UNIVERSITA' DEGLI STUDI DI GENOVA

FACOLTA' DI INGEGNERIA

PhD Program in Bioengineering and Robotics

Doctorate Thesis in
Bioengineering

Novel Bidirectional Body - Machine Interface to Control Upper Limb Prosthesis

Supervisor (UNIGE): Ch.ma Prof.ssa
Michela Chiappalone

Supervisor (IIT): Ing.
Matteo Laffranchi

Supervisor (IIT): Ing.
Nicolò Boccardo

Candidate:
Andrea Marinelli

Matr.: 442526

XXXV CYCLE 2019/2022

"When someone you love becomes a memory, that memory becomes a priceless treasure."

Dedicated to all grandparents, who protect and accompany us in life and beyond.

Abstract

Objective. The journey of a bionic prosthetic user is characterized by the opportunities and limitations involved in adopting a device (the prosthesis) that should enable activities of daily living (ADL). Within this context, experiencing a bionic hand as a functional (and, possibly, embodied) limb constitutes the premise for mitigating the risk of its abandonment through the continuous use of the device. To achieve such a result, different aspects must be considered for making the artificial limb an effective support for carrying out ADLs. Among them, intuitive and robust control is fundamental to improving amputees' quality of life using upper limb prostheses. Still, as artificial proprioception is essential to perceive the prosthesis movement without constant visual attention, a good control framework may not be enough to restore practical functionality to the limb. To overcome this, bidirectional communication between the user and the prosthesis has been recently introduced and is a requirement of utmost importance in developing prosthetic hands. Indeed, closing the control loop between the user and a prosthesis by providing artificial sensory feedback is a fundamental step towards the complete restoration of the lost sensory-motor functions. Within my PhD work, I proposed the development of a more controllable and sensitive human-like hand prosthesis, i.e., the Hannes prosthetic hand, to improve its usability and effectiveness.

Approach. To achieve the objectives of this thesis work, I developed a modular and scalable software and firmware architecture to control the Hannes prosthetic multi-Degree of Freedom (DoF) system and to fit all users' needs (hand aperture, wrist rotation, and wrist flexion in different combinations). On top of this, I developed several Pattern Recognition (PR) algorithms to translate electromyographic (EMG) activity into complex movements. However, stability and repeatability were still unmet requirements in multi-DoF upper limb systems; hence, I started by investigating different strategies to produce a more robust control. To do this, EMG signals were collected from trans-radial amputees using an array of up to six sensors placed over the skin. Secondly, I developed a vibrotactile system to implement haptic feedback to restore proprioception and create a bidirectional connection between the user and the prosthesis. Similarly, I implemented an object stiffness detection to restore tactile sensation able to connect the user with the external word. This closed-loop control between EMG and vibration feedback is essential to implementing a Bidirectional Body - Machine Interface to impact amputees' daily life strongly. For each of these three activities: (i) implementation of robust pattern recognition control algorithms, (ii) restoration of proprioception, and (iii) restoration of the feeling of the grasped object's stiffness, I performed a study where data from healthy subjects and amputees was collected, in order to demonstrate the efficacy and usability of my implementations. In each study, I evaluated both the algorithms and the subjects' ability to use the prosthesis by means of the F1Score parameter (offline) and the Target Achievement Control test-TAC (online). With this test, I analyzed the error rate, path efficiency, and time efficiency in completing different tasks.

Main results. Among the several tested methods for Pattern Recognition, the Non-Linear Logistic Regression (NLR) resulted to be the best algorithm in terms of F1Score (99%, **robustness**), whereas the minimum number of electrodes needed for its functioning was determined to be 4 in the conducted offline analyses. Further, I demonstrated that its low computational burden allowed its implementation and integration on a microcontroller running at a sampling frequency of 300Hz (**efficiency**). Finally, the online implementation allowed the subject to **simultaneously control** the Hannes prosthesis DoFs, in a bioinspired and human-like way. In addition, I performed further tests with the same NLR-based control by endowing it with closed-loop proprioceptive feedback. In this scenario, the results achieved during the TAC test obtained an error rate of 15% and a path efficiency of 60% in experiments where no sources of information were available (no visual and no audio feedback). Such results demonstrated an improvement in the controllability of the system with an impact on user experience.

Significance. The obtained results confirmed the hypothesis of improving robustness and efficiency of a prosthetic control thanks to of the implemented closed-loop approach. The bidirectional communication between the user and the prosthesis is capable to restore the loss of sensory functionality, with promising implications on direct translation in the clinical practice.

Key-words: Electromyographic Signal, Hannes Prosthetic Hand, Pattern Recognition, Body-Machine Interface, Haptic Feedback, Closed-Loop Control, Bidirectional Body-Machine Interface.

Acknowledgments

Throughout my doctoral journey, I have had the privilege of meet and collaborating with numerous remarkable individuals. Each of them has contributed a vital piece to the puzzle of my story, and for that, I extend my heartfelt gratitude to everyone. However, foremost, I wish to express gratitude to myself for the ability to assemble these diverse fragments into a breathtaking masterpiece.

I express my sincerely gratitude to the Rehab Technologies Lab, particularly Lorenzo and Matteo, for providing me the opportunity to work in an exceptional and stimulating lab. Their guidance and mentorship have not only modeled my professional growth, but also encouraged my role within a larger vision. I am immensely grateful to Nicolò for supervising the iHannes project, which has underscored the importance of our mission - to enhance the quality of life for those we assist, transcending the mere pursuit of knowledge. He has not only been an exceptional project leader, but also a dear friend. I must also extend my gratitude to Michele, whose technical expertise and unwavering support have equipped me with invaluable skills applicable across diverse domains. His presence in the lab, always ready to offer assistance and in some cases “tapullare”, is fundamental and he has become not only a source of inspiration but also a sincere friend. I am immensely thankful to all the past and current members of our group, with whom I am sharing a significant part of daily life. In particular, I would remember Lorenzo, with whom I embarked on this journey during my master's thesis, and who has now chosen to pursue new horizons abroad for love. We have formed a formidable team, continuously growing together, and I would thank each of you - Andrea, Astrid, Chiara, Dario, Giulia, Paolo Sr., Paolo Jr., Riccardo. Furthermore, I must express my gratitude to two remarkable women in the lab, Michela and Marianna, who exemplify Women in Engineering. Michela believed in me from the outset, granting me the opportunity to pursue my PhD, while Marianna has been fundamental in assisting me with paper writing and experimental setups, and for that reason and others many thanks. At IIT, there are numerous individuals whom I owe thanks to. I would like to take a moment to acknowledge the administrative staff, including the Sabrinas, as well as the Digital Production Office, Gianluca, and Caloggero (affectionately known as Lello), for their unwavering support and assistance, even in the face of the most desperate requests. Last but not least, I am grateful to Professor Strahinja Dosen for the invaluable time we shared in Denmark, which has fostered an ongoing collaboration and exchange of ideas. During my time in Aalborg, I not only had the privilege of working closely with him, but also found a reference point to admire and emulate.

Throughout these years, I had the support of the woman who shares my life, Alessandra. Her presence has enriched my personal growth and deepened my understanding of self-improvement. This, in turn, has shifted my perspective from an individualistic mindset to one of community, transcending “egoistic” behaviors. As we build our own family, I extend my profound gratitude to Alessandra for every collaborative effort we have made brick by brick. Likewise, I express my gratitude to my family -

Roberto, Ida, Eleonora, and Saretta - for the countless bricks we have laid together on our collective journey. Though physical distances may separate us, you remain forever close in my heart. My heart is filled with the love of parents, grandparents, uncles, and cousins, who, despite the miles, are an integral part of my daily life (especially when one of them sends a Sunday morning greeting). I also extend my sincere thanks to Alessandra's family, the Maturi, for hugging me as part of their ever-growing family.

Although the hard work occupies me the major time (maybe), I have been lucky to encounter a myriad of friends along this path. In Genova I had the pleasure of meeting individuals from anywhere (also Molise), who provided me with opportunities to share joyous moments and celebrate this achievement. It is with immense gratitude that I extend my thanks to Bianca, Chiara B., Chiara F., Dario, Dona, Falappone, Tonio, and Alessandro "il vecho" for the unforgettable experiences we have shared, and those that we will have together. Additionally, I would thank my roommates, who warmly welcomed me after long and taxing days of work at IIT. Some of them became my constant companions during the pandemic period, and through our shared experiences, our relation grew stronger. Thanks girl - Jessy, Caro, Fra, and Michy - for infusing my engineer's pragmatism with art, harmoncromy, and countless tea sessions. Furthermore, my time abroad holds a special place in my memory, particularly the period in Denmark where I had the pleasure of getting to know 3F (Fabio, Federico, Francesca), a French (Romain) and Caro (the little touchy one). It feels like the beginning of a joke, but with this unique combination, we shared a wonderful period during the Danish cold. There came a point when the joke became reality, as we all spent a night together at the university during a snowstorm. Although our paths have diverged since our university days, a "serata pollo" always creates an opportunity to reconnect with my university colleagues. Every time we organize this special dinner, Catto expresses gratitude, but now it is my turn to express my appreciation to all of you - Lando, Rosy, Simo, Ceci, Murru, Save, and Fede - for the moments we have shared and those that await us in the future.

Allow me to extend my acknowledgments further, as it is essential to honor every aspect of my life. In particular, I am deeply grated to my hometown friends, the "Bavose," who may be physically distant from Genova, but they are closed to my mind every day. Each member possesses their own unique story and distinctive qualities, rendering them truly exceptional. Among them, I express profound gratitude to Mando, whose solid and authentic friendship has journeyed alongside mine, transcending geographical boundaries and presenting us countless shared experiences and special moments.

I extend my sincerest gratitude to each and every one of you for your presence and for being an integral part of my life's journey.

Table of Contents

List of Figures

List of Tables

Abbreviations

#

1FB	one Feedback
2FB	two Feedback

A

A	Aim
A/D	Analog to Digital
ADL	Activities of Daily Living
ADVR	Advanced Robotics Lab
AFB	Audio Feedback
ANN	Artificial Neural Network
AP	anterior-posterior
API	Application Programming Interface
AR	Augmented Reality

B

BBT	Box and Block Test
BMI	Body - Machine Interface
BVP	Blood Volume Pressure

C

CAN	Controller Area Network
CMAC	Closed-Loop Multi Amplitude Control
CMRR	Common Mode Rejection Ratio
CNN	Convolutional Neural Network
CoP	Centre of Pressure

D

D	Degree
DASH	Disabilities of the Arm, Shoulder, and Hand
DC	Direct Current
DL	Deep Learning
DoF	Degree of Freedom
DST	Percentile Distribution

E

E	Electrodes
EC	Eyes-Closed
ECoG	Electrocorticography
EDATS	EMG Data Acquisition & Training Software
EIT	Electrical Impedance Tomography
EMG	Electromyography
EMGM	Master board
EO	Eyes-Opened
EOF	Embedded Optimization Factor
EoT	End of Travel

F

Fbt	Frequency of breath
FE	Features Extraction
FINE	Flat Interface Nerve Electrodes
FMG	Force Myography

fNIRS	functional Near-Infrared Spectroscopy
FSM	Finite State Machine
FW	Firmware

G

GSR	Galvanic Skin Response
GUI	Graphical User Interface

H

HD	High Density
HOC	Hand Open Close

I

IED	Inter Electrode Distance
iEMG	invasive Electromyography
IIT	Istituto Italiano di Tenoclogia
IMES	Implantable Myoelectric Sensor
IMU	Inertial Measurement Unit
INAIL	Istituto Nazionale Assicurazione Infortuni sul Lavoro
IOF	Index Of Fucntionality

J

JASP	JAva Structural Program

L

L	Layers
L-BFGS	Limited memory Broyden-Fletcher-Goldfarb-Shanno
LD	Low Density
LDA	Linear Discriminant Analysis
LIFE	Longitudinal Intrafascicular Electrodes

M

MAV	Mean Absolute Value
MDC	Minimal Detactable Change
MEMS	Micro-Electro Mechanical System
ML	Machine Learning
ml	medio-lateral
MLP	Multi-Layer Perceptron
MMDT	Minnesota Manual Dexterity Test
MMG	Mechano Myography
MoCap	Motion Capture
MR	Mixed Reality

N

N	Neurons
NASA-TLX	NASA Task Load Index
NIRS	Near-Infrared Spettoscopy
NLR	Non-Linear Logistic Regression
NMF	Non-Linear Matrix Factorization
NN	Neural Networks
NoFB	No Feedback

O

OPUS-UEFS	Orthotics and Prosthetics User Survey-Upper Extremity Functional Status

P

PCB	Printed Circuit Board

PDF	Probability Density Function
PhD	Doctor of Philosophy
PID	Proportional Integrative Derivative
PNI	Peripheral Neural Interface
PR	Pattern Recognition
PWM	Pulse Width Modulation

Q

Q	quaternion
QD	quick-disconnect

R

R&D	Research & Development
RAO	Relative Angle and Orientation
RBF	Radial Basis Function
RHI	Rubber Hand Illusion
RLS	Regularized Least Squares
RMS	Root Mean Square
RNPI	Regenerative Peripheral Nerve Interface
RoM	Range of Motion
RR	Respiratory Rate

S

SAR	Spatially Augmented Reality
SARB	Spatially Augmented Respiratory Biofeedback
SCMFE	Wrist FE motor control board
SCMM	Hand motor control board
SCMPS	Wrist PS motor control board
sEMG	superficial Electromyography
SHAP	Southampton Hand Assessment Procedure
SMG	Sono-Myography
SSC	Slope Sign Change
STD	Standard Deviation
STL	Standard Triangle Language
SUS	System Usability Scale
SVM	Support Vector Machine
SW	Software

T

TAC	Target Achievement Control
TAPES	Trinity Amputation and Prosthesis Experience Scales
Tb	Preliminary phase
TENS	Transcutaneous Electrical Nerve Stimulation
Tf	Final evaluation
Tf-LIFE4	Thin-Film Longitudinal Intrafascicular Electrodes
TH	Threshold Set
Ti	Initial evaluation
TIME	Transverse Intrafascicular Multichannel Electrodes
TMR	Target Muscle Reinnervation
TP	total path
TR	Training Set
TS	Tet Set
TSR	Targeted Sensory Reinnervation

U

UI	User Interface
ULP	Upper Limb Prosthesis
URD	Ulnar-Radial Deviation
USEA	Utah Slanted Electrode Array
UX	User Experience

V

VH	Virtual Hand
VHI	Virtual Hand Illusion
VR	Virtual Reality
VS	Validation Set

W

WFE	Wrist Flexion Extension
WL	Waveform Length
WPS	Wrist Pronation Supination

X

XR	Extended Reality

Introduction

The absence of an upper limb caused by amputation or congenital disabilities is a significant impairment that severely impacts daily activities and independence (refer to paragraph 1.1). The hand plays a crucial role in exploring and interacting with the external world and accomplishing simple tasks of everyday life. To address these limitations, researchers have developed active upper limb prostheses (ULP) to enhance the quality of life of individuals affected by limb loss (refer to paragraph 1.1).

Electromyographic activity is the primary method of controlling active ULPs, utilizing various control approaches and interfaces to accommodate the complexity of the prostheses (refer to paragraph 1.2.1.1 and 1.3). While literature suggests that multi-DoF prostheses can mimic the capabilities of real limbs, there remains a significant discrepancy between technology and controllability (as evidenced in section 1.3.3) [1-9]. Controllability has been identified as a major cause of prosthetic abandonment, and lack of feedback is essential in improving the usability of these devices, according to Qu, et al. [10] and Kyranou, et al. [3].

However, incorporating these aspects within the prosthesis and socket is crucial for effective implementation and real-life application, thus restoring lost functionality for ADLs. This integration is a critical aspect of the development of advanced prosthetic technologies (Figure 1) to enable effective bidirectional communication between the user and the external environment.

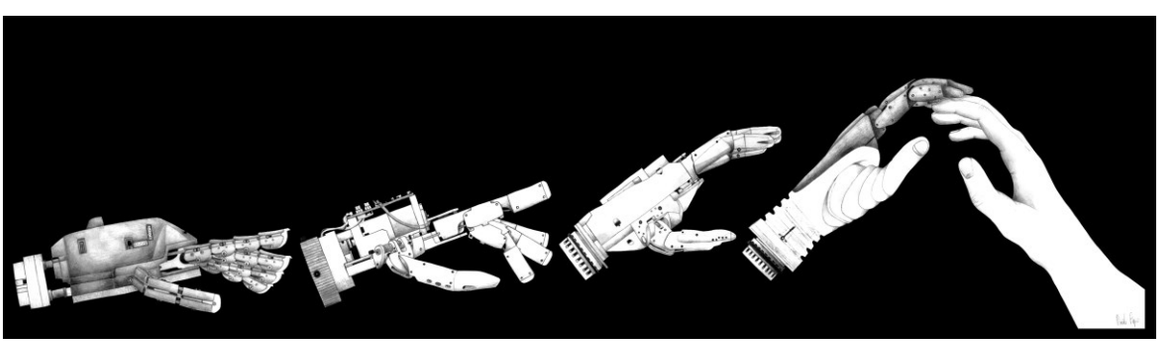

Figure 1 Evolution of robotic hand: from industry to human prosthesis.

Based on the above considerations, the three aims of this thesis are:

- **A1 – Development of the integrated *Hannes* multi-DoF system architecture.**

  This first Aim was the **development of the software and firmware architectures** for the control of the *Hannes* system [11] (Figure 2), which includes all the DoFs described in section 2.3 plus the active elbow DoF, developed but not included in the current study. The **firmware** implementation was subdivided according to the involved microcontroller-based electronic boards connected via CAN protocol. The **software** development mainly concerned a Bluetooth-based Graphical User Interface (GUI) capable of collecting data from the Master-board and setting the prosthesis parameters. This activity, performed during the first year, was instrumental in fulfilling the other Aims.

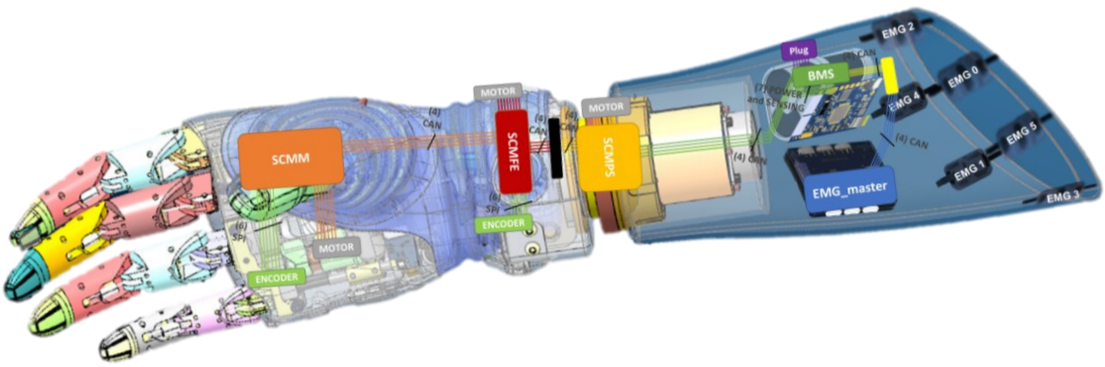

Figure 2 Hannes Multi-DoF system.

- **A2 - Closing the gap between technology and controllability**

  The second Aim had the goal to **close the gap between technology and controllability**. Thus, throughout the second year, I investigated different strategies to create a more **robust control of the Hannes multi-DoF** [12-15]. To do this, electromyographic signals (EMG) were collected from trans-radial amputees using an array of up to six EMG sensors placed over the skin. Different Machine Learning algorithms were tested and compared to study muscle synergies and state machine paradigms. The final goal was to design a **robust joint selection strategy and a human-like joint control** [12-15].

- **A3 - Haptic Feedback in Bidirectional Body-Machine Interface**

  This final Aim, which also constitutes the ultimate goal of my PhD, was focused on developing a Bidirectional BMI capable of retrieving force and/or proprioceptive information from the Hannes hand and transmitting custom haptic feedback toward the residual amputee's forearm. These new features allowed and will allow Hannes to interact more naturally with both the environment and the patient. The acquired data was "fused" with the pattern recognition algorithm. In order to deepen our knowledge of the role of tactile events in prosthetics, I have been exploring different phenomena, including the **restoration of haptic feedback** and **embodiment training based on visual-haptic respiratory biofeedback in spatial augmented reality**. These activities were performed in the third year [16].

This research was conducted at the Rehab Technologies Laboratory of the Istituto Italiano di Tecnologia (IIT) in Genova, in collaboration with Centro Protesi INAIL of Vigorso di Budrio. My role as a software and firmware engineer was integral to the iHannes project (PR19-PAS-P1). Technical activities were primarily carried out at the Rehab Technologies lab (**A1** and **A2**), and clinical validation experiments were performed with amputees through direct collaboration with INAIL. Furthermore, I had the privilege of contributing to the Sensory Motor Lab at Aalborg University, under the leadership of Professor Strahinja Dosen. During a six-month period, I focused on analyzing feedback aspects (**A3**),

specifically non-invasive proprioceptive feedback on amputees. The resulting methods were validated on both able bodies in Denmark and amputees at the INAIL prosthetic center.

The first activity I performed to reach the aims was a literature review to contextualize the amputation problem. ***Chapter 1*** presents the amputation problem with particular attention on commercial prosthesis solutions and research solutions. Subsequently, there is a description of the input signals for controlling prosthesis and feedback signals for haptic recovery. Then control strategies were analyzed at different levels, from low-level control to actuate single motor, to high-level control to perform complex tasks and actuate multi-DoF prosthesis. Such an analysis was part of a published review Marinelli, et al. [6], which offers an overview of the State of the Art in the field.

Chapter 2, ***Chapter 3***, and ***Chapter 4*** constitute the body of this thesis. These chapters include both development (**A1**) and validation (**A2** and **A3**) of the Hannes prosthetic system. In particular, ***Chapter 2*** incorporates all the works concerning the user aspects, such as functionality, efficiency, and embodiment of the Hannes prosthesis (part of **A3**) and its mechatronic improvements to cover the user needs (**A1**). This chapter describes the benefit of using a single DoF prosthetic device (section 2.1), the level of integration of such a technology into the body scheme (section 2.2), and the design of multi-DoFs Hannes to improve its functionality (section 2.3) in a User-centered prosthetic design. Subsequently, ***Chapter 3*** analyses the problem of controlling multi-DoF Hannes, with the final goal of closing the gap between technology and controllability to realize a Body – Machine Interface (**A2**). This chapter describes all the aspects related to the increase of DoFs to be controlled and how to design a robust, efficient, and human-like control solution.

Finally, ***Chapter 4*** describes the restoration of haptic information at different levels of sensory feedback, from proprioception to tactile, to cover the **A3**. Such an implementation focuses on integrating feedback on real cases of prosthesis sockets to realize a Bidirectional Body – Machine Interface.

The general ***Conclusions*** at the end of this manuscript integrated all the obtained results to outline each performed activity's role in developing a real effective prosthesis solution. Overall, the results of this Thesis, thanks to the capability to recover functionality and sensory information, allow for better prosthesis integration into the body scheme and better interaction between the human and external word [17, 18], thus making a fundamental step towards improving the amputees' quality of life.

State of the Art

Chapter 1. Active Upper Limb Prostheses: A Review on Current State and Upcoming Breakthroughs

Over the past twenty years, poly-articulated upper limb prostheses (ULPs) have undertaken several technological and scientific developments to satisfy the different needs of the upper limb amputee community. Nonetheless, in a recent study, Salminger, et al. [19] observed overall abandonment rates of ULPs of about 44% in a population of mainly (92%) myoelectric prostheses users. They also highlighted how the past decade of developments still presents technological limiting factors that did not permit the restoration of the full functionalities of a missing limb, hence leading to a substantial increased rate of prosthesis abandonment. The main cause of such ineffectiveness mainly resides in a non-sufficiently patient-tailored design process [19].

According to the American Orthotic & Prosthetic Association [20], partial amputations, i.e. finger amputations, represent the majority of upper-limb losses (75.6%), while trans-radial and trans-humeral amputations constitute a percentage oscillating between 5 and 6%. Despite this, the level of impairment caused by trans-radial and trans-humeral amputations is greater than for partial amputations.

Without tracing back all the evolution of upper limb prostheses – the reader might find useful the reviews of Trent, et al. [4] and Ribeiro, et al. [21]). Trent, et al. [4] work focuses on a classification of the upper-limb prostheses architectures based on the type of adopted actuation, e.g., passive, body-powered or active. On the other hand, Ribeiro, et al. [21]'s research investigates the most relevant control signals used for the man-machine interface.

This work focuses on trans-radial and trans-humeral devices, excluding partial amputations, and it details the latest and most technologically advanced solutions, namely poly-articulated myoelectric prostheses. Moreover, this review aims at presenting and analyzing the key elements of state-of-the-art upper limb prostheses in a user-centered and human-in-the-loop fashion and to provide guidelines for the development of such prostheses and the relative control algorithms, to possibly achieve solutions capable of promoting the systems use and overcoming the elevated abandonment rates observed so far. Overall, the reader could take advantage of this review as an analytical collection of solutions constituting a premise to provide the user with a seamless control experience.

1.1. Upper limb Prosthetics classification: a twofold perspective

An ULP system can be observed from two main points of views: its mechatronics, namely the combination of the mechanical and electronic components necessary for its operation, and the control strategies and algorithms implemented to orchestrate its functions. Research groups have therefore attempted to solve the prostheses abandonment problem by addressing different technological and scientific challenges, either focusing on mechatronic design, or on control strategies aimed at increasing

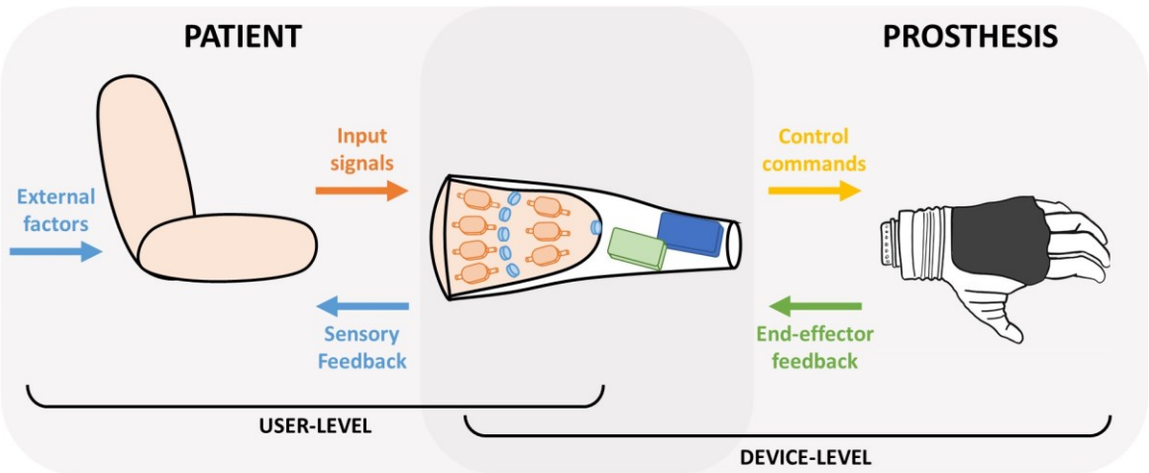

Figure 3 Graphical representation of a ULP system and its elements.
The user level (left panel) includes: input data sent from subject to the prosthesis (Input Signals), artificial sensory feedback information delivered from the prosthesis to the user (Sensory Feedback), and external sources of interaction (External Factors), such as actuation coming from the unimpaired limb or environmental/accidental sources of feedback such as vision and sound. The device-level (right panel) includes the control commands used to drive the prosthesis and the feedback information collected by the end-effector. The user-device interface is characterized by a bidirectional exchange of information (overlap of the two panels).

the human-machine interaction and, in some cases, introducing feedback sources, as detailed in the next sections.

ULP control can be divided into two synergistically interacting sub-systems: the user-level and the device-level, as depicted in Figure 3. The user-level includes the patients and the most proximal device component interacting with the user (i.e., the socket), while the device-level extends from the socket to the ULP device. These two sub-systems overlap at the socket level, which is involved in a bidirectional flow of information. On one hand, it receives inputs from the user (i.e. movement intentions) and translates them into movement commands for the device; on the other hand, it receives information (both from the device and the environment) and communicates it to the user through sensory feedback (Figure 3). Importantly, the socket itself severely limits the user comfort, and together with the prosthetic weight highly contributes to the prosthetic abandonment.

Even if the state-of-the-art in prosthetic research encompasses studies based on psychological processes too, commercial ULP systems have focused on restoring functional capabilities by capitalizing on the device-level only, therefore on mechatronic, and several solutions can be found on the market for trans-radial level of amputations. Commercially available systems merge basic functionalities and aesthetic requirements, targeting the clinical needs given by a certain kind of amputation, rather than focusing on each patient's specific needs.

Commercial solutions range from tri-digital hands, e.g., **VaryPlus Speed**, **SensorHand Speed** by Ottobock [22] and **Motion Control** Hand by Fillauer [23]; through polyarticulated hand under-actuated, e.g., **Michelangelo** by Ottobock [24]; to fully actuated polyarticulated hand, e.g., **BeBionic** by Ottobock [25], **i-Limb** by Ossur [26],**Vincent Hand** by Vincent Systems [27], **TASKA** hand by Taska Prosthetics

[28], **BrainRobotics** Hand by BrainRobotics [29], **Ability Hand** by Psyonic [30], and COVVI hand [31] by COVVI.

In the last decades, many research groups have focused on the mechatronic development of ULP devices, entrusting the intelligence of the device to the embedded mechanics in a very thorough design, structuring the development of the concept of under-actuation, such as the **Vanderbilt Multigrasp Hand** [32], the **MIA Hand** [33], the **SoftHand Pro** [34], the **KIT Hand** [35], and the **Hannes Hand** [11].

On the other hand, there is a family of very dexterous devices, not yet market-ready, that mimic the complexity of the human hand, implementing a fully-actuated multi-degrees of freedom mechatronics, e.g. the **University of Bologna Hand** [36] or the **Shadow Hand** [37].

However, this great variety of products does not match with the elevated abandonment rates, demonstrating the lack of satisfaction of the patients' needs from a mechatronic perspective. In particular, structural and supporting part lack of adjustability of user size, allow limited kinematic and motion possibilities and more advanced systems present limited operational time [38]. This leads to limited satisfaction and feeling of security. Moreover, these systems generally present poor personal and social acceptance because of limited anthropomorphism, high weight and presence of acoustic disturbances during use [38], This suggests that ULP development should not only focus on the device level, but improvements at the user level could play a key role for truly meeting the user requirements and consequently obtain device acceptance. Motivated by this, in this review, we analyse all the possible approaches that could potentially address the user needs in terms of device controllability, robustness and hence embodiment and user experience. To this end, it is fundamental not only to focus on the functionality restoration but also on the sensory information recovery, which are fundamental to effectively control the device. All the described approaches range from improvements in decoding user intentions, hence analysing all possible input sources and their related control strategies, to inclusion of additional sources of feedback capable to restore the sensory information. These approaches tackle the issues related to poor device control because of lack of intuitiveness and sensory feedback.

Therefore, in this review we present current and emerging methods in ULP development, detailing various sources of input and feedback signals, as well as control strategies. We also highlight current challenges and open issues in the field, specifically focusing on the importance of user experience and involvement in the design and development process. This is fundamental to promote patient-tailored approaches leading to the development of truly personalized devices, which are currently lacking. We finally provide an overview of the most promising approaches that if followed, may one day provide upper limb amputees with a true substitute of their missing arm.

1.2. Input and Feedback Signals for Prosthetic Control

Prosthetic control is regulated by a flow of signals, as depicted in Figure 4. *Input signal* runs from

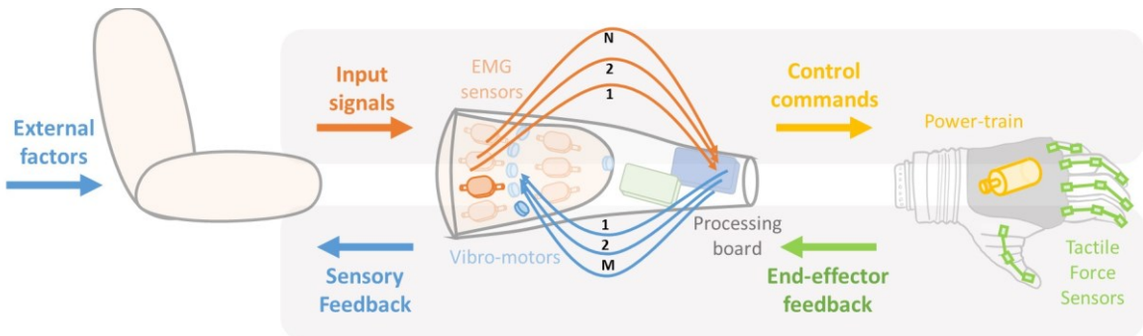

Figure 4 Graphical representation of information flow of a possible ULP architecture.
Input flow (top panel): from user (input signals i.e., from EMG sensors) to prosthesis (control commands i.e., through power train). Feedback flow (bottom panel): from prosthesis (end-effector feedback i.e., from tactile force sensors) to user (sensory feedback i.e., through vibrotactile motors).

the user to the device and they are often of biological or electrophysiological nature, in which case are called *biosignals*. Signals flowing in the opposite direction convey information from the device to the user and are therefore defined as *sensory feedback* signals. Moreover, some *external factors* convey to the user additional source of feedback (i.e., incidental feedback), such as visual or auditory information that can be used to estimate the prosthesis state [5, 39, 40].

Input signals include all the sources of information that can be taken from the amputee and translated into motor commands for driving the prosthesis (e.g., electromyography - EMG), see section 1.2.1. Instead, sensory feedback information encompasses different *prosthetic sensing* solutions acquired either from the prosthetic device or from the environment, see section 1.2.1 that can be translated into sensory stimuli for the amputee (e.g., vibrotactile stimulation, see section 1.2.3). All types of signals can

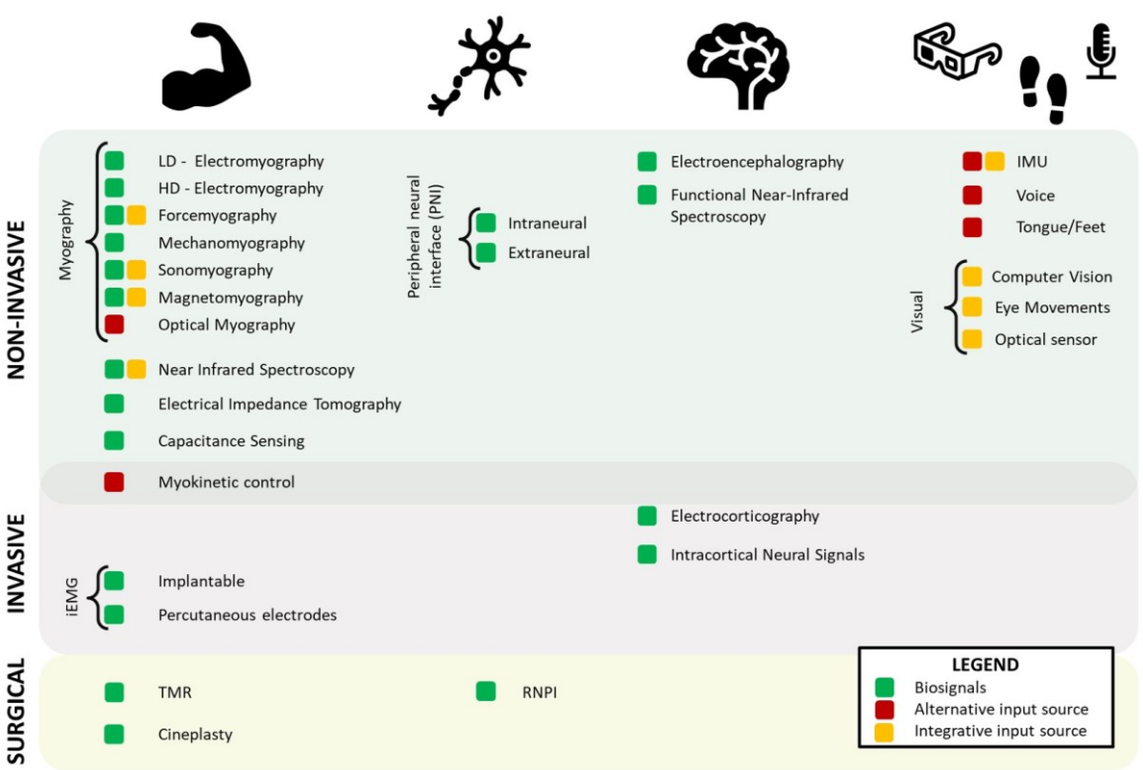

Figure 5 Input sources for ULP.

be classified according to their level of invasiveness, with consequent advantages and drawbacks.

1.2.1. Input Signals

In recent years, many research activities have focused on the extraction of useful information from the biological signals in order to suitably control upper limb prostheses. Traditionally, **the surface EMG** (sEMG) is the most widespread signal for prosthesis control but its use still faces many drawbacks [3]. In the following, we describe various methods to employ EMG as input signal for ULP control and we also explain how other input sources can be exploited to obtain more dexterous prosthetic behavior, overcoming the limitations of current ULP systems.

Figure 5 collects input signals for ULP control that will be described in the following subsections, ranging from those used by commercial systems, up to those currently under investigation.

1.2.1.1. Biosignals → Electromyography

The term *biosignal* indicates every possible signal that can be detected and measured from biological beings, humans – in our case. Usually, the term is used for signals of electric nature (i.e., EMG), but actually every signal collected from the activity of different tissues or organs belonging to the human body, can be considered as a biosignal.

We here adopt this latter definition to group input sources that are described next. Given its large use both in research and commercial ULP devices, electromyography deserves a dedicated subsection, while other biosignals are grouped together. We also dedicate a whole subsection to brain-derived signals, which are especially used in brain-machine and brain-computer interfaces (BMIs, BCIs), but that are also showing potential use for ULP applications. Table 1 summarizes biosignals for ULP control that will be described in the following subsections.

Table 1: biosignals used as input sources in prosthetic applications.

		Measured Property	Sensors' placement	PROs	CONs	Sensor Fusion	Examples
Electromyography (EMG)	Surface EMG	Muscle Electric Potentials	On the skin over targeted muscles 2–32, up to 192 sensors	Non-invasive, long-term use, a large number of people	Sweating, electrodes shift, Muscle fatigue, Electromagnetic noise	NIRS, IMU, FMG, SMG, MMG	[41] up to 27 gestures
	Invasive EMG		Underneath the skin, on or inside targeted muscles 4-8 sensors	High signal/noise ratio, directly on the nerve, no shift with respect to the source	Invasive, infections		[42, 43]

Force-myography (FMG)	Change of muscle morphology measured on the skin surface	Over targeted muscle, over related tendons 8, up to 126 sensors	Physiologic, small size, high signal/noise ratio, flexible	Muscle fatigue, sensors shift, pre-load force, small spatial resolution, crosstalk	EMG	[44] up to 8 gestures
Mechano-myography (MMG)	Muscle fiber oscillations using microphone or accelerometers	Over targeted muscle 6-20 sensors	low cost, no pre-amplification, no precise positioning, no skin impedance or sweat influence	Ambient acoustic noise, Adjacent muscle crosstalk, Sensor displacement	EMG, IMU	[45-47] up to 5 gestures
Sono-myography (SMG)	Change of muscle morphology	Over targeted muscle, over related tendons transducers of different shapes	Deep and superficial muscles, some models are cheap and energy-efficient	Probe shift, tissue impedance, no wireless, some models expensive and bulky	EMG	[48] up to 15 gestures
Near-Infrared Spectroscopy (NIRS)	Tissue oxygenation through the amount of scattered light	Over targeted muscle 2-4 sensors	Deep and superficial muscles, high spatial resolution, no electronic interference	Ambient light, Muscle fatigue, tissues heating	EMG, IMU	[49] up to 9 gestures
Electrical Impedance Tomography (EIT)	Tissue impedance	Over targeted muscle, over related tendons 8, up to 64 sensors	No need precise positioning	Low time resolution, sweating, Electromagnetic noise, high consumption	-	[50, 51] up to 8 gestures
Capacitance sensing	Tissue capacitance	Over targeted muscle, over related tendons 3 receiver sensors	Non-invasive, low cost, deep and superficial muscles	Sweating, Electromagnetic noise, displacement, ambient temperature	-	[52, 53] up to 2 gestures

Magneto-myography	Magnetic fields generated by muscle	Over/inside targeted muscle 7 sensors	Not sensitive to sensor's shift and sweat	Magnetic interference, can be invasive, movement artifacts	-	[54] concept
Peripheral Neural Interfaces (PNIs)	Electrical activity of the nerves	Microelectrode arrays placed on different fascicles within the median and ulnar nerves	Intuitive, direct maps of complex movements, high accuracy, robust	Invasive, difficult to separate EMG and PNI components, recording channels really closed each other	-	[55] up to 15 DoFs
Intracortical neural signals	Intracortical neural signals from the brain, action potentials of individual neuron	16-192 high-density channels electrodes inserted into the motor cortex tissue	Accurate and capable of collecting the most information-rich data, high spatial resolution	Very invasive, influenced by tissue reactions	-	[56-59] 7-10 DoFs
Electrocorticography (ECoG)	Electrical activity of brain's surface	32-128 high-density channels on sensorimotor regions	Less attenuated than EEG, good spatial resolution and wide frequency content	Surgical procedure and lack to measure single cell activity	-	[60-63] 4 gesture recognition and wrist movements
Electroencephalography (EEG)	Electrical activity of the brain	6-32 channels headsets	Not invasive, low cost, portable, stable, and very easy to use	Signal attenuated by the dura, the skull, and the scalp, loss of important information	-	[64-67] single DoF

Functional Near-Infrared Spectroscopy (fNIRS)	Activity-related brain oxygenation, near-infrared led, and a photodetector measure the amount of IR light absorbed by the hemoglobin in the brain	10-200 channels of optodes	Non-invasive, simultaneous detection information under the skin, low cost	Few centimeters penetration of cortical tissue, not great accuracy, and system too cumbersome	-	[68] 3 DoFs trans-humeral amputees

While cosmetics, electronic components and computational efforts have undergone a significant improvement, the control strategies currently used in prosthetic applications have not changed since their first appearance in the 1960s [69]. The EMG has been one of the major sources to control upper limb prostheses [70]. These signals carry information about neuromuscular activity, and they are used to retrieve human intention. EMG is indeed a technique for studying the activation of the skeletal muscles through the recording of electrical potentials produced by muscle contraction [71]. The theory behind the sEMG electrodes is that they form a chemical equilibrium between the detecting surface of the electrode and the skin of the body through electrolytic conduction, so that the current can flow into the electrode.

Multiple methods have been used to obtain the intended gesture from the processed EMG signals, all of which exploit the fact that the amputees can still generate different and repeatable muscular patterns related to each forearm movement with residual muscles of the stump. Low-density EMG is commonly used in prosthetic application, both in research and commercial context. Noteworthy, EMG signals can also be collected with invasive methods. The sEMG can be thus classified according to the level of resolution and density of the sensors. In the following, we provide an overview of the different types of EMG-based biosignals.

Surface EMG

The sEMG can be classified according to the number of electrodes used (Figure 6). **Low-density EMG** generally refers to the use of a small (<10) number of EMG bipolar sensors, that can be either wet, i.e. contain an electrolytic substance that serves as interface between skin and electrodes, or dry [72]. Conversely, **high-density EMG** is typically composed by wet monopolar sensors spread on a planar patch, around 1cm apart, and with the ground reference generally placed on the wrist or on the elbow [73].

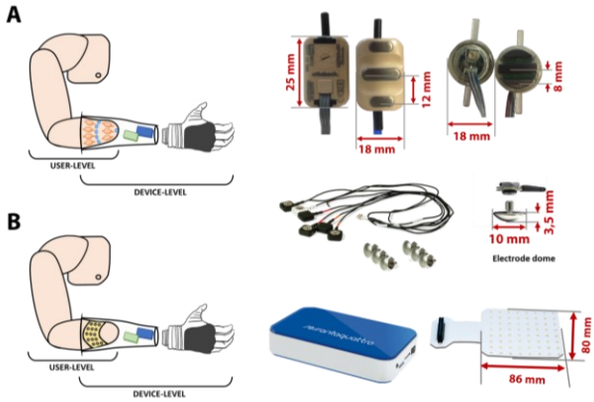

Figure 6 sEMG electrodes.
A: bipolar dry sensors, Ottobock and IIT/INAIL respectively. **B:** high-density wet sensors (OT Bioelettronica).

Importantly, sEMG electrodes also differ in their electronic configuration, as they can be either preamplified or not [74]. Merletti and Muceli [75] provided a guide with the best practice to acquire and manipulate EMG data according with the different aims, from signal analysis to motion prediction.

Prosthetic control with low-density EMG is generally obtained by using two bipolar electrodes placed on antagonist muscles. This configuration allows the control of the prosthetic system in a robust and simple way [71]. However, the detection of complex and simultaneous movements of the phantom limb can be improved by using an array of EMG electrodes placed on the superficial skin of the residual forearm [13, 76-78], The use of sEMG in prosthetic applications has become the most widespread source of information about voluntary movement [69] because of the direct correlation between EMG activity and subjects' intentions.

Differently from the low-density, the high-density sEMG (HD-sEMG) is based on a higher number of electrodes placed on a small portion of the body. Recently, a growing number of researchers has focused on the use of these electrodes aiming to increase the amount of collected data, although at the cost of a greater computational burden. HD-sEMG sensors have been used to discriminate muscular patterns related to different gestures. Their signals can be handled in various ways to retrieve unique and repeatable information, as described in section I.1.3. These sensors have to be positioned according to the distribution of the underlining muscle fibers and this configuration provides a low resolution map of the synergistic activation of the muscles during movement production [79, 80]. For example, from contraction of the muscles under the acquisition grids, it is possible to extract bi-dimensional images, in which the EMG amplitude is mapped to a color scale. These maps can be thus handled by complex algorithms, as the ones used for objects detection in robotic navigation [81]. The main limitation of the HD-sEMG, which currently bounds its application to a laboratory scenario, is the skin-electrode contact since it requires conductive gel to reduce the interface impedance. The wet area is mainly needed to reduce artifacts in the EMG signals since it is generally acquired in monopolar configuration. Another disadvantage of this technique consists in the fact that computation is time-consuming.

Overall, the main drawback of sEMG-based approaches is constituted by the influence that skin impedance, sweat, and electrode shift have on the stability of the input signals [82]. Additionally, muscle crosstalk and the difficulty to reach deep muscles further limit the quality of the collected signal. In the

context of ULP, the use of sEMG can be further complicated by the fact that the amputation strongly affects muscles strength and organization and therefore signal quality, as discussed in section 6.4 of Marinelli, et al. [6].

Invasive EMG and Surgical Procedures

The invasive approach has been exploited to explore the activity related to the production of movement for many years [83] and it is still investigated by many groups. However, the main drawback of this approach is constituted by the surgery and by the technological barriers still faced by the available equipment. On the other hand, **invasive electromyography** (iEMG) allows to measure single motor unit action potentials, enabling a higher selectivity and a better accuracy of the input signal, overcoming the limitations imposed by sEMG. There are several examples of iEMG, which vary in the type of electrodes and level of invasiveness, as detailed hereafter.

EMG can be invasively detected by inserting electrodes into the internal surface of muscles [84]. This invasive technique exploits two different percutaneous electrodes: **needles** and **fine wires** [72, 85]. The most used are *needle electrodes*. These electrodes are concentric, and their bare hollow needles contain an insulated fine wire into their cannula, which is exposed on the beveled tip, which is the active recording site. *Wire electrodes* are typically made of non-oxidizing and stiff materials with insulation, they can be implanted more easily and are usually less painful than needle electrodes.

Since both these sensors are percutaneous, i.e., passing through unbroken skin and leaving an open passage between the internal structures of the body and the external world, the risk of infection is quite probable. For this reason, and because of their intrinsic discomfort due to the percutaneous wire that can easily break, their usage is limited to laboratory research [86, 87]. A detailed description of invasive electrodes both to record biological signals and to deliver electrical stimulation can be found in Raspopovic, et al. [88].

In the last decades, growing attention has been paid to the development of **intramuscular electrodes** that could be implanted under the skin of the subject to achieve the advantages of invasive sensors and simultaneously avoid the risks and inconvenience of percutaneous instruments. For example, Weir, et al. [89] developed **an implantable myoelectric sensor** (IMES), a system able to receive and process up to 32 implanted sensors with wireless telemetry. A transcutaneous magnetic link between the implanted electrodes and the external coil allows reverse telemetry, which transfer data from the sensors to the controller, commanding the control of the prosthesis, and forward telemetry to supply power and configuration settings to the electrodes. These sensors are designed for permanent long-term implantation without any kind of servicing requirement and have been tested on animals. Four months after the implantation of IMESs in the legs of three cats, the sensors were still functioning [89]. Intramuscular electrodes have been used in prosthetic application to decode 12 different hand gestures from 4 healthy subjects [42]. Moreover, it has been shown that the application of this invasive approach enhances the simultaneous control of multi-DoFs system [90].

Recently, the group of Ortiz-Catalan showed an invasive procedure for ULP control. They positioned EMG electrodes under the skin of amputated subjects and sutured them directly on the external surface of the muscles [43]. More precisely, sensors were sewn onto the epimysium of the two heads of the biceps' muscles and the long and lateral heads of the triceps muscles. These invasive electrodes were used in combination with an osseointegrated prosthesis, i.e. a system obtained following a very invasive surgical procedure, which allows to anchor the prosthesis to the remaining limb's bone [43]. In the context of ULP, osseointegration is offered for trans-humeral amputees, and the prosthesis is anchored to the humerus with two mechanical elements: the fixture, a screw made of titanium placed inside a hole made in the bone that becomes osseointegrated, and the abutment, placed within the fixture and extending outside of the body in a percutaneous way, onto which the prosthesis is connected. This technique was tested on four osseointegrated patients.

This latter example indicates that also surgical approaches can be taken to improve the quality of the collected EMG. A promising surgical technique that is performed in case of high-level amputation is Targeted Muscle Reinnervation (TMR). This method was developed by the group of Kuiken in the early 2000s and consists in transferring residual arm nerves to alternative muscle sites. Following reinnervation, these target muscles are able to produce EMG that can be collected and used to control prosthetic arms [91]. This strategy works at the condition that each reinnervated muscle produces an EMG signal in response to only one transferred nerve, with the consequence that native nerves innervating the target muscle has to be cut during the surgical procedure to avoid unwanted EMG signals [92]. In the last 15 years, TMR has allowed intuitive control of ULP to several subjects with high-level amputation for whom standard ULP devices allowed a poor restoration of motor functions [92]. Importantly, given that it is performed on complex amputations, this technique is strongly tailored to each patient's physical and clinical status [93, 94].

Recently, a new surgical method for improving EMG-based control has emerged: the *regenerative peripheral nerve interface* (RNPI) [95]. Just as TMR, its goal is to turn a muscle into a biological amplifier of the motor command, in order to improve the quality of the EMG signal recorded, processed and used to drive the prosthesis. To this end, RNPI exploits the regeneration capabilities of nerves and muscles, to implant a transected nerve into a free muscle graft. Following regeneration, revascularization and reinnervation by the transected nerve, the muscle graft effectively becomes a stable peripheral nerve bioamplifier, able to produce high-amplitude EMG signals [96]. The potential of this novel interface has been tested by Vu, et al. [97]: they used EMG signals collected by intramuscular bipolar electrodes implanted into RNPIs obtained in amputated individuals, who could successfully perform real-time control of an artificial hand. Surprisingly, subjects were able to control the device with a high level of accuracy even 300 days post-implantation, without recalibration of the control algorithm.

Another surgical technique, not directly related to EMG signals but worth mentioning, is *cineplasty*, an old method revived in the last years with a new and more modern approach. This method was introduced for the first time by Vanghetti in 1899 and then replicated by Sauerbruch ten years later [98].

It consisted of the direct mechanical linking of residual muscles and/or residual tendons of the affected limb to the prosthesis through external cables (i.e., Bowden cables). In 2001, Heckathorne and Childress [99] implemented an evolution of this surgical solution for the control of 1 DoF ULP by exploiting exteriorized tendons directly linked to a force sensor.

1.2.2. Prosthetic Sensing

Natural movements occur with a bidirectional flow of neural information, i.e., motor commands on one direction and sensory feedback on the other. In prosthetic applications, while many efforts have been spent to provide signals carrying motor intentions, a less explored path is the integration of **sense of touch** into the prosthesis [100]. This lack is highly responsible for the missing perception of the prosthesis as part of one's own body and is also precluding a closed-loop control of the prosthesis.
More recently, the scientific community has started exploring different methods to equip prosthetic devices with perception of *tactile* and *pressure* information [101-105], although often resulting in very complex, unreliable, or unpractically cumbersome solutions. The few solutions tested on real prosthetic setups impacted on their *anthropomorphism* and *dexterity*.

To integrate *touch sensors* into robotic and prosthetic devices (Figure 4, end-effector feedback) [103, 106, 107], different technologies have been investigated and employed [108], namely **capacitive** [109, 110], **resistive** [102, 111, 112], **piezoelectric** (screen printed piezoelectric polymer, PVDF) [113], and **magnetic** sensors [114]. Other examples include technologies based on **electrical impedance** [51, 112], **pressure** and **electrical impedance** [115], **optical fibers** (Bragg fiber [116]), **Micro-electro-mechanical Systems** (MEMS**,** texture sensing [117]) combined with **Spiking** based on Izhikevich neuron model [118]) and **Optoelectronic** [119].

Examples of the application of these sensors into prosthetic devices include the **E-dermis** (piezoelectric sensors integrated on the Bebionic's fingertips) [120], **E-skin** (integrating different types of sensors) [106], and **BioTac** (impedance sensor integrated on the Shadow Hand [121]) [122].
Among commercial devices, the SensorHand Speed [123] made by Ottobock is the only one including tactile sensors based on resistive technology [123].

Therefore, tactile sensation is the first step towards novel and more efficient control strategies that do make use of feedback information [124]. To this end, artificial intelligence can be exploited to detect the grasp of different objects from sensor data [125].

1.2.3. Sensory Feedback

Sensory feedback patterns are designed to enrich the perceived responsiveness of the device and the subjective experience of its use as a limb [88, 126, 127]. Such a result derives from the elicitation of physiological and psychological reactions that promote embodiment processes (described in paragraph 5.1 of Marinelli, et al. [6]). Furthermore, such stimulations (haptic feedback in many cutting-edge devices) are designed as a fundamental component of bidirectional human-machine interfaces

empowering prosthetic control [128]. Establishing such a closed-loop can trigger learning processes even for artificial sensations [129], pointing at somatosensory plasticity processes. These phenomena provide the user with an engaging guidance within a natural interaction, facilitating the execution of prosthetic maneuvers during calibration, training, and daily use. Importantly, such an enhanced practice will ease the production of consistent biosignals that will progressively become easier to interpret as user commands.

However, current commercial prostheses generally do not incorporate an explicit haptic feedback but the incidental feedback, like visual and the sound cues, could be exploited by the user to estimate the prosthesis state [39]. For example, the acoustic feedback provides a guidance on how to reach target during the rehabilitation session, in this way the rehabilitation step can be more interactive and engaging if appropriately designed (never obnoxious, possibly plausible). Overall, the next sub-sections will discuss the design of sensory feedback in prosthetics, distinguishing invasive and non-invasive stimulation modalities.

1.2.3.1. Non-invasive methods

Non-invasive feedback restoration for upper limb amputees is a hot topic in the research community, and yet it has not achieved broad clinical application [5]. Many solutions have been proposed, but the main problem lays in their poor robustness. [21] highlighted the most widespread types of non-invasive feedback, described in Table 2.

Table 2: Non-invasive methods for sensory feedback in ULP.

Feedback sense		Instruments and feedback information	Application	PROs	CONs	Examples
Touch (cutaneous stimulation)	Vibrational	Eccentric rotating motors, proprioception, force	Array over the forearm or over the arm	Non-invasive, robustness control, brief training period, intuitive, cheap, small	[130, 131] up to 3 DoFs or different force levels	Non-physiological, need calibration, coupled intensity and rotation frequency, position displacement
	Mechanotactile	Linear actuator, pressure sensation, spatial touch sensation	Detected areas to reproduce real touch sensation, array over the arm	Non-invasive, intuitive, brief training period, decoupled intensity and frequency	[127, 132, 133] different pression level, touch sensation	Need spatial and intensity calibration, bulky, position displacement

	Electrical	Transcutaneous stimulation using bipolar electrodes, pressure, slip, proprioception	Array over the forearm or arm	No electrode displacement, low power consuming, high sensor skin contact, intensity or frequency modulation	[134-136] touch location, pression, proprioception	Noise during acquisition, long calibration, not localized sensation
Sound (Acoustic)		Acoustic speaker, proprioceptive movements	Laptop speaker to guide the training acquisition and improve the pattern recognition strategy	Low cost, no calibration, intuitive	-	[137] multiple arm positions
Vision (Visual)		Camera on board, external camera	head-mounted displays, laptop displays, virtual reality, augmented reality	Increase perceptual experience, engagement, intuitive, promote training	Bulky, not portable, uncomfortable	[138-142] trajectory, force

The most investigated feedback relies on the sense of touch and therefore consists of cutaneous stimulation. This can be performed with different modalities namely, vibrational, mechanotactile or electrical stimulation.

The **vibrational feedback** is generally implemented with the addition of eccentric rotating motors placed in contact with the skin surface of the stump [21]. This method is generally employed to augment the robustness of the control system by providing the user with additional information regarding the position of the prosthetic device but it lacks intuitiveness, as the association between perceived sensation and the corresponding information has to be learned by the user. For example, in Bark, et al. [130], the motors were placed in 4 distinct areas of the stump to guide the user through the desired trajectory while grasping object and the results showed a significant decrease in the root mean square angle error of their limb during the learning process. More recently, Markovic, et al. [131] proposed a joint-oriented feedback criterion consisting of three vibromotors placed on the arm to provide the information on which joint is currently activated by the user, thus restoring proprioceptive sensation. The experiment was performed by 12 able-body subjects and 2 amputees controlling 3 DoF prosthesis, and it was found that the myoelectric multi-amplitude control outperformed the pattern recognition method when the feedback was applied.

Differently from the vibrational, the **mechanotactile feedback** is based on the application of linear actuators on the skin and provides pressure sensation. Antfolk, et al. [132] exploited this technique and proposed a multisite mechanotactile system to investigate the localization and discrimination threshold of pressure stimuli on the residual limbs of trans-radial amputees. They demonstrated that subjects were able to discriminate between different location of sensation and to differentiate between three different levels of pressure. This study demonstrated that it is possible to transfer tactile input from an artificial hand to the forearm skin after a brief training period. Recently, Svensson, et al. [127] used it to translate the interaction between a virtual reality environment and a virtual hand into user sensation. The authors showed that by placing the tactile actuators in correspondence with the areas of the skin involved in object manipulation, subjects were able to feel a real touch sensation that increased their sense of body ownership. For example, pressure applied to the prosthetic fingers was perceived as a tactile sensation on the skin [127].

The **electrical feedback** is based on transcutaneous stimulation. The elicited sensations range from perception of pressure [134] to slip sensations [135], depending on the electrical parameters (i.e., current amplitude, pulse frequency, pulse width). One advantage of this approach with respect to the vibrotactile and mechanotactile ones is the lack of moving components avoiding problems of electrode displacement and, thus, improving the sensors-skin contact. Nevertheless, it is important to take into account that the noise introduced by the electric stimulation can corrupt the acquisition of muscular activity, causing errors if the ULP is myoelectrically controlled. Moreover, the perceptions are not strictly confined to the zone under the stimulating device but they can spread in a wider region if the area above a nerve is considered.

Another sensory modality exploited for feedback delivery is the acoustic one. Gigli, et al. [137] recently tested a novel acquisition protocol with additional **acoustic feedback** in 18 able-body participants to improve myoelectric control. The protocol consisted in dynamically acquiring EMG data in multiple arm positions while returning an acoustic signal to urge the participants to hover with the arm in specific regions of their peri-personal space. The results showed that the interaction between user and prosthesis during the data acquisition step was able to significantly improve myoelectric control. Auditory feedback has also been employed to convey artificial proprioceptive and exteroceptive information. Lundborg, et al. [143] and Gonzalez, et al. [144] employed auditory feedback by encoding the movement of different fingers into different sounds. The method demonstrated that the inclusion of auditory feedback reduces the mental effort and increase the human-machine interaction; furthermore, better temporal performance and better grasping performance were obtained.

In the last years, there have been some examples exploiting vision to deliver sensory feedback. Indeed, **visual stimulation** can be provided as explicit feedback through screens during game-like exercises, helping the prosthetic user to learn how to control the device (e.g., adjusting trajectory or grasping force) [145]. However, adding sensory information to the prosthetic user's perceptual experience in real contexts requires solutions like Augmented Reality (AR, occurring when computer-

generated items overlay a real setting) or Mixed Reality (MR, a term that represented different combinations of real and virtual items) [146, 147]. AR and MR environments, implemented through wearable solutions like head-mounted displays, can support the actual control of a prosthetic device through visual feedback that does not occlude the real context [138, 139, 141]. However, they can also be used for prosthetic use training [140, 148] – in such a case, Virtual Reality (VR, a fully computer-generated setting) can offer visual feedback too [149, 150], especially within game-based frameworks [151] for engaging the users and motivating their activity.

1.2.3.2. Invasive methods

There are different technologies that can be employed to provide a sensation directly to the nerve [88, 152]. The most used employ **intrafascicular electrodes**, such as **transverse intrafascicular multichannel electrodes** (TIME) and **wire** and **thin-film longitudinal intrafascicular electrodes** (LIFE), which can both record muscle activity (e.g., iEMG) and stimulate nerves. Other solutions are characterized by the fact that the electrodes are placed around the nerves, such as **cuff electrodes** and **flat interface nerve electrodes** (FINE).

The first example of ULP with sensory stimulation dates back to 1979 and it was based on the remapping between pressure signals acquired by prosthesis sensors to an amplitude-frequency modulation. This consisted of a series of pulses delivered with a pulse rate proportional to the increment of the pinch force and provided through dry electrodes placed over the skin in correspondence of the median nerve, as described in Shannon [153]. Later, the group of Micera employed thin-film intrafascicular electrodes longitudinally implanted in peripheral nerves (tf-LIFE4) to deliver electrical stimulation. With this method, they were able to elicit sensation of missing hand in the fascicular projection territories of the corresponding nerves and to modulate the sensation by varying the pulse width and pulse frequency [154]. Importantly, this method avoids muscle crosstalk, fundamental for guaranteeing myoelectric control. More recently, new bioinspired paradigms have been suggested to better induce natural sensations [88]. In particular, the study of Oddo, et al. [155] showed that it is possible to restore textural features recorded by an artificial fingertip. This device embedded a neuromorphic real-time mechano-neuro-transductor, which emulated the firing dynamics of SA1 cutaneous afferents. The emulated firing rate was converted into temporal pattern of electrical spikes that were delivered to the human median nerve via percutaneous microstimulation in one trans-radial amputee.

Valle, et al. [156] suggested a ‘hybrid’’ encoding strategy based on simultaneous biomimetic frequency and amplitude modulation. This kind of stimulation was perceived more natural with respect to classical stimulation protocol, enabling better performance in tasks requiring fine identification of the applied force. This paradigm was tested and validated during a virtual egg test [156], where the subject needed to modulate the force applied to move sensorized blocks. This encoding strategy not only

improves gross manual dexterity in functional task but also improved the prosthesis embodiment, reducing abnormal phantom limb perceptions.

Similarly, Osborn, et al. [120] implemented a neuromorphic feedback paradigm based on Izikevich neuron model to generate the current spike train to inject directly in the median and ulnar nerves, using beryllium copper (BeCu) probes. Their prosthesis proposes a neuromorphic multilayered artificial skin to perceive touch and pain. Their transcutaneous electrical nerve stimulation (TENS) allows to elicit innocuous and noxious tactile perceptions in the phantom hand. The multilayered electronic dermis (e-dermis) produces receptor-like spiking neural activity that allows to discriminate object curvature, including sharpness in a more natural sensation spanning a range of tactile stimuli for prosthetic hands. The authors were able not only to restore finger touch discrimination and objects recognition, but also to provide a pain sensation when the prosthesis touched sharp objects. In particular, they found that pain sensation is generated by a stimulation of 15-20Hz.

Tan, et al. [157] suggested that simple electronic cuff placed around nerves in the upper arm can directly activate the neural pathways responsible for hand sensations. This neural interface enabled the restoration of different sensations at many locations on the neuroprosthetic hand. Different stimulation patterns could transform the typical “tingling sensation” of electrical stimulation into multiple different natural sensations, enabling the amputees to perform fine motor tasks and improving the embodiment.

In George, et al. [158] a biomimetic method was described to restore both force and haptic sensation. The sensory feedback was implemented to restore the force sensation and promote objects recognition: Utah Slanted Electrode Array (USEA) electrodes were used to deliver stimulation proportional to the variation of contact force exchanged between the prosthesis and the object during manipulation. Instead, the haptic sensation was based on the distribution of stimulation delivered during contact with the object with a fixed frequency and amplitude. The characteristic of this encoding scheme is based on electrical biphasic, charge – balanced of 200- or 320-μs phase durations. The biomimetic model describes the instantaneous firing rate of the afferent population using the contact stimulus position, velocity, and acceleration simulating all tactile fibers to any spatiotemporal deformation of the skin and hand. This strategy allows the amputee to augment the active exploration experience and to discriminate object size and stiffness.

Liu, et al. [159] have shown that primary afferents encode different stimulus features in distinct yet overlapping ways: scanning speed and contact force are encoded primarily in firing rates, whereas texture is encoded in the spatial distribution of the activated fibers, and in precisely timed spiking sequences. When multiple aspects of tactile stimuli vary at the same time, these different neural codes allow for information to be multiplexed in the responses of single neuron and populations of neurons. Exploiting this sensory architecture with invasive methods may lead to the development of prosthetic devices able to truly evoke natural sensations.

Another promising approach is **targeted sensory reinnervation** (**TSR**), i.e. the sensory version of TMR, which consists in coupling a pressure sensor placed on the prosthetic device to surgically

redirected cutaneous sensory nerves [160]. This technique strongly helps discrimination of objects size and stiffness during active exploration, especially if the tactile feedback is biomimetic [158]. Recently, Marasco, et al. [161] have developed a prosthetic system based on both targeted sensory and motor reinnervation. TSR was used to deliver both touch and kinesthetic feedback. The authors showed that the system was able to significantly improve device control and promote embodiment.

These results indicate that, in order to close the loop on user and provide useful sensation (regardless the specific feedback modality), an optimal feedback control policy is necessary [5], as discussed in section 4.4 of Marinelli, et al. [6].

1.3. Prosthetic Control Strategies and Algorithms

Although the focus of this section is on the active prosthesis, it is worth mentioning that an important portion of the amputees still uses body-powered prosthesis [162]. These are cable-operated devices usually equipped with split hook or hand as terminal part [163].

Ranging from standard control approaches (e.g., dual-site control [164]) to simultaneous control of multiple degrees of freedom (e.g., pattern recognition [165]), the literature offers disparate solutions for ULP control depending on the type of input signal and the sensors density.

In general, prosthetic control is performed at different levels. The low level refers to **motor actuation** (Figure 7 D) and, more in general, to the control of the active degrees of freedom of the device; the medium level consists of the translation of **movement intentions** into joint references and gestures (Figure 7 C); the high-level control translates **input signals** collected from the user (Figure 7 A) into movement intentions (Figure 7 C, yellow panel – *layer 1*). In the next sections, we describe these different levels of control and provide examples of the different strategies that can be used.

1.3.1. Low-level control: from control commands to motor actuation

The low-level control combines the well-known strategies implemented in the automation industry to operate autonomous machines, e.g., industrial robots. We will not detail the structure and mathematical formality of these control architectures. However, if the readers are curious, a more complete and detailed analysis of robot lower-level control is provided by the comprehensive work of Siciliano, et al. [166].

In brief, at the base of these controls, there is always an active and controllable actuator, that for upper limb prosthetic solutions coincides – most of the times – with an electrical motor (either brushed or brushless) often coupled to a dedicated transmission system (e.g., a planetary gear) to reach the desired torque-speed characteristic. It is possible to present the low-level control of upper limb prostheses as the combination of three possible nested controllers: the **current**, the **speed** and the **position** control loops (Figure 7 D).

The *current control loop* takes care of reliably tracking desired current trajectories. To be implemented, it requires the presence of reliable and precise current measurement sensors. The current

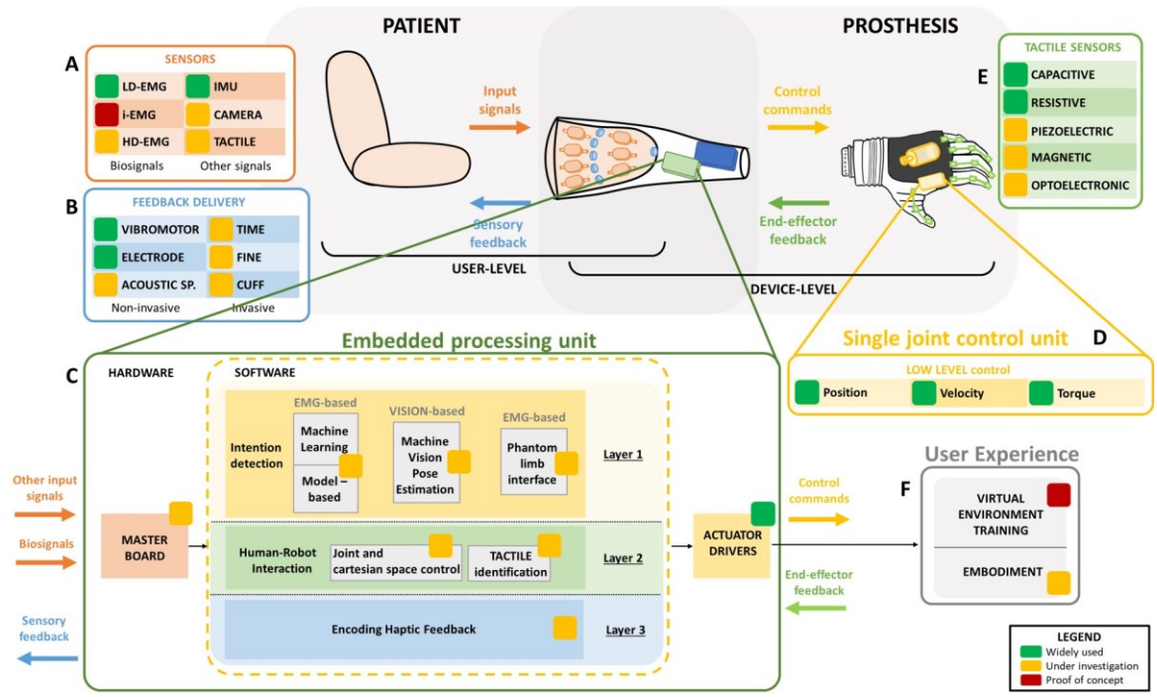

Figure 7 Architecture of ULP control:
actuation and feedback. Input signals collected from the user (A) are processed into the embedded processing unit (C) to generate control commands for the single joint control unit (D). Feedback information coming from the prosthesis or its interaction with the environment (E) are also processed in the embedded processing unit (C) to deliver sensory feedback (B). The embedded processing unit (C) can be set up by different layers: layer 1 (intention detection, yellow panel) is the software turning the input signals (A) sampled by master board into detected movement intentions, by means of specific control algorithms (e.g., machine learning or deep learning algorithms); layer 2 (human-robot interaction, green panel) is the software responsible of processing prosthesis position (joint and cartesian space control) and external information (tactile identification, E); layer 3 (encoding haptic feedback, blue panel) is the software responsible for encoding the information processed in layer 2 into sensory feedback. The output of the embedded processing unit are control commands (mediated by actuator drivers) both to move the device and to provide sensory feedback. This has a direct impact on the user experience (F) in terms of learning how to use the device (training) and of user-prosthesis integration (embodiment).

control also provides a relatively good force/torque control of the system, being the current absorbed by the actuator directly proportional to the generated output torque. On top of the current controller, it is usually found a *speed control loop* to regulate the rotational speed of the motor and, thus, the speed of the actuated system. The combination of an external speed controller with an internal current control guarantees the possibility of safely operate the actuating unit in terms of desired speeds and torques. Sometimes, on top or in substitution to the speed controller, systems also implement a *position control loop*. The position controller guarantees the tracking of desired angular trajectories. It is therefore preferable to use the speed controller if the goal is to precisely track given trajectories in specific time intervals. The implementation and application of speed and position controllers can be performed either before (fast shaft) or after (slow shaft) of the transmission system. The decision depends on the availability of sensing devices (e.g., angular sensors such as encoders or resolvers) to measure the required physical quantities.

All these controllers are implemented in a negative feedback architecture and typically controlled by means of **PID** controllers, whose *proportional* (P), *integrative* (I) and *derivative* (D) parameters are tuned to reach the desired system response in terms of control reactivity (rise time and settling time), precision (steady-state error and overshoot) and stability. It is worth mentioning that a negative feedback

architecture is typically only bounded to the low-level control of the prosthesis, while higher level controllers and especially high-level control (see Section 4.3) are often treated in an open-loop fashion, where the user directly generates the reference control signal without any feedback verification. The generated reference commands will then be directly sent to the low-level controller.

1.3.2. Mid-level control: from movement intention to control commands

The mid-level techniques (Figure 7 C, yellow panel – *layer 1*) aim to synthetize the **control commands** to suitably activate the electric motors of the multiple DoFs ULP (actuation drivers in Figure 7 C). These signals are the input of the aforementioned low-level control.

A major classification of the mid-level control strategies for multi-DoFs robots divides them in two categories: joint-space and task-space (Cartesian) controllers [167, 168].

Joint-space control strategies directly feed the commands to each of the actuated joints, namely DoFs, of the upper-limb robotic device. It is a direct approach that does not require any particular mathematical manipulation. In such a scenario, the mid-level control receives information from the high-level (see Section 4.3), then it assigns specific commands to each low-level controller (see Section 4.1). The logic used to assign the control commands is strongly based on the kind of information coming from the high-level side. Nonetheless, it will most likely reduce to a set of independent commands for each of the actuated joints.

On the other side of the spectrum, we have **task-space based control strategies**. In this case, the control commands for each of the joints are the results of a mathematical manipulation that involves the transformation from the *Cartesian space* to the *joint space*. If the aim is to regulate the Cartesian trajectory, the controller will need to translate the Cartesian trajectories into joint angles, by means of a process known as inverse kinematics. If instead the aim is to regulate the Cartesian force, the controller will transform the Cartesian forces into joint forces (or torques) utilizing the process of inverse dynamics.

Both these approaches are well known to robotic applications and will not be treated in detail in this review. Nonetheless, the authors suggest the comprehensive works of Corke and Khatib [168] and Siciliano, et al. [167] to get the fundamentals of the aforementioned approaches.

In general, Cartesian based controls are more intuitive for the external user, namely any subject interacting with the robot as an external tool. In fact, the robot behavior can be more naturally interpreted being the forces or the trajectories referred to the three-dimensional space we are used to deal with. However, from a computational and complexity point of view, task-space controllers require a bigger effort and introduce limitations to their application, e.g., singularities, redundancies. On the other hand, joint space control behavior is less intuitive to predict but it is easier and less complex to implement.

Which approach is better for upper-limb prosthetic devices is still unclear. However, it is important to notice that, even if Cartesian controls are more intuitive from an external perspective, they might

appear more complex from an internal perspective, such as the one of a prosthesis user, where the motion of the arm is more likely imagined in terms of joint motions and not Cartesian ones.

1.3.3. High-level control: from input signals to movement intentions

This section summarizes the most assessed techniques for ULP control. Considering the prostheses available on the market but also the research activities, the main input source exploited to control such devices is the EMG. On the basis of the EMG type multiple control strategies can be employed, and the last decades of studies on active prostheses mainly focused on the control strategy design and development.

The most common control strategy is based on **dual site control** which consist in two electrodes placed in two antagonist muscles [164]. This solution allows the control of the motor in two directions according to the muscle amplitude of the selected electrodes. The synthetized reference usually is proportional to the amplitude of the muscle signal in term of speed or force. With the introduction of multiple DoFs, a **co-contraction strategy** has been implemented to switch between controlled joints [169]. This allows the control of a single DoF at a time using two electrodes as in dual-site control. When both muscles are simultaneously contracted the control signal switches the joint to be controlled. This is a simple solution yet unnatural and lacking intuitiveness.

Another diffused strategy to control prosthesis with multiple active DoF is the **finite state machine** (FSM) [170]. Commercially available ULPs implement this strategy to switch the position of the thumb to reproduce different types of grasp [24-26]. For example, the Michelangelo hand allows to switch the thumb position when a signal of opening is triggered with the hand in a fully opened configuration [24].

With the aim of increasing the number of controlled DoFs, many different methods were proposed, such as **muscle synergies**, **feature extraction** (WFE), **multi-amplitude threshold control** and **machine learning methods**. Muscle synergies capture muscle activation invariance during motor production and can be exploited as control variables for ULP, with aim of obtaining a biomimetic human-like behavior [171]. The main idea is to extract motion primitives from muscle synergies and combine them to generate complex arm movements [172, 173]. Furui, et al. [174] propose a biomimetic control based on muscle synergies to extract motion primitives and combine them to generate complex movements. Feature extraction methods foresee the computation of some EMG-based metrics that reflect movement intentions [175]. Multi-amplitude threshold methods work as dual-site control, but they associate different amplitudes of the input signal to different DoFs [131]. Although robust, these techniques are poorly used because they lack intuitiveness [131].

1.3.3.1. Machine Learning Algorithms

Figure 8 illustrates the main machine learning methods employed for ULP control These methods generally solve a pattern recognition problem in which, given the input signal, an output movement have to be identified.

The first PR-based control schemes arose around the second half of 1960s [176]. In this configuration, the acquired EMG signals are elaborated by the controller to determine the action to be performed by the prosthesis. The five pillars of this computation process are: *pre-processing, data segmentation, feature extraction, classification,* and *post-processing*. Each step is briefly described in Table 3.

Table 3: Pattern recognition steps.

Pre-processing	During this phase, the incoming signals are firstly filtered to delete the interferences, such as acquisition noise and artifacts.
Data segmentation	This process divides the signals into time-windows, overlapping or adjacent [177].
Features extraction	It reduces the signal information into a set of representative features in time domain (e.g., variance, zero crossing, etc.), frequency domain (e.g., mean frequency, spectral properties, etc.) or time-frequency domain (e.g., the wavelength transform, an alternative to the traditional Fourier Transform useful for noise-removal and data compression [178]), as described in Boostani and Moradi [179]. Importantly, this part can greatly affect the computational costs.
Classification	This is the crucial step for the classifier, where the controllers recognize and classify the signals input information and generate an output for the actuators.
Post-processing	It has the main goal to reduce as much as possible the misclassification. An example is the majority vote strategy, in which the current output is calculated on the previously most recognized class. The majority vote scheme is used for eliminating spurious misclassifications caused by too short windows on which the most recurrent class is selected; it employs the previous classification results and evaluates the current output on the basis of the previously most recognized class [180].

EMG-based pattern recognition controllers are now investigated by many groups and are even available in commercial prostheses [76, 78, 181].

The PR-based controllers apply linear and non-linear methods to classify the EMG signal into a possible large number of movements. The two main families of classification methods used in this context are **regression** [182] and **classification** techniques [71]. While the former is usually simple to implement and train, the latter are generally more difficult to employ. The embedding of **neural networks** (NN) in an ULP strictly depends on the structure of the algorithm (number of layers and neurons), since complex architecture requires high computational effort [183].

Statistical regression models usually produce good results in terms of high accuracy percentages. However, the out-of-laboratory results are particularly poor, because these techniques are extremely sensitive to changes of the input signals [177]. Motivated by this issue, in the last decade, many groups focused on classification-based techniques to implement more reliable decoders. Importantly, training classifiers requires longer than training linear models, however, the formers can achieve better results during real-time execution. Different classifiers have been exploited in ULP control such as Support Vector Machine, Regularized Least Squares, whereas the gold-standard is the Linear Discriminant Analysis [12, 176, 184]. Among NN, the most common architecture is the **Multi-Layer Perceptron** (MLP) [185, 186]. The MLP is a supervised ML technique, which exploits labeled data to train the

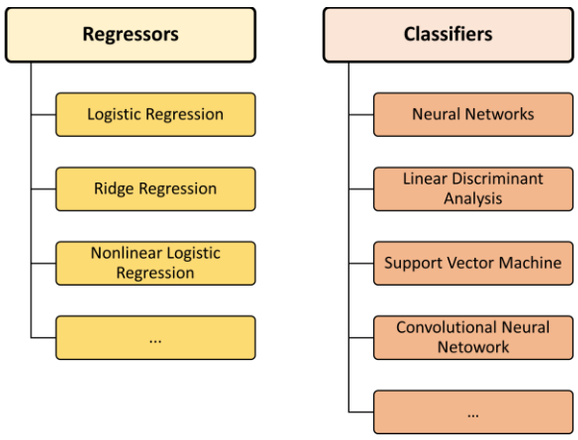

Figure 8: Division of machine learning approaches for ULP control.

algorithm. It is characterized by three types of layers: input, hidden and output layer. The first one contains the same number of neurons as the input signals (for example, features extracted from EMG signals), the second stage can have one or more layers where there are all the trainable neurons, while the last layer comprises all the output nodes representing the results (for example, classification likelihood of each class of movement). Neurons of a certain layer are fully connected to the neurons in the next layer via nonlinear activation functions. However, as for the regression algorithms, the performance results obtained in the lab are not easily replicated in the real-life scenario. Moreover, the complexity of the controlled prosthesis (e.g., the number of DoFs) corresponds to a higher number of neurons in the NN, with important consequence not only on the computational burden, but also on the memory consumption.

When considering an increase in the number of controllable DoFs, current pattern recognition approaches demonstrated poor performance [187]. As a matter of fact, to enhance the classification rate (i.e., number of correctly recognized movement) a greater content of information should be handled. The higher the amount of input data, the more complex would the ML algorithm be.

Therefore, HD-sEMG can be exploited to increase the amount of muscular information but this comes at the cost of higher computational burden. It has been proven that the use of this type of data can be helpful in increasing the robustness against electrode shift [188], allowing an improvement of the classification by exploiting spatial images of the muscular contractions [189], and for retrieving measures of motor unit potentials, which can be difficult to assess without invasive techniques [190].

Different techniques can be exploited to extract motor units' activity from the HD-sEMGs. The main used decomposition algorithm is the **blind source separation** (with the Convolution Kernel Compensation described by Holobar and Zazula [191]) which seems to be the most suitable since it does not make any prior assumptions on the action potential shapes. The main problems related to this technique is the lack of a useful output for the prosthesis control, since the decomposition provides an extraction of principal features of the EMG signals. On the one hand, the algorithm returns reliable information about neural activity, but, on the other hand, it increases the computational burden required to the system. Indeed, the Holobar algorithm has been used together with ML algorithms to control robotic arm in real-time [192].

Another approach includes the exploitation of ML algorithms where the input EMG signals are considered as numeric values and the definition of the output is based on a **Black Box technique**. Therefore, the mathematical tools contained in the Black Box do not take into account the biomechanics of the amputated limb and they are not specific for prosthetic applications.

It is relevant to feed the ML algorithm via a set of EMG signals (muscular patterns) specific for different prosthesis movements in such a way that the classifier does not misclassify. However, it is not always feasible to acquire the same signals for each movement due to different sources of errors (i.e., muscle fatigue, sweating, electrode misalignment). Indeed, more complex classifiers belonging to the **Deep Learning** (DL) field are exploited to make the control more robust. A possible application can be the use of **Convolutional Neural Network** (CNN), which exploits dimensionality reduction to extract complex features from the activation maps of the HD-sEMG without dramatically increasing the computation time [193]. This type of algorithm is also ideal for increasing the number of DoFs (and therefore the number of classes to be recognized) while keeping a quite high accuracy rate [178]. Moreover, Zhai, et al. [194] has proved that the exploitation of CNN can help in removing issues of daily life noise, updating its feature map to include this new information, avoiding the need of periodical readjustment.

Adaptive technique based on **reinforcement learning** [195, 196] has been recently investigated, with the aim of facilitating the learning process of prosthetic use. This approach is promising as it points towards the development of a "human–prosthesis symbiosis in which human motor control and intelligent prosthesis control function as one system", as defined by the group of Huang, et al. [197].

Other DL algorithms take into account time series with feedback loops with prior hidden layers [142]. This architecture allows storing the history of the input signals by considering the information of previous time instants, also resulting in performance improvements with respect to simpler DL architectures [198].

Recently, novel DL strategies have also been proposed for ULP: **Recurrent Neural Networks** process temporal or sequential information; **Temporal Convolutional Networks** take advantage of a one-dimensional convolution layer running along the time dimension to learn the time dependence of a given input signal [199]; **Transformers** are attention-based architectures applied to HD-sEMG data [200, 201].

Overall, the main problem related to ML applied to the bionic field is the evident gap between the results observed in a closed safe environment, such as a laboratory, and in real daily life [202].

1.3.3.2. Model-based approaches

To overcome the limitations of ML algorithms for ULP control, some groups investigated the model-based approach, which consists of an accurate description of the muscles and bones involved in the movements starting from the **Hill model** of muscle fiber [79]. For example, the **neuromusculoskeletal model** extracts from the residual EMGs the activation dynamics of the limb [203, 204]. The activation

dynamics combined with the kinematics of the limb produces the contraction dynamics. This consists of the modification of fiber length involved in the motion along the specific DoFs. In particular, Sartori, et al. [80] implemented a control strategy based on the physiology and kinematics of a real hand and tested it with an amputated subject performing some complex grasping tasks. This approach needs a calibration step to scale the model to the subject specific activation EMGs. Results showed great stability over the noise introduced by sensors or movements artifacts. Moreover, the amputee was able to reproduce simultaneous multi-DoF gestures. The limitation of this approach is its susceptibility to electrode shift and fatigue condition that affects the EMG acquisition. The real-life scenario is yet to be tested, but preliminary results appear very promising [80].

1.3.3.3. Sensor/Data-fusion and other techniques

For ULP control using different input sources together with or without EMG signals, other methods can be adopted. In case of force myography, the same algorithms used for EMG input can be applied. For example, machine learning techniques can be used to analyze and synthetize output starting from FMG input [205]. The adoption of other input signals different from EMG clearly requires the implementation of ad-hoc methods for their processing. For example, voice control introduces audio analysis method to detect and translate command into prosthetic movements [206, 207]. Further, tongue control allows the motion of the prosthesis using a wireless controller resembling a dental retainer and providing the functionality of a wireless joystick or keyboard [208].

The high complexity of ULP control has led to the development of sensor fusion approaches, in which input signals of different nature are simultaneously collected and then processed to estimate the intended movement more reliably and accurately.

On low-density sEMG, we can find robust and semi-autonomous control solutions based on custom multi-amplitude algorithms, as those implemented on the Michelangelo hand with Closed-Loop Multi Amplitude Control (CMAC) [131, 209]. The adoption of IMU sensors may lead to further improvements, such as the automatic adaptation to unexpected external factors, including sweat, muscle fatigue, mental stress, electrode re-positioning and weather conditions. The state-of-the-art algorithms have to cope with these challenging issues. Therefore, the combination of EMG and IMU as input to a classifier could provide useful localization information of the hand position, which could delete possible false positives, actively improving the obtained accuracy [210, 211]. Moreover, it has been observed that integrating EMG, IMU and artificial vision sensors could benefit both the classifier accuracy and the increment of available DoFs [209]. Other promising research advancements demonstrated that mixing EMG with FMG could lead to an improved multi-DoFs control as proposed by [212]. Similarly, Jiang, et al. [213] proposed a sensor fusion approach among EMG and FMG. Moreover, by fusing FMG and IMU, other interesting results were presented by [214]. In addition, other research activities treated NIRS fused with EMG [215] and IMU respectively [216].

In conclusion, a data fusion aims at compensating some of the main limiting factors of single input approaches (such as EMG-based or others) as these latter suffer from artifacts, electrodes shift, etc.

1.3.4. Control strategies for the Sensory Feedback and Closed-Loop approaches

Recent developments in the prosthetic field have focused attention on sensory feedback restoration. In particular, many groups began studying how to provide the user with information about the interaction between the prosthetic system and the physical world. This information needs to be collected (Figure 7 E), processed (Figure 7 C, green panel – *layer 2*) and encoded into control signals (Figure 7 C, blue panel – *layer 3*) for the feedback system (Figure 7 B, e.g., vibromotors, electrostimulation, etc.).

The control strategy implemented to encode this information depends on the type of sensation to restore as, for instance, tactile feedback (pressure, temperature, pain) or proprioception feedback (gestures, joint movements). o this aim, different solutions have been developed.

Mamidanna, et al. [217] focused their research activity on the force feedback that the prosthesis applies to the grasped objects by using vibromotors attached to the forearm skin. To do that, an encoding scheme of the current absorbed by the prosthetic motor was translated into vibromotors amplitude. Other sensorized solutions have been developed to directly translate the prosthesis interaction to user sensation like artificial skin able to translate the distribution of pressure and intensity to tactile and pain sensations on users with invasive interfaces [218]. Similarly, Markovic, et al. [131] implemented a proprioceptive feedback translating prosthesis movements into vibration orientation and shape to be intuitively interpreted by users.

In addition to prosthetic feedback, some groups are working on user feedback in terms of providing information about how the prosthesis is controlled by means of closed-loop approaches. For example, Schweisfurth, et al. [219] have tested on amputees a ULP system in which EMG input used to drive the prosthesis was translated into intensity of vibromotors activation. In this configuration, the amount of EMG activity detected is directly proportional to prosthesis grasping strength and to intensity of vibration amplitude. In another work, the control commands generated by the user and translated into joint angles were encoded as proprioceptive information delivered through electrical stimulation [136]. This allowed user to understand if the intended control command was correctly detected by the algorithms.

Similarly, Tecnalia developed a ULP system with sensory feedback by merging into a unique device EMG acquisition and electrical stimulation [220]. Although this solution significantly reduced the problem of encumbrance, it still faces some issues mainly related to the artifacts that the stimulation produces on the EMG signal and that cannot be removed using standard signal processing algorithms [221].

As for decoding of movement intention from input signals, the interpretation of feedback information needs a calibration procedure aimed at familiarizing the user with the ULP device. In this context, it is

fundamental to guide the user to: (i) produce the correct input signal to perform the desired movement, and (ii) to intuitively convert the feedback signal into useful information for motor planning.

Materials, Methods, and Results

Chapter 2. Beyond current prosthetic design

In the pursuit of improving the acceptance and usability of upper limb prostheses (ULPs), various approaches have been explored. A comprehensive review by Cordella, et al. [1] provided valuable guidelines, drawing insights from user requirements and case studies such as Luchetti, et al. [222]. These requirements encompassed important aspects such as the ability to perform daily activities with minimal visual attention, precise dexterity, and appropriate strength control. Furthermore, biomimetic sensory feedback and anthropomorphic features were identified as essential, alongside considerations of device duration, reliability, and technical aspects affecting comfort, such as heat dissipation and motor noise reduction [6].

To bridge the gap between laboratory research and real-life applications, it is vital to involve clinicians, researchers, and amputees themselves in co-creation frameworks and effective user research methodologies [223]. Surveys, workshops, and initiatives like the Cybathlon competitions have been instrumental in gathering insights from all stakeholders, ensuring that the issues faced by prosthetic users are accurately represented and addressed [224]. User-centered evaluation methodologies and metrics need to be tailored specifically for ULPs, considering their biomimetic behavior, feedback, and hand-like manipulation tasks [202, 225]. Such aspects were studied in the first work of this chapter (see paragraph 2.1):

- Caserta, et al. “Benefits of the Cybathlon 2020 Training for a Prosthetic Hand User: a case study on the Hannes system.” Journal of NeuroEngineering and Rehabilitation, 2022. [17]

Designing ULPs must also take into account individual preferences, which can be influenced by demographic factors, level and type of amputation, pain symptoms, and the type of prosthesis employed [226-231]. Understanding amputees' preferences is crucial not only for designing the physical interface but also for developing virtual and augmented environments for prosthetic training [232]. Engaging exercises in the form of game-like activities have proven effective in motivating users to train and provide consistent biosignals, essential for machine learning-based control systems [233]. Additionally, training programs should focus on playfully engaging users to strengthen their muscles and accurately replicate real-world prosthetic tasks, facilitating skill transfer [234]. For these reasons we studied approaches to promote such aspects in the second work of this chapter (see paragraph 2.2):

- Barresi, et al. “Exploring the Embodiment of a Virtual Hand in a Spatially Augmented Respiratory Biofeedback Setting.” Frontiers in Neurorobotics, 2021. [18]

One effective strategy for promoting positive interaction between users and ULPs is to design prostheses that closely resemble the functionality of a real hand. This approach aims to facilitate a sense of ownership and embodiment, where users perceive the artificial limb as an integral part of their body scheme [235]. The embodiment phenomenon, encompassing self-location, ownership, and agency, enhances movement control, object discrimination, manual accuracy, and sensitivity. Furthermore, it

contributes to reducing phantom-limb pain and the risk of prosthesis abandonment [236-238]. Evaluating and stimulating prosthetic embodiment is often done using methods based on the Rubber Hand Illusion (RHI) studies, involving questionnaires, biosignal analysis, and proprioceptive drift measurements [239-242].

Enhancing the embodiment of artificial limbs requires a nuanced understanding of the underlying processes. Factors such as daily prosthetic practice, individual characteristics, and multisensory feedback congruency play crucial roles in this regard. Importantly, embodiment training strategies can be explored in virtual and augmented settings, although further investigation is needed to generalize the effects to real prosthetic devices [18]. By establishing optimal techniques to promote embodiment, users can be fully engaged in exploring the potential of their prosthetic devices, creating a virtuous circle of improved acceptance and usability.

However, achieving a truly "biomimetic" experience in prosthetic embodiment presents technological challenges that must be addressed. This includes developing advanced control patterns and considering cosmetic improvements to enhance the overall user experience and acceptance of artificial limbs. In that direction we developed multi-DoF prostheses able to replicate human motions as described in the third work of this chapter (see paragraph 2.3):

- Boccardo, et al. “Improvements to an under-actuated Prosthetic Hand toward a dexterous 2-DoF Wrist” Mechatronics, 2023. (submitted)

2.1. Benefits of the Cybathlon 2020 Training for a Prosthetic Hand User: a case study on the Hannes system

2.1.1. Background

Losing a limb has devastating different consequences: the amputee is no longer able to perform his usual activities of daily living (ADLs), he is not completely autonomous and independent, and this results in a dramatic decrease of the quality of life [243]. The loss of an upper limb irreversibly alters the look and affective interactions of the amputee, causing severe repercussion such as social rejection, self-pity and low self-esteem. In addition, also the biomechanics of the body changes, trying to compensate the missing limb. This leads to the excessive use of the rest of the body or to incorrect body postures, which in turn produce extreme fatigue [244].

Typically, the main strategy for compensating a hand loss is using an artificial upper limb, a prosthesis. A prosthesis is, therefore, an assistive device which should become an essential element of the amputee's daily life. Current prosthetic options range in both cosmetics and functionality, to satisfy a variety of user needs and lifestyles. The most advanced prostheses currently available are the so called "Myoelectric prostheses". These devices use electromyographic (EMG) signals, generated from the contraction of the stump's residual muscles, for the activation of the functional elements. However, even though they offer an increased functionality compared to the simpler options such as cosmetic or body-powered, there are still problems related to weight, cost, maintenance, reliability, and complexity of control [162].

Due to all these limitations, the device abandonment rate is still high, and a large part of the amputees' population even prefers not to use any prosthesis at all during their daily life [226]. Decades of research and development (R&D) on bionic limbs suggest that the design of prosthetic hands requires accurate investigations about users' needs, paying attention at improving user experience. Indeed, this may increase the technology acceptance of the prostheses. UX depends on many factors such as the control approach used to control the prosthesis [245], interactive training methods [246], embodiment stimulation [18], and biomimetic design strategies [247]. Furthermore, the development of a prosthesis capable to induce the embodiment and to be felt as a valid and natural substitution of the missing limb by the amputee, rather than a simple tool, is an important target as well.

However, the detachment between the communities of users, researchers, developers, and all stakeholders can become an obstacle for fertile improvements in prosthetic user experience. Thus, novel strategies for gathering these communities [223] around the same scope, possibly also promoting a proper representation of the user's issues and needs, could be advantageous.

The Cybathlon competition for assistive technology have been conceived to reach such a result, reducing the gap discussed above [224]. This unique world championship proposes six different disciplines in which people with physical disabilities compete against each other with both commercial

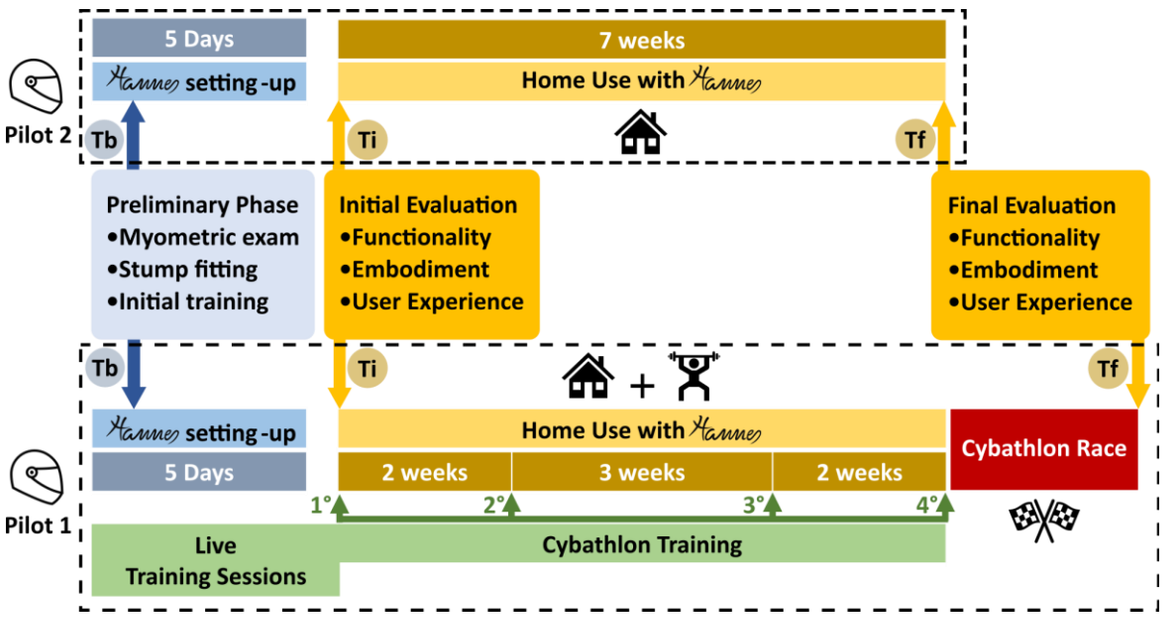

Figure 9 Scheme of planned activities:
both pilots underwent the same Preliminary Phase (Tb) of five days for the setting up of the Hannes prosthesis and then started their seven weeks of Home Use with Hannes. At the beginning of this period, they participated to the Initial Evaluation (Ti) for the investigation of functionality, embodiment and UX with Hannes. Pilot 2 repeated the same tests and questionnaires at the end of the seven weeks in the Final Evaluation (Tf). Pilot 1 participated to the same Final Evaluation right after the Cybathlon Race, performed at the end of the same Home Use period, during which he also followed four Live Training Sessions.

devices and research prototypes. Within this context, the Powered Arm Prosthesis Race is dedicated to people with transradial or more proximal arm amputation, or dysmelia, and equipped with arm prosthesis. Preparing for such a competition requires a careful attention to realistic tasks, increasing the ecological validity of the user performance assessed during the competition – potentially as in technology benchmarking [248]. On the other hand, training a prosthetic user for a Cybathlon challenge means for R&D teams the opportunity of exploit these tasks to explore novel solutions that will be extensively tested according to clinical protocols.

This paper presents the Cybathlon 2020 experience of our participating Pilot 1 with the novel prosthetic system Hannes. Furthermore, to verify if the Cybathlon-based training and related competition had a positive and substantial influence on the relationship between Pilot 1 and Hannes, we administered to both him and a non-runner Hannes user the same evaluation on functionality, embodiment and user experience with tests and questionnaires unrelated to Cybathlon.

2.1.2. Methods

Two male right transradial amputees and myoelectric prosthetic users were recruited as pilots in February 2020 to form the REHAB TECH team. The first, aged 32, has a 5-years' experience in myoelectric control with a Bebionic polyarticulated prosthesis by Ottobock, and was chosen as first pilot (Pilot 1). The second participant, age 34, is a user of a tridigital Myohand Varipuls Speed by Ottobock since 2010, and was selected as second pilot (Pilot 2). Both subjects were given the Hannes prosthetic hand and had the chance to keep it for seven weeks for Home Use. They underwent a Preliminary Phase

(Tb) with a prosthesis fitting process of five days, comprising a myometric exam for the residual muscles functional state evaluation and EMG sensors positioning, stump fitting, and preliminary training, including familiarization with the Hannes prosthesis. Due to the movement restrictions caused by the COVID-19 pandemic that hit Italy and the entire world and official institutional restrictions, we were forced to train solely Pilot 1 for the Cybathlon competition. However, we decided to still let Pilot 2 use Hannes prosthesis for the predetermined Home Use period. Given his participation, for an ease of understanding, we chose to keep referring to him as Pilot 2, even if he was completely unfamiliar with Cybathlon training, competition, tasks and anything related to it. The Cybathlon Training with Pilot 1 consisted of only four Live Training Sessions of two days each, executed during the seven weeks of Home Use. The training started at the end of September 2020, and it was completed the day before the competition, which took place on the 12th of November. This poor preparation was due to the distance of the pilot's residence from the training location, i.e. the Rehab Technologies Laboratory of Istituto Italiano di Tecnologia (IIT). Functionality, Embodiment and User Experience evaluation with Hannes was carried out for both pilots at the end of the Preliminary Phase and before the Home Use period in the Initial Evaluation (Ti). The same methods were repeated in the Final Evaluation (Tf) by Pilot 2 after the Home Use, and by Pilot 1 after the Cybathlon Race, occurred immediately after the same Home Use period (Figure 9). The evaluation was carried out with tests and questionnaires unrelated to Cybathlon race, on which both pilots were not specifically trained. During the Home Use, the pilots were encouraged to use the Hannes prosthesis in all possible activities, including work, domestic and recreational contexts, as if it was their sound hand.

2.1.2.1. The Hannes prosthetic system

The Hannes hand prosthesis is a poly-articulated myoelectric prosthetic hand. The major improvements provided by this device are the naturalness of forms, movements and orientation of the rotation axes and hand posture. Indeed, the prosthetic design was developed focusing on the anthropometry of the real human hand, both from an aesthetic and biomechanical point of view, allowing the user to perceive the device as an integral part of the body rather than a simple external tool.

The Hannes system contains four main components: an electric actuator (DC motor), two custom-made control boards (Motor control board and EMG processing board), two EMG sensors implementing a proportional dual-site control and a tendon-driven, underactuated transmission mechanism (Figure 10). The embedded differential system is capable to properly offer the patient a harmonious, quick, and precise grasping behaviour. The passive Flexion/Extension flexible wrist, separately placed at the base of the prosthetic hand to guarantee system modularity, can be fixed in five different positions (two for flexion, two for extension and one for neutral position) or left free. In addition, the wrist module offers several discrete positions in Pronation/Supination with a 360° mechanical and electrical slip ring connection. Finally, a passive thumb can be locked in three positions to allow the main grasp types:

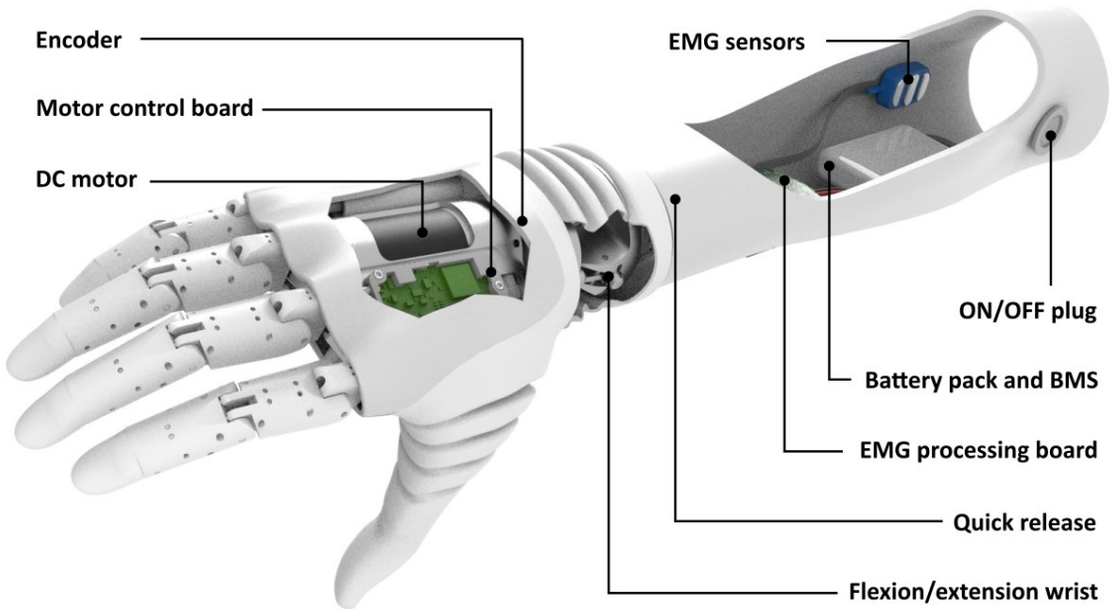

Figure 10 The Hannes Prosthetic System.

lateral, power and pinch. All these features were implemented to develop Hannes as a prosthetic system uniquely similar to the real human hand, as it is detailed in reference [247].

2.1.2.2. Cybathlon experience

2.1.2.2.1. Protocol

The Powered Arm Prosthesis Race included six consecutive tasks inspired by daily life activities, to accomplish in the minor possible time and to finish within eight minutes. Some tasks required the use of both hands and arms, simulating bimanual interactions, whereas others forced the pilot to exploit only his prosthesis. In this case, the object, or the part of it colored in blue, could exclusively be manipulated by the device. Two tasks ('Clean Sweep' and 'Home Improvement') were slightly modified, and one completely changed ('Wire Loop' into 'Stacking') after the subscription to the competition, in accordance with the new Global Edition format [249], which was designed to overcome limitations given by the pandemic crisis.

The racetrack was composed of:

1. *Breakfast task – 14 points*

   Preparing a meal using kitchen tools is a fundamental activity for an autonomous living. In this task, a breakfast table must be set up by cutting bread, opening a bottle, a jam jar and a can, unwrapping a pack of sugar cube, and lighting a candle with a matchstick.

2. *Laundry task – 15 points*

   This task challenged the practicality of the prosthesis during the wearing of standard clothes and its ability with fine activities such as tying shoes, closing and opening a zip, hanging a t-shirt with clothespins, and closing two blazer's buttons.

3. *Clean Sweep task – 16 points*

   This task required the ability to handle and grasp objects with different size, weight, texture and shape, which can be easily found in daily life. Eight blue objects (a pen, a plastic glass filled with balls, a USB pen, a ball, a key with a ring, a coffee mug filled with balls, a credit card, and a DVD case) must individually be moved from a table to another one, also testing the prosthetic user's capability to maintain the grasp and the grip force during big movements. Originally, all these objects were supposed to be located in a dedicated wooden support.

4. *Home Improvement task – 17 points*

   Being able to accomplish manual duties during maintenance work at home is again important for the independent living of an amputee with his prosthesis. Indeed, in this task the pilot must cut a paper with scissors, drive in a nail, and insert a light bulb in a lamp.
   In the last version, stair climbing and descending with hammer and scissors in a toolbox was removed.

5. *Haptic Box task – 20 points*

   The sensory feedback implemented in a prosthetic system could improve control, acceptance, and embodiment of the prosthesis. By relying only on this feedback from the prosthesis, for example with vibrations at the socket, sounds or haptic feedback, the pilot should be able to recognize and match six different objects in shape and texture, hidden from the view and inserted in wooden boxes.

6. *Stacking task – 18 points*

   To test the ability in the maintenance of a solid grasp during big postural movements of the arm and the body, in this task the pilot must flip ten blue cups and stack them into a vertical pyramid. This task substituted the old 'Wire Loop' one, where pilots were supposed to hold a conductive wire loop with a blue handle in a curved metal wire without touching it.

Each team had three attempts for the race. The total score was calculated as the sum of the successful tasks, and the best attempt was considered for the final ranking. In case of equal scorings between two or more teams, the ranking was established using the total completion time, which included only successful tasks. In Figure 11 our Pilot 1 performing some previously mentioned tasks during the official competition.

2.1.2.2.2. Training

The REHAB TECH Pilot 1's training consisted in the repetition of each task multiple consecutive times to become familiar with the proposed activities. The most difficult tasks and specific exercises were identified, and a particular attention was given to them. During the trainings and the Home Use, Pilot 1, together with the help of the team, focused on overcoming these difficulties, searching for the right strategy to successfully complete the tasks.

In the first training session each task setup was prepared one by one, and Pilot 1 repeated each task until it was accomplished. Accordingly, we collected the time of the best performance of each successful task, and during the data processing we summed these times to recreate a complete race. For this reason, this first simulated race, highlighted with a black squared box in Figure 12, does not contain any failure. Afterwards, three other simulated races were performed at the end of each successive training session, following official rules of the competition, with the six tasks performed in a row on the racetrack. We then examined all these simulated races and the official one, reporting the time of completion of each single task, to investigate the evolution of the performances achieved during the training.

Throughout the training period we additionally collected notes and considerations about the pilot's strategies, its performances and the type of proposed tasks and activities, which could be useful to improve the training of future Cybathlon competitions and even the practicing of an amputee with a new prosthesis.

Figure 11 REHAB TECH Pilot 1
driving Hannes during the Powered Arm Prosthesis Race of the Cybathlon 2020 Global Edition.

After the competition, a further analysis was carried out to better understand Pilot 1's results with respect to the other participants. We analysed the time of each task of the best race of each team, from which the ranking of individual task is appreciable.

2.1.2.3. Hannes's evaluation

The aim of the evaluation, which involved both pilots, was to assess possible progresses and improvements in the dexterity while using Hannes (from a functional point of view), its embodiment process, and user experience, focusing the attention on a possible positive impact of the Cybathlon-based training and competition in Pilot 1's results. Both pilots executed the protocol twice (Ti and Tf) and were not trained on the proposed evaluation protocol during the Home Use.

2.1.2.3.1. Functional evaluation

The functional evaluation was executed with three standard and globally validated clinical tests, performed only with the prosthetic hand, to measure the level of dexterity:

- *Minnesota Manual Dexterity Test (MMDT)* [250], only the Placing Test

  This test evaluates the dexterity obtained with the prosthesis by measuring the time spent to reorder a set of sixty small plastic discs. These latter must be placed, starting from the corner corresponding to the amputated side (in order not to invade and obstacle the field of view), one column after another in the board below, from the top to the bottom. The score is the time required to complete the task; therefore, lower scores indicate better performances.
- *Southampton Hand Assessment Procedure (SHAP)* [251]

  This clinical test, designed to evaluate the functionality of the upper limb, measures the time spent to move forward on a board six different objects, both light and heavy, with six different grips, and the time needed to accomplish fourteen ADLs. These results are then used to calculate six indices, one for each grip, and an overall index called Index Of Functionality (IOF) (0-100), which provides an overall assessment of hand function. Scores between 95 and 100 are considered referable to the normality range. Accordingly, higher scores suggest better functionality.
- *Box and Block Test (BBT)* [252, 253]

  BBT test is composed by a wooden box divided into two compartments, separated by a wall, and by 150 wooden cubes with a lateral length of 2.5 cm. The subject must move, one by one, the maximum number of cubes from one compartment to the other one, without touching the wall, within 60 seconds. The final score is the total number of transferred cubes, hence higher scores manifest better dexterity.

Furthermore, two standard and globally validated questionnaires were administered with the same aim:

- *Quick Disabilities of the Arm, Shoulder, and Hand (QuickDASH)* [254]

This questionnaire provides a general measure of the functional activities and the musculoskeletal disorders of the upper limb, validated for amputated patients. The subject must evaluate his capacity in performing eleven actions while thinking about his last week, by choosing from a 5-point scale where 1 is "No difficulty" and 5 is "I could not do it". The final DASH score is a number between 0 and 100, and lower scores indicate better performances.

- *Orthotics and Prosthetics User Survey-Upper Extremity Functional Status module (OPUS-UEFS)* [255, 256]

  This scale is specifically designed for amputees, and it includes twenty-eight activities concerning the self-care and the usage of daily life instruments. The evaluation method consists in a 5-point scale from 4 (the subject can easily perform the task) to 0 (the subject is not able to perform the task), besides the "not applicable" choice, with the additional information about the performing of the task with or without the prosthesis. The outcomes are the percentage of usage, exploiting the number of tasks indicated to be executed with the prosthesis, and its goodness.

2.1.2.3.2. Embodiment evaluation

The embodiment is the integration of an external object into the internal body scheme: an embodied object is hence perceived as if it is part of the body itself [257]. The level of embodiment was first evaluated with postural sway, searching for potential variations, and preferably decreases, with Hannes over time. The postural balance test required the subject to be motionless standing on a force plate, with his knees straight and arms down at his sides. First, the participant had to look at an eye-level fixation point on the wall for 60 seconds (eyes-opened - EO - condition). Immediately afterward, he had to close his eyes and remained standing for 60 seconds (eyes-closed - EC - condition). The sample frequency of the data acquisition, made with the force plate (AMTI), was 1000 Hz, while the data were extracted and elaborated by a custom-made Matlab software [258] and filtered with a low-pass filter with a cut-off frequency of 20 Hz. The required parameters were calculated and generated in an Excel file as described in [258]. The programmed outputs were:

- Centre of Pressure (CoP) medio-lateral (ML) path length, calculated as the cumulative displacement in the medio-lateral direction of the CoP [259, 260];
- CoP anterior-posterior (AP) path length, calculated as the cumulative displacement in the anterior-posterior direction of the CoP [259, 260];
- CoP total path (TP) length, calculated as the cumulative displacement of the CoP [259, 260];

Furthermore, three items of an ad-hoc questionnaire (item 1, 2, 3; subsection 'Embodiment'), inspired by the RHI questionnaires [257, 261], explored the embodiment obtained with Hannes in a subjective way and are shown in Table 4. The ad-hoc questionnaire was formulated with statements as in [242] and as the standard validated questionnaires exploited in this evaluation.

Table 4 Ad-hoc subjective questionnaire.

SUBSECTIONS	ITEMS
Embodiment	1. When I look at the prosthesis it seems to look directly at my own hand instead of a device
	2. The prosthesis seems to be part of my body
	3. I feel the prosthesis belongs to me
System use	4. I feel I can exploit the device at its best
	5. I manage to well coordinate the two hands using them together
	6. I am immediately able to understand if an object was reachable or manipulable with the prosthesis
	7. I don't think the device presents usage risks (that do not depend on me)
Daily life impact	8. I think I can use the device in different daily contexts
	9. The device brought positive changes in relationship with others
	10. The device usage improves my quality of life in terms of autonomy

2.1.2.3.3. User experience evaluation

The user experience is intended as the set of subjective consequences of all relationships between the user and the prosthesis [262], in term of individual perceptions, expectations, and reactions, also about aesthetics, comfort and technology acceptance [263]. User experience can be investigated through questionnaires filled out by the subjects. In our case, seven statements of the already cited ad-hoc questionnaire had the goal to evaluate these aspects and are reported in Table 4. Four of them belong to the 'System Use' subsection (item 4, 5, 6, 7), the remaining three (item 8, 9, 10) to the 'Daily life impact' one.

The ad-hoc questionnaire (Table 4) hence contained a total of 10 statements, to which assign a score within a 5-point Likert type scale, where 1 was 'Strongly Disagree' and 5 'Strongly Agree' in order to maintain the same form of the previous validated questionnaires. In all items, an increase in the scoring means an improvement.

The user experience was also investigated with three other standard and validated questionnaires:

- *Raw NASA Task Load Index* (*Raw NASA-TLX*) [264]

  This questionnaire measures the workload perceived to assess a task or a series of performances. The perception of the workload can change, depending on the level of UX reached. It consists of 6 subjective subscales, rated within a 20-point range with 1-point steps. The raw version of the NASA-TLX, exploited in this evaluation, lacks the individual weighting of the subscales, there is evidence supporting this shortened version, which could even increase experimental validity [265]. The NASA score is calculated as a percentage, and lower scores represent better performances.

- *System Usability Scale* (*SUS)* [266]

This scale provides a validated tool for measuring the usability of a system. It comprises 10 statements with five response options, from 'Strongly disagree' (1 point) to 'Strongly agree' (5 points). It is a very easy scale, and it can be used on small sample sizes, assuring anyway reliable results. Therefore, it can effectively differentiate usable and unusable systems. The SUS score is calculated as a number between 0 and 100, and it is considered above average when higher than 68 points, meaning that the system is usable. Hence, higher scores indicate higher usability.

- *Trinity Amputation and Prosthesis Experience Scales (TAPES),* only part 1 [267]

  This questionnaire measures the overall appreciation in using the prosthesis and its influence in the performance of ADLs. Part 1 of TAPES consists of two subscales with a 5-point rating scale regarding, respectively, the psychosocial adjustment, and the prosthetic satisfaction. The overall index is shown in the form of a percentage, and higher scores indicate greater levels of adjustment.

Results obtained in both Initial and Final Evaluation are analysed, together with the difference between the final and the initial value (Tf - Ti).

In addition, rates of improvement/deterioration of the Final Evaluation (Tf) with respect to the first one (Ti) are evaluated with the following formula:

$$T_f - T_i\ [\%] = \frac{(T_f - T_i)}{T_i} * 100 \qquad (1)$$

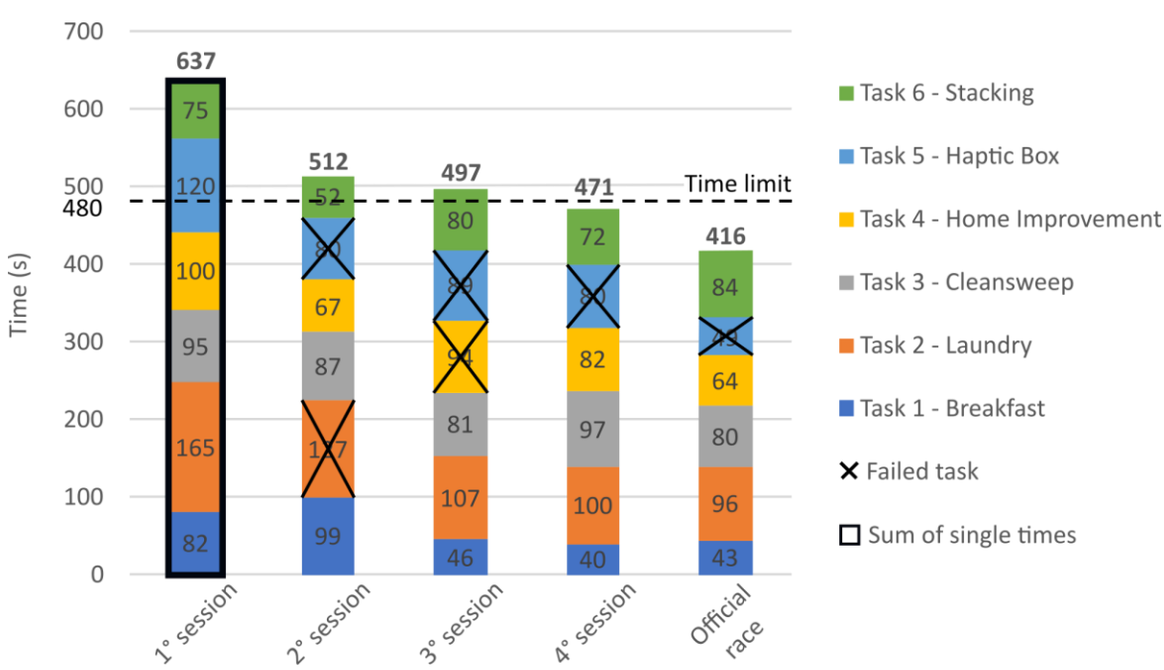

Figure 12 Performance evolution:
the four simulated races executed during live training sessions and the performance of the official race.

2.1.3. Results

2.1.3.1. Cybathlon training sessions

The results of each simulated race executed during the training period are reported in Figure 12, showing performance progresses achieved during the training by our Pilot 1. A gradual decrease can be appreciated over time. From the first simulated race (637 s), higher than the time limit (480 s equal to 8 minutes) of more than two minutes and half, the total time decreased and became lower than the limit in the last training session (471 s) and in the official race (416 s). In the second simulated race Pilot 1 failed task 2 and task 5, in the third one task 4 and 5, while in the last simulated race only failed task 5, as in the official competition.

The result trend followed the learning process of our Pilot 1. Some tasks and relative subtasks were performed very easily and quickly, whilst others, which initially seemed to be even physically impossible, required a more intense training. Indeed, it took several trials for Pilot 1 to formulate appropriate strategies to best exploit his Hannes device. Analysing in depth each task, no specific difficulties were found in the execution of the subtasks composing task 1 and task 3, since they were all bimanual exercises very similar to usual daily life activities, typically performed during the home use. Hence, the training was immediately focused on reducing the completion time. In contrast, the clothespins subtask of task 2 revealed to be challenging. Indeed, it was difficult to manipulate the clothespin while also having a strong-held grip in a comfortable posture. With some practice, Pilot 1 was able to identify the right strategy, which permitted a strong and safe grasp in a natural way, with him in front of the clothesline holding the clothespin between the index and thumb, as performed by non-amputees. Task 4 was found tough in all subtasks, as only the prosthetic hand was allowed to manipulate the blue objects comprised in it: hammer, bulb and scissors. Regarding the scissors, it was

Table 5 Final ranking of the Powered Arm Prosthesis Race of the Cybathlon 2020 Global Edition.

RANK	TEAM	SCORE	TOTAL TIME (s)
1	Maker Hand	100	344
2	SoftHand Pro	100	403
3	e-OPRA	100	452
4	SuperMotorica	86	390
5	BFH HuCE	86	425
6	**REHAB TECH**	**80**	**367**
7	x-OPRA	80	414
8	Hands On	70	319
9	Viswajyothi	51	360
10	Smart ArM	49	366
11	Touch Hand	34	252
12	CyberTum ARM	35	360
13	Imperial ARM	15	151

not possible to hold them with the sound hand to insert the prosthetic fingers in the finger holes. After the training, the adopted strategy consisted in sliding the scissors till the edge of the table and exploit it to insert thumb, index, middle and ring prosthetic fingers roughly about half their length, to have a firm grip but with a certain range of motion to allow the continuous scissors' operating for cutting the paper. The lamp subtask, which consisted in inserting and screwing the bulb in the lamp shade, needed long training to find the optimal postural movements' combination of legs, prosthetic side elbow and shoulder for the screwing of the bulb without active pronation/supination of the wrist. Instead, the hammer subtask was relatively easy, as the strong grasp and mechanical resistance provided by the prosthesis allowed nail hammering without risk of tool loosening and prosthesis rupture. Also task 6, where only the prosthetic hand was allowed to touch blue cups, needed an intense training to overcome the absence of wrist active pronation/supination, forcing compensatory movements of the prosthetic side shoulder and the constant bending of the legs. For our Pilot 1, the most difficult faced task was task 5, as the

Table 6 Evaluation of Hannes's functionality, embodiment, and user experience.

		PILOT 1			PILOT 2		
		Ti	**Tf**	**Δ**	**Ti**	**Tf**	**Δ**
FUNCTIONALITY							
MMDT [s]		180.0	150.0	-30.0	196.0	179.0	-17.0
SHAP IOF [%]		58.0	76.0	18.0	61.0	75.0	14.0
BBT [n°]		18.0	24.0	6.0	16.0	21.0	5.0
QuickDASH		11.4	11.4	0.0	13.6	11.4	-2.2
OPUS-UEFS: usage [%]		50.0	75.0	25.0	67.9	71.4	3.5
OPUS-UEFS: goodness [%]		71.4	79.8	8.4	69,7	75.0	5.3
EMBODIMENT: POSTURAL BALANCE TEST							
TP length [mm]	EO	477.9	411.9	-66.0	482.7	500.7	18.0
	EC	589.7	479.4	-110.3	665.7	808.2	142.5
ML path length [mm]	EO	222.1	177.2	-44.9	251.4	186,2	-65.2
	EC	270.4	177.2	-93.4	323.7	387.9	64.2
AP path length [mm]	EO	356.9	334.9	-22.0	360.3	433.5	73.2
	EC	438.6	410.9	-27.7	514.7	638.8	124.1
EMBODIMENT & USER EXPERIENCE: AD-HOC QUESTIONNAIRE							
Embodiment		7	10	3	8	8	0
System use		17	20	3	17	17	0
Daily life impact		13	15	2	10	12	2
USER EXPERIENCE							
raw NASA-TLX [%]		34.2	11.7	-22.5	40.8	25.8	-15.0
SUS		95.0	100.0	5.0	87.5	90.0	2.5
TAPES, part 1 [%]		80.0	93.3	13.3	83.3	89.2	5.9

prosthetic hand Hannes is not equipped with systems able to provide haptic feedback. Hence, a safe strategy capable to assure a successful result in a very short time and with the pressure of the competition was not found. Pilot 1 tried to recognize the texture, soft or hard, of the hidden objects by slamming the prosthesis on it, listening to the sound response, and sensing the mechanical resistance of the squeezed object. The shape was instead evaluated by slipping the back of the hand on the object's surface, looking for edges or curves. However, this task's outcome was still an uncertainty also right before the competition.

2.1.3.2. Cybathlon official competition

The final ranking of the Cybathlon 2020 competition is shown in Table 5. Only three teams over thirteen succeeded in all tasks, obtaining the maximum score of 100 points. Our team REHAB TECH placed in the sixth place with a score of 80 points due to the error occurred in task 5 (which had the highest scoring of 20 points), and with a total time of 416 seconds.

Figure 13 graphically shows the time of completion of each team for each task. Precisely, the main light orange bars represent our team REHAB TECH's performance, whilst other teams' times are reported as coloured points. No time was reported for each team if the task was failed. Lower times indicate better performance. Task 1 was completed by only six teams out of thirteen, task 2 by eleven, task 3 by ten, task 4 by eight, task 5 by eight and finally task 6 by ten.

Our Pilot 1 had the best time performance in task 1, which was failed by many teams (seven on thirteen). Same result, but on par with the winner team Maker Hand, was obtained in task 4. The sixth and fifth places achieved respectively in task 2 and task 3 shows anyway a good mid-table result in the handling of different common objects with different grasp types. Task 5, as can be appreciated by the

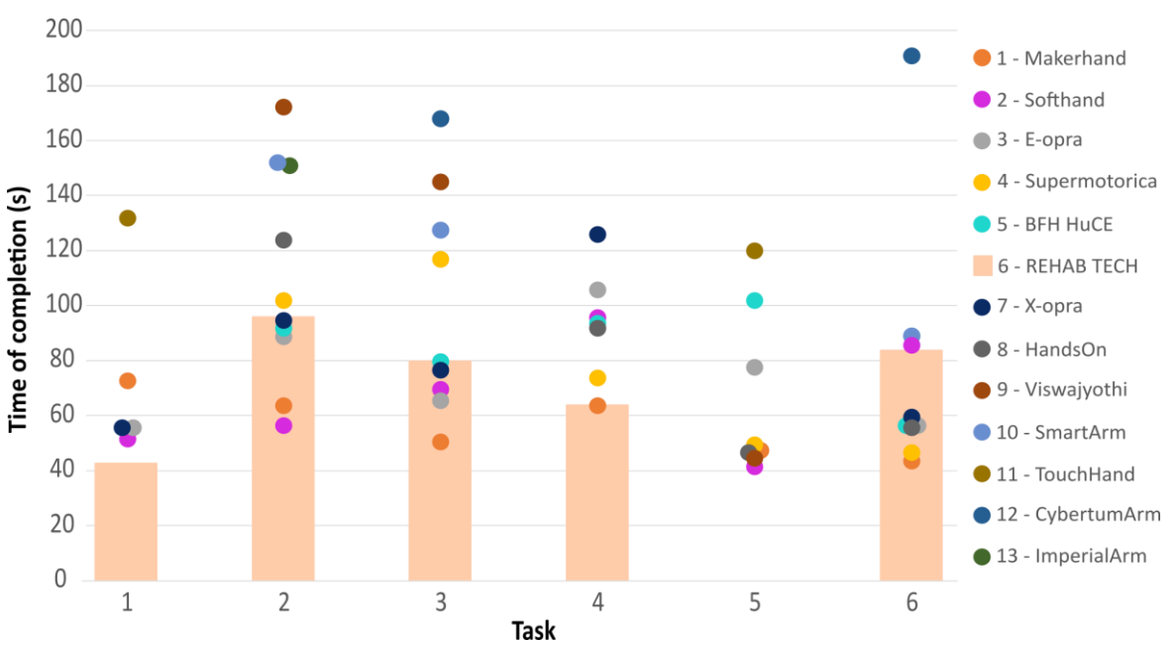

Figure 13 Time of completion of each team for each task:
REHAB TECH's times are enhanced and reported with light orange bars, whilst the rest of the teams' results are shown with coloured points. Each team is correlated with a colour, as explained in the legend on the right.

absence of REHAB TECH's time of completion in Figure 13, was failed. Only in task 6 our team REHAB TECH ranked in the second half of the ranking.

2.1.3.3. Functionality, embodiment, and user experience evaluation

The scores of functionality, embodiment, and user experience measures of the two evaluations (Ti, Tf) for both pilots are shown in Table 6, together with the difference between the two values (Δ). In Functionality section, both pilots decreased their times in the execution of MMDT and SHAP tests (which accordingly increased the IOF), while increased the number of transferred cubes in BBT test and their questionnaires' scores, except for the QuickDASH of Pilot 1. In the Postural balance test, which was employed to measure the embodiment, the body oscillations decreased in Pilot 1 in each investigated condition. Differently, Pilot 2's sway increased, except in the medio-lateral direction and in the eyes-opened condition. Pilot 1's ad-hoc questionnaire total scores increased respectively of 3 points in subsections 'Embodiment' and 'System use' and 2 points in subsection 'Daily life impact', whilst Pilot 2 made the same total score in the first two subsections, and slightly increased the last one (2 points more). Regarding the last validated questionnaires investigating User experience, both raw NASA-TLX scores decreased, while both SUS and TAPES ones increased.

Figure 14 graphically shows the rate of improvement/deterioration of both pilots over the evaluations. Regarding the functionality, a general improvement can be observed in Figure 14 (**A**) for both pilots, however Pilot 1 exhibits overall higher percentages of improvement, especially for the OPUS-UEFS usage (50,0% against 5,3%). Only the QuickDASH score shows a small improvement for Pilot 2 and a stable result for Pilot 1.

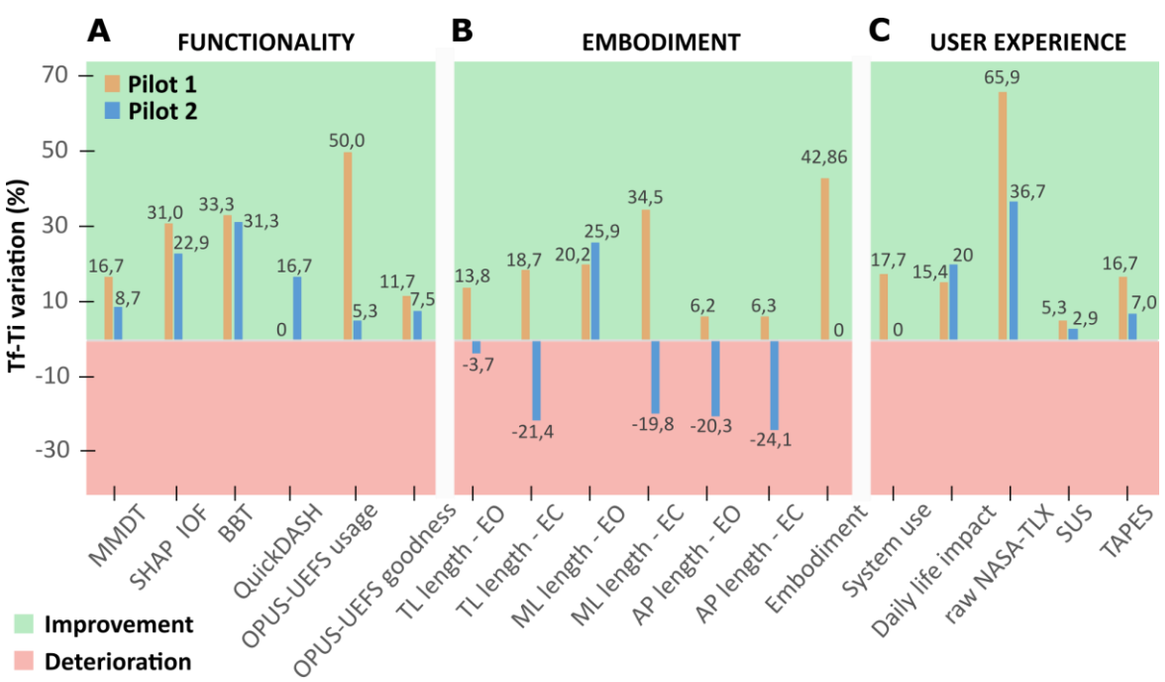

Figure 14 Rate of improvement/deterioration of the scores
for the three investigated areas: (**A**) the functionality, (**B**) the embodiment and (**C**) the user experience. Positive values correspond to improvements, negative values to deteriorations.

In the postural balance test Pilot 1 improved all his parameters in each of the investigated condition, whilst Pilot 2 had an overall worsening. He only improved one variable (ML length) in one single occasion (EO), with a percentage of improvement slightly higher than Pilot 1's, as shown in Figure 14 (**B**). In the ad-hoc questionnaire Pilot 1 improved his total scoring in 'Embodiment' (Figure 14, **B**) and 'System use' (Figure 14, **C**) subsections, whilst Pilot 2 did not show any improvement over time. Instead, in 'Daily life impact' module, the percentage of improvement was higher for Pilot 2, as shown in Figure 14 (**C**). The highest percentages of improvement in the last three validated questionnaires of the user experience belong to Pilot 1, as it can be seen in Figure 14 (**C**).

2.1.4. Discussion

2.1.4.1. Cybathlon training and competition

As expected, a gradual improvement in the tasks' completion time was observed with the advance of the training (Figure 12), which allowed Pilot 1 finding the most reliable and fast strategy to accomplish each task.

The result trend followed the learning process of our Pilot 1, who learnt how to exploit Hannes and to formulate successful strategies. Some tasks and relative subtasks were performed very easily and quickly, whilst others, which initially seemed to be physically impossible, required a more intense training. No specific difficulties were found in the execution of the subtasks of task 1, since they were all bimanual exercises very similar to usual daily life activities, typically performed during the Home Use. Hence, the training was immediately focused on reducing the completion time. In contrast, the clothespins subtask of task 2 revealed to be challenging. Indeed, it was difficult to manipulate the clothespin while also having a strong-held grip in a comfortable posture. With some practice, Pilot 1 was able to identify the right strategy, which permitted a strong and safe grasp in a natural way, with him in front of the clothesline and the clothespin held between index and thumb, as performed by non-amputees. Subtasks composing task 3 were accomplished quite easily as they were performed using common grasp strategies. Task 4 was found tough in all subtasks, as only the prosthetic hand was allowed to manipulate the blue objects comprised in it: hammer, bulb and scissors. The adopted strategy exploited the edge of the table to insert thumb, index, middle and ring prosthetic fingers into the scissors' handle to assure a firm grip and a continuous scissors' operation for cutting the paper. The lamp subtask needed long training to find the optimal postural movements' combination of legs, prosthetic side elbow and shoulder for the screwing of the bulb without active pronation/supination of the wrist. Instead, the hammer subtask was relatively easy, as the strong grasp and mechanical resistance provided by the prosthesis allowed nail hammering without risk of tool loosening and prosthesis rupture. As well, task 6, where only the prosthetic hand was allowed to touch blue cups, needed an intense training to overcome the absence of wrist active pronation/supination, forcing compensatory movements of the prosthetic side shoulder and the constant bending of the legs. The most difficult task was task 5, as Hannes prosthetic

hand is not equipped with a haptic feedback. Hence, a safe strategy capable to assure a successful result in a very short time, and with the pressure of the competition, was not found. Pilot 1 tried to recognize the stiffness (soft or hard) of the hidden objects by slamming the prosthesis on it, listening to the sound response, and sensing the mechanical resistance of the squeezed object. The shape was instead evaluated by slipping the back of the hand on the object's surface, looking for edges or curves.

In the official competition (Figure 13), the peculiarity of the prosthetic hand Hannes, capable to adapt to the grasped object, and the flexible wrist module in flexion/extension helped Pilot 1 in succeeding in task 1, in which a high number of objects with different sizes and type of grasps were included. The same key role was played by Hannes in task 2 and task 3. However, both completion times were not low. This might be a consequence of Pilot 1's approach, who gave priority to grasping precision to replicate natural hand strategies, rather than execution's speed. For example, the tridigital grasp implemented by thumb, index and middle fingers and used for the clothespins of task 2 and the USB pen of task 3 resulted to be very natural. However, more time was required to manage this grip, as the object needed to be precisely picked with the distal phalanges. The absence of active wrist pronation/supination negatively influenced task 6, in which a flipping movement was required, leading to consistent compensatory movements and slowing down the performance. Furthermore, a small error occurred during the pyramid construction, as one cup slipped over another one and the pilot had to relocate it. The lack of active wrist pronation/supination also impacted in the bulb insertion of task 4. Nevertheless, the quick execution of the rest of the task, permitted by the strong and natural grasp of the hammer and the continuous actuation of the scissors offered by Hannes, allowed our pilot to obtain the best time, together with the Maker Hand team. The failure in task 5 was quite expected, considering Hannes is not equipped with haptic feedback system and the difficulties faced during the training to conceive an effective and reliable strategy.

Eventually, the times of completion of each task was very good or in line with the average times, meaning that Hannes performed better or similarly compared to other prosthetic devices (Figure 13). The participation to the Cybathlon competition allowed Hannes to be compared with many other hand prostheses. Considering the position in the first half of the final ranking (6 of 13), Hannes's performance can be considered above the average (Table 5). The absence of an active wrist module and a system capable to restore haptic feedback could be considered as limiting factors, which on our team will focus for future developments.

2.1.4.2. Functionality, embodiment, and user experience evaluation

As expected, after almost two months of Home Use, both pilots improved their performances in all investigated areas over time, except for Pilot 2's embodiment domain, which worsened. Moreover, it can be noted that Pilot 1 had a better learning curve and better progresses, as improvements were higher than the ones of Pilot 2.

Concerning functional clinical tests, major improvements were noticed in the most complex ones: MMDT and SHAP. In BBT test, the easiest one, both pilots improved almost in the same manner. Differently, in MMDT, which required a specific fine control for the correct inserting of the disks into the board, and in SHAP test, where several different grasps were required, higher improvements were shown by Pilot 1. This difference may be related to the additional training he faced for the Cybathlon competition, which included tasks very similar to these clinical tests. Even if the training was focused on the fast and correct execution of specific exercises and tasks, the control of Pilot 1 with Hannes seemed to improve. Differently, Pilot 2 made use of Hannes freely, without periodic training and a specific goal to achieve. This could be one of the reasons his functional improvements were lower compared to Pilot 1's.

The difference obtained by Pilot 2 in the QuickDASH score is much smaller than the Minimal Detectable Change (MDC) (12.85) [268], implying a not relevant clinical improvement, as the stable score of Pilot 1. These results can depend on the low specific nature of this questionnaire in evaluating amputees' dexterity, since it provides a general measure for everyone with upper limb problems. The OPUS-UEFS scores improved for both pilots, but more for Pilot 1. He notably improved in the 'Percentage of usage' score, in which the difference between the final and initial value also overcomes the MDC (12.07) [256]. This parameter can be considered important because it means Pilot 1 involved his prosthesis Hannes in many more activities over time. This outcome could depend on the positive influence of the Cybathlon experience. In fact, the training and the competition seem to have improved maneuverability and functionality when compared to Pilot 2. This is confirmed by the functional tests' outcomes reported above. Again, the training and the purpose to compete with Hannes might have motivated Pilot 1 in increasing the prosthetic usage. On the contrary, since Pilot 2 was extraneous to such experience and involvement, he may have involved Hannes in a small number of activities.

The evaluation of the embodiment, executed with an objective (postural balance test) and a subjective (items 1,2 and 3 of the ad-hoc questionnaire) measure, seems to show an improved embodiment only for Pilot 1. Probably, the regular and increased usage of the prosthesis made by Pilot 1 due to the training had a positive impact on the embodiment domain. Overall, the results suggest that the engagement produced by the participation to the Cybathlon competition could be intertwined with the one depending on the embodiment processes. Thus, the daily usage of the system was promoted by the motivation to perform successfully during the official challenge and by the sensation that the prosthesis was part of one's body scheme. The engagement [269] can constitute a factor promoting the embodiment of a wearable technology or can be a phase of embodiment itself thanks to the motivation to improve for the competition, in our case. However, these hypotheses will need further investigation to be evaluated. In contrast, Pilot 2 worsened the scores used to evaluate the embodiment process. Even though Pilot 1 and Pilot 2 spent almost the same total amount of time with Hannes (except for some additional days to compete the race for Pilot 1), it seems that Pilot 2 was not capable to establish a real connection with Hannes prosthesis. This could be a consequence of a basic domestic use, without the involvement driven

by the motivation to prepare for a challenge. Furthermore, the difference in their results could also depend on the subject's personality and willingness in approaching a prosthetic device as a part of the body rather than a tool: we cannot imply that Pilot 2 had a more resistive behavior, but such an interpretation suggests us to adopt personality questionnaires in future studies for checking this hypothesis.

TAPES questionnaire and subsection 'System use' of the ad-hoc questionnaire investigate similar situations and evaluate the perception of the subject towards the prosthesis. In our view, this represents a very important argument, and the highest improvements in relation to these two assessment tools belong to Pilot 1, as if the training and the Cybathlon competition increased such a perception. Similarly, the raw NASA-TLX scale, which measured the perceived workload while using the prosthesis, shows an improvement for Pilot 1 that is almost twice the one of Pilot 2. This may indicate that Pilot 1's Cybathlon experience permitted to reduce the perceived workload. Overall, the higher improvements obtained by Pilot 1 suggest that the participation in the Cybathlon competition might have had a beneficial influence on his global user experience and the prosthesis impact on daily life situations. On the other hand, again, the more basic environment of Pilot 2 resulted in smaller improvements, which is in accordance with the other two evaluations.

The evaluation simultaneously conducted to the Cybathlon experience, concerning functionality, embodiment and user experience achieved with Hannes, showed overall improved scores for both pilots (except for the embodiment of Pilot 2), leading to assume that the constant and prolonged Home Use of Hannes can improve the amputee-prosthesis relationship. However, the most interesting outcome of this study is the consistent greater improvement exhibited by Pilot 1 with respect to Pilot 2. We could assume that this outcome may depend on the training, the tasks and the speed running challenge of Cybathlon 2020 competition performed by Pilot 1. Hypothetically, the engagement produced by the expectation to compete in a challenge affected the amount of daily practice of the user. Such an additional use time could have accelerated the prosthetic embodiment processes of Pilot 1, improved his speed performances, and stimulated him in finding strategies and solutions for the achievement of everyday actions, consequences not found in Pilot 2's results, as a plausible effect of the non-attendance to the Cybathlon competition.

The embodiment phenomena are intertwined with cognitive and affective processes as in the case of motivation: motivation sustains our efforts and push us to improve our skills and performance. We hypothesize that the motivation generated by the purpose of preparing for Cybathlon competition affected the engagement of Pilot 1 in - carefully and continuously - employing the device. Such an effect helped him to establish a connection with Hannes through a steady enhancement of his skills in controlling it, directly enriching the sense of agency (a component of the embodiment).

As a limitation, only short-term benefits of the Cybathlon-based training and competition are analysed in this case study. Hence, it is not possible to state that these benefits could last in the long-term period, maintaining a consistent difference between pilots' results in the investigated areas. Further

analysis, comprising longer total time of usage and multiple follow-ups, may clarify long-term implications, evaluating if these differences persist or if both pilots reach, at some point, same level of improvement.

2.1.5. Conclusion

Considering this was our first approach toward the Cybathlon experience, we can consider our sixth place a very good result. Pilot 1 learnt how to take advantage of our novel prosthetic system Hannes and was able to accomplish 5 out of 6 tasks, with execution times on average. Hannes demonstrated to be a valuable competitor, capable to perform a variety of natural grasps and to realize most of the tasks with human-like behaviors and biomimetic performances.

The results of the comparison between the user who was involved in the Cybathlon experience and the one who was not suggest that the training of a user with a prosthesis could benefit from Cybathlon's proposed tasks and structure. The inclusion of more exercises inspired by real daily life activities, requiring their execution within a certain amount of time, could stimulate the patient's dexterity, prosthetic embodiment and UX in a short time. It seems that timed races or trainings designed as competitions, like Cybathlon, could facilitate and even accelerate the prosthetic learning phase, decreasing the perceived workload, as possible consequences of the high developed engagement between the user and the prosthesis. This novel methodological approach should be further investigated with a precise protocol and with a consistent sample size to obtain significant results, both to improve the ADLs amputee's performances and to better prepare our pilot for the next competition using the Hannes hand.

frontiers in Neurorobotics
ORIGINAL RESEARCH
published: 27 August 2021
doi: 10.3389/fnbot.2021.683653

2.2. Exploring the Embodiment of a Virtual Hand in a Spatially Augmented Respiratory Biofeedback Setting

2.2.1. Introduction

Artificial limbs are designed to assist and increase the manipulation capabilities of human beings in contexts from teleoperation to virtual rehabilitation, to bionic prosthetics [270]. In order to nurture the progress of this research domain, scientists considered the results of studies on topics like the proprioceptive illusions in people with a spinal cord injury [271] or the applications of error-related potentials in neuroprosthetics [272]. Through the integration between neuroscience and engineering, interdisciplinary research has offered inspiring strategies like, developing neurointerfaces to control virtual and robotic systems [273], neuromorphic systems to bring the sense of touch to the prosthesis users [274].

Artificial limbs can be perceived by certain users as tools, while others can feel them as corporeal structures [275]. In this second case, these robotic or virtual extensions of the user can trigger the phenomenon of embodiment, i.e., the psychological process occurring when subjects feel external objects as integrated in their own body scheme [276].

However, the embodiment process is not limited to artificial limbs, and can involve any artifact or tool [277]. Initially, this process makes the device more familiar for the users who have become curious about it. Subsequently, the mental representations of the users start to adjust to progressive human-artifact integration [269]. Feeling a device as embodied leads to improvements in user's engagement, technology acceptance, control transparency, and, consequently, human-machine system performance [278].

Typically, the investigations in this domain aim at establishing effective methods to enhance the embodiment through the manipulation of the stimulus-conditions [279] or the active control conditions of artificial limbs [280]. However, literature on interoceptive processes [281] suggests that an individual’s psychophysiological control potentially impacts on embodiment components like body ownership. It is hypothesized that respiratory entrainment techniques [282] like those used in contemplative mental training and biofeedback [283], may influence the embodiment process.

This paper preliminarily investigates whether modulating one's psychophysiological state via respiratory biofeedback can enhance the embodiment of a virtual, computer-generated hand**.** Our research was carried out through a pilot study using common devices like a computer monitor, a smartphone, and a microphone. This last choice was made to explore the potential of a setup that can be replicated at home without the need for special equipment. Evaluating the feasibility of this setup is our second scope for extending the upcoming data collection (bypassing also the restrictions of the current pandemic) (Woolliscroft, 2020) through this innovative “embodiment training” approach.

2.2.2. Background and Scope

2.2.2.1. Related Works

As hinted above, several studies on embodiment [284] aim at improving human-machine interaction with special attention to artificial limbs user experience, especially to reducing prosthetic devices abandonment [238] and promoting their acceptance and integration [285]. Indeed, the results of embodiment studies are quite helpful to guide the design of novel artificial limbs through an improved understanding of user experience: a survey involving 2383 limb amputees highlighted how naturalistic prostheses designed with sensory feedback were associated with higher feeling of prosthesis ownership and reduced phantom pain [286].

According to literature [278], the sensations of ownership (the feeling that non-bodily objects are body parts and sources of bodily sensations, depending on the integration of multisensory inputs), self-location (the feeling of the body location in space, depending on the co-location of fake and real elements), and agency (the feeling of being the cause and the author of observed actions, depending on the efficiency of limb motor control) constitute the embodiment [287] process itself.

Considering the case of artificial upper limbs, the investigation of their embodiment is usually entrusted to methods for evaluating a well-known phenomenon that demonstrated high potential in experimental and clinical neuroscience research [288]: the Rubber Hand Illusion (RHI) [239]. RHI is typically induced by the co-occurrence of visual stimulations on an inactive fake limb observed by the subjects and tactile stimulations on their real hand [289].

In particular, RHI studies offer important pointers towards investigating the ownership component of embodiment. The body ownership is especially critical in the acceptance of artificial limbs - see [241] and [235]. This aspect of the embodiment was investigated through multiple studies, considering, for instance, its relationships with sensory stimulations [290] and other embodiment components - agency [291] and self-location [292]. Interestingly, RHI can also generate phenomena of disembodiment as the disownership of the hidden real hand [293]. These and other seminal studies have contributed to the research in this area, which embraced topics like the impact of affective processes [294], the psychopathological aspects [295], and the individual differences [296] in body ownership representations.

These are just examples of the body ownership literature, which is rich with original methodological solutions to assess how this phenomenon occurs in different conditions. Overall, the body ownership is typically evaluated in RHI paradigms through measures like subjective evaluations (e.g., self-report questionnaires) [242] or physiological reactions (e.g., Galvanic Skin Response, GSR) [297]. Another classic measure of ownership is the proprioceptive drift [240] towards the artificial limb when the subjects are asked to estimate the actual position of their own hand, usually hidden and apparently replaced by a fake one during the experimental session. This implicit measure is performed in different ways according to the experimental setting - e.g., a virtual version in [298].

It must be noted that the use of such body ownership measures in RHI studies is still debated: for instance, distinctions between subjective questionnaire scores and proprioceptive drift (Gallagher, Colzi, & Sedda, 2021) should be further investigated to understand different processes underlying the subjective evaluation and the proprioception.

Alongside the research on the heterogenous manifestations and measures of the ownership, literature has also shown structured models to understand its role within the bodily representations. According to [299], body ownership depends on the interplay between the current multisensory input (bottom-up processes) and the internal models of the body (top-down modulation) that phenomenologically lead to conditions like the RHI [240]. Specifically, the malleability of bodily representations can depend on interoception [300], the perception of the internal state of the body. In particular, individuals with low interoceptive sensitivity (assessed through a heartbeat monitoring task) experience a stronger illusion of ownership in RHI [301].

Within this research domain, typical methodologies based on purely exteroceptive visuo-tactile stimulations tend to be substituted by combinations of interoceptive and exteroceptive signals, like cardio-visual stimulations [281]. For instance, observing a virtual hand that is pulsating in synchrony with participant heartbeat can induce body ownership changes as reported in RHI experiments [302]. Other studies investigated heartbeat-evoked electroencephalographic (EEG) potentials and their role in bodily self-consciousness [303].

The role of interoceptive sensitivity in RHI was also investigated in [304]. Specifically, authors studied the effects of meditation and mindfulness practices – like respiratory control or heartbeat control – on RHI susceptibility. Authors highlighted how meditators subjectively rated the RHI less strongly than non-meditators. These results are coherent with the ones of [305] on the agency perceived by meditators in RHI, and with [301]. However, in [304], no difference in proprioceptive drift was found between these meditators and non-meditators, and different interoceptive awareness factors were associated with RHI intensity in meditators. Thus, it can be inferred that practicing meditation could lead to different embodiment experiences when subjected to an interoceptive training to flexibly shift attention along the body; it makes the person more resistant to abnormal sensations.

This conclusion suggests the possibility that our malleable body representations could be affected by meditation exercises. However, the evidence in [304] was based on a typically passive RHI procedure executed by people who previously practiced meditation techniques. The prior meditation experience had, apparently, shaped the people's interoceptive sensitivity and body awareness before any RHI experience. This led us to a question: how could these exercises affect the embodiment of an artificial limb if they directly contribute to making an artificial limb illusion happen? A positive answer to this question could lead to novel approaches of embodiment training based on active self-regulation techniques that assist the artificial limb ownership.

In the current study, we targeted a core component of meditation practice, i.e., the breathing [306], particularly slow breathing, which is commonly performed at 10 or 6 breaths per minute. Slow paced

breathing produces multiple psychophysiological changes (Zaccaro et al., 2018), characterized by a generalized relaxation across, for instance, cardiovascular and cortical domains, especially with regard to meditation (Yu, Hu, Funk, & Feijs, 2018). Overall, this respiratory exercise has pervasive effects on autonomic functions, downregulating them [307] with long-term therapeutic responses [308]. Furthermore, these effects can involve the interoceptive awareness [309] through a self-regulation that is relatively easy for a practitioner. Here, we considered respiratory biofeedback (targeting 0.1 Hz respiratory rate) – self-modulating the Respiratory Rate (RR) according to its visualization [310] – for its effectiveness in influencing the physical and mental states has been shown in literature [311].

In order to proceed with our investigation, we decided to adopt a promising approach for exploring embodiment processes like the body ownership through an interactive solution with high perceptual versatility: the Virtual Hand Illusion (VHI) [312]. VHIs are produced through a setup that offers a complete experimental control of engaging computer-generated scenarios [146] of Virtual Reality (VR - where the perceptual scenario is fully generated by a computer) or Augmented Reality (AR - where virtual items are placed within a real perceptual scene) or Mixed Reality (MR - where virtual items and real items co-exist, often emphasizing the possibility to interact with the first ones as physical objects, according to some authors) [147]. Overall, these systems can be considered as cases of Extended Reality (XR), which is becoming a trend in neuroscientific research as well [313].

Thanks to their versatility in controlling the perceptual scene [314] and to their capability to motivate and engage the subjects through game-based features [315], XR systems offer fertile opportunities for body ownership studies as demonstrated by [316] and [317] – for a review on this topic, read [318]. Such solutions, extremely valuable in clinical applications too [319], demonstrate further potential through their compatibility with other technologically advanced approaches like neuromodulation [320]. Furthermore, AR solutions are currently explored to train the control of prosthetic systems [321].

Interestingly, the study in [322] adopted a VR-based RR biofeedback approach to generate and investigate an "embreathment" illusion by ecologically mapping the subjects' breaths onto a virtual body observed from a first-person perspective, improving the embodiment of the individual on the avatar. The authors highlight the potential of breathing as a natural, continuous, multisensory self-stimulation. Furthermore, they demonstrate the opportunity of implementing such a self-regulation process through an engaging virtual environment.

Summing up, XR settings can be exploited to investigate the effects of a slow respiratory biofeedback exercise as a method to enhance the embodiment of an artificial limb.

2.2.2.2. Research Objectives

Our hypothesis is that slow respiratory biofeedback, as a self-regulation strategy, can facilitate the embodiment of a virtual hand during a biofeedback training designed to evoke a VHI. Accordingly, this pilot study aimed at comparing two conditions of respiratory biofeedback – slow breathing and normal breathing – in terms of indices of virtual hand ownership sensation. We considered an interactive setup

that enables the person to control the perceptual features of a computer-generated hand without moving it (as in typical RHI and VHI). This allows us to focus on the body ownership component of embodiment as a premise for further studies.

Through this proof of concept, we also investigated the feasibility of a protocol designed for remote use, which only requires a computer, a microphone, a monitor, and a smartphone. If successful, this would provide a portable and affordable solution to enable anyone (for example an amputee waiting to receive a prosthesis) to perform at home a novel biofeedback-enhanced embodiment training. This choice was also driven by the need of creating a remote version of this setup for upcoming studies due to the limitations imposed by COVID-19 (e.g., stay home orders).

2.2.3. Materials and Methods

2.2.3.1. Participants

All participants were volunteers from IIT, signed the informed consent and followed the IIT ADVR TELE01 experimental protocol approved (on March 16th, 2020) by the Ethical Committee of Liguria Region in Genoa, Italy. All participants were volunteers from IIT, signed the informed consent and followed the IIT ADVR TELE01 experimental protocol approved (on March 16th, 2020) by the Ethical Committee of Liguria Region in Genoa, Italy. Before recruiting the participants, the sample size was calculated through G*Power v3.1.9.7 [323] according to the results of preparatory tests (involving 8 subjects) performed to improve the user-centered design of the setup. These results were based on the differences between 2 conditions in mean (-2.55) and standard deviation (4.36) of proprioceptive drift scores (see 3.5.1) compared through paired samples t-test (more restrictive in terms of requirements than non-parametric tests used for other measures like questionnaire scores). Thus, with $\alpha = 0.05$, power = 0.8, G*Power estimated a sample size of 22 subjects.

Twenty-two (six females) adults (Age, mean ± SD: 27.4 ± 2.4 years) without disabilities participated in the study. Twenty subjects were right-handed, one subject was left-handed, one subject was ambidextrous. Only two subjects declared to have had respiratory difficulties (respectively moderate asthma and rhinosinusitis) in past. All individuals were free from sensory and cognitive disabilities, and motor impairments derived from neurological conditions, and psychoactive drugs consumptions in previous 6 months. To avoid any potential RHI-resistance of meditators [304], all participants were selected as naïve about mindfulness and meditation techniques.

To assess how prosthesis users could approach this kind of task with the proposed setup within an embodiment training protocol, two (66 and 33 years old) male amputees (users of transradial prostheses for the right upper limb) without respiratory issues were also recruited and performed the same procedure as the 22 participants described above, except for the biosignal data collection (simulating the home setting).

2.2.3.2. Experimental Setup

All experimental sessions took place at Istituto Italiano di Tecnologia (IIT - Genoa, Italy). However, to design a setup compatible with upcoming home-based data collection, we did not use any head-mounted display typically adopted in highly immersive VHI settings with advanced haptic feedback systems [324]. Thus, we considered the options offered by Spatially Augmented Reality (SAR) [325] environments, where the real world is enriched by displays (including projections) placed across the real setting instead of being worn by the user as in the most typical AR paradigms based on visors [326]. In our case, a computer monitor became a screen-based display for SAR. The final setting (Figure 15) was constituted by basic equipment available to anyone at home (monitor, smartphone, headphones) with the addition of professional systems for recording biosignals.

To use the setup, the participants (Figure 15 A) were positioned in front of a monitor (21" with 16:9 ratio, laid-out horizontally, slightly tilted towards them), wearing a headset with a microphone placed in front of their mouth. Black blankets covered the subjects' arms and surrounded the monitor to make the subject focus on the non-immersive virtual scenario presented by the screen (Figure 15 B) – for the same reason, during the experimental session the environmental light was dim. A laptop (Alienware M15; Windows 10 Home 64 bit) was used to perform real-time processing of the audio data and extract breathing information used for visuo-tactile biofeedback. All participants wore photoplethysmography sensors to collect Blood Volume Pressure – BVP – data (providing a second estimation of breathing events, thus the RR in Hz, in respect to our custom microphone-based system) and skin conductance sensors collecting GSR data (source of potential embodiment-related reactions, expressed in μS) on left hand fingers. Specifically (Figure 16 A), the BVP sensor was placed on the middle finger, the GSR sensors – Ag/AgCl electrodes mounted without conductive gel as in [327] - were placed on the middle phalanges of the index finger and the ring finger as in [328].

These sensors constituted an acceptable compromise to record biosignals without excessively altering the individual experience (this reason led to exclude the use of a chest belt). All biosensors were

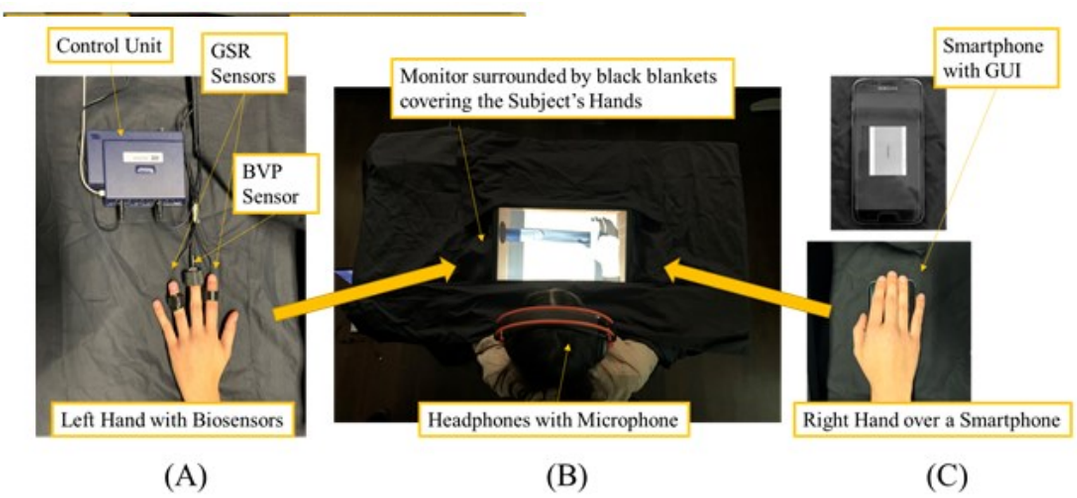

Figure 16 Experimental setup.

connected to the FlexComp Infiniti control unit (Figure 16 A), connected to the laptop enabling the SAR scene (Figure 15 B) and setting (Figure 16 B). A smartphone (Samsung S7) for vibratory stimulations was placed under their right hand (Figure 16 C).

Coherently with the SAR concept, this setting showed a continuity between the subjects' body and the virtual hand presented by the display, just like a prosthesis would replace a missing limb or a rubber hand would be placed in the typical RHI studies. Specifically, the screen presented an interactive environment developed in a Unity (https://unity.com) game project comprising 13 scenes per experimental condition.

This environment represented the inside of a cardboard box containing, on the right half, the 3D model of the Hannes [11] prosthetic hand (Figure 15 B). The choice of using the model of an actual prosthesis was made to allow for upcoming comparisons with real settings including the actual Hannes system in RHI-like studies. The hand model was created with the 3D design program Blender (https://www.blender.org/) starting from single-part STL files of the Hannes prosthetic hand to preserve the real joint axes and related joint movements of the human hand. The Blender object was, then, imported in the Unity scenes, maintaining the properties of its different parts.

Inside the virtual cardboard box, a blue sphere "made of energy" (an engaging game-like design imported from a Unity package: ArtStation - Glowing orbs VFX, Vladyslav Horobets) slid from left to right on an inclined surface, coming out from a hole on the left side of the box. In 1 minute, the sphere reached a black area (designed to magnify the position of the trial goal) with a hole placed under a right virtual hand, leant on a support that represents the presence of the smartphone under the real limb of the subjects. A hole through the virtual support enables the "contact" between the computer-generated hand and sphere. Figure 15 B depicts the scene.

This SAR setting was then enriched by respiratory biofeedback features (based on RR data collected through the microphone of the earphones) within a Spatially Augmented Respiratory Biofeedback – SARB – paradigm. In this SARB implementation, the subjects modulated their own RR according to a target frequency in order to minimize the transparency (managed through a Unity package: Unity Stipple Transparency Shader - Alex Ocias Blog) of the virtual hand (Figure 17) according to the biofeedback procedure described in sub-section 3.2. If the transparency index was over a certain threshold, the hand was visible enough to trigger a visuo-tactile event when the sphere approached the hand. In that case the virtual hand on the screen showed a "shaking" animation and the smartphone under the real hand of the subject vibrated. Overall, the SARB is characterized by gamification features (from the challenge to the set of feedback) designed to engage the user in self-regulation activities [329] that will be described in next paragraphs.

2.2.3.3. Respiratory Biofeedback and Data Acquisition

The SARB was adopted to evaluate 2 experimental conditions: slow RR and normal RR. The following sub-sections describe how the data were collected and processed for implementing the SARB

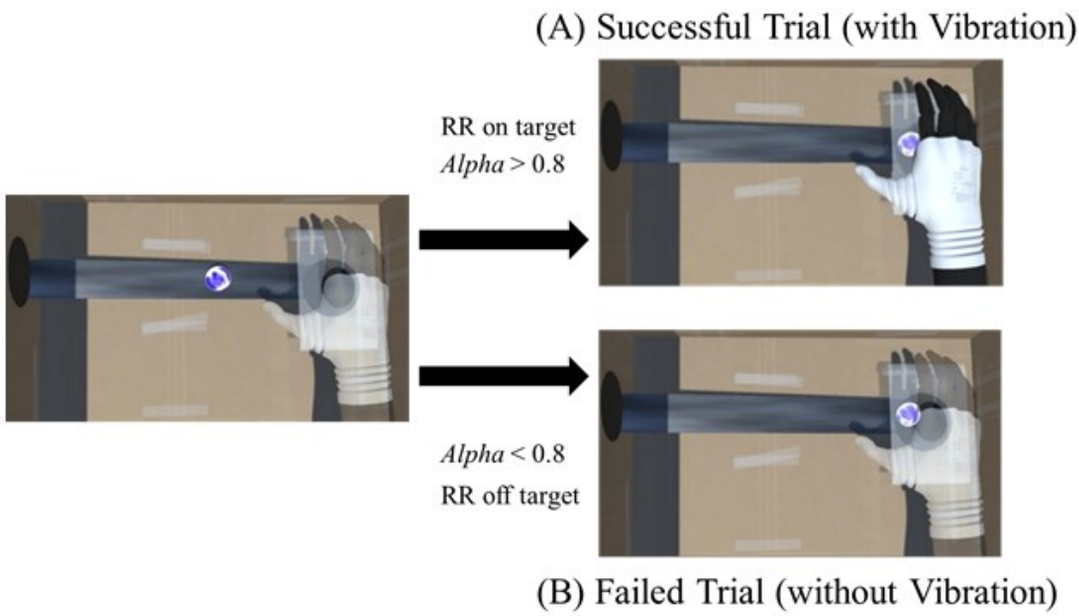

Figure 17 Trial examples of Spatially Augmented Respiratory Biofeedback.
Examples of **A:** successful trial (the sphere reaches the virtual hand in fully visible state) and of **B:** failed trial (the sphere reaches the virtual hand in transparent state).

and assessing the presence and the entity of the expected effects of slow RR.

2.2.3.3.1. Breathing Data

Breathing data was extracted by analyzing audio signal acquired during the experimental sessions. The procedure aims to detect the current breathing state of the subjects, and their changes: Rest, Inhalation, Exhalation.

The breath states detection was based on the loudness of the signal using an automated custom software (based on C# within a Unity project). The values used depended on this implementation of the SARB system, and they were manually defined by adjusting the values in [330]. Specifically, we classified the breath events with respect to the maximum amplitude of the recorded breath signal.

A headset was provided to the subjects to be used as an audio recording source. This allowed to comfortably keep a microphone close to the breathing sound source. The headset is a Canyon CORAX Gaming Headset CND-SGHS5, representative of entry level, non-professional devices which might prove affordable for home setups. The experimental setup is positioned in a controlled room to exclude major sources of noise.After acquiring the audio signal, a custom software evaluated current breath states of the subjects: Rest, Inhalation, Exhalation. This step was performed by computing the signal loudness and testing it against a set of threshold values. Starting from the signal loudness, the baseline noise allows to detect the Rest State: $Loudness < InhaleMin$. Small amplitude variations determine the Inhalation State: $Loudness \in [InhaleMin, InhaleMax]$. Big amplitude variations determine the Exhalation State: $Loudness > ExhaleThresh$. The thresholds chosen for the present experiment are: 0.05 for *InhaleMin*, 0.1 for *InhaleMax*, 0.3 for *ExhaleThresh*. A different microphone setup might require an adjustment of these values, since they strictly depend on the characteristics of the analyzed signal, which is itself heavily influenced by the audio acquisition factors mentioned above.

Breath frequency detection was performed over audio signal blocks of the duration of 1s each. This analysis was executed by design at 50Hz (every 20ms): this implies an overlap of 980ms between consecutive audio signal blocks. The sequential steps to detect the breathing frequency were: (i) acquisition of an audio signal block of the duration of 1s, (ii) calculation of the envelope of the signal representing the loudness (expressed as the root mean square of the raw signal) of the microphone signal multiplied by a scale factor of 10 and the pitch (power spectrum of the signal), (iii) detection of the breathing phases (Rest, Inhalation, Exhalation), (iv) removal of artifacts, (v) computation of the breathing frequency.

Artifact removal (step iv) is required since, despite the controlled setup (headset microphone + controlled room), the recording arrangement for this experiment is still extremely sensitive to background sound and to speech. As a consequence, artifacts had to be removed by filtering the signals and excluding what had to be considered false breathing states triggers. In particular, a rejection procedure was implemented which excluded all the Exhalation and Inhalation state change triggers that were produced by a sound pitch out of the 500 – 4000 Hz band. Artifact removal was performed through our custom software solutions, developed in C#.

The exhalation loudness is considerably higher than the inhalation loudness. Therefore, the exhalation event is easier to detect and for each of them a time stamp (Te_t) is saved to finally determine the frequency of breath (Fb_t):

$$Fb_t = \frac{60}{Te_t - Te_{t-1}} \tag{2}$$

Where *Fb* is the new breath frequency at the time *t+1*, Te_{t+1} is the time stamp event of exhalation at time *t+1* and Te_t is the time stamp event of exhalation at time *t* (time in seconds, breathing frequency in breaths per minute).

2.2.3.3.2. Respiratory Biofeedback

The biofeedback depended on the condition of the task, asking the subjects to keep a "Slow Breathing" rate (about 6 breaths/minute) [331] or "Normal Breathing" rate (about 14 breaths/minute) [332].

For both conditions, when a new frequency of breath was detected, it was compared with the target breathing rate (*Fopt*) to produce a value between 0 (transparent) – 1 (opaque) of transparency (*Alpha*):

$$Alpha_t = \begin{cases} \frac{Fopt}{Fb_t}, & Fb_t > Fopt \\ \frac{Fopt}{(2 * Fopt) - Fb_t} & Fb_t < Fopt \end{cases} \tag{3}$$

For the success of the task in each trial (fully visualizing the 3D model of the prosthesis before the sphere disappears), the hand transparency (*Alpha*) needs to be higher than 0.8 (Figure 17 A). When transparency was lower than 0.8 (Figure 17 B) at the end of the trial, the sphere fell down the hole and the task was considered failed. Each trial started with an *Alpha* = 0.5.

During preparatory tests of the initial prototypes of the setup, the quick changes in the hand visibility often constituted a serious obstacle to the subjects' training to perform the task, especially when the sphere was approaching the hand.

Consequently, a facilitation ($f = 0.05$) of the task was introduced to increase the degree of success in case of occasionally breathing rate far from the target during the entire task:

$$Alpha_t = \begin{cases} Alpha_t, & Alpha_t > Alpha_{t-1} \\ Alpha_{t-1} - \mathrm{f} & Alpha_t < Alpha_{t-1} \end{cases} \quad (4)$$

If *Alpha* was greater than 0.8 at the end of the trial, the visuo-tactile vibration feedback was generated as co-occurrence of the visual shaking of the virtual hand on the screen and the vibration of the smartphone, placed under the real right hand, as caused by the collision of the sphere and the hand.

To enable such a haptic event, an API was developed for allowing the control of smartphone vibration and to set up wireless communication (based on a local network) between the laptop and the smartphone. This connection was based on a Unity (Windows) desktop app sending to a Java back-end (running on a Tomcat server) a request for a Unity (Android) mobile app that triggers the vibration of the smartphone when the virtual hand-sphere collision happens.

It must be noted that latency is expected when triggering events across a network. Even for a LAN network, latency is usually negatively affected by wirelessly connected components (e.g. the smartphone used for the experiment). Nonetheless, such latency was not noticeable (under 100 ms) when triggering the events required by this experiment, even more so given the slow pace of the tasks.

2.2.3.4. In-Session Data Collection and Processing

During the experimental sessions, both data collection programs (Unity custom program and BioGraph) were running on the same laptop, allowing for a data synchronization based on the laptop-generated timestamps. The data generated by the Unity software were collected in a text file, named with the ID of the subject and containing the list of breathing events with their time stamps during the experiment. The data collected through the FlexComp Infiniti system were recorded and exported in a text file through the BioGraph software at 2048 Hz. Downsampling at 256 Hz was performed to allow data synch with the breathing data generated by the Unity software.

The power spectrum of each BVP sequence was reconstructed through the Welch method (8 Hamming windows with 50% overlap). Frequencies in the 0.05 to 0.5 Hz (corresponding roughly to 3 to 30 breath per minute) have been considered as generated by respiratory activity, thus the center of the frequency bin with the highest power provides a good estimate of the RR. The RR value, expressed in breaths per minute, was then simply estimated by multiplying the obtained frequency by 60.

GSR in each trial was compared for checking potential anticipatory responses to upcoming virtual stimuli (possibly related with the hypothetical different degrees of embodiment in slow and normal breathing conditions): each sequence was normalized as to have a mean value of 0 and a standard deviation of 1, then the value at time 0 was subtracted from each sequence. Normalized sequences were

then averaged over trials and subjects for each experimental condition. It must be added that, in RHI studies, skin conductance typically offers information on individual reactions to threatening events [333]. However, this signal increases to both aversive [334] and appetitive stimuli [4]: thus, we decided to adopt it to evaluate potential anticipatory reactions to the (uncertain) outcome of the trial, when the hand could vibrate (marking a successful trial) or not.

2.2.3.5. Experimental Procedure

2.2.3.5.1. Instructions and Tasks

Session preparation

Initially, the subjects were asked to wear the (appropriately sanitized) headset and biosensors comfortably. All participants were asked to sit in front of a desk and to place their hands at the sides of a monitor lying (slightly tilted on a foam support towards the subject) on it.

Then, their right hand was placed on the smartphone (the amputees did not wear any prosthesis during the session, thus they placed the right stump on the phone). The position of the phone was marked with tape as a reference for the post-session estimation of the proprioceptive drift.

After this, the subjects agreed to start the experimental session, allowing the experimenter to begin the acquisition of the respiratory events and the physiological data and to change the Unity scenes (observed through a secondary screen) according to the commands of the participants during the session itself. Figure 18 shows the main Unity scenes and phases of the experimental procedure.

In the first scene (Figure 18, scene 1), the experimenter inserted the subjects' number, set the connection between the laptop and the smartphone through the local network, and chose the breathing condition. In the second scene, the investigator filled the subjects' personal data while reading aloud the different sections to properly transcribe the subjects' answers.

After this, the first instructions scene introduced a 3-minute video (Figure 18, scene 2). This video had the goal to induce a neutral mental state before initiating the actual experimental session. The investigator asked the subjects to stay still while fixing the cross in the middle of the screen.

Training and testing trials

Subsequently, the second instructions scene was read aloud by the experimenter (Figure 18, scene 3), who explained the upcoming short training sample. This scene contained different instructions about the task according to the experimental condition of the ongoing session:

- in the Slow Breathing (low RR) condition, the subjects were asked to maintain the respiratory rate at a slow pace (about 6 breaths/minute) to make the virtual hand "materialize" (become visible) enough for feeling the energy of the sphere when it approached the virtual limb,
- in the Normal Breathing (typical RR) condition, the subjects were asked to maintain the respiratory rate at a normal pace (about 14 breaths/minute) to achieve the same goal.

In both cases, the subjects were invited to blow on the microphone when they were breathing out. This instruction was given to help the participants in maintaining the expected pace and to produce a sound correctly interpreted by the SARB system.

As described before, by maintaining the right RR of the assigned condition (Slow Breathing or Normal Breathing), during the sliding of the energetic sphere from the hole on the left wall to the hole under the Hannes 3D model, the participants were able to decrease the transparency of the virtual hand to make the virtual hand solid enough to "feel" the energy of the approaching sphere as a vibration. This event meant that the trial was successfully accomplished (Figure 17 A). This task was expressed by asking the subjects to "make the hand visible and solid enough to intercept and the sphere and feel its energy". The duration of each trial was 1 minute: the time spent by the sphere to move from the left hole to the right hole on the screen.

Once a training session constituted by 2 trials (Figure 18, scene 4) was completed, the subjects had to decide to repeat the training or proceed. There was no limit in the repetition of the training trials.

When the participants declared to be ready to start the experimental session, a series of 16 trials started (Figure 18, scene 5), each one based on the 1-minute animation and the respiratory biofeedback task described above. Each trial started after the end of the previous one within the same scene: the sphere disappeared into a hole under the virtual right hand and re-appeared on the left side of the screen. The resulting visuo-haptic events are far less frequent than the ones in typical RHI and VHI studies: this choice depended on the need to perform the biofeedback exercise over an appropriate time to reach the target respiratory pace.

Subjective questionnaire

After completing the experimental trials, the subjective questionnaire scenes appeared instantaneously (Figure 18, scene 6).

The experimenter read aloud the questionnaire instructions, asking the subjects to rate their experience during the session through a score from 1 for "Total Disagreement" to 5 for "Total Agreement" per each statement. Through this, the participants defined how much they disagreed/agreed with the following 14 statements that represented different aspects of virtual hand ownership (items 2, 3, 4) and real hand disownership (items 9, 10, 11) and individual experience – stress (item 1), emotional engagement (item 12), interoceptive intensity (item 13), perception of the relationship between virtual hand visibility and breathing rate (item 14) (Table 7). Control items (5, 6, 7, 8) were included for checking the subject's compliance with the experimental instructions.

The subjects read silently by themselves each of the 14 statements, divided in 3 scenes, and told the investigator the different scores. To conclude, the experimenter asked the subjects to estimate the duration of the experimental session (in minutes) for evaluating further potential effects of the breathing condition. The questionnaire was partially adapted to the case of the amputees, referring to their "limb" instead of their "hand".

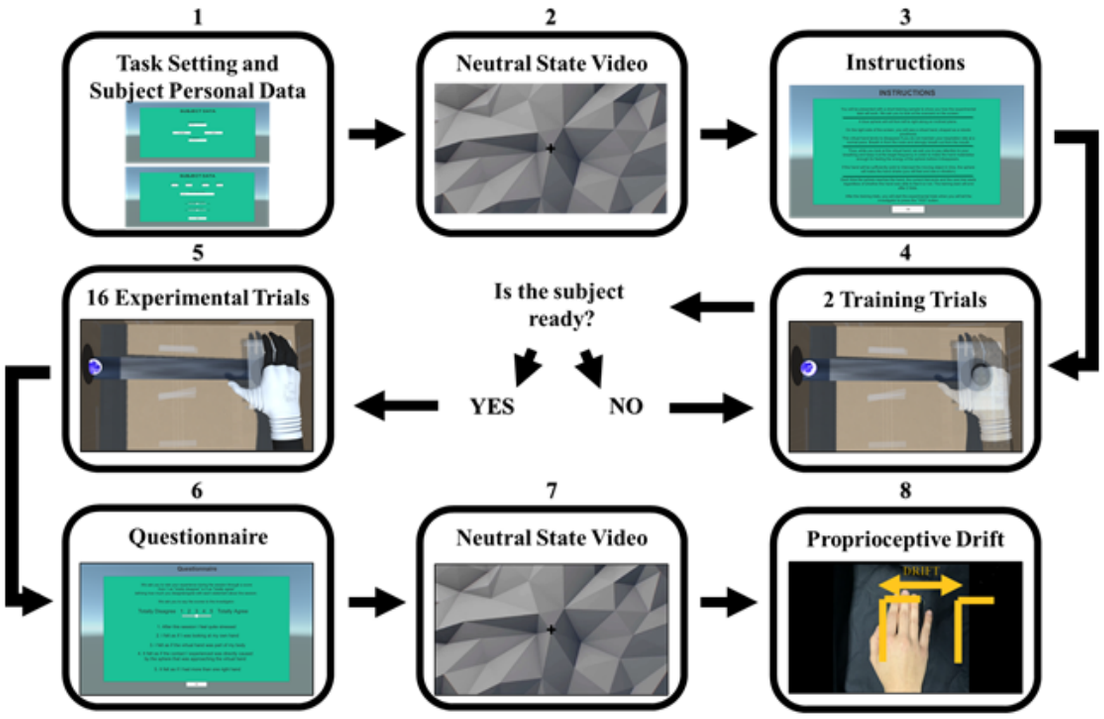

Figure 18 Experimental phases.

Proprioceptive drift measurement

After collecting the questionnaire answers, the experimenter moved to another instruction scene concerning the final 3-minute video to induce a neutral state (Figure 18, scene 7) for restoring the neutral state before measuring the proprioceptive drift (Figure 18, scene 8). Once the video was over, the participants were asked to close their eyes, and the black blanket on the right arm was removed. The reference position of the phone (previously marked by tape) was checked after removing the blanket. If the phone had been moved during the session by more than 5 mm in any direction the following measure of the drift would have been considered unreliable. Otherwise, the researcher marked this position of the phone as final reference position, representing where the phone (thus, the right hand) was during the experiment. After this, the participants were asked to raise their right arm while holding the smartphone and to wave it around to briefly stretch.

Thus, the participants were asked to relocate the smartphone in the perceived initial position, always while keeping the eyes closed. Differently, the prosthesis users only raised their right limb (always with closed eyes) and, after the experimenter removed the smartphone to avoid obstacles, they placed the stump where they felt it was during the session. The estimated position of the phone (which, in the case of the prosthesis users was re-placed by the experimenter under the relocated stump) was marked with tape to facilitate the measurement of the drift from the reference position, previously marked with tape too.

The lateral distance between the reference position of the phone and the one estimated by the participants were measured by the experimenter, together with the direction of the deviation (Figure 19). To measure the drift we assumed the reference position of the phone during the session as 0 point of a

continuous horizontal scale with negative values to the left (towards the virtual hand) and positive to the right.

This strategy to estimate a proprioceptive drift was specifically devised for this setup, considering how it could facilitate this part of the experiment in home training sessions: marking with tape the position of a rectangular object representing the hand position is far easier than performing the same operation with the hand itself as a reference.

After this, the sensors, the headphones, and the blankets were removed, and the subjects were free.

2.2.3.5.2. Experimental Design and Statistical Analysis

In a within-group experimental design, all participants performed the tasks under Slow Breathing and Normal Breathing conditions. Each condition was experienced by the participants in different days

Table 7 Subjective questionnaire scores (median, Mdn; median absolute deviation, MAD; mean, M; standard deviation, SD).

N	Questionnaire Items	Slow Breathing				Normal Breathing				
		Mdn	MAD	M	SD	Mdn	MAD	M	SD	
1	After this session I feel quite stressed	2	1	2.55	1.26	3	1	3.00	0.93	
2	I felt as if I was looking at my own hand	2	0	2.14	0.71	2	0	1.91	0.53	
3	I felt as if the virtual hand was part of my body	3	0	2.50	0.60	2	0	2.05	0.65	*
4	It felt as if the contact I experienced was directly caused by the sphere that was approaching the virtual hand	3	1	2.95	0.90	2	0	2.27	0.83	**
5	It felt as if I had more than one right hand	1.5	0.5	1.77	0.92	2	1	1.68	0.72	
6	I felt as if my real hand was turning virtual	2	0	1.91	0.53	2	0	1.73	0.63	
7	I felt as if I could move the virtual hand	2	0	1.95	0.58	2	0	1.82	0.59	
8	It felt as if the contact I experienced came from somewhere between my own hand and the virtual hand	2	1	1.91	0.81	2	0	1.86	0.56	
9	It seemed as if my hand had disappeared	2	0	2.23	0.87	2	1	2.32	0.89	
10	It seemed as if I could not really tell where my hand was	3	0	2.50	0.80	2	1	2.36	0.95	
11	It seemed as if I was unable to move my hand	3	0	2.77	0.75	2	0.5	2.36	0.73	**
12	I felt emotionally involved in the situation	3	1	3.05	1.00	3	1	2.95	1.09	
13	I perceived intensely my bodily sensations	3	1	3.14	1.21	3	1	3.18	1.01	
14	I felt the relation between my breath and my virtual hand	3	1	3.18	1.22	4	1	3.55	0.96	

*, $p < 0.05$; **, $p < 0.01$ (Wilcoxon signed-rank test between conditions of Slow Breathing and Normal Breathing).

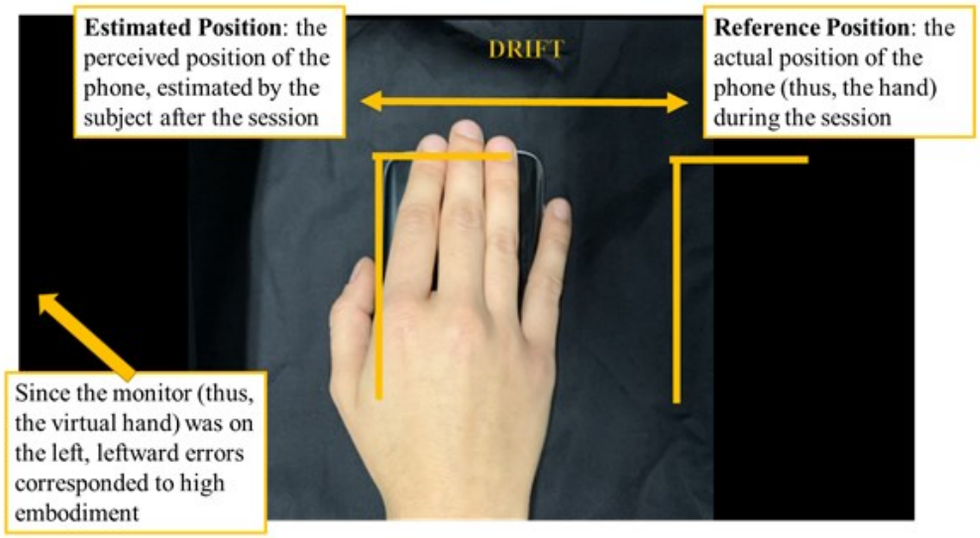

Figure 19 Proprioceptive drift measurement
only the lateral error from the actual phone position (reference position) was considered.

with max 14 days between sessions. The order of sessions was counterbalanced, by also accounting for gender and age (as much as possible) to compose the resulting 2 sub-groups: eleven (3 females) subjects (Age, mean ± SD: 27.6 ± 2 years) who were presented the Slow Breathing condition in first session and the Normal Breathing condition in second session, and eleven (3 females) subjects (Age, mean ± SD: 27.2 ± 2.8 years) who were presented the condition in the opposite order. Following the exploratory function of this preliminary study, we used two-tailed tests for observing potentially significant differences in both directions.

The questionnaire data were analyzed via Wilcoxon signed-rank test with the breathing condition - Slow Breathing vs. Normal Breathing - as factor. The scores of each item were compared. Further comparisons were based on average scores per sub-set of questionnaire items as global indices of ownership, disownership, and control as in [335].

Session time estimation and proprioceptive drift were analyzed via paired samples t-test with breathing condition as a factor.

The frequency of respiratory events was analyzed to assess the feasibility of this setup by evaluating the participants' capability to control their own number of breaths per trial (being each trial 1-minute long) according to the instructions. The breathing condition being the factor, the breaths per trial were analyzed via Student's t-test. The same comparison was performed for the number of successful trials as a performance measure (the number of trials in which the subjects made the virtual hand vibrate).

GSR signals have been analyzed to identify possible time segments for which responses differed significantly from the end-point value, implying a possible anticipatory response. Given the normalization described in 3.4, this analysis consisted simply in testing grand-averages across subjects and trials to identify time segments with median values different from zero. Specifically, a Wilcoxon signed-rank test for zero median has been conducted on the skin conductance signal. In order to prevent

possible false positives due to slow signal drift, this analysis has been limited to the last 10 seconds of recording before each visuo-tactile event.

All analyses were performed using JASP (https://jasp-stats.org) [336], R (https://www.r-project.org/), and Matlab (MathWorks, Inc.), and $p < 0.05$ was considered significant. The next section focuses on the significant results in all comparisons, with statistically relevant information like the effect size (Cohen's d for the parametric tests, rank-biserial correlation for the Wilcoxon signed-rank test) [337] and the test assumption check (only Shapiro-Wilk test of normality for repeated measures parametric tests with one 2-level independent variable).

2.2.4. Experimental Results

2.2.4.1. Virtual Hand Ownership

In the Slow Breathing condition, participants reported stronger feelings that the virtual hand was part of their body (item 3, with $W = 106$ and $p = 0.035$), that the contact experienced was directly caused by the sphere that was approaching the virtual hand (item 4, with $W = 122$ and $p = 0.003$), and that they were unable to move their own right hand (item 11, with $W = 96$ and $p = 0.022$), compared to the Normal Breathing condition (see Table 7). Rank-biserial correlation was used to estimate the effect size and the related confidence interval, respectively with values of: (item 3) 0.559 and 95% CI [0.074, 0.83], (item 4) 0.794 and 95% CI [0.482, 0.927], (item 11) 0.6 and 95% CI [0.117, 0.853].

Significant differences were found between the control (5, 6, 7, 8) items average score and, respectively, the ownership (2, 3, 4) items average score ($W = 220.5$ and $p < 0.001$ in Slow Breathing, $W = 195$ and $p = 0.027$ in Normal Breathing) and the disownership (9, 10, 11) items average score ($W = 206.5$ and $p < 0.001$ in Slow Breathing, $W = 223.5$ and $p = 0.002$ in Normal Breathing). Rank-biserial correlation was used to estimate the effect size and the related confidence interval. For the ownership-control comparison: 0.909 and 95% CI [0.776, 0.965] in Slow Breathing, 0.542 and 95% CI [0.128, 0.794] in Normal Breathing. For the disownership-control comparison: 0.967 and 95% CI [0.912, 0.988] in Slow Breathing, 0.767 and 95% CI [0.489, 0.903] in Normal Breathing.

A significant difference ($W = 153.5$ and $p < 0.001$) was also found between the ownership average scores in each breathing condition (Table 8). According to rank-biserial correlation, the effect size and the related confidence interval are respectively 0.795 and 95% CI [0.508, 0.923].

Overall, the participants estimated the total duration of the task (16 minutes) as: 11.55 ± 5 minutes in Slow Breathing, 12.77 ± 4.03 minutes in Normal Breathing (no significant difference between conditions).

Considering the proprioceptive drift, no subject moved the phone during the session (before the drift estimation) by more than 5 mm in any direction: thus, all measures were included in our analysis. According to the collected data, the breathing condition significantly affected the proprioceptive drift: $t(21) = -3.558$, $p = 0.002$, $d = -0.759$, CI [-1.23, -0.276] (Figure 20). The drift comparison between Slow

Breathing and Normal Breathing successfully passed the Shapiro-Wilk test of normality, with 0.975 ($p = 0.824$). The participants estimated the position of the smartphone, i.e., their right hand, to the left of its actual location (averagely by 0.91 ± 2.58 cm) and closer to the monitor i.e., the virtual hand, in the Slow Breathing condition. The same estimation was to the right of its actual location (averagely by 1.45 ± 2.45 cm) in Normal Breathing condition.

The analysis of GSR (planned as in 3.5.2) shows that, in the considered time window, the measured values are significantly different from the end value at the 0.05 significance level only in Normal Breathing condition (between 1.7 s and 1.3 s before the end of the trial).

2.2.4.2. SARB Feasibility

Figure 21 highlights how the subjects followed the instructions for each condition according to the data collected through the microphone and processed by the custom Unity software. No significant difference can be found considering both the breathing condition and the trial repetition as factors. However, in the Slow Breathing condition participants maintained 5.8 ± 2.5 breaths per trial, overall. This value was significantly lower than the Normal Breathing condition, 10.7 ± 2.6 breaths per trial, as expected: $t(21) = -8.382$, $p < 0.001$, $d = -1.787$, CI [-1.459, -1.098]. The comparison successfully passed the Shapiro-Wilk test of normality, with 0.951 ($p = 0.335$).

Additionally, an exploratory analysis of BVP values was performed for extracting the frequency of respiratory events and comparing it to the data collected by the Unity software, showing no significant difference between them in each breathing condition.

Before moving on to the experimental session, 4 participants asked to repeat (1.75 ± 0.5 times, by average) the training session in Slow Breathing condition. 3 of these subjects needed to repeat (1.33 ± 0.58 times, by average) the training session in Normal Breathing condition too. Then, over 16 total trials, the participants were able to make the virtual hand “shake” (when, at the end of each trial, the transparency index *Alpha* > 0.8) by average (without significant differences): in 10.77 ± 4.94 trials under Normal Breathing condition, and in 9.36 ± 3.44 trials under Slow Breathing condition.

2.2.4.3. Preliminary Test with Users of Prostheses

Both the users of upper limb prostheses involved in this study followed our instructions in terms of breath control. In Slow Breathing condition, one subject (who repeated the training session 2 times) had a mean 6.3 ± 2 breaths per trial and the other (1 repetition of the training) had 4.94 ± 2.5 breaths per trial. In Normal Breathing condition, they respectively had (after repeating 2 times and 1 time the training) a mean number of breaths per trial of 11.31 ± 2.5 and 13.19 ± 3.02. About task performance: in Slow Breathing condition they respectively achieved 8 and 12 successful trials over 16, and in Normal Breathing condition 15 and 11. These preliminary tests with 2 amputees suggested the potential for implementing home-based embodiment training systems with affordable solutions for respiratory biofeedback in amputees.

Table 8 Average scores of items on ownership, control, disownership (median, Mdn; median absolute deviation, MAD; mean, M; standard deviation, SD).

Questionnaire Items Average Scores	Slow Breathing				Normal Breathing				
	Mdn	MAD	M	SD	Mdn	MAD	M	SD	
Ownership (items 2, 3, 4)	2.67	0.333	2.53	0.54	2.17	0.167	2.08	0.52	**
Control (items 5, 6, 7, 8)	1.88	0.375	1.89	0.45	1.75	0.25	1.77	0.42	
Disownership (items 9, 10, 11)	2.67	0.5	2.5	0.66	2.33	0.5	2.35	0.75	

**, $p < 0.01$ (Wilcoxon signed-rank test between conditions of Slow Breathing and Normal Breathing).

Overall, their questionnaires showed higher scores than the individuals interviewed for the main study, surpassing the middle value of the 5-point Likert-type scales. The scores (Table 9) demonstrate medium-high values of ownership and engagement with a minimal stress. The session time estimation reported by each subject in both conditions was lower than the actual 16 minutes of trials, respectively: 10 minutes and 15 minutes in Slow Breathing, 5 minutes and 10 minutes in Normal Breathing.

The proprioceptive drift of each subject tended in both conditions towards the virtual hand, respectively: 3 cm and 4.7 cm in Slow Breathing, 3 cm and 2.5 cm in Normal Breathing.

2.2.5. Discussion

This study provides preliminary evidence of how self-regulation techniques (via respiratory control) can increase the processes of body ownership underlying the embodiment of a virtual right hand. It also highlights the feasibility of the implementation of SARB within the boundary of remote studies.

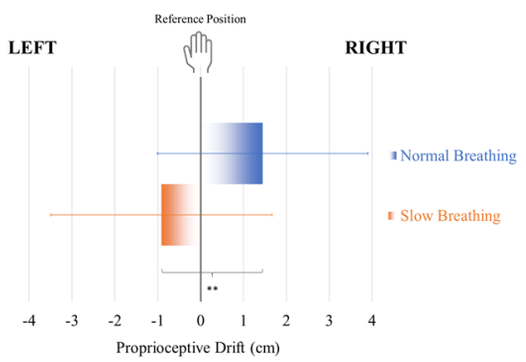

Figure 20 Comparison of proprioceptive drift (cm) from the reference position of the hand (0) in conditions of Slow Breathing and Normal Breathing, with means and standard deviations. **, $p < 0.01$ (pairwise Student's t-test between conditions of Slow Breathing and Normal Breathing).

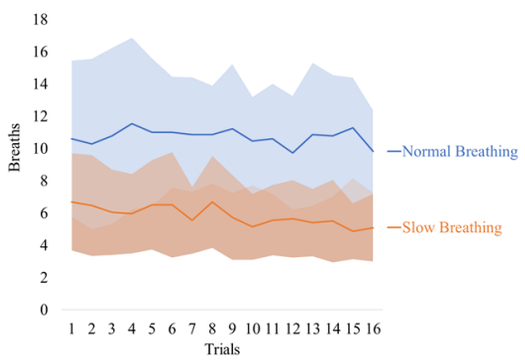

Figure 21 Means (continuous lines) and standard deviations (shaded areas) of breaths per trial in conditions of Slow Breathing and Normal Breathing, along the 16 trials (1 trial per minute).

Table 9 Post-trials subjective evaluation questionnaire scores reported by the two users of upper limb prostheses.

N	Questionnaire Items	Slow Breathing		Normal Breathing	
		Subject A	Subject B	Subject A	Subject B
1	After this session I feel quite stressed	1	2	1	2
2	I felt as if I was looking at my own limb	4	3	4	3
3	I felt as if the virtual limb was part of my body	5	2	4	3
4	It felt as if the contact I experienced was directly caused by the sphere that was approaching the virtual limb	5	4	3	4
5	It felt as if I had more than one right limb	1	1	2	1
6	I felt as if my real limb was turning virtual	5	1	3	1
7	I felt as if I could move the virtual limb	3	2	2	3
8	It felt as if the contact I experienced came from somewhere between my own limb and the virtual limb	1	2	1	4
9	It seemed as if my limb had disappeared	1	1	5	2
10	It seemed as if I could not really tell where my limb was	1	1	1	3
11	It seemed as if I was unable to move my limb	5	3	5	2
12	I felt emotionally involved in the situation	4	3	4	3
13	I perceived intensely my bodily sensations	5	3	5	3
14	I felt the relation between my breath and my virtual limb	5	3	5	3

Our results (questionnaire scores, proprioceptive drift) indicated that slow feedback-controlled breathing vs normal breathing may improve the ownership process, i.e. increasing the sensations that the virtual hand was part of the subject's body and that the vibration experienced by the subject was caused by the sphere on the screen. While both aspects are directly connected to the embodiment process (which depends on the perceived relation between self and body), the last one could also be related to the feeling of presence: the experience of "being there" in a mediated environment [338].

Thus, we can infer that the Slow Breathing condition made the participants feel that their body was extended (through the artificial limb) into the digital on-screen component of the SARB environment, when compared to normal breathing. Such an effect needs further investigation while studying the role of Slow Breathing in improving presence and avatar control, also considering the relationships between embodiment and presence [339]. Interestingly, the assessment of the subjects' feeling (reported through questionnaire responses and spontaneous remarks) of being unable to move their own right hand, unveils a side-effect of Slow Breathing in terms of disownership.

The SARB setup was effective in monitoring individuals' breathing, processing the respiratory rate and providing the desired feedback to the users. The subjects were able to follow the instructions properly, generating two different condition-specific breathing rates. However, we noticed that the subjects tended to have a lower respiratory rate than the target, and their performance in terms of successful trials was quite variable across the subjects (highlighting how maintaining an appropriate RR to trigger the vibration can become complex to manage). These observations point at the need of a task re-design for facilitating the execution of the biofeedback training, especially considering the high inter-subject variability of the successful trials in this study (pointing at potential usability issues for certain participants) and the potential effects of workload on body ownership measures [10].

Furthermore, such a re-design should also focus on improving the user engagement, since the setup was just moderately able to stimulate the participants through its current gamification features. Indeed, most questionnaire scores did not overcome the middle point of 3 in the 5-point Likert-type scales, and anticipatory responses were just weakly detected in GSR patterns only under Normal Breathing condition. This could depend on the fact that our implementation of SARB was based on a limited number of tactile events: 16 occurrences (1 per minute) just in case the person performs the task correctly in each trial. In classic RHI studies, these stimulations are more frequent and numerous in a shorter time, making most people experience the illusion within the first minute of the session [340]. Furthermore, our SAR environment was probably less immersive than the ones used in most VHI settings. VHI studies typically provide a strong perceptual continuity between computer-generated body parts (hand and arm) of the subject within the same immersive context, with advantageous effects on the embodiment measures. However, our goal was to observe if these measures were significantly different in Slow Breathing condition and Normal Breathing condition within the same setting, and this was confirmed by our preliminary data. In any case, the role of the attentional effects of respiratory control needs to be also considered by, for example, separating focus-attention on breathing from the feedback-control components.

Considering its methodological value, our SARB-based procedure can be considered an original addition to the heterogenous family of RHI studies [341]. Specifically, SARB can constitute an affordable home training system for the embodiment, but it needs further design improvements, possibly exploiting more game-based features to engage the users, This can be a promising strategy, especially if validated through long-term home experiments [232], even within wider and engaging digital health

protocols [342]. The opportunity of using this kind of approach for developing novel strategies to investigate psychopathological conditions will also be considered, especially when the interoceptive processes are involved, as in [343], for example.

Being aware of the limitations of this initial study, we are anyway encouraged by the current preliminary results: SARB constitutes a viable approach in implementing a self-regulation of psychophysiological states to promote the embodiment of an artificial limb through a Slow Breathing condition. Furthermore, this study offered the opportunity of preliminarily testing our hypothesis and our setup before proceeding with further laboratory investigations and with extensive home data collection sessions.

Accordingly, the dual value of the investigation presented in this paper suggests 2 possible directions for the next steps of this research (envisioning their subsequent convergence too).

- Psychophysiological studies (in laboratory) would allow to investigate specifically the EEG correlates of the virtual hand embodiment [344] in a SARB setting (using chest belts to precisely monitor RR). A potential target could be the study of Slow Cortical Potentials (SCPs, 0.01–0.1 Hz) [345] correlated with the heartbeat and the respiration cycle, thought to be also implicated in stimuli integration [346].

- User experience studies (in laboratory and in remote contexts) on the SARB setting would initially help to improve the usability of the setup, making the task easier and more engaging (possibly personalizing the target RR through adaptive and co-adaptive features) for the participants in upcoming remote online sessions (even as daily game-like training) [347]. The visual scene will be improved with further graphic details to achieve a more compelling experience (e.g., substituting the black area around the right hole with a more realistic texture). This would include amputees exploiting the respiratory biofeedback strategy for training the embodiment of artificial limbs.

Extending the sample size will also allow for controlling factors based on the subjects' traits and habits (e.g., playing videogames or sports, smoking). Importantly, their body image and interoceptive awareness should be assessed [348] alongside the personality features [349].

Further investigations must also demonstrate if the effects of the SARB-based training persist over time, and if an actual generalization of the embodiment of the 3D model of a prosthesis can be observed for the actual device [11], possibly exploiting the latter in game-like XR remote trainings designed to engage the users. This solution (alongside with the adoption of ecologically valid settings as in neuroergonomics research) [350] could counter the apparent lack of RHI-susceptibility in subjects who feels prosthetic limbs ownership mainly when the devices are used in daily life (Zbinden & Ortiz-Catalan, 2021).

As discussed above, this kind of RHI-resistance was found in meditators [304]. However, differently from previous studies, we explored the embodiment as a process affected by an active respiratory control within a biofeedback protocol instead of just presenting a typically passive RHI-like test without asking to perform any respiratory task. Accordingly, we hypothesize that the fine control of RR matured through meditation practices could be advantageous in SARB procedures, possibly working as a

preparatory activity to our respiratory biofeedback for embodiment training – especially for patients attending telerehabilitation protocols and amputees waiting for their prosthesis.

2.2.6. Conclusion

This pilot study presented a novel, affordable strategy for empowering the feeling of owning a virtual hand through an individual self-regulation method based on a respiratory control aiming at slow breathing. The design of the setting, targeting remote studies, showed the feasibility of implementing such a system with common devices owned by users like a computer, a monitor, a smartphone, and a microphone. Thus, this proof of concept offered a preliminary (methodological and technological) background for developing novel user-centered strategies in research and design to facilitate the embodiment of artificial limbs.

2.3. Improvements to an under-actuated Prosthetic Hand toward a dexterous 2-DoF Wrist

2.3.1. Introduction

The human hand is the most complex and functional part of the human body [94, 244], therefore, the loss of the upper limb is a highly traumatic event. Engineering a replacement is, till nowadays, a challenge both from mechanical and control perspectives. Due to these difficulties in the correct development of a prosthetic device, the long-term abandonment is still high, 30-50% [226, 243].

A forearm-level amputation does not only involve the loss of the hand but, in many cases, also the loss of the wrist. The human wrist is a 2 Degrees-of-Freedom (DoFs) joint, namely the ulnar-radial deviation (URD) and the flexion-extension (WFE). Nonetheless, with forearm-level amputation also the pronation-supination (WPS) is lost, even though its anatomical joint is located in the elbow. As consequence these three DoFs are crucial for manipulation and interaction and their loss affects greatly the amputees' quality of life. It is known, from splinting studies of the wrist, that if a subject is not able to pose the hand in the correct orientation, even the most advanced hand struggles in performing prehensile tasks [351, 352].

As a consequence, the absence of wrist mobility limits the orientation capability of the hand hence leading to compensatory movements [353], adding stress on the body and causing overuse complications for the remaining joints [351, 354]. Bertels [355] demonstrated how even a single DoF prosthetic wrist coupled with a prosthetic hand can greatly reduce the amplitude of compensatory movements.

According to the assessment of user-needs, it is crucial to mimic the native human wrist, both in terms of available DoFs and control capability [356]. During Activities of Daily Living (ADLs), users underlined the need for several improvements such as multiple and selectable wrist active movements, simultaneous control of wrist and grasps, wrist position feedback and others [356].

Nonetheless, user-controllable actuated prosthetic wrists have largely been ignored in the literature, in comparison to the efforts devoted to hand prosthesis development [351, 357, 358]. In fact, there are very few commercial myoelectric wrist prostheses available on the market, chiefly the Ottobock pronation-supination Electric Wrist Rotator [359], the Fillauer MC Wrist Rotator [360] and Fillauer Powered Flexion Wrist [361], all of them offering just one active DoF. In addition, research devices such as the Keshen KS-Bionic Hand with an actuated pronation-supination and flexion-extension wrist [362], the ToMPAW modular arm [363] and DARPA Modular Prosthetic Limb [364] DEKA "Luke" Arm [365] have been developed, but have yet to be made commercially available for a prosthetic use [366].

This paper hence presents an innovative 2-DoFs prosthetic wrist, analysing its design and demonstrating its mechatronic performances according to the user's needs. Therefore, we underline how the combination of the CE marked underactuated prosthetic hand Hannes [11] and this avant-garde 2-

DoFs wrist, addresses the most demanding tasks which, usually, other devices fail to accomplish. To meet the assessment of users' needs [356] we aim to control this innovative wrist by means of leading-edge strategies such as pattern recognition (PR) [12]. This led to improved control, both in terms of naturalness and intuitiveness, of the multi-DoF prosthetic device.

Moreover, we demonstrate that advanced PR techniques presented in [13] can be successfully applied to the presented new system, by considering its application to real-life scenarios.

In this paper, we present the design and the realization of such 2 DoFs wrist for prosthetic applications. We preliminarily identify the system requirements as highlighted in section I.2.3.2, to then address a detailed description of the mechanical, electrical and control design of prosthetic systems in section I.2.3.3. Moreover, a description of the performed testing methodology phase is disclosed to validate the overall design in section I.2.3.4, whereas the corresponding experimental results are presented in section 2.3.5. Finally, in sections I.2.3.6 and I.2.3.7 we outline the impact of this work and propose future applications of the system.

2.3.2. System Requirements

The Hannes hand was designed using a bio-inspired and holistic approach. The result was an under-actuated hand prosthesis that nonetheless strongly exhibits biomimetic behaviour of the human hand [367]. Hannes is already capable of performing three main categories of grasp, using a passive, manually operated thumb adduction: power grasp, precision grasp and lateral grasp. The under-actuated differential mechanism of the Hannes hand has been already presented and discussed [367], therefore, we focus here on the novel design of the 2 DoFs wrist.

With a similar design approach, our goal was to develop a 2-DoFs prosthetic wrist including flexion-extension (WFE) and pronation-supination (WPS) characterized by biomimetic performances in terms of range of motions (RoMs), speed and torque hence consenting user to perform the most demanding ADLs.

In the following part of this manuscript, we firstly present the biological and technical requirement as inspired by ADLs (Section A and B respectively), followed by the kinematic layout (Section C) and finally the power and safety aspects (Section C and D respectively) considered along with the development phases.

2.3.2.1. User's needs-driven requirements

The human wrist joint has three DoFs that can be simultaneously moved. The wrist itself possesses two DoFs: WFE and URD. In addition, the forearm ulnar and radius bones provide WPS movement [368-370]. Since this rotation ability is largely lost by trans-radial amputees it can be considered integral to wrist functionality and a relevant characteristic for a prosthetic wrist system to fulfil. To be able to effectively replicate the functionalities of its biological counterpart, the hand-wrist prosthetic system, should possess the following features:

1) RoMs, torques and speed must be comparable to the ones attained by humans during ADLs [11];
2) Robustness – each actuator must resist peak loading forces substantially above peak torques exerted during ADLs, in case of a fall or improper use [11]
3) Anthropomorphism – the system must approximate the size of the human hand and forearm [11]
   a. Low weight – Since this characteristic is strongly correlated with abandonment rates [371, 372], the system must weigh less than the human hand and arm, needing to be similar to commercial prostheses (see Table 10)
   b. Low overall length – The type of arm amputation and lost functionality is unique for each patient. The minimum overall length will maximise the number of patients that can benefit from a wrist prosthesis system. As up to 70% of amputations are distal to the elbow [373], and assuming that the average trans-radial amputation occurs halfway along the forearm, then the total length of the wrist prosthesis should not exceed 50% of the female 5th percentile of forearm length (around 97mm) [374].
4) Ease of Control and low latency – From the Assessment of user needs [356], it emerges how the wrist is explicitly required by the amputees, since, as already stated, the positioning of the hand is crucial in everyday activities. Moreover, focusing on the users' requirements, the ease of control and the non-disturbing time delay in wrist movements are both crucial. To deal with these, we developed a low-level control strategy (section I.2.3.3.3) for the wrist and tested the device involving an online control through PR.

2.3.2.2. Design Requirements from the perspective of ADLs

Literature on RoMs, torques and speeds characterizing each joint of the human arm during 23 ADLs and the SHAP Test [375] was used to define the desired DoFs, kinematic layout, and desired peak torque and peak joint velocity of each wrist. The SHAP test is a standardized clinical protocol for estimating and comparing patient hand and wrist dexterity in ADLs [376]. Although simulated activities only approximate functional ones [377] they can estimate the minimum required prosthesis performance.

In addition, whilst RoMs during ADLs are well defined by studies of wrist motion, with the worst-case values found in literature used for each joint [378], there is much fewer data and much higher variation regarding joint speeds and torques [357]. Commercial WPS wrist devices are capable of 80 deg/s whereas others are as high as 300 deg/s. Previously published researches on wrist WPS and WFE speeds have noted that 175deg/s is a suitable value to be functional [379], whereas for WFE prosthesis the target rotation speed is 150deg/s [380]. Information on nominal and peak wrist torques is even more lacking as most studies focus on maximal wrist torques, nevertheless, minimum torque requirements for

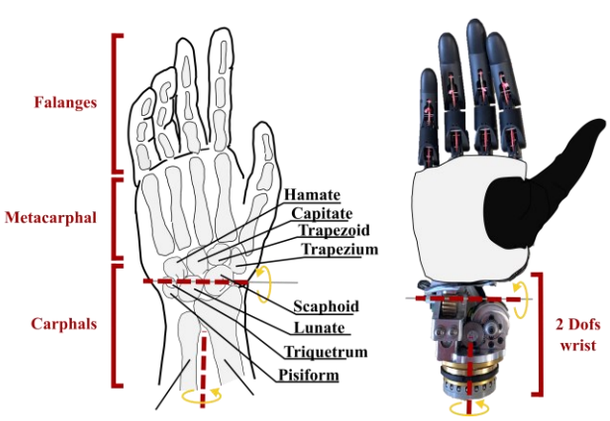

Figure 22. Individual joint rotation axes and layout of prosthesis vs human hand and forearm.
4 mm of misalignment among the human and the 2 DoF wrist.

TABLE 10 BIOLOGICAL & ADL REQUIREMENTS

Joint	Length [mm]	Mass [g]	ADL RoM [deg]	Peak Torque [Nm]	Velocity [rad/s]
Wrist FE	20-30	100	-70 to 50	-3.5 to 3.5	4
Wrist PS	60	100	-65 to 77	-6.0 to 4.0	7
Wrist URD	50	150	-18 to 20	-0.2 to 0.3	-0.2 to 0.3

the WFE and WPS wrist can be estimated from the literature [381]. However, in Section **2.3.4**, it was decided to estimate more accurate values from able-bodied volunteers using motion capture hardware.

2.3.2.3. Kinematic Layout Required for ADLs

F. Montagnani et al. demonstrated that the removal of the ulnar-radial deviation DoF using a custom-designed orthosis resulted in the smallest increase of compensatory movements during the SHAP test Southampton [382]. In fact, a 2-DoF wrist (WPS and WFE) coupled with a 1-DoF hand (open/close), performed very similarly to an anatomical hand during SHAP tests. Other studies conducted on able-bodied subjects similarly demonstrated how the URD can be regarded as the least important upper limb movement [383, 384].

Based on these findings and the limiting requirement to minimize the prosthetic wrist weight and overall length, a 2-DoFs device with WFE and WPS was developed, as this would offer similar functionalities compared to a 3-DoFs wrist prosthesis. Moreover, to increase the human-like behaviour, we decided to couple the 2-DoFs wrist with an underactuated prosthetic hand (Hannes) capable to express very high biomimetic performance as demonstrated in [385].

2.3.2.4. Power Consumption Requirements

As an upper limb prosthesis must embed the power source, the aim is to minimize the motors power consumption, to gain a sufficient battery autonomy during daily use. As stated in [222], and confirmed during the clinical evaluation performed in 2017 with Hannes [386], transradial amputees perform an average of 150000 main grasp movements per year, resulting in 411 movements per day.

Therefore, we set the requirement to perform at least 500 combined hand and wrist movements with a single battery charge, considering a 1:1 ratio between hand and wrist usage. Moreover, we designed the WFE drivetrain to be non-backdrivable, allowing static loads to be resisted without motor torque contribution, therefore greatly minimizing current consumption in static poses [357]. Non-backdrivable transmissions allow to choose smaller motors, since the dynamic active torque requirements during ADLs are low compared to the maximum passive torques that the human wrist can be subjected to [387]. Additionally, the joint will remain static when subjected to sudden external load changes or during a power loss, also resulting in a more predictable control and safer use by upper-limb prosthetic users.

2.3.3. Design of Prosthetic System

In this chapter, the prosthetic system will be analyzed in all its parts. Firstly, in Sections 2.3.3.1 and 2.3.3.2, respectively the mechanical and electrical architectures of the device will be described in their entirety. Subsequently, in Sections 2.3.3.3 and 2.3.3.4, the control strategies, both low and mid-level, applied to this system will be discussed and detailed.

2.3.3.1. Mechanical Architecture

The arm mechanical architecture is serial and modular by design (Figure 22): the WPS and the WFE wrist joints are separate, to allow the insertion of an Ottobock-style quick-disconnect (QD) Locking Unit [388] and electrical slip-ring namely Coaxial Plug [389] with its counterpart within the wrist in the socket, named Co-Axial Bushing [390] (Figure 23B, Figure 24B and C). The slip-ring provides power and control signals to the hand during WPS rotation. Moreover, this architecture provides a variable total system length making the prosthesis adaptable to the type and severity of patient amputation (distal or proximal) by also maintaining the compatibility with the existing amputee socket design. This precluded the investigation of an integrated parallel wrist mechanism for simultaneous multiple DoFs motion such as Stewart-platforms or quaternion wrists, even though such systems are often more compact than serial chain devices [391].

2.3.3.1.1. WFE Wrist Design

According to the previously presented design requirements (section 2.3.2), hereafter we describe the design solution to match the anthropomorphism of the WFE wrist rotation axis equipped on the Hannes hand. The misalignment between the mechanical and the anatomical rotation axis should not be greater than 5-7mm (Figure 22). Moreover, the overall mechanism should be as small and noiseless as possible to prevent user discomfort [392]. On the other hand, to prevent excessive battery consumption in case of high static loads, non-backdrivability is another crucial aspect to consider. Therefore, the WFE wrist powertrain presents a 3-stage gearbox directly connected to the drive motor (Faulhaber BXT22H) and a slow shaft encoder (Figure 23). In detail, the first stage is a [(13/3):1] planetary gearbox, that allows lowering the revolutions-per-minute (RPMs) of the BLDC motor while keeping high efficiency ($\eta \approx 0.9$) that guarantees high torque to drive the subsequent gear-stage. The second stage shifts the rotation

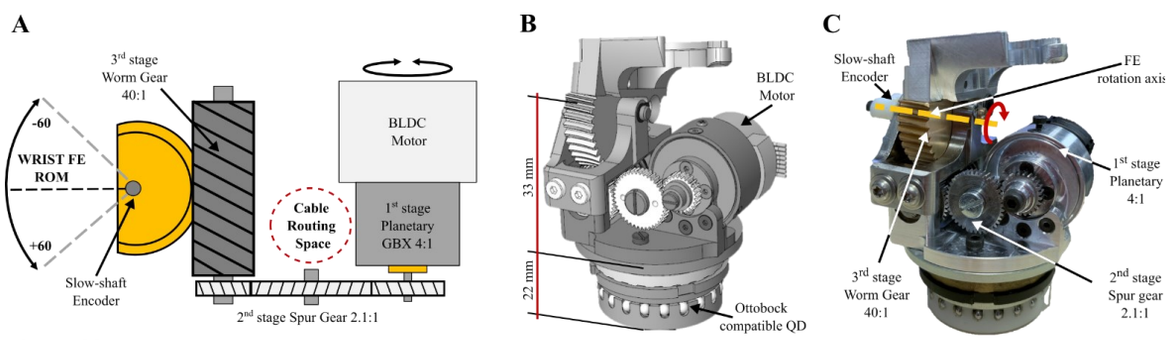

Figure 23.
WFE wrist: A) Simplified diagram of mechanical design, B) Placement of the mechanical components and C) the real WFE wrist device.

axis to the physiological position of the human wrist with a [1:2] spur gear to reduce still maintaining high efficiency ($\eta \approx 0.9$).

The supplementary reduction of the resultant angular velocity is fundamental to reduce the noise of the previous gear's stages and to provide a sufficiently high torque to the third stage that will then waste a considerable amount of torque due to its low efficiency ($\eta < 0.4$, $0.25 < \eta < 0.4$) [30:1]. Thanks to its precise dimensioning, this third stage allowed to achieve the correct alignment of the rotation axis. Moreover, it is crucial to grant the non-backdrivability of the entire mechanism, by means of its low efficiency. This characteristic, coupled with the correct dimensioning of the frame and the third gear stage, make the wrist able to hold up to 50kg in steady condition without any battery consumption and makes it possible for the user to lean on the wrist, for example, when standing up from a chair leveraging on the upper limb for stability purposes and reducing harmful compensatory movements.

The design of the entire wrist WFE mechanism allows 82 deg of RoM in detail having 33 deg in extension and 49 deg in flexion, mimicking the natural conditions (40 deg in extension and 38 deg in flexion hence having 78 deg of RoM) of healthy subjects [384].

2.3.3.1.2. WPS Wrist Design

The WPS wrist main design requirement was to be hollow shaft, to allow fitting the single slip-ring located in the Ottobock-style Laminating Ring [393]. The actuator unit is composed of a frameless PMSM motor (TQ Motors ILM25x04) [394] directly integrated with the strain-wave reducer's wave generator [100:1] (Harmonic Drive HFUC 11-100-2A R), forming a hollow shaft actuator, allowing cable passage between the hand prosthesis and the socket electronics. The output of the strain-wave reducer is connected to the female output of the quick-disconnect adapter. The design permits the hand prosthesis and WFE wrist actuator to be quickly attached and detached by the patient, whilst ensuring a robust electrical connection between the two halves of the prosthesis system, namely the hand and the socket.

The resultant mechanism is characterized by an overall length of 55mm (Figure 23B) and a 45mm diameter which offers a one-to-one replacement with the Ottobock-like Locking Unit and its related counterpart, the Ottobock-like Laminating Ring [395] which is also capable to accommodate the active component namely Electric Wrist Rotator [396] by Ottobock.

On the mechatronic side, our custom device can exert higher angular velocity and torque on the slow shaft in respect to existing commercial solutions. The direct connection between the Harmonic Drive and the BLDC motor [394] grants a single reduction stage (Figure 24). The overall power-train efficiency of 80% can be achieved by aligning the bell-shaped efficiency behaviour of the reducer with the one described in the motor datasheet. Conversely, commercial prosthetic wrists offer a cascade of reduction stages that lower the device's efficiency. As consequence, our solution aims at increasing the overall efficiency to design a reversible mechanism that, at the same time, allows the Ottobock-like Locking Unit to disconnect the wrist from the hand thanks to the breakaway torque of the powertrain.

2.3.3.2. Electrical Architecture

From an electrical point of view, the system is conceived to be modular and self-contained (Figure 25): the hand itself contains all the motor drive electronics necessary to move the main grasp motor and the WFE wrist motor in closed-loop. All the hand and wrist movements are controlled via a single microcontroller (Texas Instruments TM4C123GH6PM [397]) embedded in a single rigid-flex control board system (SCMM), minimizing space requirements and power consumption overhead. The onboard electronics include a 9-axis IMU module [398], to provide the angular orientation of the hand expressed in quaternions via I2C protocol to the motor control unit of WPS wrist (SCMPS) . The system includes two contactless absolute on-axis magnetic encoders (AMS AS5045B [399]), to provide absolute position feedback and diagnostics via SPI protocol. The SCMM allows to implement all the necessary safety features as for IEC60601-1 medical device standard, including sensor diagnostics, overcurrent, overload and short circuit protection on all the active joints. The overall system architecture includes a central processing board (EMGM) and up to 6 surface electromyography (EMG) sensors, compatible with both Ottobock electrode or custom circular EMG sensor Marinelli, et al. [15] developed by Rehab Technologies lab of Italian Institute of Tecnology. The EMGM board hosts a microcontroller (Texas Instruments TM4C123GH6PM), acquiring the EMG signals. The EMGM board is placed above the wrist joint, and acts as a master of a CAN Bus network, sending position references to the SCMM board, for controlling hand and wrist WFE via SCMFE, and retrieving various measurements from the SCMM board, such as the joints current, the measured joint position, the angular orientation, and the system status. Additionally, the EMGM board hosts an IMU module, to gain information about the angular orientation of the stump and control directly the WPS wrist control board (SCMPS) movement accordingly (Section 2.3.3.3).

All the information gathered by the prosthetic systems is then provided via Bluetooth Low Energy to a host system graphical user interface (GUI), which can allow both therapists or researchers to perform tuning of the control parameters, the activation thresholds, check the system diagnostics,

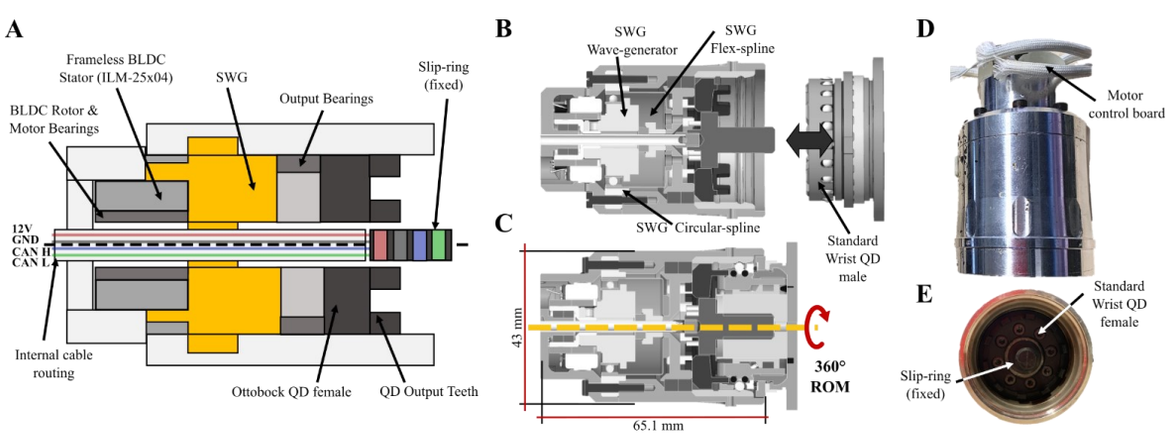

Figure 24.
PS wrist: A) Simplified diagram of mechanical design, B) Placement of the mechanical components and C) the real WFE wrist device.

TABLE 11 DAILY POWER CONSUMPTION

Joint	Average Current [A]	Average Power [W]	Energy per Movement [J]	Movement Time [s]	Number of Movements	Overall day energy consumption [J]	Percentage on battery charge [%]
Hand	0.75	9.2	7.4	0.8	500	3700	3.7
Wrist PS	0.2	2.4	3.5	1.5	500	1750	1.75
Wrist FE	0.16	2	5	2.5	500	2500	2.5
Idle state	0.07	0.86	-	-	-	48240	48
Total			-			**56209**	**56.2**

visualise, and log the data in real-time. All the data are available to a frequency up to 100Hz via custom communication protocols.

The system is equipped with a custom battery pack, made of 3 lithium-ion certified cells in series (11.1V nominal, 2.5Ah capacity, 27.75Wh energy, 99900Joule) and a battery management system, carefully designed to fit in the gap between the residual stump and the wrist joint, hence allowing to directly embed the system electronics and power supply in most of the transradial amputation cases. To confirm that, we made a simple evaluation of the power consumption, measuring the battery current absorption at a fixed voltage (12.28 V) in respect of the worst-case movements of each joint (highest speed), using an oscilloscope (Tektronix MDO3034) and a current probe (Tektronix TCP0020). We then computed the net electrical power and the energy absorbed for each task. Additionally, we measured the overall system consumption in an idle state, with all the motors enabled but not moving with respect to the daily energy balance we considered a 16 hours per day duty cycle, compared to the energy available with a full charge. The results of this analysis are resumed in Table 11: it can be observed that the main energy use is due to the idle state (48%) rather than during the movements.

However, is shown that the system can be easily operated, in an average use, for 16 hours consecutively with a single charge, having a good residual charge (43.8%).

2.3.3.3. Low-Level Control Design

We developed a control strategy that allows both intuitiveness and non-disturbing time delay ,in agreement with the assessment of user needs [356]. For the WFE wrist joint we implemented a position Proportional-Integral-Derivative (PID) controller by using the custom encoder as feedback (see Figure 23*C).* Conversely, due to the lack of space, no embedded encoder was possible to fit in the WPS joint. Therefore, a virtual encoder was used as feedback to the WPS position loop. In particular, the virtual encoder is obtained by using two IMU (Bosch Sensortech BNO055 [398]) located on the two links, respectively the hand and the socket. These sensors extract quaternions used to compute the angular WPS position via a custom algorithm. The “Relative Angle and Orientation” (RAO) algorithm computes the angle between the hand and the forearm, avoiding singularities. The procedure is presented hereafter.

Knowing the standard definition of a quaternion (***Q***) and its conjugate (***Q****):

$$\begin{aligned} Q &= [q_w, q_x, q_y, q_z] \\ Q^* &= [q_w, -q_x, -q_y, -q_z] \end{aligned} \tag{5}$$

setting Q_{pre} and Q_{post} as quaternion relative respectively to pre-joint and post-joint link, it is possible to define the rotation quaternion of the joint as follows:

$$Q_R = [Q^*_{pre} \cdot (Q_{post} \cdot Q^*_{pre})] \cdot Q_{pre} \tag{6}$$

Once Q_R is evaluated by knowing the actual possible DoFs of the joint, the angles along the principal axis (α_x, α_y, α_z) can be computed. Knowing the structure of the quaternion from Eq.1, the angles can be calculated as follows:

$$\alpha_i = 2 \cdot atan\left(\frac{Q_{R_i}}{Q_{R_w}}\right) \quad \text{, with } i \in [x, y, z] \tag{7}$$

Calculations run in a built-in routine on the EMGM board, retrieving link quaternions from the peripheral sensors and computing the RAO algorithm. This computation efficient routine can run in real-time, as it computes the angles in 0.172 ms (13760 clock cycles) on an ARM Cortex M4F running at 80MHz.

2.3.3.4. Mid-level Control Design

Furthermore, we implemented PR to control the Hannes system. To this aim, Nonlinear-Logistic Regression (NLR) algorithm was embedded into the EMGM's microcontroller as presented in two our previous works of Marinelli, et al. [13] and Di Domenico, et al. [12]. After the algorithm training phase, the users were able to operate the prosthesis in real-time by controlling 2 and 3 DoFs respectively.

The software architecture presents two main layers: the joint selection layer, which selects the joints to be controlled and the joint control layer, which computes the position references according to the EMG signal intensity.

Therefore, PR algorithm decodes the user intention and translates it into motor activation patterns by using up to 6 EMG electrodes, as shown in Figure 27 Each joint reference position is modulated

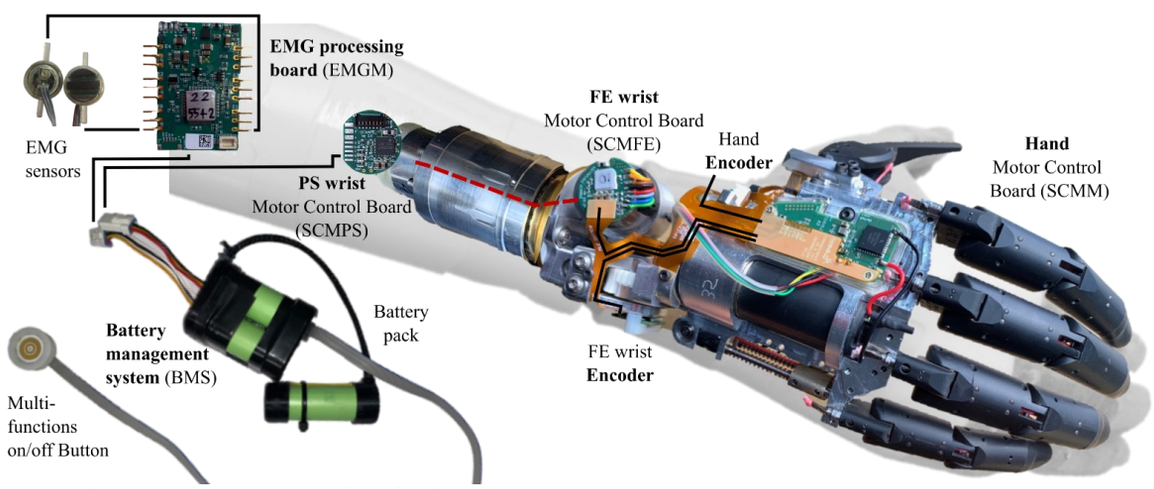

Figure 25. Electronic architecture of the full Prosthetics system.

according to the RMS of the 6 EMG signals, which is compared with two thresholds and amplified via a gain according to the formula:

$$Joint_{pos} += \frac{(RMS(sEMG) - LTh)}{H} * Gain \quad (8)$$

where, RMS is the root mean square of the EMG signals, LTh is the activation threshold optimized according to the validation set, H is a coefficient used to normalize the EMG amplitude according to the recorded signals during the calibration phase and Gain is a parameter to tune the joint speed according to the user needs.

2.3.4. Test Methodology

We developed a 3-phases testing methodology to gradually characterize and validate the performance of the device. A preliminary analysis in the frequency domain was performed to identify the dynamic behavior of the single joints' movements as presented in Section 2.3.4.1. Subsequently, in Section 2.3.4.2 we acquired the kinematics of able-body subjects performing ADLs and then used this information to validate the prosthesis' performances in mimicking these movements. Finally, a speed-torque analysis was conducted to outline the mechatronics performances achieved during ADLs as presented in Section 2.3.4.3. Moreover, to examine the control capabilities, an EMG-based PR algorithm was developed and tested on amputee as presented in Section 2.3.4.4.

2.3.4.1. Dynamic tests

We aimed at estimating the bandwidth of the wrist actuation unit in both WPS and WFE joints. To this end, we imposed a sequence of sinusoidal speed references, by increasing the frequency with step increments of 0.25Hz from 0.25 to 4.5Hz. Moreover, we chose the reference amplitude according to the mechanical RoMs of the system not to impact with the end of travels. We supplied the motor drive with fixed voltage and measured the joint speed output response comparing them with the imposed references. We then interpolated the voltage-speed transfer function to estimate the closed-loop mechanical bandwidth.

2.3.4.2. Able-Body Kinematics Recording

To the best of the authors' knowledge, there is a lack of accurate velocity (and torque) profiles of the human wrist joint during typical ADLs in literature. Therefore, we built a dataset of healthy subjects' wrist speed profiles performing multiple tasks. We then obtained reference kinematic trajectories to be applied to the 2-DoF wrist [377] to test its dynamic performance under load. The considered tasks were divided into two sections, namely the basic functional tests and fully functional tests. In the former, the subject separately performed simple movements (i.e., wrist flexion, wrist supination) and their combination (i.e., infinite trajectory). In the latter, we selected ADLs activities where the wrist movements play an essential role and recorded the joint angles via a Motion Capture (MoCap) system

described below. Eventually, each subject was asked to perform 5 tasks divided as presented in Table 12.

In detail, during the trials, the subjects were asked to perform each one of the tasks three times. Using a metronome, a rhythm was prescribed to impose three different speeds, namely “slow” (30bpm), “normal” (45bpm) and “fast” (60bpm). The subjects were asked to perform the task in the most natural way while following these rhythms to start each movement. Imposing a defined time frame to execute the task prevented unnecessary interruptions which could bias the acquired speed distribution. Therefore, a distribution of natural speeds was acquired and compared with the speed performances of the two wrist motors.

As shown in Figure 26, the setup consisted of a Vicon Nexus MoCap system, based on 10 Infra-Red (IR) cameras that record the movement of 12 IR-reflecting markers. This MoCap system, can guarantee a 0.01mm precision over a 48 m^3 of total volume of acquisition. This setup with the 12 IR markers allows the tracking of the whole arm, and, for this case, the detailed movement of wrist WPS and WFE. The VICON system has a fixed frame rate of 100Hz. This is consistent to Khusainov et al. [400], as 90% of human movements are under the 5Hz threshold. Therefore, we asked 8 able-bodied volunteers (age range: 25-32 years, 5 males and 3 females with self-reported hand and wrist dominance) to sit on a chair with their elbows fixed and close to their torso to minimize elbow and shoulder contribution. After the participants were marked with the 12 IR markers (according to the marker placement depicted in Figure 26C) they were asked to perform the 9 tasks. During each task, the movement was repeated 10

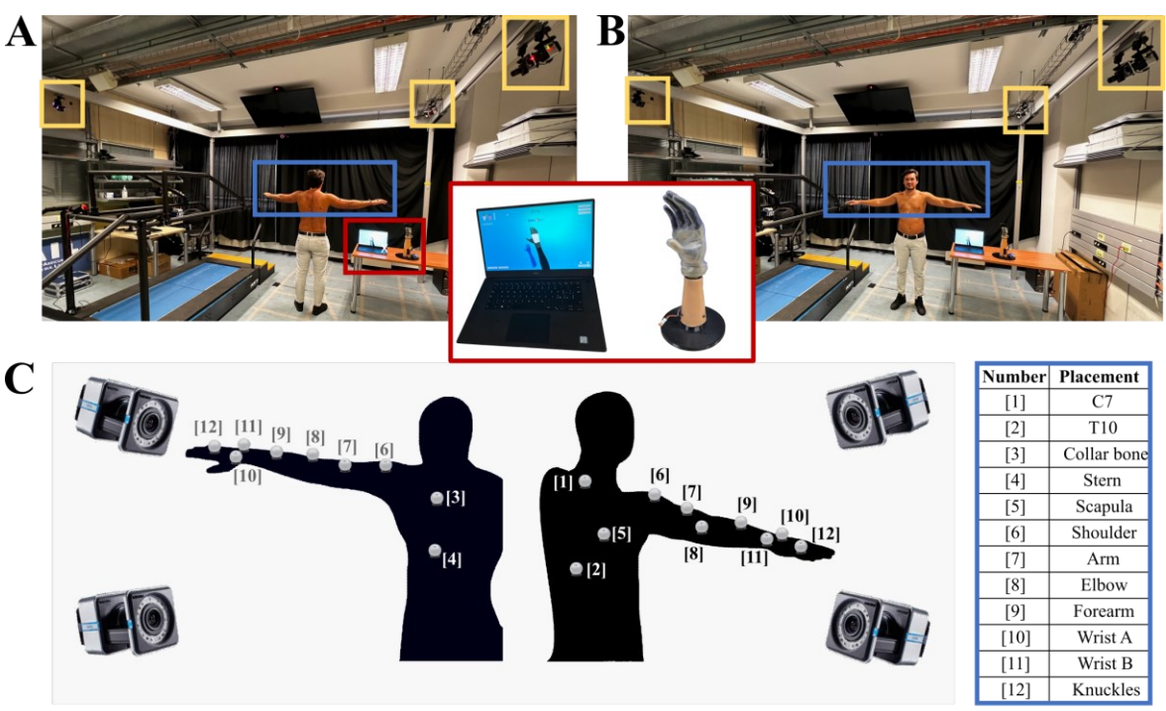

Number	Placement
[1]	C7
[2]	T10
[3]	Collar bone
[4]	Stern
[5]	Scapula
[6]	Shoulder
[7]	Arm
[8]	Elbow
[9]	Forearm
[10]	Wrist A
[11]	Wrist B
[12]	Knuckles

Figure 26.
Human-Prosthetic validation setup. (A-B) VICON Mo-Cap room, in yellow squares the IR VERO Cameras for marker tracking while in blue square the subject wearing the 12 markers. (C) Marker positioning scheme according to VICON user’s manual.

TABLE 12 PERFORMED TASKS.

Basic functional	Fully functional
Wrist Flexion-Extension	Stirring
Wrist Pronation-Supination	Jar Pouring
Infinite shape (combo WFE and PS)	-

times. Each subject performed each task with a 30s pause between them to prevent muscular fatigue. The test duration was approximately 20 minutes per participant.

2.3.4.3. Prosthesis Kinematic and Dynamic Test

We tested the speed and torque performances of the novel prosthetic wrist with the aim of assessing its reliability and its consistency in comparison with the natural equivalent. Therefore, we computed the joints speed Probability Density Function (PDF) of healthy subjects examined to obtain a reference distribution curve. The percentiles distribution (DST) of angular velocities were compared with respect to the speed performances for both WPS and WFE mechanisms. To this end, we chose the two most demanding basic functional tasks mentioned before for each DoF, executed at maximum achievable rotational speed. To stress the overall system in a realistic scenario, we loaded the prosthetic hand with a glass jug (300 gr) with 500 ml of water for the jug pouring task (WPS), and a heavy aluminium sphere (532 gr) for the lifting task (WFE). We recorded the joint position and the motor current to compute both speed and torque achieved. From this data we extracted the speed-torque required by the two powertrains while executing the tasks.

2.3.4.4. High-level Control Design

With the goal of validating the full system on a real application scenario, we tested advanced control strategies on the Hannes system [176, 356], first on healthy subjects and then on amputees. An EMG-based PR algorithm including proportional and simultaneous control of three active DoFs was developed by Di Domenico, et al. [12]: the Hannes hand's main motor, the WPS and WFE wrist. In this algorithm, the speed amplitude is proportional to the RMS value computed on the EMG signals, while the simultaneity is achieved by activating multiple movements of different joints. Both the setup and the classification algorithm were tested on 10 healthy subjects and 3 mono-lateral amputees (transradial amputation of the dominant limb). Each subject was asked to perform 10 repetitions of each gesture to be decoded (i.e., hand opening, hand closing, wrist pronation, wrist supination, wrist flexion and wrist extension) and to maintain the contraction for 2s. The acquisition of the muscular activity was performed by using 6 MyoBock (Ottobock) electrodes placed on the forearm (Figure 27) as described in [12]. The data collection was performed by using an ad-hoc software, EMG-Data Acquisition and Training Software [12], to associate the muscle contraction to the prosthetic movements. For each movement and

DoF the activation of the six EMGs generate a different pattern associated to the movement intention, Figure 27A.

Non-Linear Logistic Regression [12, 13] was used as PR algorithm to select the joint to move, as already offline tested by our group in different configurations. Moreover, we mapped muscle activation amplitude to selected joints' reference position Figure 27C), as described in formula (9):

$$\begin{cases} P_t = P_{t-1} + \Delta S \\ \Delta S = \dfrac{\left\| \sqrt{\frac{1}{N}\sum_{n=1}^{N} |EMG_n|^2} \right\|}{Fc} \end{cases} \quad (9)$$

where P indicates the position, the sum of the previous position and the increment (ΔS). ΔS is calculated with the normalized RMS of the N = 6 EMGs divided by the loop frequency of the microcontroller (300Hz) to limit the maximum increment to a value that controls the prosthesis full-RoM movement in 1s.

2.3.5. Results

Correspondingly with the methods presented in Sec. IV, we computed the open-loop Bode diagram (Section A), the able-body kinematics analysis (Section B) and the joint's speed-torque dynamic performances (Section C). Finally, in Section D we present the results obtained in a real scenario, in which machine learning techniques were used to offer an intuitive control strategy for the multi-DoFs Hannes system via EMG.

2.3.5.1. Dynamic test results

This analysis (Figure 28A) shows the speed closed-loop mechanical bandwidth of the prosthetic wrist drive at the maximum battery voltage (12.6V), defined as the intercept of the magnitude system response with the -3dB attenuation red line. The measured dynamic is around 1Hz for wrist WPS joint and 2Hz for WFE joint in their complete RoMs.

2.3.5.2. Able-Body Kinematic recordings results

Throughout the trials, the participants were instructed to perform movements without any specific guidance, ensuring that the angles measured were not influenced by any bias. Despite this, as depicted in Figure 28B boxplot, the healthy subjects' executed movements were contained within the mechanical Range of Motion (RoM) of the Hannes system. The prosthesis minimum and maximum RoM are indicated by the dotted lines. Specifically, the End-of-Travels (EoT) for the WFE wrist were designed to span from -49 deg to +33 deg, while the Wrist WPS could move freely without any restrictions; however, the EoTs were set to span from -90deg to +90deg. Therefore, these EoTs could be adjusted according to the subject's natural contralateral anatomy. In the boxplots, the squared regions represent the population from the 25th to the 75th percentile, the grey dashed lines indicate the entire population span and the red crossed indicates the outliers outside the Tukey fence.

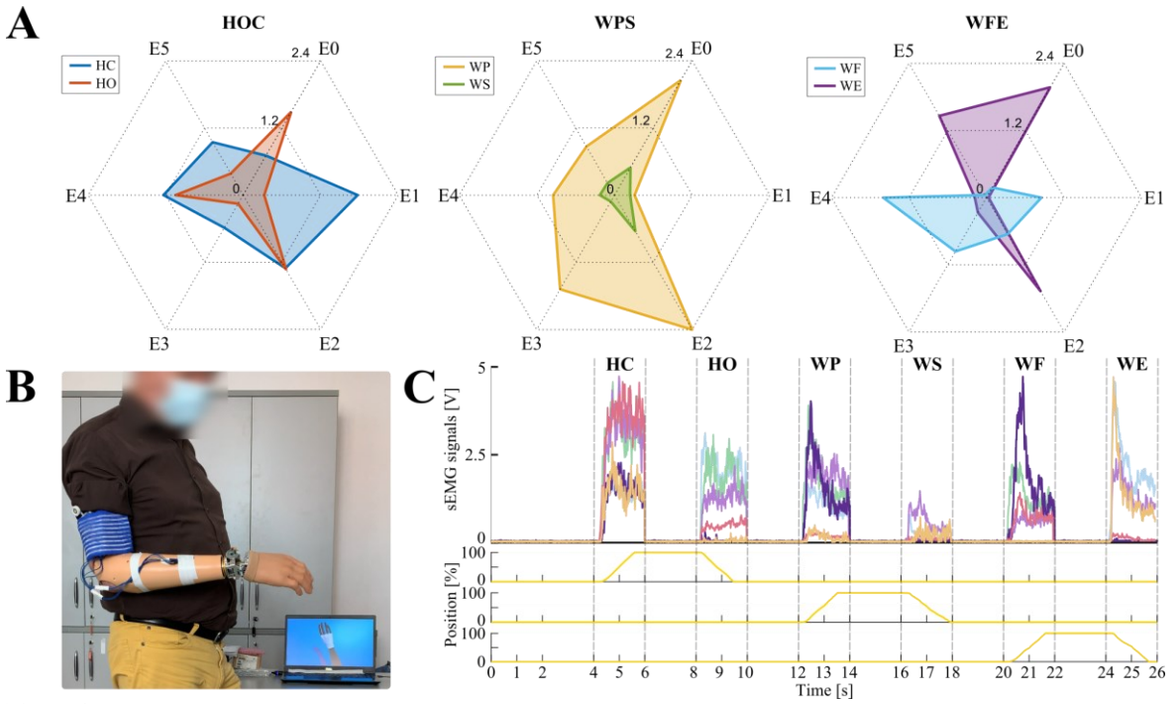

Figure 27.
(A) Radar plots of EMG signals amplitude for the various voluntary movements: Hand Open and Closure (left), Wrist Pronation and Supination (center), Wrist Flexion and Extension (right). (B) Fully integrated, wearable system fitted on a transradial amputee while operating the prosthetic arm. (C) Plot of 6 EMG signals amplitude (top) compared to the normalized position measurements of the controlled joints (bottom).

2.3.5.3. Performance Characteristics during ADLs

Figure 29A presents the human wrist's speeds distribution compared to the prosthetic wrist speed performance. The Probability Density Function (PDF) of healthy speeds, as well as the Distribution of the speed population (DST) in the form of a boxplot can be appreciated for both WPS and WFE wrist. These results are compared to the Hannes wrist's performance, represented by the grey shaded area. For the WPS joint, we observed a median value of 5.82 rpm (34.95deg/s), a 25th percentile of 1.51 rpm (9.06deg/s) a 75th percentile of 16.39 rpm (98.34 deg/s) and a maximum of about 38.7 rpm (232.2 deg/s). For the WFE joint, we observed a median value of 4.77 rpm (28.62 deg/s), a 25th percentile of 1.25 rpm (7.5deg/s) a 75th percentile of 10.12 rpm (60.72 deg/s) and a maximum of about 23.43 rpm (140.58 deg/s). The red crossed indicates the outliers outside the Tukey fence. Moreover, we observed that the data are substantially symmetric in respect of the sense of rotation.

Figure 7A depicts the torque-speed behaviour of the WPS and WFE wrist respectively performing the two most demanding selected tasks. The maximum rotational speed achieved by WPS wrist joint was around 360 deg/s (60 rpm) during glass jug pouring task whilst was around 180 deg/s (30 rpm) for WFE wrist while lifting a heavy sphere. The maximum torque exerted by WPS wrist joint was around 5.27 N during glass jug pouring task whilst was around 2.38 Nm for WFE wrist while lifting a heavy sphere. The dashed grey lines represent the power rating under load and no load, respectively 20 W and 10 W for the WPS and 4 W and 2 W for WFE wrist. We measured and RMS torque of 1.55 Nm for WPS and 0.88 Nm for WFE.

2.3.5.4. Control Design Test

Once the NLR classifier was trained, each subject was able to intuitively control the 3 different joints. The implemented control strategy (NLR) was able to suitably discriminate the patterns for the 6 different gestures as presented in Figure 8A. The radar plots show the6t EMG signals contribution among the classified movements. As consequence, the trained algorithm was able to decode the user intention and translate them into prosthesis actions. In Figure 27C, it is possible to appreciate the synthesis of the position references according to the EMG signals: in the upper side of the graph, EMG rectified signals are grouped together, in the lower side, we show the respective reference positions after the regression. Figure 27B shows the fully integrated system controlled by a transradial amputee. Since the NLR algorithm runs directly embedded in the EMGM control electronics, the system is wearable and usable in a realistic clinical scenario. As a result, the subjects were able to control the prosthesis' ROMs by combining each movement as for ADLs.

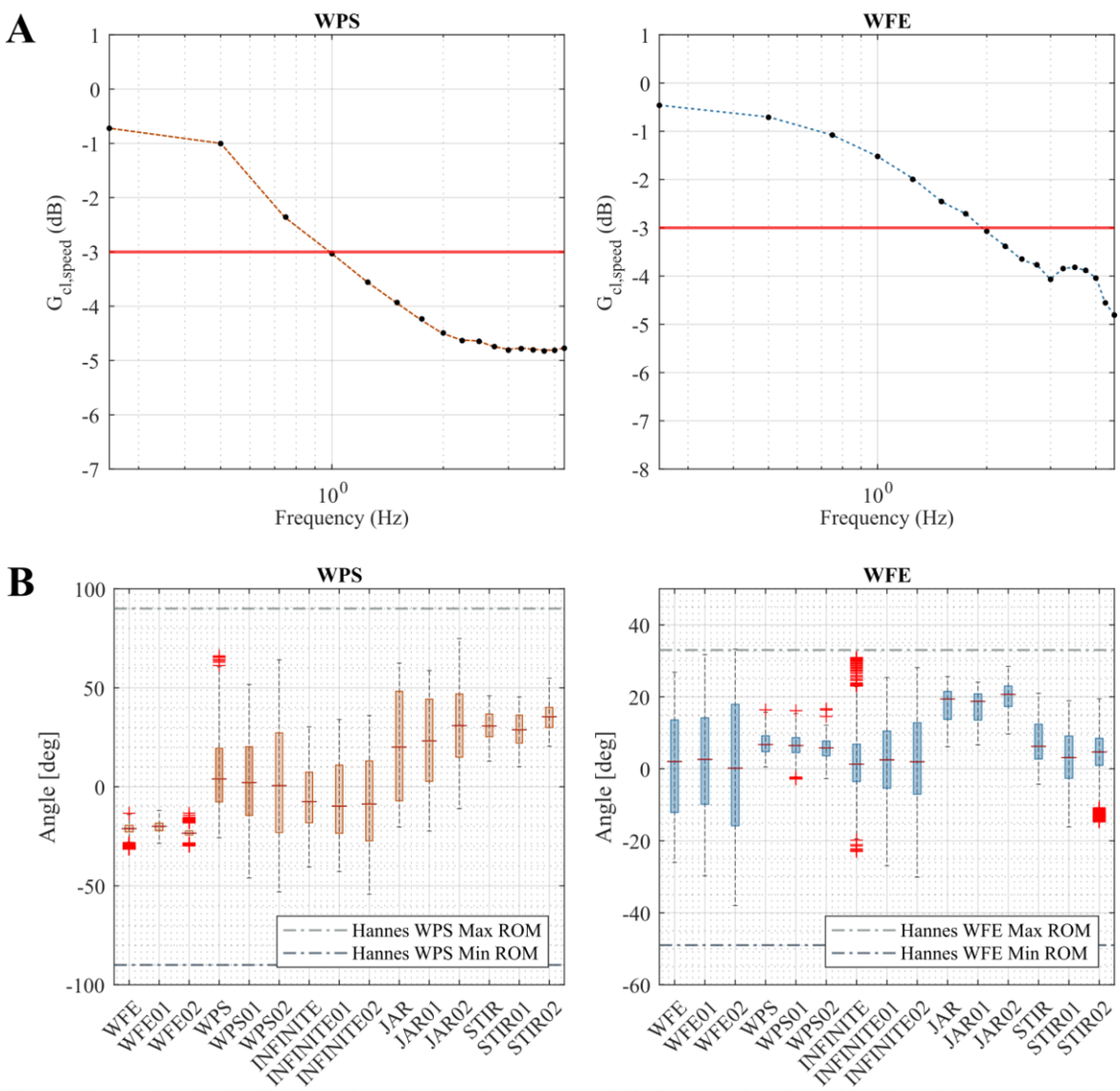

Figure 28. (A) Bandwidth diagram of prosthetic wrist motors, and (B) Ranges of motion of healthy subjects during trials.

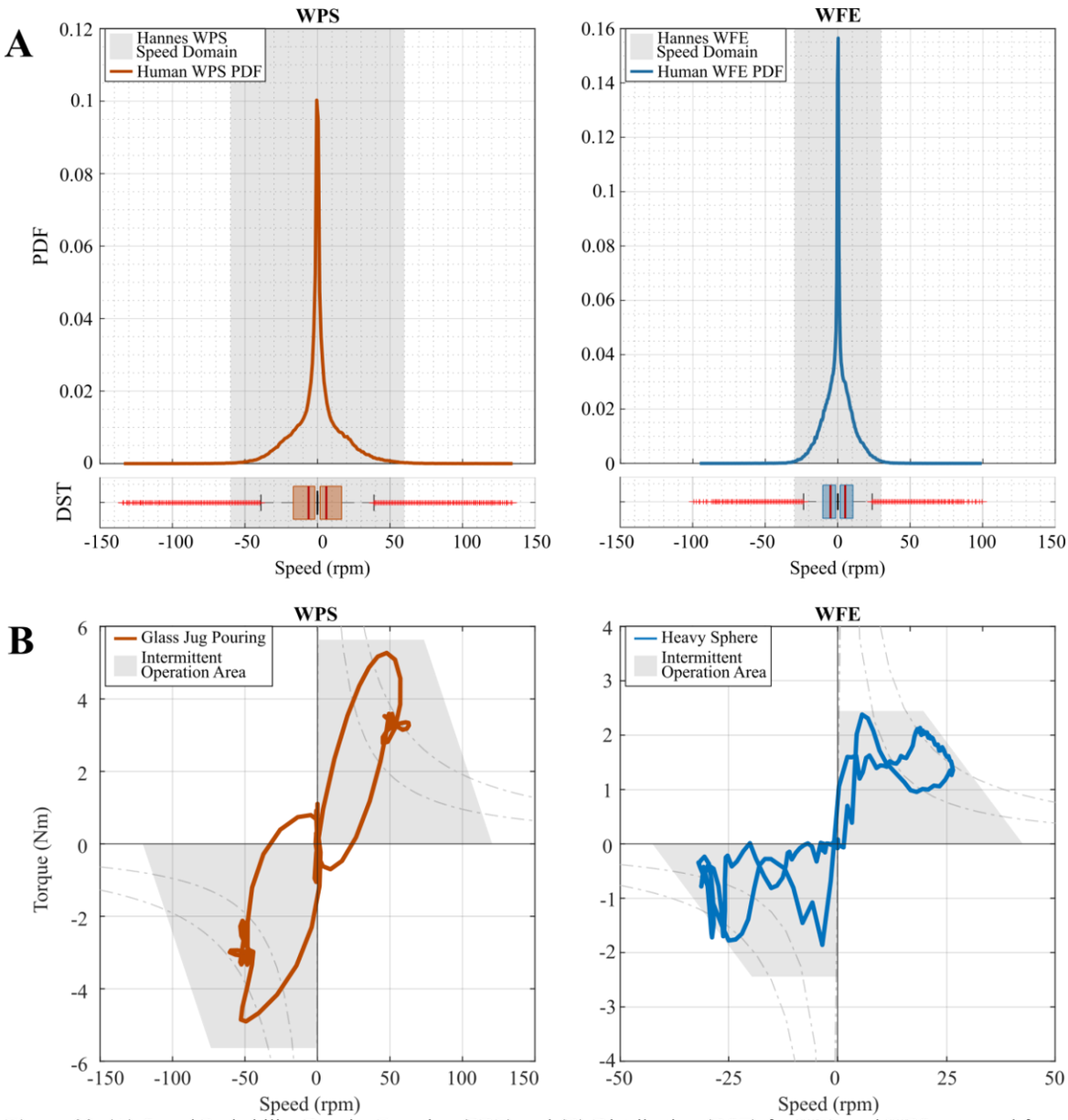

Figure 29. (A) Speed Probability Density Function (PDF) and (B) Distribution (DST) for WFE and WPS extracted from humans.

2.3.6. Discussion

The objective of this study was to propose a novel 2-DoFs prosthetic wrist combined with a poly-articulated prosthetic hand. We assessed its reliability as a viable replacement for its natural counterpart via a multi-level validation. With the aim of meeting the requirements explained in Section 2.3.2 we developed a fully integrated solution, comprehending a very compact mechanical assembly, a modular, wearable and battery-operated electronic structure and an advanced software to control the prosthesis in the most natural way.

We firstly performed a mechanical bandwidth analysis with the purpose of investigating the frequency response of the two powertrains. The results of this analysis can be used as a reference for further improving the drivetrain structure. It is worth noticing that even if the Hannes system has been designed

to mimic human motion, the performances are limited due to the anthropomorphism and low-noise requirements. This implies a trade-off between performances and user-needs: with this purpose, we performed an acquisition campaign on healthy subjects, recording the wrist movements in common ADLs to extract realistic dynamic requirements for wrist in daily life. During the trials, the participants were not instructed to restrict their movements in any way. We then compared the performances of healthy wrists to the prosthetic equivalent, to examine the biomimicry of the proposed mechatronic system, both from a range of motion point of view and speed performance under maximum load. As shown in Figure 28B diagrams, the RoMs achieved by Hannes wrist are suitable for executing all the tasks examined. From the dynamic performance point of view, the speed was statistically analysed to determine a reasonable performance which could represent a natural healthy wrist behaviour in the selected tasks. From Figure 29A, it can be appreciated that the Hannes wrist speed performance exceeds the maximum statistical speed required for the natural tasks, excluding the outliers. This is coherent with the torque-speed performance graphs (Figure 29B), which shows that the worst-case load speed-torque trajectory examined falls inside the limits of the mechatronic system.

Furthermore, the human-like dexterity was confirmed via a final validation, using a ML-based multi-DoFs control strategy, first on healthy subject and then on amputees. At this point, the requirements of low control latency and anthropomorphism are fundamental to correctly map the residual muscular contractions to the prosthesis movements, to give a natural and embodied control experience. To this extent, the proposed ML approach offers a possible strategy to suitably control the system: the patient was able to perform the wrist movements in a repeatable and predictable way since, as shown, in Figure 27A, each movement intention is well separable using 6 EMG sensors. Figure 27B shows the amputee wearing the prosthesis: it can be appreciated how a compact wrist mechatronic solution can help in achieving a good overall anthropomorphism. Figure 27C shows the effect of the joint position control strategy: according to the joint selection as output of the NLR, the user was able to control each joint separately, by proportionally regulating the movement speed by increasing the amount of contraction. This allows to stop the movement and remain in a fixed joint configuration by relaxing the muscles, with the advantage, for instance, of promoting the grasp robustness while controlling the wrist to change the orientation of an object by maintaining a certain wrist configuration while controlling the hand to grasp an object.

2.3.7. Conclusion

The Hannes System is a prosthetic device for trans-radial amputees whose aim is to mimic the human capabilities therefore restoring most of the lost functions. The two power trains for wrist motion allow an overall satisfactory RoM, that, after the analysis of human movements performed for validation purposes, was found to be coherent with the natural equivalent.

To validate the performances of this prosthetic device, a set of functional tasks was conceived due to the lack of information about the human wrist capabilities in literature. Therefore, we conducted a

measurement campaign, providing a statistical analysis of the RoMs and velocities of healthy subjects during ADLs. The Hannes system demonstrated to mimick human movements according to the presented analysis. In addition, we estimated the motors' torque and power effort in worst-case load and speed scenarios, validating the mechatronic design of the wrist. The obtained results proved the Hannes system to be a promising prosthetic device for promoting wrist dexterity for trans-radial amputees. The 2-DoFs wrist motors combination achieves both fast and slow motions hence restoring the ability of the final user to move freely in the three-dimensional world. Thanks to the non-backdrivability of the wrist in flexion-extension, amputees can rely on the wrist for holding weights, or leaning on it to stand up from a chair therefore restoring not only the functionality, but also self-confidence during daily activities while operating their prosthesis.

The resulting findings serve as evidence of a favorable balance between performance and the necessary requirements for a medical wearable device. Further developments will include an increased number of inspected subjects in a long-term scenario along with a clinical trial. This will enable a long-term investigation for receiving user feedbacks and iterate the design assessing the device efficacy. Moreover, the mechatronic system can be used as a mean for developing novel AI control strategies, both in the invasive and non-invasive domain, bridging the gap towards a realistic neuroprosthetic device. Finally, the proposed development approach could also be applied to the design of a novel trans-humeral prosthetic solution.

2.4. Chapter Discussion and Remarks

Advancements in prosthetic technology have paved the way for innovative designs that can mimic natural human capabilities, promoting greater functionality and ease of use. In this context, three fascinating aspects have been uncovered in recent research. Firstly, the Hannes system has proven to be a promising solution, boasting adaptive grasping capability and a flexible wrist module that has enabled prosthetic users to complete tasks successfully. Secondly, self-regulation techniques via respiratory control have been found to increase the embodiment of virtual limbs, but further development is required to improve user engagement. Lastly, a novel 2-DoFs prosthetic wrist has been developed, offering human-like dexterity and control via a machine learning-based multi-DoFs control strategy, bringing us one step closer to achieving the ultimate goal of prosthetic devices that can mimic natural human movements. These advancements are promising and demonstrate the exciting possibilities that lie ahead for prosthetic technology.

In summary, the following outcomes were achieved:

1. A case study on the Hannes system showed gradual improvement in completion time as training progressed, with successful strategies developed for each task. The Hannes prosthetic hand was helpful in some tasks, but the absence of active wrist pronation/supination negatively impacted others. Despite some limitations, Hannes performed well in the Cybathlon competition, ranking 6 out of 13. The team will focus on developing an active wrist module and a system capable of restoring haptic feedback for future developments.
2. Self-regulation techniques via respiratory control can increase body ownership processes and the embodiment of a virtual right hand. Slow feedback-controlled breathing may improve ownership processes, while normal breathing may cause disownership of the right hand. The SARB setup was effective in monitoring individuals' breathing and providing feedback, but a task redesign is needed to improve biofeedback training and user engagement. SARB is a viable approach in implementing self-regulation of psychophysiological states to promote the embodiment of an artificial limb through a Slow Breathing condition.
3. A study proposed a novel 2-DoFs prosthetic wrist combined with a poly-articulated prosthetic hand and developed a fully integrated solution for it. The prosthetic wrist was found to have suitable range of motion and speed performance under maximum load, and human-like dexterity via a final validation using a ML-based multi-DoFs control strategy. The proposed ML approach offered a possible strategy to suitably control the system.

Chapter 3. Body – Machine Interface

The translation from user intention to prosthetic action is a crucial aspect of the effective usability of the device. The PR algorithms developed in this project included a Joint-Oriented control strategy that resulted in a more robust and efficient approach with respect to the commercial solutions (MyoPlus [78] and Coapt [76]) in terms of robustness and speed. The other goal is to guarantee the simultaneity and naturalness of multi-DoF control. Movement robustness and naturalness are fundamental aspects of control that improve the system when embedded in a microcontroller inside a prosthesis. This activity aimed at realizing a control algorithm with a high classification rate to guarantee robustness for the user and, at the same time, a low computational burden to be fast executable. Finally, the simultaneity of movements ensured a natural control of the device tanks to the combination of joint movements.

The literature analysis allowed me to identify the more promising algorithms for a 2 DoF prosthetic application that satisfied the needs described. Consequently, the performance analysis of each algorithm allowed me to select the most promising one. The best algorithm was optimized in terms of accuracy and speed. I realized an embedded version on a microcontroller to test the online performance of the prosthetic system. Finally, a validation framework was developed, based on a virtual environment (Unity), to systematically test the prosthetic performance for both algorithms during the development phases using a clinical protocol dedicated (e.s., Target Achievement Control Test - TAC).

In this section, the results for each activity are described, presenting the relative scientific papers:

- Marinelli, et al. “Performance Evaluation of Pattern Recognition Algorithms for Upper Limb Prosthetic Applications.” BioRob 2020. [13]
- Marinelli, et al. “Miniature EMG Sensors for Prosthetic Applications.” NER 2021. [15]
- Marinelli, et al. “A Comparative Optimization Procedure to Evaluate Pattern Recognition Algorithms on Hannes Prosthesis.” Neurocomputing, 2023. (submitted)
- Marinelli, et al. “Improved Pattern Recognition Control of Hannes.” IRIM 2021. [14]
- Di Domenico, et al. “Hannes Prosthesis Control Based on Regression Machine Learning Algorithms.” IROS 2021. [12]

Chapter 3

DOI: 10.1109/NER49283.2021.9441111

3.1. Miniature EMG Sensors for Prosthetic Applications

3.1.1. Introduction

A crucial feature for the functionality and usability of a poly-articulated myoelectric hand prosthesis is its controllability. Indeed, poor controllability is one of the major causes of prosthetic system abandonment. Traditionally, myoelectric hand prosthesis control relies on the use of two electromyographic (EMG) sensors, respectively placed on flexor and extensor muscles. The muscle contraction was detected by EMG sensors, and the control policy regulates prosthesis velocity [401]. However, this solution does not allow simultaneous multi-DOF control and this prevents users from perceiving the prosthesis as a true substitute of the missing limb [402]. Recently, many groups focused on investigating solutions to improve the control of multi-DoF myoelectric hand prostheses [80, 165, 403]. One possible strategy consists in increasing the number of EMG sensors in order to provide the pattern recognition algorithm with more data for decoding hand posture [165]. However, one of the major drawbacks of current systems is that the gold standard Ottobock has a rectangular shape that badly adapts to the limited amount of space available within the socket, which also has unpredictable shape due to the residual limb. Moreover, the mechanical integration of EMG electrodes within the socket, strongly affects the physical robustness of the entire prosthetic system. This design is developed with an Inter Electrode Distance (IED) of 12 mm accordingly with the Nyquist theorem that suggests 8-10mm minimum [41]. To address these issues, we designed circular EMG sensors with a smaller design and a IED of 8 mm that is the minimum dimension for EMG application following the Nyquist theorem [41] and compared their performance versus the gold standard, while training a pattern recognition algorithm based on Non-Linear Regression (NLR) for decoding multi-joint hand posture. The NLR algorithm was chosen, instead of the gold standard Linear Discriminant Analysis, following on from the results showed on [13]. We tested both sensors on a group of healthy volunteers and on three trans-radial amputees using the Hannes hand [11] to understand the feasibility of this sensors on a prosthetic scenario.

3.1.2. Material and Methods

3.1.2.1. Subjects and Experimental Protocol

We recruited 10 right-handed able-bodied (6 males, age 36 ± 9 years) and 3 amputated subjects (mono-lateral, right trans-radial amputation of the dominant limb; all males; aged 72, 43 and 39, respectively). All subjects provided written informed consent. The study conformed to the standard of the Declaration of Helsinki and was approved by the ethical committees of Bologna-Imola (CP-PPRAS1/1-01).

Six standard EMG sensors (OTTOBOCK), and six custom-made (IIT) sensors (see section 3.1.2.2) were used. Each set of sensors was embedded into a custom-made elastic brace placed around the forearm for collecting electrical activity from 6 relevant muscle groups involved in grasping and

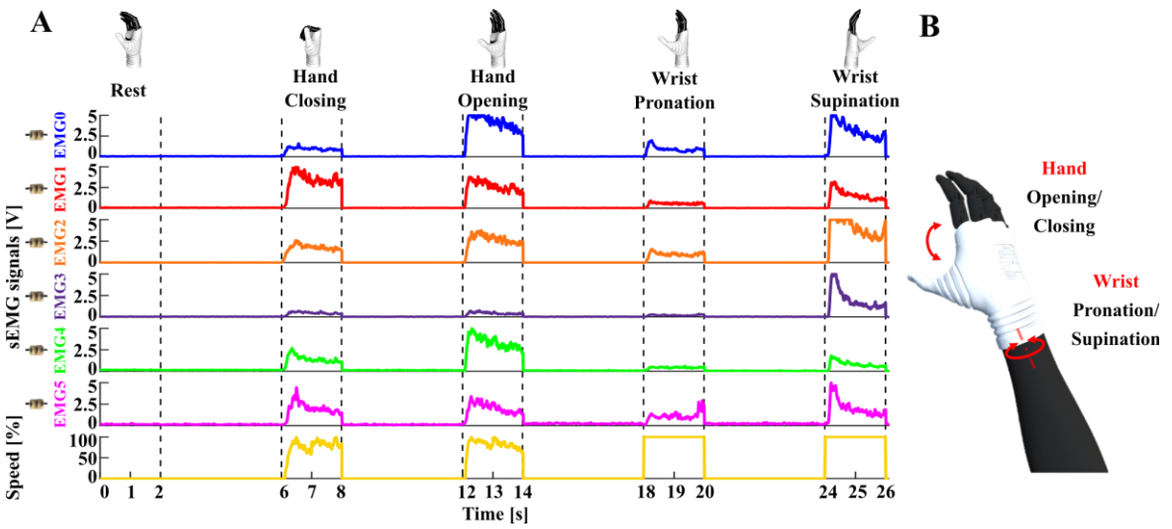

Figure 30 EMG activity associated to related joint movement.
A: EMG activations and Hannes system speed during different hand and wrist movements. **B**: DoFs of the Hannes system.

pronation/supination of the wrist (Figure 30 A). The muscles groups were: Extensor Carpi Radialis Longus Muscle (EMG0), Palmaris Longus Muscle and Flexor Carpi Ulnaris Muscle (EMG1), Extensor Digitorum Muscle (EMG2), Flexor Carpi Radialis Muscle (EMG3), Extensor Carpi Ulnaris Muscle (EMG4), and Brachio-Radial Muscle (EMG5). Subjects performed the experimental protocol twice: first with one set of EMG sensors (i.e. OTTOBOCK or IIT) and then with the other set. The order of EMG set placement was randomly assigned and 30 minutes of rest were allowed between sessions.

After sensors placement, subjects were positioned in front of a monitor displaying a virtual hand (VH) emulating the controlled prosthesis (see section 3.1.2.3). We asked subjects to sequentially perform hand opening/closing and wrist pronation/supination for 10 times, then we collected 16 repetitions of resting state (duration 2 s, Fs 1 kHz).

3.1.2.2. EMG Sensors

In this study, two different set of EMG sensors were compared: the commercially available 13E200 MyoBock (OTTOBOCK, Figure 31 A) and the custom-made circular sensors (IIT) newly developed. IIT sensors were created to minimize the occupied surface of the internal lamination of the socket: this feature allows to fit a higher number of sensors around the residual limb, without compromising the mechanical strength of the prosthesis. Moreover, to facilitate the socket manufacturing process, we designed a custom PCB assembly composed by two boards fitting within a circular shape enclosure with a final diameter of 18 mm and a thickness of 9.5 mm, (Figure 31 B). According to the identified shape, three custom titanium electrodes were designed a connected directly to the lower side PCB via epoxy conductive glue. Consistently with the OTTOBOCK devices, the IIT sensor employs a bipolar configuration with differential sensing electrodes placed on the side with IED of 8 mm with a central reference electrode. The output amplified signal range is compatible with the 0 ÷ 5 V signal commonly needed by the standard prosthetic systems. The filtering stages consist in a cascade of a band-pass filter (from 90 to 450 Hz), a notch filter (to reject the mains common mode noise), and an envelope detector

DOI: 10.1109/NER49283.2021.9441111

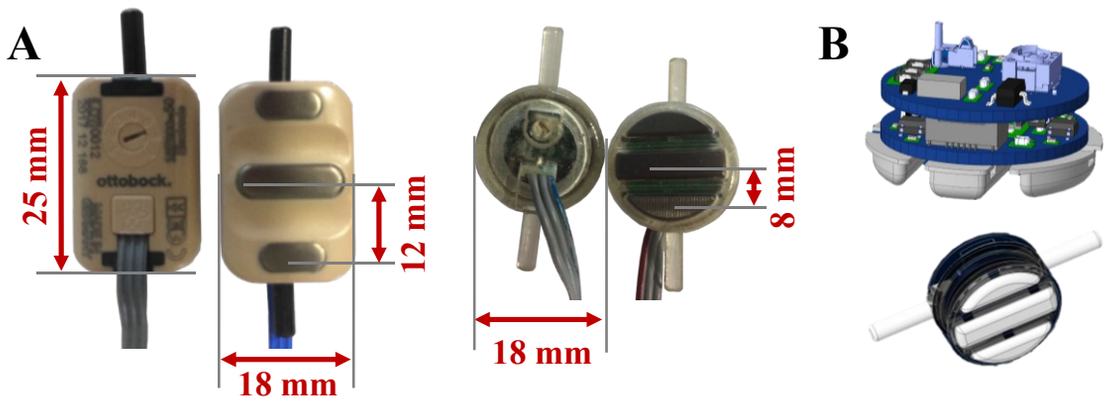

Figure 31 EMG sensors.
A: Ottobock (rectangular shape) and IIT (circular shape) sensors. **B**: Mock-app IIT sensor.

circuit with adjustable gain via a trimmer. Thanks to the input instrumentation amplifier configuration used in the very first stage, supplied by a very low noise voltage reference, a CMRR (Common Mode Rejection Ratio) of 100 dB was achieved. The output contacts can provide enveloped and raw EMG signal, both after the common mode rejection stage. Currently, on our pattern recognition application, the enveloped signal has been used: we are considering to use the raw EMG signal for further investigations.

3.1.2.3. EMG Signal Processing

Regardless of the sensors used, all EMG signals were sampled (12bit resolution) by a custom EMG processing board based on an ARM Cortex M4 microcontroller, performing A/D conversion and then Bluetooth streaming of real-time data to a host PC.

NLR classifier (see section 3.1.2.4) were then off-line trained using single samples of EMG signals recorded both during movement and rest. EMG signals were collected by a customized version of the EMG Data Acquisition & Training Software (EDATS), developed by Centro Protesi INAIL [13, 77] (Figure 32 A), implemented in MATLAB (MathWorks).

Following NLR calibration, subjects were allowed to freely explore its control by performing any of the 4 movements, which were real-time decoded and replicated onto the VH, whose joint velocity was linearly dependent with EMGs RMS.

3.1.2.4. Training, Optimizing and testing of the NLR model

We used NLR classifier because in a previous study we found that it produces comparable or better results than the gold standard Linear Discriminant Analysis [13]. NLR is a supervised algorithm and thus needs a specific calibration procedure to estimate the best set of internal parameters for its further on-line use. The Dataset is acquired at a sample frequency of 1 kHz and divided into test set (TS), training set (TR) and validation set (VS). The TS was obtained after a down-sampling operation from 1 kHz to 40 Hz according with the optimal down-sampling found in [77]. The TR was composed by 70%

Figure 32 Experimental Setup.
A: EMG processing board, power supply, sEMG armband, EDATS software, VH and Hannes system. **B**: VH control performed in Real-Time by a healthy subject. **C**: VH control performed in Real-Time by an amputee.

of the remaining data, while the VS was finally composed by 30% of the remaining data.

Through a custom MATLAB API, the parameters of NLR were off-line tuned on the TR and validated on the VS to prevent overfitting (step 1 in Figure 33). It followed an evaluation phase in which the calibrated algorithm was used to on-line decode hand motion using a real-time PC based PR simulator (step 2 in Figure 33). The resulting outcomes were finally uploaded (step 3 in Figure 33) to the EMG processing board for the final on-line classification (step 4 in Figure 33), during which the user was able to freely control the VH or the Hannes prosthesis. For online use the NLR receives input data composed by a single sample of EMG array at 300 Hz, fast enough to detect variation of human movements and to guaranty the control loop execution.

We aimed at estimating the minimum number of EMG sensors able to provide top performance of the NLR algorithm, in terms of F1Score [404]. Further, we also considered the role of the degree (D) of complexity able to provide top performance in terms of Embedding Optimization factor (EOF), as in [13]. We also introduced a "truth index", based on Likelihood threshold [405]. The Likelihood maximizes the efficiency of algorithms: we set the threshold of likelihood around 70-80% in order to

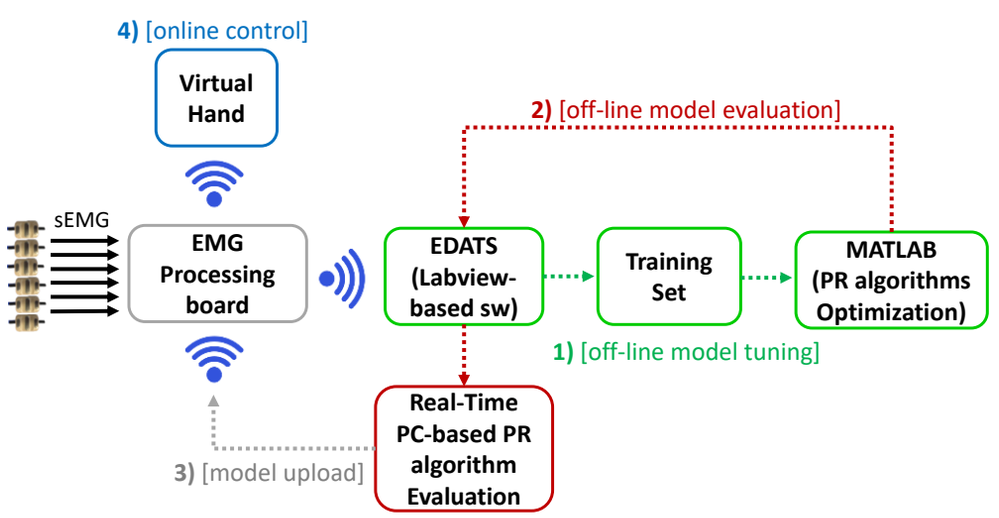

Figure 33 Experimental Setup block diagram.

guarantee the classification of the voluntary movements only. Movements discarded from classification were considered as "abstentions" and did not produce any movement.

A comparison of NLR performance with different EMG sensors was evaluated in terms of classification (% of correctly decoded movements), F1Score, and abstention (% of non-assigned movements). The best NLR configuration (optimal number of sensors and degree of complexity) was then used for training the algorithm on the amputees' dataset, with both types of sensors. We assessed whether the obtained scores were comparable with those of the healthy population. Statistical analysis was performed with Wilcoxon signed rank test and Bonferroni correction for multiple comparisons [406].

3.1.2.5. The Hannes system

The *Hannes* hand prosthesis was jointly developed by INAIL and IIT. It allows to restore around 90% of motor capacity in trans-radial amputees [11].

The Hannes system (Figure 32 A) consists of: (i) a set of six EMG electrodes, (ii) a custom EMG processing unit, (iii) a myoelectric poly-articulated prosthetic hand, (iv) an active wrist pronation/supination (WPS), and (v) a battery pack. The EMG processing unit ("EMG-Master") acquires the analog sensor output and synthesizes the control signals for each active joint. The extent of the activation is proportional to the RMS of the six EMG signals, normalized in the range 0 to 100% for the hand control, while WPS is always controlled at the maximum velocity. The control signals are then sent to the respective motor control boards within the prosthetic system. Each motor driver is equipped with an on-board control loop to ensure the correct joint movement: closed-loop speed control for the hand and open loop for WPS. The WPS consists in a standard motor-gearbox actuation and can provide 360° rotation. The description of the mechanical design of the Hannes prosthetic hand is provided in [11].

3.1.3. Results

3.1.3.1. Effect of EMG sensors number on performance

We first explored the minimum number of sensors required to achieve the saturation of performances, expressed as non-statistical difference between F1Score. Starting from the full configuration including 6 EMG sensors, we progressively reduced the number of EMG sensors by removing those placed on smaller muscles, according to the following order: EMG5, EMG2, EMG3, EMG4. We found that three OTTOBOCK sensors were enough to reach the same performance as with maximum number of sensors and that four IIT sensors reached the same performance as with maximum number of sensors (Table 13 and Figure 34).

3.1.3.2. Effect of D parameter on performance

We assessed performance in terms of EOF with different values (from 1 to 7) of the parameter D,

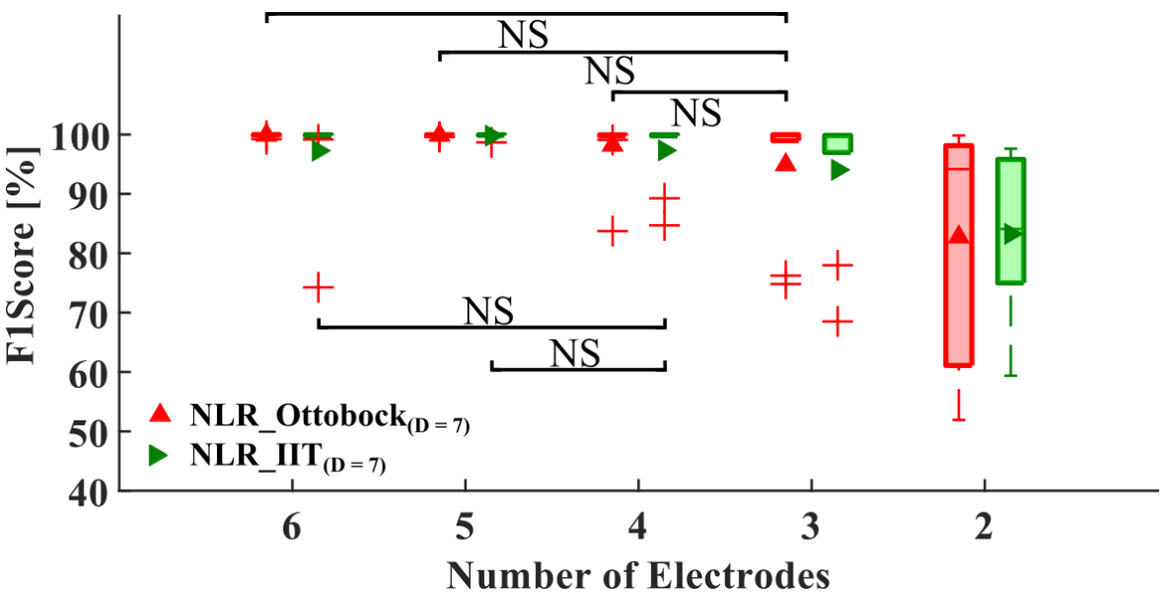

Figure 34 F1Score obtained for both sensors typology using different number of electrodes. The value of D is fixed to 7. NS: not significant.

which regulates the maximum polynomial degree. As shown in Figure 35, we found that both for Ottobock and IIT sensors D = 3 maximized the performance.

3.1.3.3. Sensors comparison

We compared F1Score obtained by both sensors' type through a Wilcoxon Signed-Rank test and found no statistical difference. Table 13 summarizes classification, F1Score, and abstention for both sensors type with the optimized number of sensors, as determined by the previous analysis.

We observed no significant difference, but IIT sensors led to more consistent results, as indicated by smaller standard deviation.

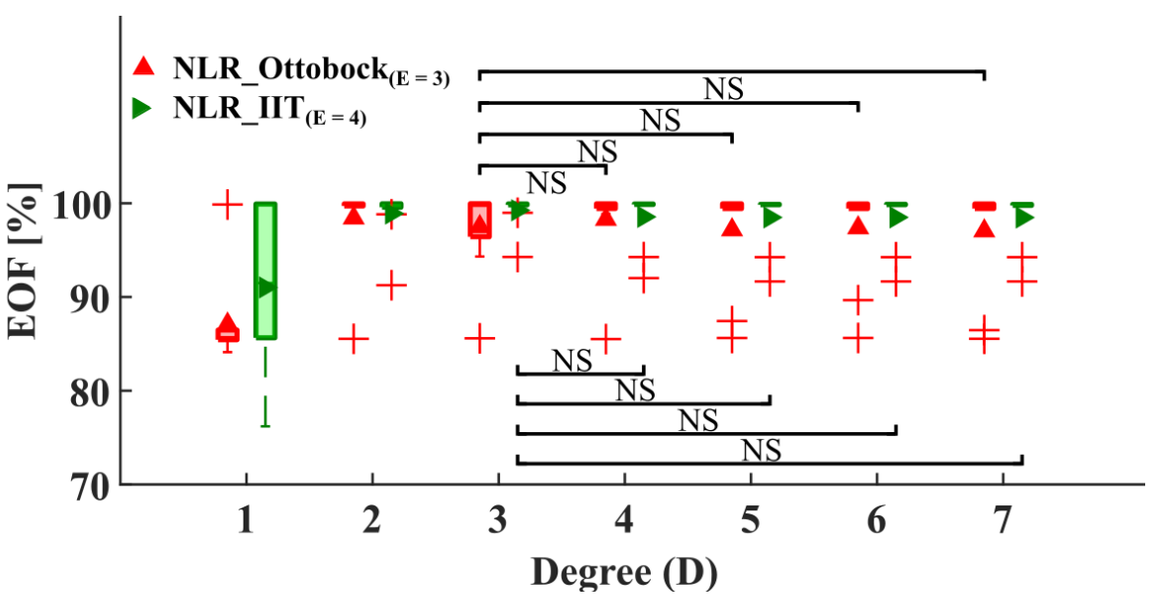

Figure 35 EOF obtained by NLR using different maximum value of parameter D and fixing number of electrodes to 3 for Ottobock sensors and 4 for IIT sensors, respectively. NS: not significant

DOI: 10.1109/NER49283.2021.9441111

Table 13 NLR performances obtained for OTTOBOCK and IIT with different number of sensors on Healthy.
In bold are indicated the number of sensors which saturated the F1Score.

Sensors	EMG (#)	Classification accuracy (%)	F1Score (%)	Abstention (%)
OTTOBOCK	2	98.2 ± 2.8	82.2 ± 12.3	82.4 ± 6.9
	3	**99.8 ± 0.2**	**94.1 ± 11.2**	**69.8 ± 9.6**
	4	99.9 ± 0.1	97.2 ± 5.6	60.7 ± 9.1
	5	99.9 ± 0.1	99.8 ± 0.4	60.0 ± 8.2
	6	99.9 ± 0.2	97.3 ± 8.1	55.1 ± 9.0
IIT	2	99.1 ± 0.8	82.7 ± 19.7	82.0 ± 7.8
	3	99.8 ± 0.2	95.0 ± 10.2	64.2 ± 8.4
	4	**99.9 ± 0.1**	**98.1 ± 5.0**	**57.2 ± 8.8**
	5	99.9 ± 0.1	99.9 ± 0.2	54.3 ± 8.1
	6	99.8 ± 0.2	99.9 ± 0.2	53.6 ± 7.8

We also ran tests on three trans-radial amputees, using optimized number of sensors. Table 14 shows the values of classification, F1Score, and abstention obtained by amputees with both EMG sensors. Scores match those obtained by healthy subjects, with highest scores for IIT sensors.

3.1.4. Discussion and Conclusion

We developed miniaturized circular EMG sensors for prosthetic applications and compared their performance in decoding hand movements using the NLR algorithm, with the commercially available gold standard. We performed tests on healthy subjects and found that IIT sensors led to similar or better performance. OTTOBOCK sensors reached highest classification performance with only three EMG sensors, while IIT sensors with four. However, IIT sensors are smaller and the overall areas occupied is 254 mm^2, while three OTTOBOCK sensors occupy a total of 486 mm^2. This is a clear advantage for prosthetics applications, because placing each sensor requires the opening of a hole in the socket. Therefore, the smaller the area occupied by sensors, the smaller the possibility of undermining socket

Table 14 NLR PERFORMANCE SCORES OBTAINED BY AMPUTEES.
In bold are reported the best scores according to each indicator (classification, F1Score, and abstention).

P.	Sensors	Classification accuracy (%)	F1Score (%)	Abstention (%)
1	OTTOBOCK	**99.8**	**98.4**	83.4
	IIT	99.4	89.6	**79.5**
2	OTTOBOCK	99.8	90.9	76.4
	IIT	**99.9**	**99.9**	**53.3**
3	OTTOBOCK	100	99.9	69.4
	IIT	**100**	**100**	**51.5**

robustness and system stability. This is crucial with proximal residual arm and reduced socket internal lamination. We also found that keeping a small degree of polynomial complexity (D = 3), maintained the same level of performance as with higher degrees in both Ottobock and IIT sensors. Therefore, the computational burden was still kept at a minimum.

Overall, we found that IIT sensors are promising for prosthetic applications, as indicated by upper limb amputees, who were able to move a VH by controlling residual muscles of the stump. More studies are needed to evaluate IIT sensors for prosthetic control in activities daily life and to validate them by testing frequency and time response.

3.2. A Comparative Optimization Procedure to Evaluate Pattern Recognition Algorithms on Hannes 2DoFs Prosthesis

3.2.1. Introduction

Nowadays, the field of multi-functional upper limb prostheses is marked by important technological and scientific developments aimed to satisfy the users' needs. The loss of a hand is a crucial impairment due to the limitation on the activity of daily living [407] and the development of high advanced prostheses is a real opportunity to compensate the lack of a limb. However, anthropomorphism and the human-like performances are not aligned with the controllability that such devices can offer [19]. Indeed, an important drawback on modern prostheses is the lack of control robustness [177]. Moreover, the dimensions of the advanced electronics systems needed to operate complex devices, result in a difficult integration within the custom socket [7-9].

A myoelectric prosthesis is commonly controlled using electromyographic signals (EMG) coming from the remaining muscles after the amputation. EMG signals are first collected using sensors, and then translated into prosthesis commands [74]. However, the stochastic nature of EMG makes the search for repeatable and reliable characteristics of the signals very challenging [133, 177, 408]..

Multi-DoF pattern recognition algorithms improve the controllability of the system, but they are affected by different problems [3] such as: electrode shift, sweating, fatigue, and the stochastic nature of the signal that eventually lead to an overall performance degradation [1, 3, 177].

Unfortunately, most of the algorithms applied in the literature are tested on healthy subjects [3] rather than on amputees [77].So far, the most promising result has been obtained by Nguyen, et al. [409], but with significant drawbacks in term of computational burdening, invasive signals acquisition, overall encumbrance and overheating of the computation unit.

In this context, researchers attempted to increase algorithms performances via parameters optimization only. However, the obtained results are not one-to-one reflecting to the final application in term of both control and mechatronics device [2, 4, 8, 9, 21, 74]. As a consequence, we here address this challenge by implementing a fully optimized pattern recognition control for the Hannes prosthetic system [11]. To achieve this objective, we first identified the mostly used pattern recognition algorithms for prosthesis application. Then, we opportunely adapted all the algorithms for controlling the Hannes hand. The study compared several approaches (i.e. Non-Linear Logistic Regression (NLR) [77], Regularized Least Squares (RLS) [410], Artificial Neural Network (ANN) [411], and Support Vector Machine (SVM) [412]) with the gold standard for prosthetic application, the Linear Discriminant Analysis (LDA) [77]. Additionally, we combined NLR, RLS and LDA methods, with an "abstention" criterion by evaluating the likelihood of each decoded class and enabling the "abstention" criterion (i.e., confidence-based rejection).

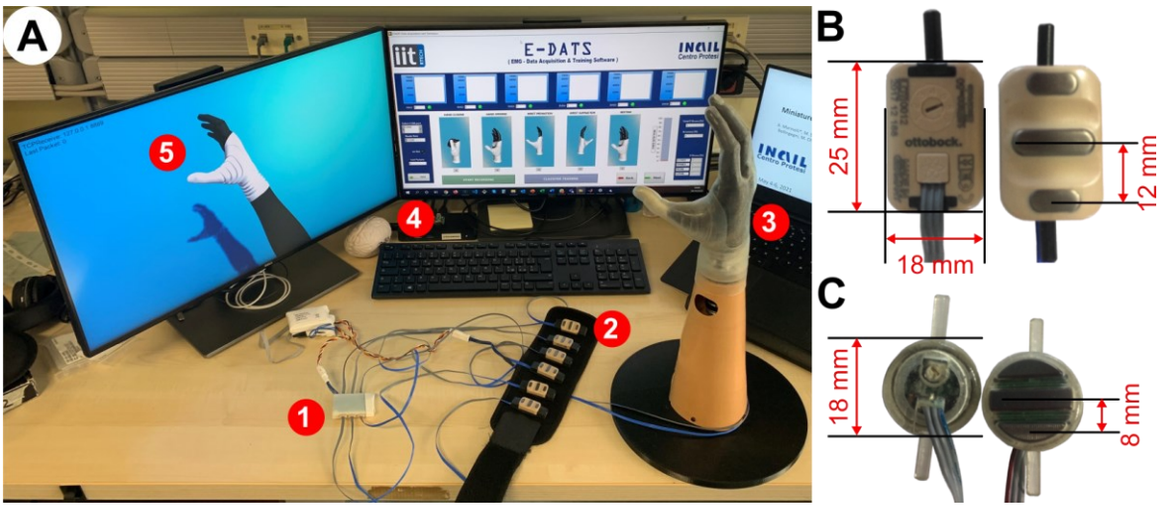

Figure 36 Experimental setup.
A) the system used to perform data acquisition and training of algorithms: 1) the emg-master; 2) the six EMG sensors; 3) the Hannes hand; 4) the EMG-data acquisition and training system (E-DATS) user interface; 5) the Hannes virtual reality hand. B) The Ottobock sensors. C) the IIT sensors

As the aim of this study was to reduce the encumbrance of the system, several interventions were performed. The maximum number of EMG sensors (E) that saturated performances of each algorithm were first investigated. Moreover, the parameters of algorithms that saturated performances were also optimized to reduce both complexity and computational burdening. Additionally, custom made EMG sensors (i.e. IIT sensors) validation was performed by comparing their performance with commercial gold-standard ones, i.e. the Ottobock sensors. The main goal of this novel design was to preserve space on the socket [15]. Finally, we then implemented the resulting 'best performing' algorithm for the online control of the Hannes system joints. Our group already tested a set of pattern recognition algorithms on healthy subjects for translating muscular activity into Hannes movements (rest, hand opening/closing (HOC), wrist pronation/supination (WPS)) [13]. We here extend that work by including a population of amputees to detect and generalize the right combination of parameters to be applied for the real-time control of the Hannes prosthesis.

3.2.2. Materials and Methods

3.2.2.1. Subjects

Eleven trans-radial amputees (45.3 ± 2.6, 8 right-handed), with no prior experience in controlling multi-DoFs prostheses via Pattern Recognition algorithms, participated in this study. Before starting the experiment, the subjects were informed about the protocol, and they signed the informed consent form. The experimental protocol was approved by the AVEC (Area Vasta Emilia Centro) Ethics Committee (Protocol Code: CP-PPRAS1/1-03).

3.2.2.2. Experimental Setup

The experimental setup (Figure 36) was composed by: (A) a standard laptop (DELL XPS 15, Intel Core i9 @2.60GHz, 32GB RAM) running Windows 10, to collect the EMG data, train the algorithms and perform the experiment; (B) a 18'' computer monitor to show the movement to be performed; (C) a custom made master PCB (EMGM) to communicate via Bluetooth with the PC for sending EMG data, running the Pattern Recognition algorithm and operating the prosthesis; (D) a 12V, 3000mAh battery pack; (E) two arrays of six EMG sensors (Ottobock, Duderstadt, Germany, 13E200=50 AC and IIT, custom made circular electrodes [15]) to acquire and amplify the muscular activity; (F) the Hannes prosthetic hand [11-13, 15]. The EMGM board collected the EMG signals from two types of sensors (see later in this paragraph). Data could be transmitted first to the laptop (to train the algorithm) and then to the EMGM (to translate them into control movements for the Hannes hand). The User Interface (UI) was designed by using Labview (National Instruments Corp., Austin, TX, USA) development suite, while Matlab (MathWorks, Natick, MA, USA) to collect data and train the algorithm. This framework acquired the EMG data from EMGM and sent the model parameters back to EMGM for real-time movement decoding and therefore to control the prothesis. The virtual reality (VR) framework was developed by using the Unity development suite (Unity Technologies, San Francisco, CA, USA).

As explained below (section 3.2.2.3, 2 types of EMG sensors were tested during each experimental session and were used in a random order to offline compare the classifier performances. Both sets were placed circumferentially and equidistantly around the subject's stump, approximately 10 cm distal to the elbow, and strapped using an elastic band. The amplification gain of each EMG was individually adjusted to cover the range of values during maximum muscle contraction for every subject, avoiding electrodes saturation.

The subjects sat comfortably in front of the monitor, with their amputee arm placed towards the desktop, taking care to avoid the contact between the EMG sensors and the table. The computer monitor was placed approximately 50 cm from the subject. The UI environment displayed the movements to be performed by subjects to create the dataset and tuning the models to control the prosthesis. Afterwards, the subjects proportionally controlled the Hannes prosthesis movements with their muscle contraction, in opening and closing the hand or rotating the wrist.

3.2.2.3. EMG sensors

In this study, two different sets of EMG sensors were compared: the commercially available 13E200 MyoBock (Ottobock, Figure 36 B) and the custom-made circular sensors (IIT) newly developed. We designed the IIT sensors to minimize the space occupancy within the socket therefore permitting to fit a higher number of sensors around the residual limb, without compromising the mechanical strength of the prosthesis. Moreover, to facilitate the socket manufacturing process, we designed a custom PCB assembly composed by two boards fitting within a circular shape enclosure with a final diameter of 18 mm and a thickness of 9.5 mm, (Figure 36 C). According to the identified shape, three custom titanium

plates were designed and directly connected to the lower side PCB via epoxy conductive glue. Consistently with the Ottobock devices, the IIT sensor employs a bipolar configuration with differential sensing electrodes placed on the side with an interelectrode distance of 8 mm. The amplification range of the output signal is compatible with the 0 ÷ 5 V signal commonly needed by the standard prosthetic systems. The filtering stages consist of a cascade of a band-pass filter (from 90 to 450 Hz), a notch filter (to reject the main common mode noise), and an envelope detector circuit with adjustable gain via a trimmer. Thanks to the input instrumentation amplifier configuration used in the very first stage, supplied by a very low noise voltage reference, a CMRR (Common Mode Rejection Ratio) of 100 dB was achieved. The output contacts could provide enveloped and raw EMG signal, both after the common mode rejection stage. For our pattern recognition application, we used the enveloped signal.

3.2.2.4. The Hannes system

Hannes is an anthropomorphic, poli-articulated upper limb system comprising a prosthetic hand and wrist that allows patients to naturally recover most of the lost functionalities [11]. The underlying mechanism of the hand is a mechanical differential system that allow Hannes to adapt to the grasped object. This results in a grasp that is efficient, robust against external conditions and natural. The system also permits to actively pronate and supinate the wrist ('key turning movement'), allowing grasps in different orientation without relying on harmful patient compensation.

The Hannes prosthetic system is myoelectric as it relies on biopotentials to be controlled. An array of up to six surface electromyographic sensors [15], placed within a custom socket, records the muscle activity in the residual limb. The system has been developed to record the intensity of the muscular activity. As a consequence, the Root Mean Square (RMS) values acquired by each sensor are computed, to run PR algorithm and to identify the Sought-after movements to be reproduced by the prosthetic system [13]. In particular, opening and closing of the hand can be proportionally controlled whilst the pronation and supination of the wrist are commanded in open loop at its maximum speed.

3.2.2.5. Pattern Recognition algorithms

A wide range of supervised machine learning algorithms were tested to perform EMG Pattern Recognition online: Non-NLR [77], RLS [410], ANN [411], SVM [412], and LDA [77]. Both model and optimization criteria were defined according to the cited references. ANN and SVM are classifiers, therefore the related output is the decoded movement (class). Oppositely, the other algorithms are regressors and their output is a classes' likelihood estimation. In the following, all the algorithms involved in this study are described, and the related model training and parameters optimization are presented.

3.2.2.5.1. NLR

The NLR [413] calculates the class membership probability using the following logistic function:

Table 15 Polynomial features extraction varying the parameter D of NLR

D	Description	Example
1	Linear case (LR)	x_1, x_2, x_3, x_4, x_5, x_6
2	max 2nd degree	x_1, …, x_6, x_1x_2, x_1x_3, …, x_5x_6, x_1^2, x_2^2, …, x_6^2
3	max 3rd degree	x_1, …, x_6^2, $x_1x_2x_3$, …, $x_4x_5x_6$, x_1^3, …, x_6^3
4	max 4th degree	x_1, …, x_6^3, $x_1x_2x_3x_4$, …, $x_3x_4x_5x_6$, x_1^4, …, x_6^4
5	max 5th degree	x_1, …, x_6^4, $x_1x_2x_3x_4x_5$, …, $x_2x_3x_4x_5x_6$, x_1^5, …, x_6^5
6	max 6th degree	x_1, …, x_6^5, $x_1x_2x_3x_4x_5x_6$, x_1^6, …, x_6^6
7	max 7th degree	x_1, …, x_6^6, x_1^7, x_2^7, x_3^7, x_4^7, x_5^7, x_6^7

$$P(1|x,\theta) = \begin{cases} g(\theta^T * x) = \dfrac{1}{1+e^{-(\theta^T * x + \theta_0)}} \\ 1 - P(y=0|x,\theta) \end{cases} \quad (10)$$

where θ and θ_0 are the classification parameters vector and the bias term, and g(·) is the sigmoid (logistic) function. The level of non-linearity (D) is achievable thanks to the interaction terms as described in Table 15. The NLR algorithm is characterized by polynomial input features which are obtained from the combination product of the starting input features (i.e., x_1; x_2; x_1*x_2; x_1^2; x_2^2; …, see Table 15) [77]. The complexity of the NLR classifier is determined by the internal parameter D (ranging from 1 to 7, in this case), which encodes a structure of polynomial features as reported in Table 15: from the linear terms up to the D-power elevation and all the possible permutations without repetitions of a maximum number of elements corresponding to the indicated degree (D).

3.2.2.5.2. RLS

The RLS evaluates the class membership probability using the following linear relation:

$$f(x) = W^T x \quad (11)$$

where W is the weight vector of angular coefficient and x is the EMGs input vector. In addition, several features (X) in the time domain are extracted from the EMG signals for enhancing the classification performances: Variance (σ^2), Sum, Standard Deviation (STD), Mean Absolute Value (MAV) and RMS. Once the features (X) have been extracted, a gaussian kernel (K), symmetric and positive defined, was introduced:

$$K(X,X') = e^{-\frac{\|X-X'\|^2}{2\sigma^2}} \quad (12)$$

where the standard deviation σ (set between 20 monospaced values from 10^{-3} to 5) of the non-linear Gaussian kernel has to be tuned. So, the solution of the problem is:

$$f(K(X,X')) = K(X,X')^T C \tag{13}$$

where the term C is obtained by using a root mean square technique:

$$C = (K(X,X) + \lambda I)^{-1} Y \tag{14}$$

The regularization term λ (set to be around 20 values monospaced from 10^{-4} to 10) was properly chosen through CrossValidation, *Y* is a vector containing the output classes as entries and *I* is the identity matrix. Known C, it is possible to classify the new data as input through the function (13).

3.2.2.5.3. ANN

The ANN [411, 413] is a supervised classification algorithm where each neuron inside the architecture implements a logistic function. The net architecture is composed by a first input layer, one or more hidden layers (L, with the same number of neurons), and an output layer with a neuron for each class. The output vector of *l-th* layer ($a^{(l)}$) of this classifier is obtained through a forward propagation:

$$a^{(l)} = \begin{cases} x & ,l = 1 \\ g\left(\theta^{(l-1)} * a^{(l-1)} + \theta_{0^{(l-1)}}\right) & ,l = 2,3,\dots,L \end{cases} \tag{15}$$

where $\theta^{(l-1)}$, $\theta_0^{(l)}$ are respectively the matrix of classifier parameters and the bias vector associated to *l-th* layer and *L* indicates the output layer. The output of the net is a vector, *Pv(y| x)*, whose elements represents the probability to belong to a given class expressed in the following way:

$$Pv\left(y\middle|x,\theta^{(l)},\theta_0^{(l)}\right) = a^{(L)} \quad ,l = 1,2,\dots,L \tag{16}$$

It is important to consider that the ANN classifier's complexity is defined by the maximum number of layers (ranging from 1 to 10) and the maximum number of neurons (N) for each L (ranging from 1 to 30).

3.2.2.5.4. SVM

The SVM [414] is a supervised classifier with a One vs All approach to obtain a multiclass classification. The corresponding formulation is:

$$h_\theta(x) = \begin{cases} 1 & ,(\theta^T * x + \theta_0) \geq +1 \\ 0 & ,(\theta^T * x + \theta_0) \leq -1 \end{cases} \tag{17}$$

where, θ and θ_0 are the parameters vector and the bias term of classifier.

To achieve high classification performances, a non-linearity has been introduced. For this reason, a kernel function (*f*) was used to solve the Mercer theorem. This theorem describes the similarity between a generic input vector *x* and a support vector, *landmark* (*s*), which represents one of the two classes. A subvector of the all-vectors *x* recorded to train the SVM algorithm is typically chosen as *landmark*, so that the *j-th* element of *f*, for a Radial Basis Function (RBF) kernel can be expressed as follow:

$$f_j = \exp\left(-\frac{\left|x - s^{(j)}\right|^2}{2\gamma}\right) \quad ,j = 1,2,\dots,n. \tag{18}$$

where *n* is the number of support vector chosen as representative vector of class 0 and 1, and *y* is the internal parameter of RBF (variable from 0 to 50 with sequence step of 0.1). The algorithm, developed by using the library *libsvm3.20* [412], allows to set the regularized parameters value C (varying from 0 to 10^4 with sequence step of 0.01) which appears within the loss function and the value of internal RBF kernel parameter γ. In this specific case, a *One vs. One* method can be adopted to solve the multi-class

classification problem as suggested by the library developer [412, 415, 416]. The *Limited memory Broyden-Fletcher-Goldfarb-Shanno* (L-BFGS) [417] was chosen for minimizing the algorithm. The SVM was iteratively trained with all the possible configurations of internal parameters C and γ, by varying each of those within a proper range of values. Hence the best combination of hyperparameters was selected for evaluating the classifier performances.

3.2.2.5.5. LDA

The LDA algorithm is a linear supervised classifier where the class index (c) is predicted as follow:

$$\begin{cases} h_\theta(x) = \max_c({}_c\theta^T * x + {}_c\theta_0) \\ {}_c\theta = \Sigma^{-1} * \mu_c \\ {}_c\theta_0 = -{}_c\theta^T * \left(\frac{\mu_c}{2}\right) + ln(\Pi_c) \end{cases} \quad (19)$$

where ${}_c\theta$ e ${}_c\theta_0$ respectively are the vectors of parameters and the bias term of c class. This type of classifier, thanks to its intrinsic formulation, does not have internal parameters to be optimized, thus it does not need a Cross Validation approach to be validated. A *One vs. All* approach can be adopted to solve the multi-class problem. Moreover, in order to improve the classifier's percentage, five features in the time domain are considered: MAV, RMS, Slope Sign Change (SSC), Waveform Length (WL) and Variance (σ^2). The MAV formula is:

$$MAV(t) = \frac{1}{\Delta t + \Delta_0 t} \sum_{i=t-\Delta_0 t}^{t+\Delta t} |x_i| \quad (20)$$

The SSC is the number of time that the signal changes sign:

$$SSC(t) = \sum_{i=t-\Delta_0 t+1}^{t+\Delta t-1} \left((x_{i+1} - sign(x_i - x_{i-1})) \sim 0 \right) \quad (21)$$

given the EMG signal in three subsequent time instant *x(i-1)*, *x(i)*, *x(i+1)*, with *i* that varies from t-$\Delta_0 t$+*1* to t+Δt-*1*, it is possible to calculate the number of times where a variation trend occurs.

Finally, the Waveform Length (WL) can be expressed as follow:

$$WL(t) = \sum_{i=t-\Delta_0 t+1}^{t+\Delta t} |\Delta x_i| \quad (22)$$

where Δx_i is defined as $\Delta x_i = x_i - x_{i-1}$. In all the cases, the features were extracted in a temporal window of 250 ms (Δt) with an overlap with the previous window of 200 ms ($\Delta_0 t$) [418].

3.2.2.5.6. Training and testing of the classifiers model

As all the algorithms (see section 3.2.2.5) were supervised, they needed a specific calibration procedure to estimate the best set of internal parameters for their online usage. It is important to highlight that the calibration regarded the optimization of internal parameters of each classifier, therefore it should not be confused with the optimization procedure related to the other hyperparameters (see section 3.2.2.5.7.

As a consequence, the input dataset was composed by single samples of EMG data for NLR, ANN, and SVM, while for RLS and LDA some features (see paragraph 3.2.2.5.5 were extracted, by using a sliding window of 200ms with an overlap of 200ms. The algorithms were first calibrated to optimize the

internal parameters that achieve high performances with the lowest computational effort during the online control (see details in [13]). For what concerns LDA algorithm, we split the dataset into a training set (70% of the data) and a test set (30% of the data). The other algorithms were used after downsampling the data from 1kHz to 40Hz thus obtaining a training group (4% of the data) and a test set (TS, 96% of the data). The training group was in turn divided into a training set (TR, 2.4% of the data for offline tuning of the internal parameters), validation set (VS, 0.8% of the data for tuning the hyperparameters to prevent overfitting), and a threshold optimization set (TH, 0.8% of the data for tuning the likelihood threshold for the abstention criterion).

Through a custom Matlab API, the parameters of the selected model were offline tuned on TR. Afterwards, a validation phase on the VS for tuning the internal parameters to prevent overfitting was performed. Then, the likelihood threshold was optimized using the TH set to improve the accuracy of the model. Lastly, the performance of the model was assessed on the TS. Each classifier was optimized according to its model parameters with a computational time ranging from few seconds to few minutes, depending on the algorithm.

Abstention criteria

In NLR, RLS and LDA regression algorithms, the maximization of the voluntary gestures recognition was implemented through the introduction of a "truth index", based on Likelihood threshold [405]. The threshold, ranging between 0.7 and 1, was optimized for each subject and each algorithm in terms of F1Score [404]. During offline optimization, in the cases of movements under threshold or simultaneous above-threshold movements, the classifier abstained without classifying. During online classification, above-threshold movements belonging to the same DoF were considered as "abstentions", while above-threshold movements belonging to different DoFs produced simultaneous movements.

Voting criteria

The voting criteria was introduced to make the classification more robust to misclassifications due to the high sampling rate of the signal. In particular, the output class (calculated each 3.3ms) was considered valid if it was predicted more than 70% of the time within the decoding window (160ms). This criterion is a sort of a low pass filter that allows to mitigate the artefacts due to rapid variation of EMG signals during muscle contraction.

3.2.2.5.7. Optimization and testing of the best configuration of hyperparameters

We first optimized the number of EMG electrodes (E) for each classifier by computing the F1Score for every single configuration of EMG sensors. For each number of E, the best configuration was chosen by exploiting the Non-negative Matrix Factorization (NMF) on the training dataset [419]. The NMF allowed to select the most significant sensors to better discriminate the classes to be detected. This method associated each sensor to a certain weight representing the information carried out by such electrode. The greater the weight the higher the information. Therefore, we selected the desired number of E starting from those having higher weights.

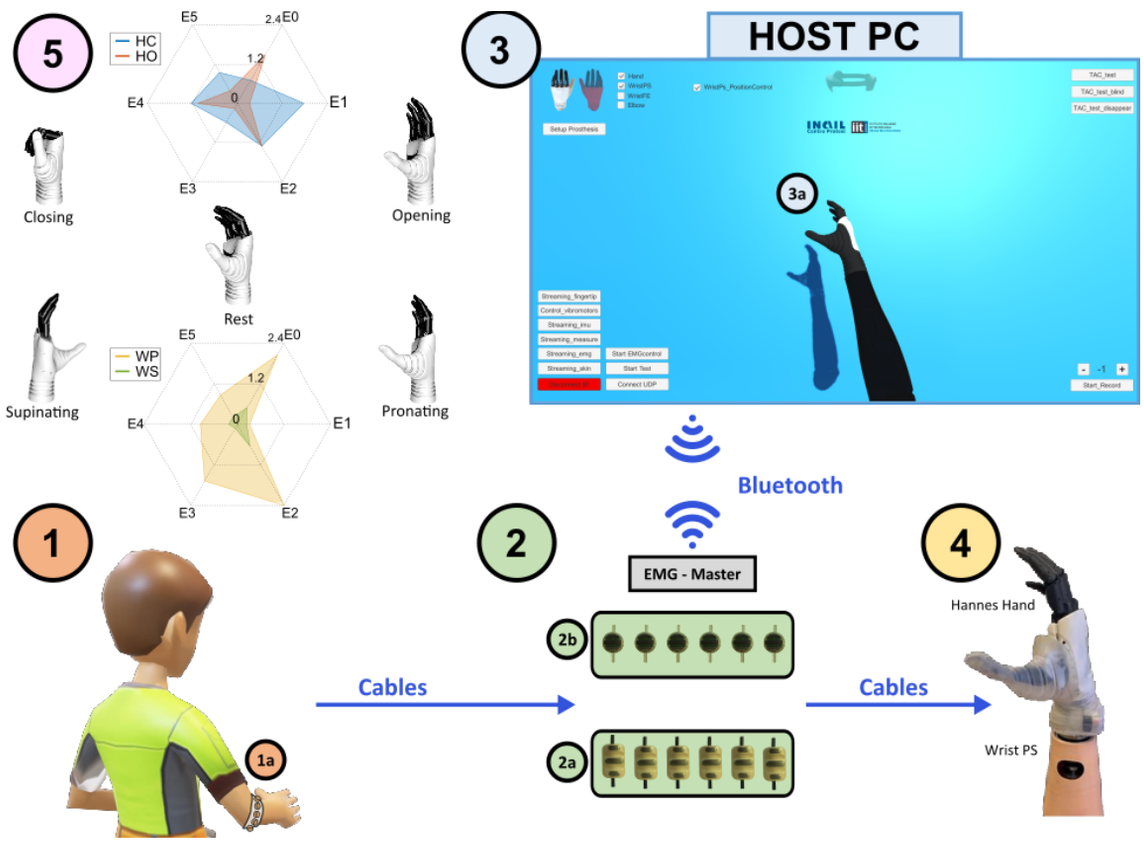

Figure 37 Experimental protocol.
1) the user wears the 6 EMG sensors with wristband; 2) the EMG-master acquires data from EMGs (either collected with commercial – 2a, or custom – 2b, electrodes) and send them to 3) the Host PC via Bluetooth and it controls 4) the Hannes hand sending the references via CAN, after model calibration. 3) The Host PC creates the dataset, calibrates the models and controls the virtual Hannes hand. 5) Available movements on Hannes and the relative EMG pattern activation to

Subsequently, for every implemented algorithm we focused on the optimization of the hyperparameters. Concerning the NLR classifier, we optimized the polynomial degree (D), which plays an important role since it represents the complexity of the algorithm, as described in [13]. The higher the complexity, the greater the computational burden required to the processing board. Regarding the ANN, we investigated the importance of the number of L by fixing the number of N to the highest value (30) and then we optimized the number of N, considering the previously obtained optimal number of L. Those analyses were performed using the Embedding Optimization Factor (EOF) as parameter to analyze the role of computational burden on saturation of performances. The EOF explains the trade-off between performance accuracy and complexity of the algorithm, which is strongly related to the computational burden on the EMG processing board [77]. This index is strongly related to the available memory on the EMG-Master. Therefore, it may happen that in some cases (e.g., full configuration of EMG sensors), the model has too many parameters for the available flash memory, resulting in EOF obtaining negative scores (see [77] for EOF calculation).

3.2.2.6. Experimental Protocol

First, the amplitude gain for each EMG sensor (Figure 37.2 a or b) was determined to let the signal cover the whole range of values during contractions. To this aim, the subject (Figure 37.1) was asked to

contract at the maximum power the muscle and the gain was manually set to amplify the visualized signal.

After the calibration, the subject was asked to repeat the 4 movements (hand open/close, wrist pronation/supination) and the rest for 10 times to create the training dataset for the algorithms (Figure 37.5). After the calibration, the model of the best algorithm was uploaded to the EMGM for the online control of both the VR (Figure 37.3) and the Hannes hand (Figure 37.4) to verify the effectiveness of the control.

Then the subject was asked to perform again the calibration with the second set of EMG sensors (Figure 37.2 b or a), and control in real-time the prosthesis and the VR.

After each calibration, the subject was free to move the prosthesis using the resulting best performing algorithm embedded on the microcontroller to see the ability of that approach to decode and control in real-time the prosthesis (Figure 37.3 and Figure 37.4).

3.2.2.7. Data Analysis

The primary outcome measure analyzed was the minimum number of EMG sensors (E) that produced a saturation of performances in term of F1score. Those results were computed for each algorithm by setting the hyperparameters to maximum complexity (i.e., D=7, L = 10, N = 30). When the number of E was decreased, the choice of active EMG was done using the Non-Negative-Matrix-Factorization (NMF) to detect the most significant sensors. The second outcome was the minimum level of complexity that produced a saturation of performances in term of EOF. This parameter considered both the accuracy of the classifier and its computational burden. For this analysis the number of E was set to the result obtained in the previous analysis, while for ANN the L parameters was optimized putting the N to maximum complexity and then the N was optimized putting L to the level of complexity found at the previous optimization phase.

After this analysis, the performances of the algorithms were compared to each other to find the best solution that produced the best results with the lower computational cost. In this case the algorithms were compared with all the internal and external parameters optimized.

Finally, a comparison between electrodes (Commercial vs Custom was performed to find possible differences in their working performance.

For each type of comparison, a Wilcoxon sign-rank test was performed to verify the statistical differences. The multiple comparison test was Bonferroni corrected. Matlab 2020b were used for the statistical analysis. The F1score, the EOF, the classification, and the Abstention were computed for each subject and condition and compared across conditions. The threshold for statistical significance was set at $p<0.05$. Outliers were excluded from the statistical comparisons. The results in the text are reported as median (interquartile range).

3.2.3. Results

The following results present the offline analysis performed both using commercial Ottobock EMG sensors and custom made IIT EMG sensors.

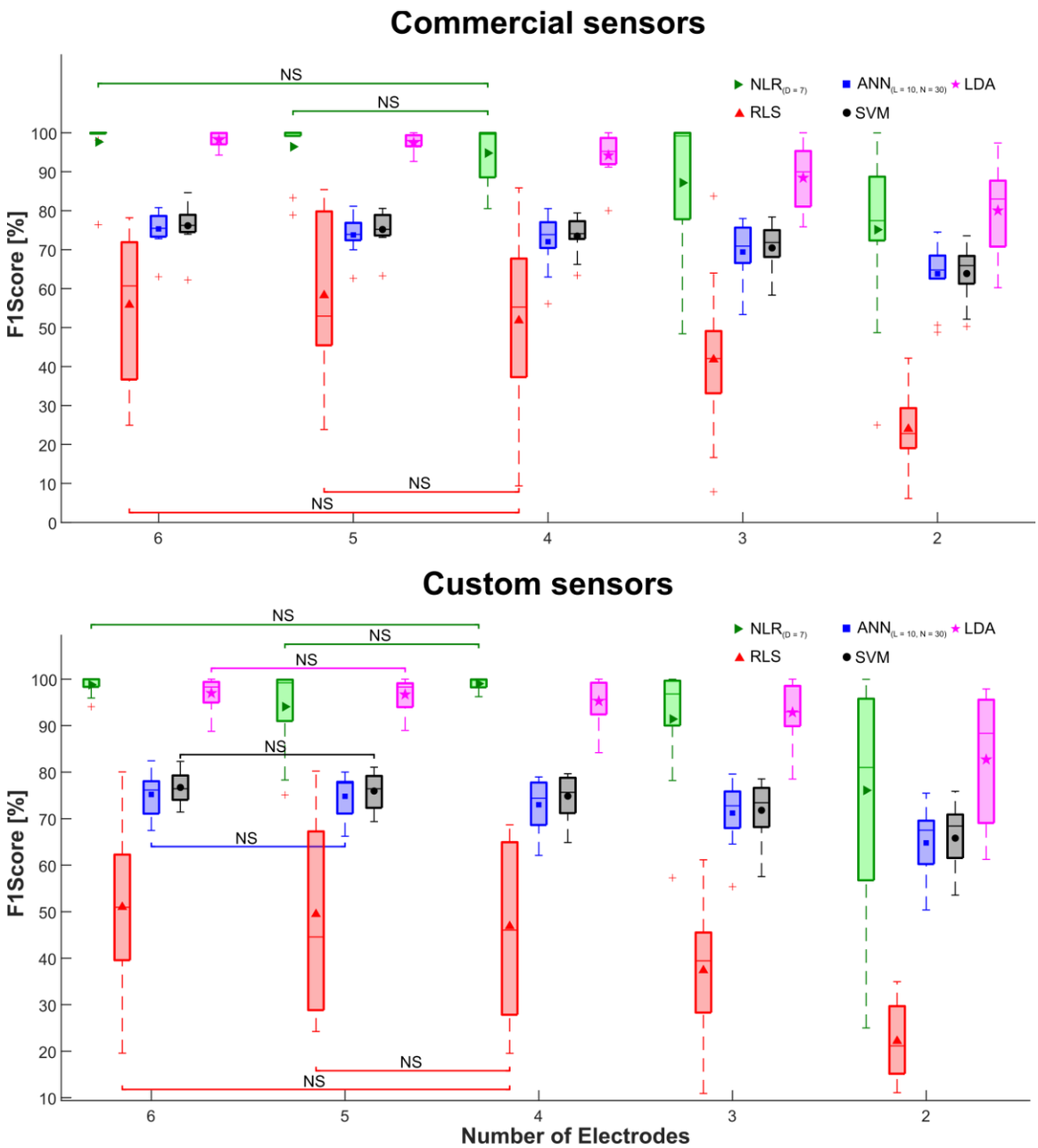

Figure 38 Electrodes' number optimization based on F1Score.
We reported data acquired using the Ottobock sensors in the upper panel, and data acquired using the IIT sensors in the lower panel. The 5 PR algorithms were optimized varying the number of E using NMF to select the optimal set, by keeping fixed the hyperparameters of each algorithm to the maximum complexity. In the boxplots, the small icons are the means for each algorithm. The lower and upper quartiles are shown as the bottom and top edges of the box, respectively. The line inside the boxes indicates the median, whiskers represent min/max values and crosses are outliers. The horizontal lines denote not-statistically significant differences for the comparisons across the values of number of electrodes for each algorithm (NS, $p > 0.05$ with Bonferroni correction).

Table 16 Number of optimized sensors for each algorithm using both Commercial and Custom.

Algorithm	EMG [#]	
	Commercial	Custom
$NLR_{(D=7)}$	**4**	**4**
RLS	**4**	**4**
$ANN_{(L=10, N=30)}$	6	5
SVM	6	5
LDA	6	5

3.2.3.1. Effect of EMG electrodes number on performance

Figure 38 reports the analysis performed for each algorithm varying E, the number of EMG sensors. The results show that using Commercial EMG, only NLR and RLS had a saturation of performances with 4 electrodes ($p > 0.0674$ and $p > 0.1016$ respectively) while the other algorithms need the full E to reach the maximum performances in term of F1Score, as shown in Figure 38 upper graph. By using custom EMG, NLR and RLS had again a saturation of F1Score with 4 electrodes ($p > 0.2061$ and $p > 0.3203$ respectively), while ANN, SVM, and LDA had a saturation of F1Score with 5 electrodes ($p > 0.3203$, $p > 0.1016$, and $p > 0.1934$ respectively), as shown in Figure 38 lower graph. For each algorithm and each type of sensors the number of electrodes is summarized in Table 16.

3.2.3.2. Effect of D parameter on NLR performance

For NLR algorithm, the role of D parameter was analyzed fixing E on the basis of previous analysis, see Table 16. Figure 39 shows that using both commercial and custom sensors, the performance in term of EOF saturated with a D = 2 ($p > 0.0537$ for commercial sensors, and $p > 0.7002$ for custom sensors).

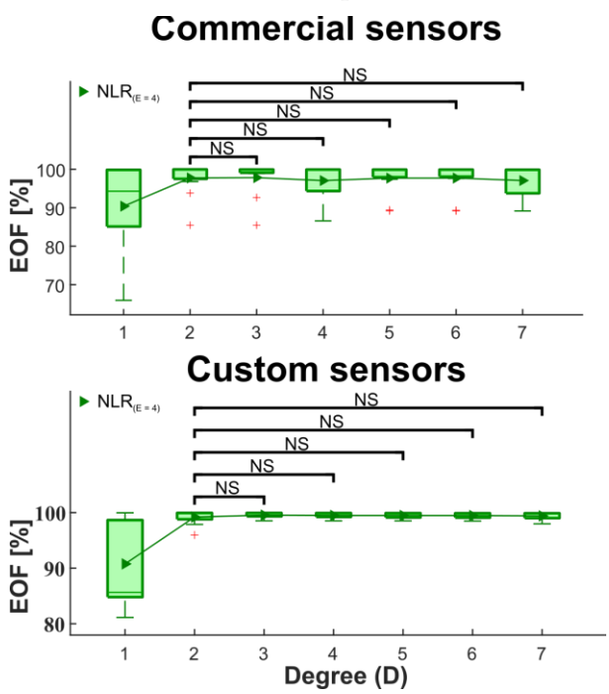

Figure 39 NLR degree (D) optimization based on EOF.
The upper panel reports the data acquired using the commercial sensors, the lower panel that acquired using the custom sensors. The NLR algorithm was optimized varying the polynomial D complexity, by using the previously optimized E (E=4 for both commercial and custom sensors). In the boxplots, the small triangles are the means for each D. The lower and upper quartiles are shown as the bottom and top edges of the box, respectively. The line inside the boxes indicates the median, whiskers represent min/max values and crosses are outliers. The horizontal lines denote not-statistically significant differences for the comparisons across the values of D for NLR algorithm (NS, $p > 0.05$ with Bonferroni correction).

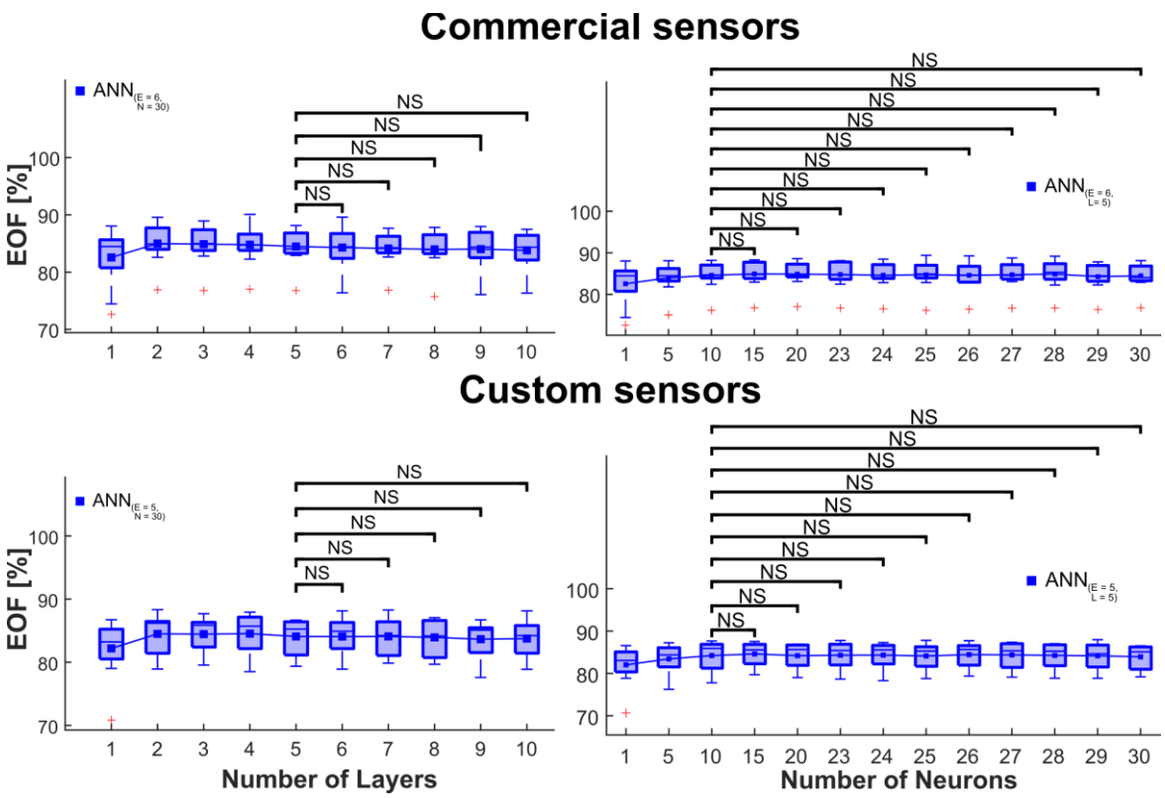

Figure 40 ANN hyperparameters optimization, layers (L) and neurons (N), based on EOF.
In upper panels is present the data acquired using the Ottobock sensors, in the lower panels is present the data acquired using the IIT sensors. The ANN algorithm was optimized, firstly, varying the L complexity, by keeping fixed the N to the maximum value (30). Secondly, the N was optimized by keeping fixed the L previously minimized (5 for both Ottobock and IIT sensors). The number of E in both the optimization phases was keeping fixed to the previously optimized value (E=6 for Ottobock and E=5 for IIT sensors). In the boxplots, the small squares are the means for each L and N. The lower and upper quartiles are shown as the bottom and top edges of the box, respectively. The line inside the boxes indicates the median, whiskers represent min/max values and crosses are outliers. The horizontal lines denote not-statistically significant differences for the comparisons across the values of hyperparameters (L and N) for ANN algorithm (NS, $p > 0.05$ with Bonferroni correction).

3.2.3.3. Effect of network architecture on ANN performance

For ANN, two hyperparameters were tested: number of L and number of N. In the first case, E was fixed to the obtained results in section 3.2.3.1 and the number of N to the maximum complexity of 30. In this case, using the commercial and custom electrodes, we found a saturation of EOF with L = 5 ($p > 0.1474$ for commercial sensors, and $p > 0.2061$ for custom sensors) as shown in Figure 40 top panels.

The optimization of N was done fixing E according to the results of section 3.2.3.1 and then fixing L, as described above. Figure 40 bottom panels show that also in this case the saturation of performance in term of EOF was with N = 10 both for commercial and custom sensors ($p > 0.083$ for commercial sensors, and $p > 0.3203$ for custom sensors).

3.2.3.4. Comparison of algorithms performances

The comparison among the algorithms was done with all the parameters optimized as detailed in sections 3.2.3.1, 3.2.3.2, 3.2.3.3. Figure 41 shows the comparison between the different algorithms for all type of performances, upper panels for commercial sensors and lower panels for custom sensors.

Table 17 Summarization results calculated on amputees. In table are reported the mean and standard deviation over subjects for each parameter of performances with all the hyperparameters of PR algorithms optimized.

Algorithm	F1Score [%]	Classification [%]	EOF [%]	Abstention [%]
$NLR_{(E=4, D=2)}$	95.98 ± 8.0	**99.3 ± 1.7**	97.7 ± 4.5	65.8 ± 16.8
RLS	51.8 ± 22.7	55.2 ± 22.4	61.9 ± 20.6	48.2 ± 10.2
$ANN_{(E=6, L=5, N=10)}$	73.7 ± 4.9	73.0 ± 4.8	84.6 ± 3.3	-
SVM	76.1 ± 5.7	75.1 ± 5.8	81.5 ± 4.1	-
LDA	**98.1 ± 2.1**	98.2 ± 1.9	**99.0 ± 1.1**	**38.8 ± 7.7**

Algorithm	F1Score [%]	Classification [%]	EOF [%]	Abstention [%]
$NLR_{(E=4, D=2)}$	**98.5 ± 2.5**	**99.8 ± 0.3**	**99.2 ± 1.3**	68.2 ± 15.5
RLS	46.9 ± 19.1	49.7 ± 18.5	58.7 ± 17.1	43.3 ± 7.1
$ANN_{(E=5, L=5, N=10)}$	73.4 ± 5.2	73.2 ± 5.3	84.4 ± 3.5	-
SVM	75.9 ± 3.9	75.7 ± 4.1	81.5 ± 2.9	-
LDA	96.7 ± 3.6	96.8 ± 3.5	98.2 ± 1.9	**38.1 ± 7.0**

As regard commercial sensors, we found a non-statistical difference between NLR and LDA in term of F1Score ($p = 0.6377$), EOF ($p = 1$), and Classification ($p = 0.0674$); while for custom sensors, the F1Score presented a non-statistical difference between NLR and LDA ($p = 0.0068$); while the abstention criterion had no statistical difference between RLS and LDA ($p = 0.0186$). All the other parameters presented statistical differences between algorithms.

3.2.3.5. Comparison of custom vs commercial electrodes

The comparisons between commercial electrodes and custom electrodes demonstrated that there was no-statistical difference for all algorithms except for RLS, Table 17. The performances were consistent and similar using both type of sensors.

3.2.4. Discussion

In this study, an in-depth analysis on four of the most adopted classifiers for EMG signals has been carried out, using LDA with time domain features extraction as ground truth for the final validation of the performed analysis. Furthermore, a comparison between commercial and custom electrodes was conducted to determine if it was possible to reduce the dimension of EMG sensors and consequently the interelectrode distance, without affecting the performances.

The different number of classification parameters extremely affected the computational burdening of the system. Therefore, we evaluated both parameters and performances to develop a fully custom embedded classifier. We conducted an intensive analysis on data acquired from 11 people with trans-radial amputation. This study provides a reflection upon the trade-off between performance and computational burdening of these classifiers, with particular attention on the final integration of the entire system.

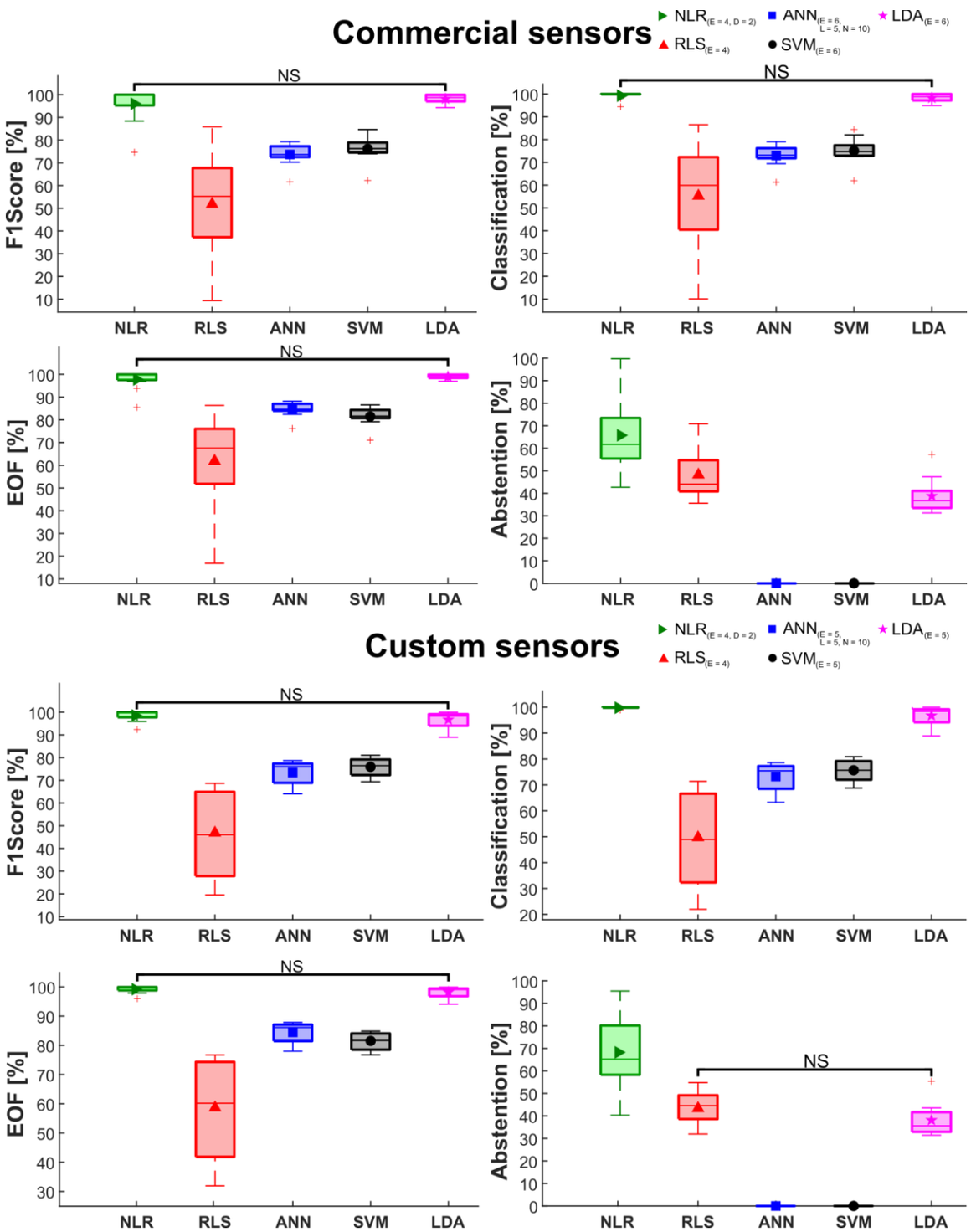

Figure 41 Algorithm comparisons with all hyperparameters (E, D, L, N) optimized.
In upper panels is present the data acquired using the Ottobock sensors, in the lower panels is present the data acquired using the IIT sensors. In the boxplots, the small icons are the means for each PR algorithm. The lower and upper quartiles are shown as the bottom and top edges of the box, respectively. The line inside the boxes indicates the median, whiskers represent min/max values and crosses are outliers. The horizontal lines denote not-statistically significant differences for the comparisons across the PR algorithms (NS, $p > 0.05$ with Bonferroni correction).

The performances were first evaluated by varying the number of sensors and then analyzed with the Wilcoxon Signed-Rank test on the TS. The results showed that for NLR and RLS no significant improvement of performance can be obtained with more than 4 EMG sensors, either commercial or

custom. While for the other algorithms there was no significant improvement in performance with more than 5 sensors only for the custom sensors, Figure 38. This result sets a benchmark on the necessary amount of space for sensors depending on the type of algorithm used. The commercial sensors, with 6 EMG electrodes fitting within the socket occupy 27 cm^2, while our optimization in term of number of electrodes can reduce to 4 sensors (18 cm^2). This permits to save about 9 cm^2. Oppositely, when the custom sensors are used in their full configuration, the amount of space occupied by 6 sensors is 15.3 cm^2. This means around 11.7 cm^2 less compared to the one occupied by the commercial ones. Moreover, by optimizing the number of custom sensors up to 4 EMGs (10.2 cm^2) it is possible to save ~16.8 cm^2 respect to commercial ones, and 5.1 cm^2 with respect to the custom full configuration. Overall, in the ideal case, custom sensors can reduce up to 27-10.2 = 16.8 cm^2 of the overall encumbrance which is fundamental in case of very proximal amputations. Furthermore, it is worth underling that decreasing the number of inputs for the algorithms also reduces the time to compute the trained model and, therefore, the output during an online classification.

Following optimization of E, we tuned the parameters of those algorithms needing optimization. The performance of NLR and ANN algorithms were then evaluated and analyzed by varying the complexity in term of both maximum polynomial features D and maximum number of L and N. The results showed that for NLR no significant improvement of performance could be obtained for a D greater than 2 for both commercial and custom sensors (Figure 39), and for ANN no significant improvements could be achieved by increasing the complexity of the network up to 5 L and 10 neurons for both commercial and custom sensors (Figure 40).

These results set a boundary on the complexity of the classifier, allowing to reduce the training and cross-validating times and the output generation during an online classification of amputees' gestures. It is also relevant to observe that NLR, in the linear case analysis (D = 1), obtained the lowest F1Score value with respect to the other higher grade of polynomial features, suggesting the use of a non-linear classifier when as inputs were used directly the EMG data of commercial or custom sensors.

Finally, the comparison between the two types of sensors demonstrated no statistical difference in performances. This means that if there is a need to decrease the number of motors in the array and reduce the amount of occupied space, the custom sensors could be used maintaining the same level of performances.

The next step in this research will be to expand the proposed approach using the best algorithm and the best configuration of parameters to online test the performance of that control. As explained above, the limit space of the socket reduces the possibility to use a large number of EMG electrodes, for this reason when a NLR is applied the number of EMGs can be safely reduce to 4 without any significant impact on performances.

The present experiment was performed by collecting EMG data from 11 trans-radial amputees performing 4 different movements, then an offline analysis was executed to determine the best parameter and configuration of algorithms to determine the best solution for online application. However, in the

envisioned practical application, the analysis was performed offline, and this can affect the final online control, but the controllability of the Hannes system performed by subjects confirmed the results we achieved. Therefore, the next step in this research will be to test the NLR that results as the best algorithm in an online scenario produce a target achievement control test (TAC) to obtain a complete evaluation on the usability of this solution. The aim of the present study was not a direct clinical translation but a systematic investigation of the effect of algorithm parameter on performances. Further, the results obtained confirmed our hypothesis that the number of sensors in specific configuration can be reduced without any significant impact on performances. In the case of a reduce amount of space available, that could give a guideline for the future clinical application on upper limb prosthetic use.

3.2.5. Conclusion

The present study aims at comparing different algorithms for pattern recognition, by optimizing the external and internal parameters and analyzing the role of the EMG sensor type of performances. The quality of the produced accuracy, namely, the F1Score and EOF, depends on the number of EMG sensors, the algorithm chosen, and the level of complexity used. Overall, the present study provides a clear scenario to better choose the algorithm and its parameter to decode muscle activity for prosthetic application. Nevertheless, there was a clear outperform towards the choice of the algorithm and the number of sensors. A higher number of sensors was more robust with respect to a lower number when using specific algorithms, indeed in other cases the number of sensors could be safely reduced, up to 4. This is an important outcome for the application of pattern recognition algorithms, as it points out that the encumbrance of the system for a general purpose multi-DoF prosthetic use, can be reduced in a more compact solution without any loss in performance.

3.3. Improved Pattern Recognition Control of Hannes 2 DoF: Hand Aperture and Wrist Flexion Extension

3.3.1. Introduction

Poly-articulated myoelectric hand prostheses are characterized by a high number of degrees of freedom (DoF). A crucial feature for their functionality and usability is their controllability. Indeed, low usage intuitiveness, often due to the poor ergonomics of the control system [420], lies among the main causes for prosthesis abandonment.

To promote a natural usage of a multi-DoF prosthetic hand in daily life scenario, here we propose an ergonomic decoder that is characterized by high accuracy, it does not rely on additional sources of input and it does not require the rearrangement of the natural contraction schemes. We also aimed at reducing the number of EMG sensors. We tested and optimized Linear Discriminant Analysis (LDA), gold standard in EMG pattern recognition application, and Non-Linear Logistic Regression (NLR) to decode hand and wrist movements, from up to 6 EMG electrodes, and to online control the Hannes system [11]. The performances improvement was observed not only on healthy subject data, but also on upper limb amputees when Hannes movements (rest, hand opening/closing – HOC) and wrist (flexion/extension - WFE) [13] were controlled.

3.3.2. Material and Methods

3.3.2.1. Subjects and Experimental Protocol

We recruited 10 able-bodied, right-handed subjects (6 males, age 36 ± 9 years) and 4 trans-radial amputated subjects. Six commercial EMG electrodes (13E200 AC, Ottobock) were embedded into a custom-made elastic brace placed around forearm or stump to collect electrical activity from 6 relevant muscle groups involved in grasping and wrist's flexion/extension movements (Figure 42 B).

We asked subjects to sequentially perform HOC and WFE 10 times (Figure 42 A). We also collected 16 repetitions of hand at rest (duration 2s, sampling frequency 1kHz).

3.3.2.2. Training and testing of the classifiers model

The analysed classifiers first underwent a calibration procedure to estimate the best set of internal parameters for further on-line use, as detailed in [13]. For the LDA algorithm, we split the dataset into a training set (70% of the data) and test set (30% of the data). For the NLR algorithm, we first down-sampled the data from 1kHz to 40Hz, obtaining a training group (4% of the data) and a test set (96% of the data). The training group was in turn divided into a training set (2.4% of the data for off-line tuning of the internal parameters), validation set (0.8% of the data for tuning the hyperparameters to prevent overfitting), and threshold optimization set (0.8% of the data for tuning the likelihood threshold for the

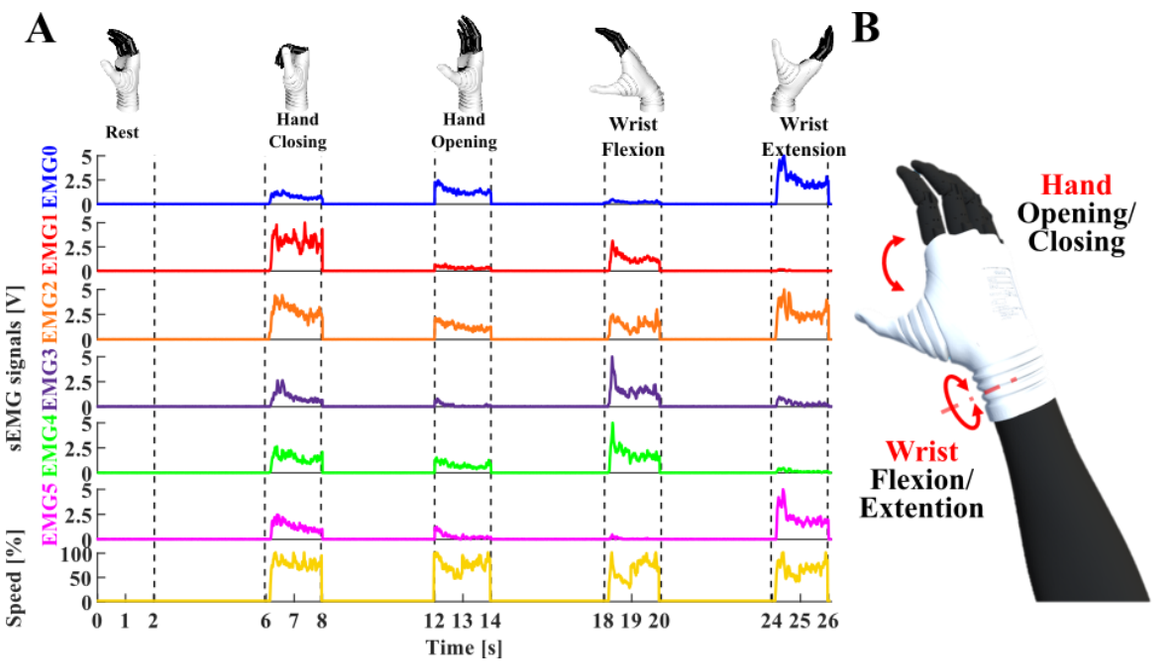

Figure 42 Surface EMG activities related to the single joint movement.
A: EMG signals and Hannes system speed during different hand and wrist movements. **B**: available DoFs of the Hannes system.

abstention criteria [421]). During validation, we tested the F1Score, calculated on the test set, with respect to the number of EMG electrodes. This analysis was used to estimate the minimum number of electrodes. Then, we compared algorithms performance, evaluated in terms of F1Score and abstention (% of non-assigned movements). The best configuration of classifiers was then used for testing the algorithms on amputees' dataset.

Finally, we used the resulting best algorithm, already calibrated, for on-line decoding of hand motions and control the Hannes system with sampling frequency set to 300Hz. Statistical analysis was performed with the Wilcoxon-Signed-Rank test using a Bonferroni correction [406].

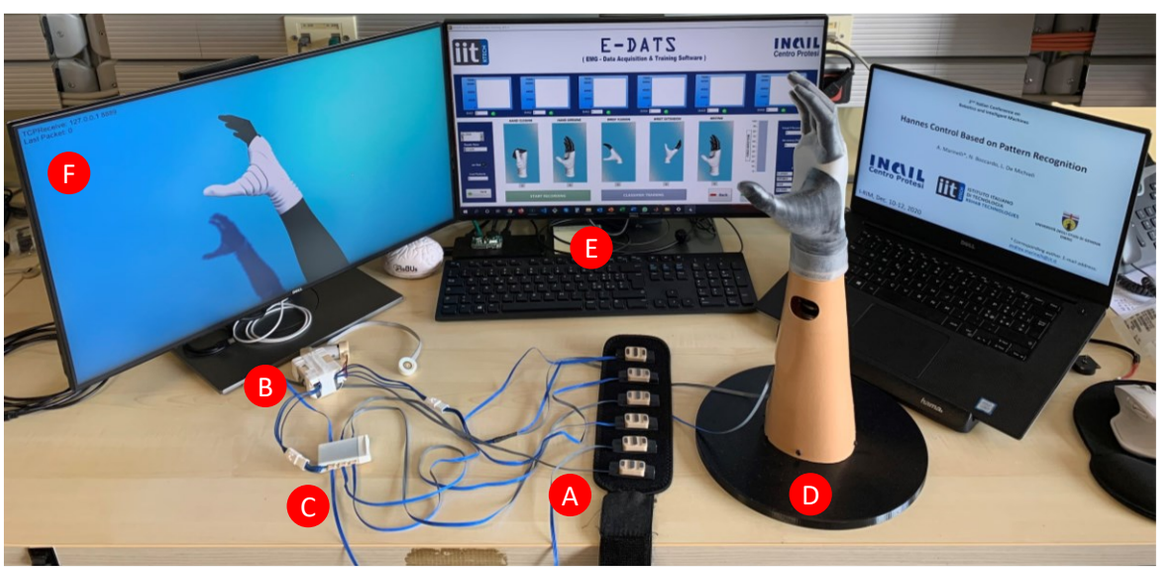

Figure 43 Experimental Setup.
A: EMG electrodes, **B**: power supply, **C**: EMG processing board, **D**: Hannes system, **E**: E-DATS software, **F**: Hannes system in a non-immersive virtual-reality on Unity.

3.3.2.3. Hannes System

The Hannes prosthetic system consists of: (i) a set of six EMG electrodes, (ii) a custom EMG processing unit, (iii) a myoelectric poly-articulated prosthetic hand, (iv) an active WFE, and (v) a battery pack (Figure 43). The EMG processing unit ("EMG-Master") acquires the analog sensor output and synthesizes the control signals for each active joint. The movements of the hand and wrist are proportional to the RMS of the six EMG signals, normalized in the range 0 to 100%.

3.3.3. Results

3.3.3.1. Effect of EMG electrodes number on performance

We first established the minimum number of EMG electrodes needed to maximize performance of algorithms, expressed as the non-statistical difference between the distributions of F1Score obtained from the test set (Figure 44).

For the NLR, we found that a configuration of five electrodes was enough to reach the same performance as with six electrodes. For LDA algorithms, the full configuration with 6 EMG sensors saturated its performance.

3.3.3.2. Comparison of algorithms performances

Figure 45 summarizes the performance scores in terms of F1Score and abstention obtained by the algorithms in their optimized configurations (i.e., with the optimized number of electrodes and hyperparameters).

With respect to F1Score (Figure 45 A) NLR always obtained the highest value. Although NLR has no statistical difference with LDA (gold standard). However, NLR also obtained highest percentage of abstention (Figure 45 B).

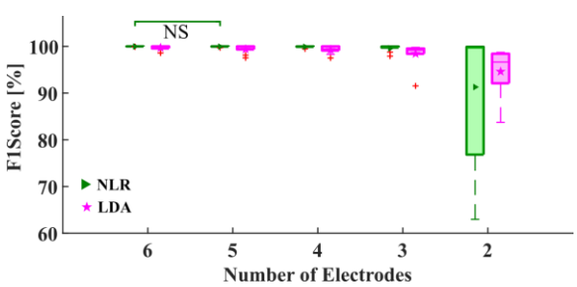

Figure 44 F1Score obtained by the classifiers using different number of electrodes.
For NLR the value of D is fixed to 7. NS: not significant

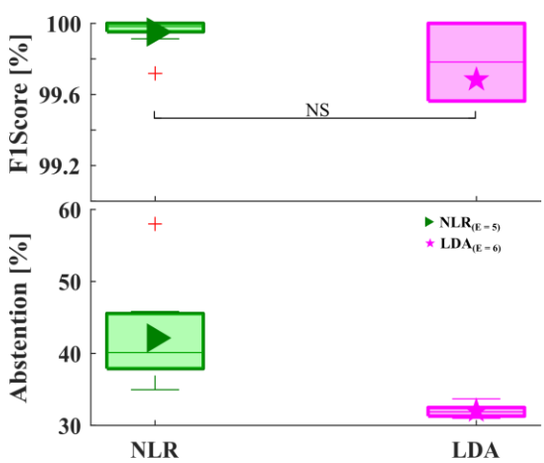

Figure 45 Algorithm comparison.
A: F1Score. **B**: Fraction of abstention. NS: not significant

3.3.3.3. Algorithms evaluation on the amputees' dataset

We tested the classifiers on four trans-radial amputees, using an optimized configuration, as obtained from the analysis of the healthy dataset. Table 18 shows the values of F1Score, classification, and abstention obtained from patients. Scores of the amputees matched those obtained by healthy subjects: NLR obtained the highest F1Scores, classification, and abstention score.

3.3.4. Discussion and Conclusion

We tested two pattern recognition algorithms to decode hand movements and we identified NRL is the one producing the best performances. Indeed, our results demonstrate that NLR is the only algorithm which reached the highest classification performance with five EMG electrodes. This is crucial for amputees whose residual arm is proximal, the smaller the number of electrodes, the smaller the possibility of undermining the socket robustness as well as the stability and costs of the entire prosthetic system.

When comparing classifiers in their optimized form, we found that, also in this case, the NLR outperform LDA in term of F1Score. NLR also obtained a greater number of abstentions. However, this apparent weakness is counterbalanced by the high classification frequency set.

We confirmed these results with upper limb trans-radial amputees, who were able to successfully control the Hannes system by activating the residual muscles of the stump in a natural way. Clearly, we need to extend the study to a wider population of amputees and we also need to confirm these promising results with clinical trials. However, as verbally described by the amputees, NLR algorithm allows them to reliably translate real-time movement intentions into actions.

DOI: 10.1109/IROS51168.2021.9636391

3.4. Hannes 3DoFs Prosthesis Control Based on Regression Machine Learning Algorithms

3.4.1. Introduction

Myoelectric prosthetic devices represent a real opportunity for enabling upper limb amputees to perform various activities of daily living (ADLs). These prostheses typically exploit flexor and extensor muscles of the wrist through surface electromyographic (EMG) electrodes [82]. Additionally, the level of recorded muscular contraction modulates the speed of the prosthesis, implementing a proportional control [401]. Due to the high complexity of the muscular system, the relationship between EMG signals and upper limb movements is remarkably nonlinear and generally only dual-site control has been employed [422]. Moreover, the prosthesis control is narrowed to the single articulation preventing the simultaneous movement of multiple joints. Indeed, when two or more DoFs are considered, only one joint is controlled at a time, and co-contraction strategies are used to switch between DoFs [423]. Other groups have attempted the direct control of multi-DoF prostheses by implementing a multi amplitude strategy using dual-site electrodes, by thresholding the muscle contraction intensity [131]. However, this strategy is not intuitive, with movements appearing to be clumsy and unnatural, therefore preventing users from feeling the prosthesis as part of their body [402]. In order to overcome these limits, pattern recognition algorithms were adopted by many groups to decode the intended movement, with the final goal of increasing the controllability of multi-DoF prosthetic devices [80, 165, 403]. However, current pattern recognition approaches demonstrated poor performance with DoFs higher than 2 [187]. Another limitation of these studies is that the outcomes achieved during laboratory experiments are poorly assessed in real ADL applications [401].

Therefore, there is an urgent need of a reliable and stable classifier able to deal with unknown situations typical of ADLs [405, 424-426]. We addressed this challenge by implementing a pattern recognition control specifically optimized for the Hannes system, a novel poly-articulated hand prosthesis [11], to generate a robust, intuitive and human-like simultaneous DoFs control. Concerning the previous work where only hand opening and closing were actively controlled [11], we here include the classification of other two DoFs of the wrist. We optimized and tested several pattern recognition algorithms that process information coming solely from the EMG electrodes embedded in the prosthetic device. We then implemented the resulting best performing algorithm for simultaneous online control of the Hannes system joints. Our group already tested pattern recognition algorithms for translating muscular activity into virtual hand movements in 2 DoFs only (rest, hand opening-closing (HOC), wrist pronation-supination (WPS)) [13]. We here extend this work by including the detection of wrist flexion-extension (WFE) for the real-time control of the Hannes prosthesis [13]. We assessed the performance of the detection algorithms for the control of the Hannes prosthetic hand both with 10 healthy subjects and with 3 trans-radial amputees. The examined classifiers were: Non-Linear Logistic Regression

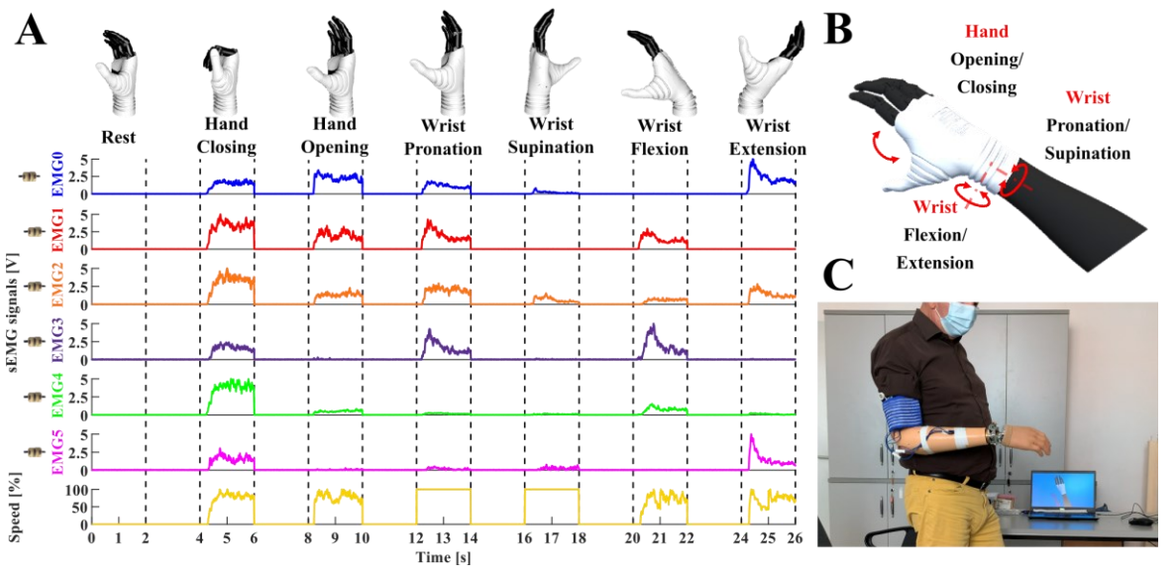

Figure 46 sEMG activities related to each gesture.
A: EMG signals and Hannes system speed during different gestures. **B**: available degrees of freedom of the Hannes system.
C: Amputee performing Real-Time control of Hannes and VR.

(NLR) [77], Regularized Least-Square (RLS) [410], Artificial Neural Network (ANN) [411], Support Vector Machine (SVM) [412], and Linear Discriminant Analysis (LDA) [77]. For NLR, RLS and LDA methods, we combined pattern recognition with an "abstention" criterion. This consists in evaluating the likelihood of the decoded joint movement and enabling an "abstention" criterion (i.e. confidence-based rejection) [421]. The hyperparameters calibration and the integration of abstention inside each algorithm greatly improved the classifier accuracy. The increased number of DoFs to be simultaneously classified could lead to lower algorithms accuracy with respect to simpler settings [11, 13], nevertheless we here show that performances were still suitable for prosthetic control. We also found that both for amputees and able-bodied subjects, the NLR outperformed the other classifiers.

3.4.2. Materials and Methods

3.4.2.1. Subjects

We involved ten healthy subjects aged between 22 and 33 years (27.1 ± 3.2) and three mono-lateral amputees (trans-radial amputation of the dominant limb, already users of active prostheses). Written informed consent was obtained from all subjects. The study adhered to the standard of the Declaration of Helsinki and was approved by the Bologna-Imola ethical committees (CP-PPRAS1/1-01).

3.4.2.2. Experimental Protocol

Six Ottobock EMG electrodes (13E200=50 AC) were attached to an elastic band (Figure 47 A) wrapped around the forearm or stump approximately 5cm distal to the olecranon. These electrodes measured muscular electrical activities during grasping, WPS and WFE movements (Figure 46 A). Muscles involved were identified by manual inspection and they were: Extensor Carpi Radialis Longus (EMG_0), Extensor Digitorum (EMG_2), Extensor Carpi Ulnaris (EMG_4), Palmaris Longus and Flexor

DOI: 10.1109/IROS51168.2021.9636391

Carpi Ulnaris (EMG_1), Flexor Carpi Radialis (EMG_3) and the Brachioradialis Muscle (EMG_5).

After electrodes positioning, users were placed in front of a display showing the virtual Hannes system (Figure 47 E). We required subjects to sequentially execute HOC, WPS and WFE 10 times. Then, we also recorded 16 repetitions of resting position (2s time-window and 1kHz sampling frequency) and combined their samples into a random distribution, obtaining a total of 24 repetitions (4 repetitions x 6 gestures). This resting data was then randomly arranged for each gesture to create an indecision region.

3.4.2.3. Processing of EMG signals

EMG signals followed the same processing already described in [13]. Briefly, a custom EMG-master board implements the A/D conversion of the input data, which are subsequently sent to the PC via Bluetooth. We then used a customized version of the EMG - Data Acquisition & Training Software (E-DATS [13, 77], Figure 47 E) to both collect data and offline train the algorithms. The model generation was realized through a MATLAB script (MathWorks).

Following classifier training, real-time recognition of the available gestures was performed. Afterward, the Hannes system, equipped with the resulting best classifier, was controlled in real-time by each subject.

3.4.2.4. Train and test the algorithms

Algorithms (see paragraph 3.4.2.6) were first calibrated, in order to obtain internal parameters able to satisfy high performances with the lowest computational effort during the online control, as detailed in [13]. For the LDA algorithm, we split the dataset into a training set (70% of the data) and a test set (30% of the data). The other algorithms were used after down-sampling the data from 1kHz to 40Hz, obtaining a training group (4% of the data) and a test set (96% of the data). The training group was in turn divided into a training set (2.4% of the data for offline tuning of the internal parameters), validation set (0.8% of the data for tuning the hyperparameters to prevent overfitting), and threshold optimization set (0.8% of the data for tuning the likelihood threshold for the abstention criterion). Afterward, we used the resulting best algorithm, already calibrated, for online decoding of hand motion using a real-time PC

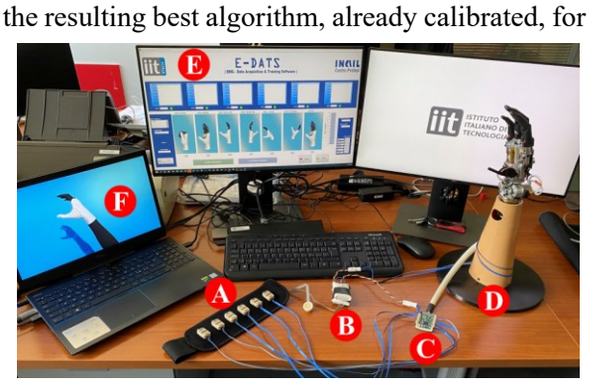

Figure 47 Experimental Setup.
A: EMG electrodes, **B**: power supply, **C**: EMG processing board, **D**: Hannes system, **E**: E-DATS software, **F**: Hannes system in a non-immersive virtual-reality on Unity.

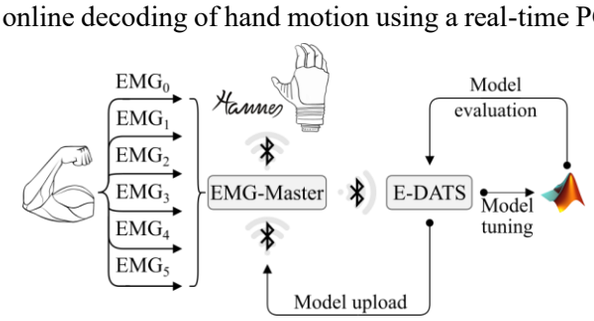

Figure 48 Diagram of the model generation and Hannes control.

simulation based on pattern recognition (Model evaluation in Figure 48). The optimized model was then uploaded (Model upload in Figure 48) to the EMG processing board (TiVa Cortex-M4) for final online classification (Hannes in Figure 48), used to freely control the Hannes with sampling frequency set to 300Hz.

3.4.2.5. Hannes hand

The Hannes prosthetic system consists of: (i) a set of six EMG electrodes, (ii) a custom EMG processing unit, (iii) a myoelectric poly-articulated prosthetic hand (Figure 47 D), (iv) an active WFE, (v) an active WPS, and (vi) a battery pack (Figure 47 B). The EMG processing unit ("EMG-Master" Figure 47 C) acquires the analog sensor output and synthesizes the control signals for each active joint. The extent of the activation is proportional to the RMS of the six EMG signals, normalized in the range 0 to 100%. An exception is the WPS, which is always controlled at the maximum velocity. The references are then sent to the respective motor control boards within the prosthetic system. Each motor driver has an on-board control loop to ensure the correct joint movement: closed-loop speed control for the hand and WFE, and open-loop for the WPS. A detailed description of the mechanical design of the prosthetic hand is provided in [11]. To the architecture described in [11], the current system adds the two active DoFs for the wrist. The WFE consists of a custom drivetrain based on a worm gear, ideal to withstand the high external loads. The overall range of motion achieved is ±65°. Similarly, the WPS consists of a standard motor-gearbox actuation, and it can provide 360° rotation. The "de-facto" standard quick disconnect system by Ottobock was replicated, as described in [11].

3.4.2.6. Algorithms and hyperparameters optimization

Following previous work on prosthetic control [405], we compared supervised machine learning algorithms: NLR [77], RLS [410], ANN [411], SVM [412], and LDA [77]. We first estimated the minimum number of EMG electrodes for each classifier by computing, for each configuration of EMG sensors, the F1Score performance. For the NLR classifier, we optimized the polynomial degree (D), which plays an important role since it represents the complexity of the algorithm, as described in [13]. The higher the complexity, the greater the computational burden required to the processing board. Regarding the ANN, we investigated the importance of the number of hidden layers by fixing the number of neurons to the highest value (30) and then we optimized the number of neurons, considering the previously obtained optimal number of hidden layers. Furthermore, in RLS, LDA and NLR, the maximization of the voluntary gestures recognition was implemented through the addition of a Likelihood threshold [405]. The threshold, ranging between 0.7 and 1, was optimized for each subject and each algorithm in terms of F1Score [404]. During offline optimization, in the cases of movements under threshold or simultaneous supra-threshold movements, the classifier abstained without classifying. During online classification, supra-threshold movements belonging to the same DoF were considered as "abstentions", while supra-threshold movements belonging to different DoFs produced

DOI: 10.1109/IROS51168.2021.9636391

simultaneous movements. We used the test set (paragraph 3.3.2.2) to assess the performance of each algorithm in terms of F1Score and Embedding Optimization Factor (EOF), considering different configurations of hyperparameters. The EOF explains the trade-off between performance accuracy and complexity of the algorithm, which is strongly related to the computational burden on the EMG processing board [77]. This index is associated to the available memory on the EMG-Master. Therefore, it may happen that in some cases (e.g. full configuration of EMG sensors), the model has too many parameters for the available flash memory, resulting in EOF obtaining negative scores (see [77] for EOF calculation). We compared the performance of each algorithm in terms of F1Score, EOF, classification (percentage of correctly decoded movements, i.e. accuracy), and abstention (percentage of not assigned movements). Afterward, the optimized hyperparameters were exploited to build optimal classifiers on the amputees dataset. We used Wilcoxon-Signed-Rank test and Bonferroni correction [406] for statistical analysis.

3.4.3. Results

3.4.3.1. Variation of EMG electrodes number

The minimum number of EMG electrodes was first determined to optimize the performance of each algorithm, highlighted by the absence of statistical difference in the F1Score (NS in Figure 49). Then, starting from the setup with 6 EMG electrodes, we successively decreased the number of sensors by ignoring EMG signals coming from muscles with lower activity, according to the following order: EMG_5, EMG_2, EMG_3, EMG_4. Regarding the LDA and the NLR classifier, the best configuration was obtained either with five or six electrodes. For SVM and ANN, only four electrodes were required to maximize the performance, while for RLS the full configuration with 6 EMG sensors saturated the

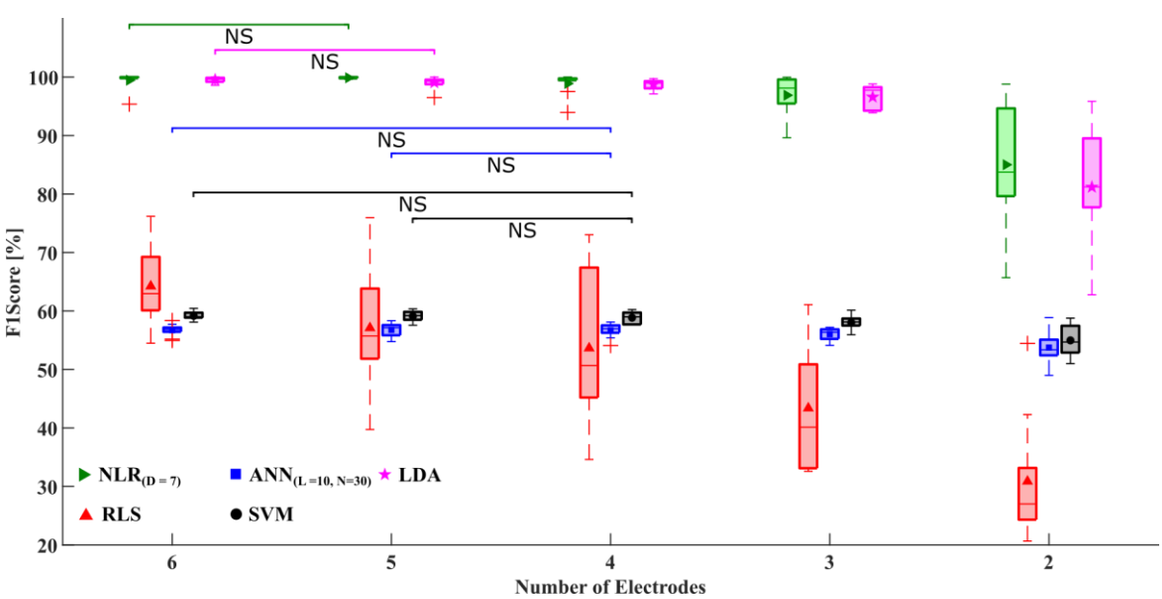

Figure 49 Performance of F1Score when varying the number of electrodes for each classifier.
In the NLR the D-value is fixed to 7, while for ANN the number of hidden layers is 10 and the number of neurons is 30.
NS: not significant.

performance. However, F1score was highest for NRL and LDA with any configuration of electrodes, while in other cases, it was always lower than 65%.

3.4.3.2. NLR: variation of polynomial degree D

Regarding the NLR classifier, we swept the polynomial degree (D-value) in the range 1-7 to assess the performance in terms of EOF. As represented in Figure 50, we obtained the optimal behavior for D = 2.

3.4.3.3. ANN: variation of network architecture

Concerning the ANN classifier, we evaluated how the number of hidden layers affects performance using a configuration of 4 EMG electrodes. We tested the EOF performance when varying the number of hidden layers (L) from 1 to 10 (according to [77]) and keeping fixed to 30 the number of neurons. We found optimal EOF values with L=5 or greater (Figure 51 A). Subsequently, we considered as the optimal choice L = 5 and we varied the maximum number of neurons (N) between: [1, 5, 10, 15, 20, 23, 24, 25, 26, 27, 28, 29, 30]. We compared the performance of the different configurations to establish the best hyperparameters setup. We set N=1 since we found that performances do not degrade when considering more neurons (Figure 51 B).

3.4.3.4. Analysis of algorithms performance

Figure 52 highlights the behavior of the classifiers in terms of F1Score, EOF, classification, and abstention obtained by the various algorithms in their optimized configurations (i.e. optimal values of hyperparameters). With respect to F1Score, EOF and classification (Figure 52 A, B and C), NLR always

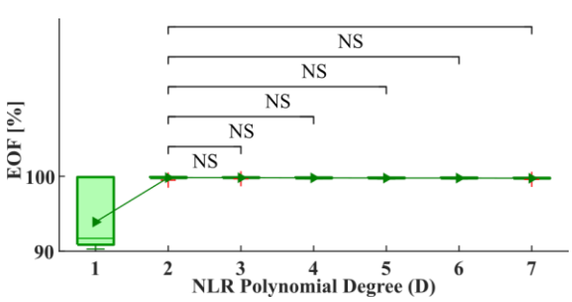

Figure 50 NLR optimization with 5 electrodes: EOF performance when varying the maximum D-value.
NS: not significant.NS: not significant

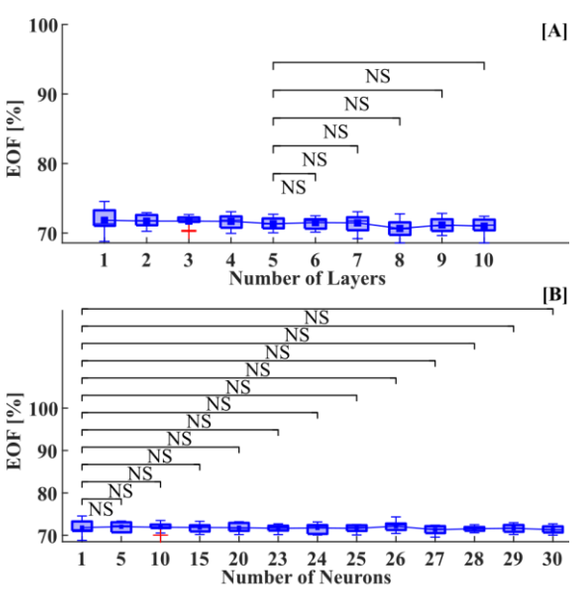

Figure 51 ANN optimization with 4 EMG sensors.
A: EOF performance when the maximum number of hidden layers varies and the maximum number of neurons is fixed to 30. **B**: EOF performance when the maximum number of neurons varies and the maximum number of hidden layers is fixed to 5. NS: not significant.

DOI: 10.1109/IROS51168.2021.9636391

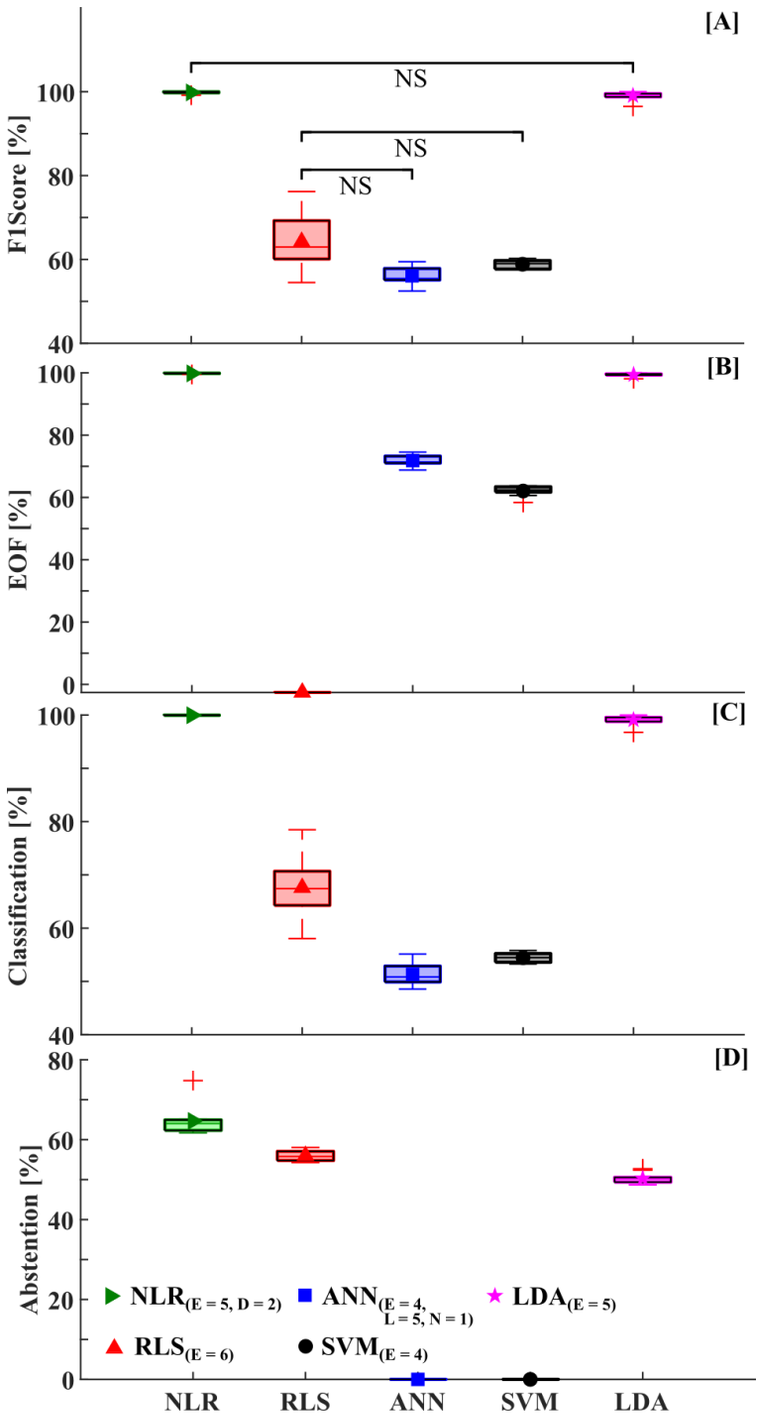

Figure 52 Algorithms comparison. **A**: Performance of F1Score. **B**: EOF index. **C**: Percentage of correctly classified outputs. **D**: Percentage of abstention. NS: not significant.

reached the highest value. Although the F1Score has no statistical difference between NLR and LDA (gold standard), the former obtained less dispersed results, as indicated by small standard deviation. However, the highest abstention was reached by NLR (Figure 52 D).

3.4.3.5. Tests on amputees

With trans-radial amputees, we used the optimal configurations of the classifiers obtained from the analysis on able-bodied subjects. Moreover, we compared the performance obtained by amputees with those of the healthy subjects to assess whether the algorithms perform differently in the two cases. Table

18 highlights the values of F1Score, EOF, classification, and abstention achieved by amputees. Scores of the patients matched those obtained by able-bodied subjects: NLR had the highest classification score, followed by LDA. F1Scores and EOF were highest for NLR, followed by LDA for patients #1 and #3, vice versa for the other subject. NLR obtained greater abstentions. During the experiments, the amputees verbally expressed their satisfaction towards the improved controllability of the tested system with respect to their usual prosthesis.

3.4.4. Discussion

We tested multiple supervised machine learning algorithms to decode prosthesis movements. We found NLR and LDA algorithms as top performers, with respect to EOF, with a configuration of 5 EMG electrodes. In a previous study including only 1 DoF for the wrist [13], our group found that 3 EMG electrodes were enough for NLR to reach top performance. We here show that the successful decoding of 3 DoFs movements came at the cost of increasing the number of EMG electrodes needed (from 3 to 5). NLR maintained the same performance when the degree of polynomial complexity is higher or equal than 2. This guarantees that the computational burden is still kept at a minimum, even with a greater number of decoded classes, with respect to [13]. Regarding the ANN algorithm, we optimized the architecture of the network with respect to our previous study [13]. Indeed, the optimal maximum number of hidden layers decreased to 5 (6 in [13]) and that of neurons decreased to 1 (24 in [13]). However, the performances dramatically dropped as both classification and F1scores decreased to 51.3% and 56.1%, respectively (80.3% and 80.2%, respectively, in [13]), presumably as an effect due to the increased number of decoded classes that causes less separation of gestures into the parameter hyperspace. Differently from [187], where they achieved degraded performance for the 3-DoFs control, we here discovered that, with the same number of DoFs, the NLR algorithm is the most suitable for a prosthesis control based on pattern recognition. Although no statistical difference was found between NRL and LDA algorithms, NRL showed smaller standard deviations (see Figure 52 A). NLR and LDA were also the best performing algorithms for amputees, who succeeded in the control of the Hannes system through the residual muscular activity of the stump. With respect to other classifiers, NLR also reached a higher percentage of abstentions. Nonetheless, due to the high classification frequency, set to 300Hz, 300 movements per second were decoded. Consequently, latency between movement intentions and resulting action was not perceived by users even in case of high abstention rate. The abstention criterion reduced the number of classification artifacts, leading to more robust and consistent classification with respect to the state of the art systems in a similar context [3, 427]. The NLR algorithm was therefore implemented on the microcontroller board for online control of Hannes. Subjects could then freely explore the human-like behavior of the system, which was able to achieve simultaneous and intuitive control of multi-DoFs, a fundamental feature for bioinspired prosthetic use, not yet achieved by current state-of-the-art systems [3, 401]. Indeed, as reported by amputees, the NLR classifier allows the reliable translation of the gesture intentions into actual movements (Figure 46 C). However, online

DOI: 10.1109/IROS51168.2021.9636391

Table 18 AMPUTEES RESULTS.
In bold are highlighted the best performances of each index (F1Score, EOF, classification, and abstention) for each amputee. The number of electrodes is fixed from the results on the able-bodied subjects.

S.	*Alg.*	*EMG sensors*	*F1Score [%]*	*EOF [%]*	*Classification [%]*	*Abstention [%]*
1	*NLR*	5	**99.73**	**99.77**	**99.96**	**82.21**
	RLS	6	38.22	-2.62	42.27	52.99
	ANN	4	54.63	70.64	49.21	-
	SVM	4	59.37	61.86	55.06	-
	LDA	5	97.86	98.80	98.51	57.88
2	*NLR*	5	93.81	96.71	**98.91**	**77.95**
	RLS	6	35.09	-2.63	37.47	56.04
	ANN	4	44.45	61.54	41.70	-
	SVM	4	50.88	54.23	47.54	-
	LDA	5	**94.73**	**97.18**	94.59	54.88
3	*NLR*	5	**99.91**	**99.86**	**99.99**	**77.08**
	RLS	6	44.75	-2.61	48.12	56.82
	ANN	4	49.29	66.02	44.61	-
	SVM	4	55.31	59.28	51.64	-
	LDA	5	96.46	98.08	96.69	53.63

control was not systematically tested as for the offline phase, leaving online control to be further assessed in future experiments. Moreover, we need to increase the number of amputated subjects in order to properly perform statistical analysis. Finally, to truly assess the validity of NLR for simultaneous multi-joint prosthetic control, it will be fundamental to perform tests outside the lab and in the context of ADLs.

3.4.5. Conclusion

We here assessed the ability of multiple supervised machine learning algorithms to simultaneously control upper limb prosthesis through EMG signals detected at the forearm level of healthy subjects. NLR turns out to be the best operating algorithm and we further supported this result by tests on trans-radial amputees controlling the Hannes system (see the attached VIDEO). We will now extend this study to a wider amputees population in the context of ADLs, in order to truly test NLR control of prosthetic devices in real life context.

3.5. Chapter Discussion and Remarks

The promising capabilities of prosthetic devices can be enhanced significantly by leveraging the recent developments in electromyography (EMG) sensors and algorithms. In recent research, miniature EMG sensors were developed and compared to the gold standard, with impressive results. The sensors led to similar or better performance than the gold standard. An in-depth analysis was also conducted on the most commonly used classifiers for EMG signals, revealing that no significant improvement in performance could be obtained with more than 4-5 EMG sensors for the algorithms tested. Such preliminary result allows a reduction of occupied space in the socket up to 16.8 cm^2 guaranteeing an easiest integration with the final device for A3 of Chapter 4. Furthermore, NRL was found to be the best algorithm for decoding hand movements with the highest classification performance enabling successful control of the Hannes system by upper limb trans-radial amputees. Finally, NLR algorithm achieving simultaneous and intuitive control of multi-DoFs, a fundamental feature for bioinspired prosthetic use. These developments are significant for improving the functionality and usability of prosthetic devices, potentially enabling greater independence and mobility for those with limb loss.

In summary, the following outcomes were achieved:

1. Miniature EMG sensors for prosthetic applications were developed and compared to the gold standard. IIT sensors led to similar or better performance than the gold standard, and Ottobock sensors reached the highest classification performance with only three EMG sensors. IIT sensors required four sensors but were smaller in overall area, which is an advantage for prosthetic applications.
2. An in-depth analysis was conducted on four of the most adopted classifiers for EMG signals, and it was found that no significant improvement of performance could be obtained with more than 4 EMG sensors for NLR and RLS, and no significant improvement in performance with more than 5 sensors for the other algorithms. The performance of NLR and ANN algorithms were evaluated, and it was found that no significant improvement of performance could be obtained for a D greater than 2 for both commercial and custom sensors.
3. NRL is the best algorithm for decoding hand movements with the highest classification performance using five EMG electrodes, which is important for amputees with a residual arm. Upper limb trans-radial amputees were able to successfully control the Hannes system using the NRL algorithm and translate real-time movement intentions into actions.
4. NLR and LDA algorithms were found to be the top performers for decoding prosthesis movements with 5 EMG electrodes. NLR maintained the same performance with a greater number of decoded classes and polynomial complexity, keeping the computational burden at a minimum. The NLR algorithm was implemented on the microcontroller board for online control of Hannes, achieving simultaneous and intuitive control of multi-DoFs, a fundamental feature for bioinspired prosthetic use, not yet achieved by current state-of-the-art systems.

Chapter 4. Bidirectional Body – Machine Interface

The bidirectional communication between the user and the external word is crucial for an effective acceptance and reintegration of the device into the body scheme. The haptic feedback methods developed in this project included proprioceptive and tactile feedback strategies that result intuitive, compact, and non-invasive respect to the literature solutions [136, 428]. Providing subjects information on how the prosthesis moves is a fundamental aspect to remove the continuous visual attention on the prosthesis during tasks [429], reducing the mental demand while using multi-DoF systems [1, 430]. This activity aimed at realizing a feedback system able to restore the bidirectional communication between the user and the prosthesis in a compact solution for its integration on a prosthetic socket.

During the six months at Aalborg University, I was able to deeply investigate and implement methos to provide proprioceptive feedback. The literature analysis allowed me to identify non-invasive methods to provide proprioceptive feedback. Consequently, I developed a novel method to restore a continuous wrist rotation proprioception. Then, the approach was extended to include the hand aperture proprioception in a compact solution without increasing that solution's cumbersome. I integrated such methods into the prosthesis and implemented a closed-loop control to EMG drive the prosthesis and receive back the proprioception information in both able body and amputees. Finally, a validation framework was developed, based on a virtual environment (Unity), to systematically test the user performance on perceiving and recognizing the feedback information received using a clinical protocol dedicated (e.s., Target Achievement Control Test - TAC).

In this section, the results for each activity were described, presenting the relative scientific papers:

- Marinelli, et al. “A Novel Method for Vibrotactile Proprioceptive Feedback Using Spatial Encoding and Gaussian Interpolation.” IEEE Transactions on Biomedical Engineering, 2023. (submitted)
- Marinelli, et al. “A Compact Solution for Vibrotactile Proprioceptive Feedback of Wrist Rotation and Hand Aperture.” Journal of Neural Engineering, 2023. (submitted)
- Marinelli, et al. “Object Stiffness Recognition and Vibratory Feedback without Ad-hoc sensing on the Hannes Prosthesis: a Machine Learning Approach.” Frontiers in Neuroscience, 2023. [16]

4.1. A Novel Method for Vibrotactile Proprioceptive Feedback Using Spatial Encoding and Gaussian Interpolation

4.1.1. Introduction

Over the past twenty years, the field of multi-functional upper limb prostheses was marked with important technological and scientific developments aiming to better satisfy the needs of prosthesis users. The loss of an upper limb is a traumatic event with a strong impact on the ability to participate in the activities of daily living [6, 407], thereby leading to a substantial decrease in the quality of life [9]. Despite the aforementioned developments, in a recent study, Salminger, et al. [19] reported overall abandonment rates of about 44% for the users of upper limb myoelectric prostheses. An important drawback of modern prostheses is that they lack explicit somatosensory feedback. Without the feedback, the user can still estimate the state of the device using incidental cues, such as visual observation and motor sound [39, 145], but this requires constant attention to the prosthesis. Providing explicit feedback can reduce the cognitive load and fatigue when using prostheses [5, 6].

To mitigate this drawback, methods to restore the missing sensory information were proposed in the literature, and the results demonstrated that the haptic feedback can enrich the prosthesis-user interaction by improving performance [156, 428, 431] and subjective experience [432, 433] as well as by facilitating the feeling of embodiment [88, 126, 127]. Reestablishing the closed-loop control, characteristic of sound limbs, can trigger somatosensory plasticity and promote long-term learning and adaptation processes for artificial sensations [129].

To provide haptic feedback, the information about the prosthesis state can be conveyed to the subject invasively [88, 106, 155, 434, 435], by electrically stimulating peripheral nerves that innervated the lost hand, or non-invasively [5, 100, 220, 436, 437], by delivering mechanical or electrical stimulation to the skin of the residual limb. Despite the invasive methods needing a surgical procedure to implant the electrodes, they allow providing somatotopic feedback, where the tactile sensation is experienced as coming from the missing limb (phantom sensation) [434]. Such invasive feedback was used to convey pressure [120], textures [155], slippage [438], pain [106], and proprioception [5, 88]. However, this approach has several drawbacks including the risks of surgery, subject reluctance to undergo additional surgical operations, high cost, lack of access, and limitations in perceptual performance due to the difficulty in selective activation of target nerves. Non-invasive methods are simpler to implement and can be particularly relevant in those subjects that are reluctant to undergo further surgical procedures [1]. Although the non-invasive stimulation results in a less natural sensation (e.g., non-somatotopic), the subjects can quickly learn to interpret the feedback and integrate it into the body scheme [401]. In most studies, prosthesis grasping force was selected as the variable to be transmitted to the user [5, 100, 217, 220, 428, 437, 439-442], while the artificial proprioceptive feedback, conveying the position of the

prosthesis joints (e.g., wrist rotation and hand aperture), was seldom considered [136, 408, 436, 443-446].

Different methods have been presented in the literature to provide artificial proprioceptive feedback. The most natural approach is to induce a realistic kinesthetic illusion [161, 408, 444, 447], where a phantom sensation of the movement of the missing limb is created, for instance, by vibrating muscles to activate muscle afferents [448-450]. This is modality-matched feedback and hence likely most intuitive for the subject but the setup can be cumbersome. Another approach that can be implemented using a more compact setup is the sensory substitution feedback, where proprioceptive information (e.g., wrist angle) is provided indirectly, using tactile stimulation [5]. In this approach, at least a brief training is required to teach the subject to associate the tactile sensation with the provided information. Tactile stimulation can be delivered mechanically (e.g., using vibration motors) or electrically, but regardless of the stimulation interface one of the critical questions when designing such feedback is the choice of the encoding scheme, which defines the mapping between the feedback variable and stimulation profile [5].

When a single-channel stimulation is used, the feedback information can be encoded by modulating stimulation parameters, such as intensity. A conventional approach would be to modulate the intensity or frequency of electro or mechanotactile stimulation [439, 451, 452]. Recently, Battaglia, et al. [444] and Kayhan, et al. [443] presented a novel solution to convey wrist rotation and/or hand aperture by stretching the skin. When multiple stimulation channels are available, feedback information can be conveyed also by changing the location of stimulation (active channel), the approach known as spatial encoding. Witteveen, et al. [453] used arrays of vibromotors or electrotactile stimulators to convey hand aperture feedback. In Garenfeld, et al. [454] wrist orientation and hand aperture information were provided using electrotactile stimulation delivered through a 16-pad electrode array. Finally, the most flexible scheme is to combine spatial encoding and parameter modulation, which is a so-called mixed encoding approach. For instance, Erwin and Sup IV [455] combined the spatial activation of three vibration motors with the modulation of vibration frequency to convey the position of a virtual wrist. Despite different methods have been used to encode the proprioceptive information, they are rarely compared against each other (see [136] for the comparison between spatial and amplitude schemes). In addition, the methods are usually implemented by heuristically predefining the configuration parameters (e.g., number of motors, intensity) instead of systematically investigating the performance across the parameter space. However, such comparisons are important as they can help making informed choices when designing feedback interfaces.

The present study describes a novel approach to providing wrist rotation feedback using an array of vibromotors and a mixed encoding paradigm. Multiple vibrators were activated simultaneously to produce the moving phantom sensation, while the vibration intensity was interpolated across the array following the Gaussian profile. This approach provided a continuous sensation of motion around the forearm that was congruent with the motion of the prosthesis. In this scheme, the quality of the elicited

sensations critically depends on the number of motors in the array as well as the "width" of the Gaussian. For instance, increasing the width makes the change in sensation around the forearm more smooth and hence continuous. In addition, decreasing the number of motors can simplify the integration of the feedback interface into the prosthetic socket. Such continuous feedback that directly follows the motion of a prosthesis would be intuitive and thereby easy to interpret (direct relation between sensation and feedback variable), could enable higher spatial resolution, and improve user experience by generating smooth and pleasant sensations [456]. These factors could in turn lead to more effective control and a decrease in the cognitive load and fatigue required to use a prosthesis. However, a "wider" Gaussian could also jeopardize the identification of the current wrist orientation conveyed by the momentary location of the peak of the Gaussian profile. In the present study, we have therefore investigated the impact of both of these factors on the effectiveness of haptic feedback during the closed-loop control of a hand prosthesis. To this aim, the subjects performed a virtual target achievement control test (TAC) [457], using a novel framework that simulates the behaviour of the Hannes prosthesis [11] while providing vibrotactile feedback to control the rotation of the virtual hand. The subjects performed the task with different combinations of the number of motors and Gaussian width, thereby systematically exploring the parameter space of the novel feedback approach. With the small width of the Gaussian, our method "reduces" to discrete spatial feedback used previously in the literature [450], where a single vibromotor is activated at a time (hence, localized stimulation which "jumps" around the forearm). Therefore, in addition to exploring the parameters, the present study also compares the conventional approach (discrete feedback) to the novel method that produces smooth sensations congruent to the orientation of the prosthesis.

4.1.2. Materials and Methods

4.1.2.1. Subjects

Fifteen healthy able-bodied subjects (aged 26.7 ± 3.2, 8 males), and an individual with congenital limb deficiency subject (aged 25, female) with no prior experience with proprioceptive tactile feedback, participated in this study. Before starting the experiment, the subjects were informed about the protocol, and they signed the informed consent form. The experimental protocol was approved by the Research Ethics Committee of the Nordjylland Region (approval number N-20 190 036).

4.1.2.2. Experimental Setup

The experimental setup (Figure 53) comprised the following components: (i) a virtual reality (VR) environment simulating the Hannes prosthetic hand [11-13, 15] with 3 active DoFs (hand open/close, wrist pronation/supination, and wrist flexion/extension), (ii) fourteen eccentric rotating mass vibromotors (Vybronics, VC0625B001L) with a custom-made control unit to provide tactile feedback, (iii) a custom-made master board to establish the communication between a host PC and feedback

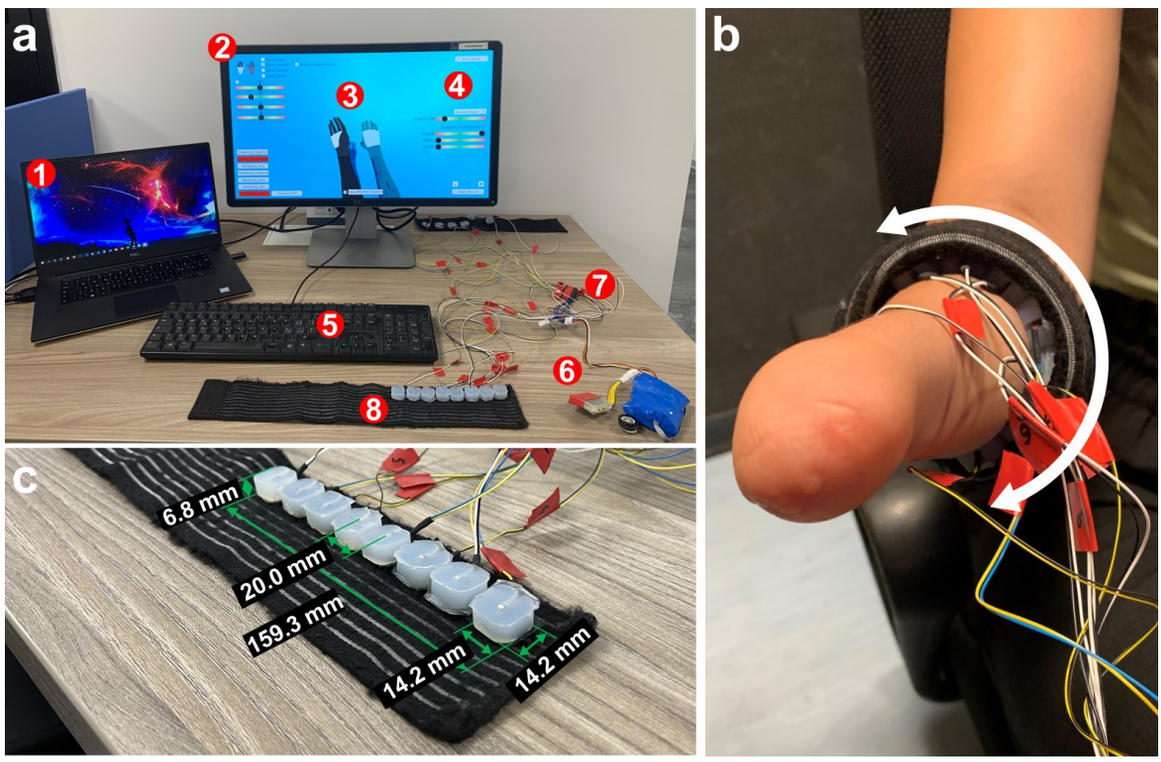

Figure 53 Experimental Setup.
a: The subjects were seated in front of the monitor (2) wearing the armband with the vibromotors (8) placed equidistantly around the interior aspect of the right forearm. The virtual reality scenario showed the orientation of the target and the controlled hand (3). The graphical controls (4) allow setting the parameters of the feedback scheme. The keyboard (5) was used to move the controlled prosthesis while its state (wrist angle) was conveyed through vibrotactile feedback. The setup also included a laptop (1), a master board with a battery pack (6), and a feedback control board (7). **b**: The elastic band with vibromotors placed around the medial part of the right forearm of an amputee participant. **c**: a detailed photo of the wrist band with vibromotors with indicated dimensions.

control unit, (iv) a battery pack, and (v) a standard laptop (DELL XPS 15, Intel Core i9 @2.60GHz, 32GB RAM) running Windows 10, an 18'' computer monitor and a keyboard. The master board communicated with the feedback controller using CAN Bus protocol, while it was connected to the laptop via Bluetooth. The VR framework was developed using the Unity development suite and C# language. The framework acquired the data from the master board and sent control commands to the feedback controller to generate desired vibrotactile stimulation.

As explained later (see section 4.1.2.4), up to eight vibromotors were placed circumferentially and equidistantly around the subject's right forearm (see Figure 53 a and c), approximately 15 cm distal to the elbow, and strapped using an elastic band (Figure 53 c). Regardless of the number of motors used (i.e., 8, 6, 4), the first vibromotor was always placed in the middle at the volar side while the last was positioned in the middle of the dorsal side, covering thereby the half of the forearm (its internal portion). The rest of the motors were then placed equidistantly between the first and the last motor. This placement was selected because the spatial extent of the vibrotactile interface matched the range of motion of the virtual prosthesis and the elicited sensations were thereby congruent to the prosthesis motion. More specifically, the generated sensation indicated the position of the dorsal side of the prosthetic hand, as shown in Figure 54. Alternatively, the vibromotors could have been placed to cover the full circumference of the forearm. This would increase the spatial separation between the neighboring

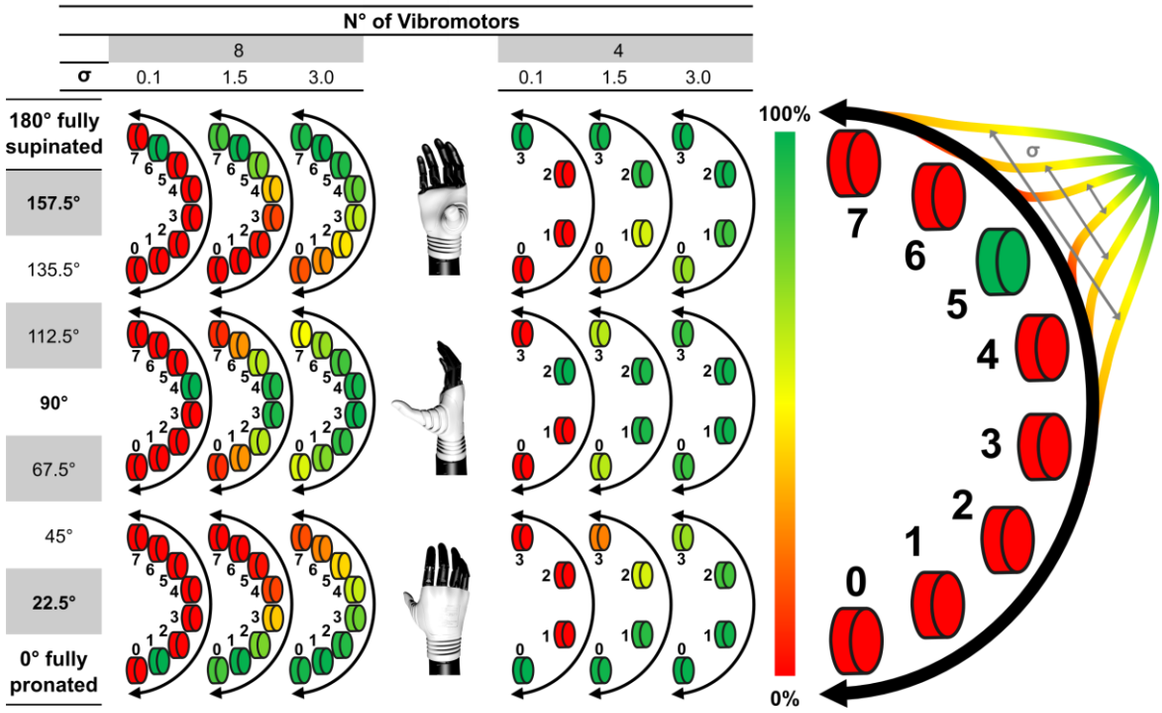

Figure 54 Illustration of the novel feedback encoding approach.
The left panel displays three wrist positions and the corresponding stimulation profiles (vibration intensity across motors) generated for the different numbers of motors (8 or 4) and values of standard deviation (σ) of the Gaussian profile. The representation on the right shows the concept: a Gaussian profile with variable width (standard deviation parameter) that "rotates" around the forearm.

motors, potentially facilitating their discrimination, but the exact correspondence between the spatial configuration of the prosthesis and the forearm sensation would have been lost. Only up to eight vibromotors, out of fourteen available, were used in the present study.

As noted in the introduction, the proposed approach provides feedback to the user by generating a specific intensity profile (Gaussian interpolation) that moves across multiple vibromotors. To be able to generate a well-controlled complex sensation, the elementary sensations elicited by a single motor need to be localized below the motor. Therefore, the vibromotors were covered with a soft silicone case to absorb the stimulation radiating from each motor. The case was thicker laterally (10mm) to separate two consecutive vibromotors while the side in contact with the skin was thin (1mm) to enable vibrations to be delivered effectively while avoiding the heating of the skin during prolonged motor activity. Finally, the silicon case allowed placing the vibromotors vertically to further spatially separate the consecutive motors and thereby allow the subjects to better detect the transitions between active motors. Vertical placement also provides a stronger sensation as shown in the pilot test that we conducted. The center-to-center distance between the consecutive motors is 20 mm, which is within the ranges of the two-point discrimination (2PD) thresholds reported in the literature [458]. However, for our encoding approach, it is not critical that the motors are separated by the 2PD. This is because the subjects do not need to recognize the activation of a random motor (absolute recognition); instead, they can rely on detecting the smooth transitions between active motors (relative recognition), as explained in section 4.1.2.3.

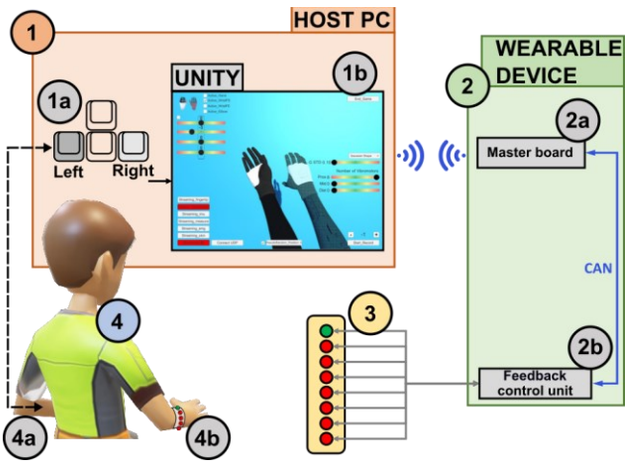

Figure 55 Closed-loop control of a virtual prosthesis.
The subject controlled the rotation of the virtual hand by pressing on the keyboard (1a) with the left hand (4a). The Unity virtual environment (1b) visualized the target hand and recorded the trajectory performed by the controlled hand. The laptop (1) communicated via Bluetooth with the master board (2a) sending the feedback shape, while the master board in turn sent the commands to the feedback control unit (2b), which activated the vibromotors (3) to provide the feedback to the subject's right forearm (4b).

The silicone case had a Velcro on top to be fixed to the elastic band, to prevent slips. The elastic band was strapped to the subject forearm with Velcro by applying the level of pressure which was enough to hold the motors securely in place, without masking the vibration sensation and/or constricting blood flow. To check the tightness, the subject was asked to rotate the forearm, and if the elastic band moved accordingly without slipping, the band was deemed tight enough. The appropriate level of tightness was additionally confirmed during the calibration phase by checking that the sensation thresholds were not excessively high (compared to those obtained during pilot tests).

For each vibromotor, the vibration frequency was set to 200Hz using a supply voltage of 2.5V [459], which lay within the range of maximum sensitivity of the Pacinian corpuscles [460]. The gain of each vibromotor was individually adjusted for every subject (see section 4.1.2.4).

Despite the virtual hand implementing 3 DoFs, only wrist rotation was controlled in the present study. The subject controlled the prosthesis movements using the keyboard and contralateral hand ("3" key for pronation, "4" key for supination). Such a setup provided reliable control and focused the subjects' attention on the feedback, ensuring thereby that the results reflected the changes in the feedback parameters (σ and the number of motors) rather than the influence of control strategy (e.g., changes in sensation due to movement of the forearm). The subjects sat comfortably in front of the monitor, with their right arm relaxed over the desk, taking care to avoid contact between the vibromotors and the table. The computer monitor was placed approximately 50 cm from the subject. The VR environment displayed two prosthetic hands, where one showed the target position (Figure 55.1b, transparent) while the other was controlled by the subject (Figure 55.1b, solid).

4.1.2.3. Vibrotactile feedback encoding

A novel encoding scheme was implemented to provide proprioceptive feedback (Figure 54). The rotation angle of the prosthesis wrist was conveyed to the subject by modulating both vibration intensity and location. To convey feedback that is spatially congruent to the prosthesis movement, a Gaussian profile of vibration intensity was "rotated" around the forearm in synchrony with the rotation of the hand (Figure 54, right). More specifically, the location of the profile peak always matched the orientation of

the wrist, i.e., the Gaussian was centered at the first vibromotor (volar side) when the wrist angle was 0° (wrist starting orientation, completely pronated), then gradually moved across the vibromotors, to reach the last vibromotor (dorsal side) for the wrist angle of 180° (wrist end orientation, completely supinated). Interpolating the intensity using a "rotating" Gaussian function elicited a smooth sensation that was gradually moving around the forearm, thereby replicating a smooth movement of the prosthetic hand.

The following equation was used to define the Gaussian mapping between wrist orientation and vibration intensity:

$$\begin{cases} y = e^{-\frac{(k-m)^2}{g*\sigma^2}} \\ m = p * N \end{cases} \tag{23}$$

where y is the normalized vibration amplitude of the motor k, m is the mean of the Gaussian computed as the normalized position (p) of the virtual hand multiplied by the number of motors (N) in the array, g is a parameter set to 2.25, and σ is the standard deviation of the Gaussian. Effectively, m determines the location of the peak of intensity within the array of vibration motors while σ adjusts the spread of intensity across the motors. The interpolation function (23) can be used to define the mapping for different numbers of motors in the array, as determined by the parameter (N). The effect of the different number of vibromotors and the values of σ is visualized in Figure 54. In general, the σ adjusts the level of interpolation across the given number of motors thereby generating a more discrete or continuous sensation of movement around the forearm.

4.1.2.4. Experimental protocol

First, the minimum and maximum amplitude for each vibromotor were determined using the method of limits [461]. To this aim, the vibration intensity was increased in small steps (i.e., 4-5% in the normalized scale of pulse width modulation (PWM)). When the subject reported a sensation or discomfort felt for the first time, the momentary PWM was adopted as the sensation and discomfort threshold, respectively. This procedure is standardly performed to compensate for the individual perceptual abilities, and in this case, the possible differences in the tightness of the band holding the motors against the forearm. During the rest of the experiment, the vibration intensity was then modulated between these two thresholds, to generate clearly perceivable and localized vibrations that were not intrusive to the subject.

The subjects then performed the main experimental task, namely the target achievement control test (TAC) [457]. They used the keyboard to rotate the virtual prosthesis to bring it into the target orientation (desired rotation angle). Importantly, the hand indicating the target position was always shown on the screen, whereas the hand controlled by the subject was not visible while the subject performed the task. At the beginning of each trial, both hands were visible thereby showing the target orientation and the starting position of the controlled hand. When the trial started, the controlled hand disappeared and its momentary wrist angle was then conveyed to the subject through the vibrotactile feedback. To ensure

minimally intrusive feedback and avoid adaptation to stimulation, the vibration was provided only while subjects pressed the control keys, otherwise, the vibration was deactivated. The subjects were asked to press the space bar key when they thought to have reached the correct position. At that moment, the controlled hand was revealed to the subjects (however, the vibration was deactivated) so that they could see the deviation from the target rotation angle. This was done to increase the subjects' motivation during the experiment.

Each subject performed the task in 21 conditions, i.e., using 8, 6, and 4 vibromotors × 7 values of σ (0.1 – 3, in steps of 0.5). These values were determined heuristically and via pilot tests. For instance, the maximum number of vibromotors was set to 8 as this was the highest number that could be reasonably fitted around half of the forearm in most people. The minimum standard deviation was set to the value (0.1) that elicited discrete motor activation (hence discrete feedback). The other values were selected so that the parameter space was well explored while still maintaining a reasonable overall duration of the experimental session. In each condition, the subjects first received a short training to associate the new sensation scheme to the hand orientation. We also asked the subjects if the sensations were clear, to further check that they received the correct feedback and that the sensation was not affected by adaptation during the experiment. Although the adaption was not explicitly measured, it is highly unlikely that it had an impact on the results of the present study, as the stimulation profiles were dynamic (varying in both intensity and position) and they were delivered intermittently [462]. Indeed, none of the subjects complained about the loss of sensations during the experiment. The virtual prosthesis was programmed to rotate back and forth, 5 times through the full range of motion. On this occasion, the controlled hand was visible to allow the subjects to associate the visual feedback of hand orientation with the feedback sensation. Afterward, they performed an assessment block comprising 21 trials. Seven orientations, equally distributed between 0° and 180° excluding the extremities (Figure 56), were used as targets and each target was repeated 3 times. The sequence of target positions was randomized while ensuring that the same position was not repeated in succession. Furthermore, the order of target positions was different across conditions. At the beginning of each trial, the controlled hand was placed at the opposite end of the range of motion (0° or 180°) furthest from the target orientation, as shown in Figure 56. In addition, to prevent the subjects from using feedforward control and motivate them to rely on the feedback, the velocity of the prosthesis was changed across trials by multiplying the maximum speed (1.26 rad/s) with a gain randomly selected from the interval 0.4 – 1. The order of conditions was obtained by randomizing the tests with the different number of vibromotors. For the given number of motors (4, 6 or 8), the subjects then tested all σ values in random order. Before switching to the next number of motors, the subject was asked to choose which σ produced the best sensation. Similarly, when all the numbers of motors were tested, the subjects chose the preferred number of vibromotors.

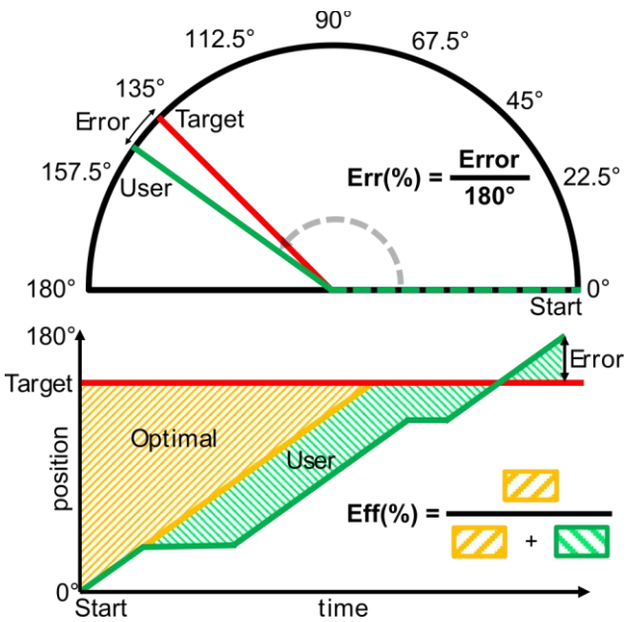

Figure 56 Target positions and outcome measures. The top panel is the error between target and reached position (control accuracy) and the bottom panel shows the ratio between the area enclosed by the optimal trajectory and the trajectory generated by the subject (control efficiency).

4.1.2.5. Data Analysis

Two outcome measures were used for this study: error and efficiency (Figure 56). The end-point error in orienting the hand (Figure 56, top) was computed as the difference between the final position of the controlled hand and the target position, expressed as the percentage of the range of motion. The end-point error measures how accurately (close to the target) the subject can orient the hand using vibrotactile proprioceptive feedback. In addition, for the given motion speed of the controlled hand in each trial, the path efficiency was calculated as the ratio between the area associated with the optimal trajectory (Figure 56 bottom plot, yellow area, optimal path) and the area associated with the trajectory generated by the subject (Figure 56 bottom plot, green plus yellow area, generated path). The optimal path corresponded to reaching the target orientation from the initial position in one uninterrupted motion at a fixed speed imposed by the TAC test at the beginning of each trial. Therefore, while the literature normally uses only the length of the trajectory [457], the efficacy in the present study was a function of both trajectory and time and was thus computed as the ratio of the respective areas. This parameter is always less or equal to 100% and indicates how much the subject deviated from the optimal path in each feedback condition. These values were calculated for each condition varying the number of vibromotors and the Gaussian σ.

The data were tested for normality using the Shapiro-Wilk test. As the test showed that the data were not normally distributed, the Friedman test was performed, while the post-hoc pairwise comparisons were performed using Wilcoxon signed rank test with Bonferroni correction. OriginPro 2020 Graphic & Analysis (OriginLab Corporation, Northampton, MA, USA) and MATLAB 2020b (The MathWorks, Inc., Natick, MA, USA) were used for the statistical analysis. The average of the outcome measures (error and efficiency) was computed for each subject and condition and compared across conditions.

More specifically, the performance achieved with different σ values was compared for the given number of vibromotors, to test how sensitive were the different number of vibromotors to the modulation of σ. In addition, the performance achieved with different numbers of vibromotors was compared for the given value of σ, to assess whether the number of motors could be reduced without sacrificing the performance.

In addition, the error and efficiency were calculated individually for each target angle. In this case, the angle error and efficiency were calculated by varying the number of vibromotors (averaging across σ), and by varying σ (averaging across the number of vibromotors).

The threshold for statistical significance was set at $p < 0.05$, and outliers were excluded from the statistical comparisons. The results in the text are reported as mean ± standard deviation.

4.1.3. Results

The overall results for error and efficiency are summarized in Figure 57, Figure 58, and Figure 59.

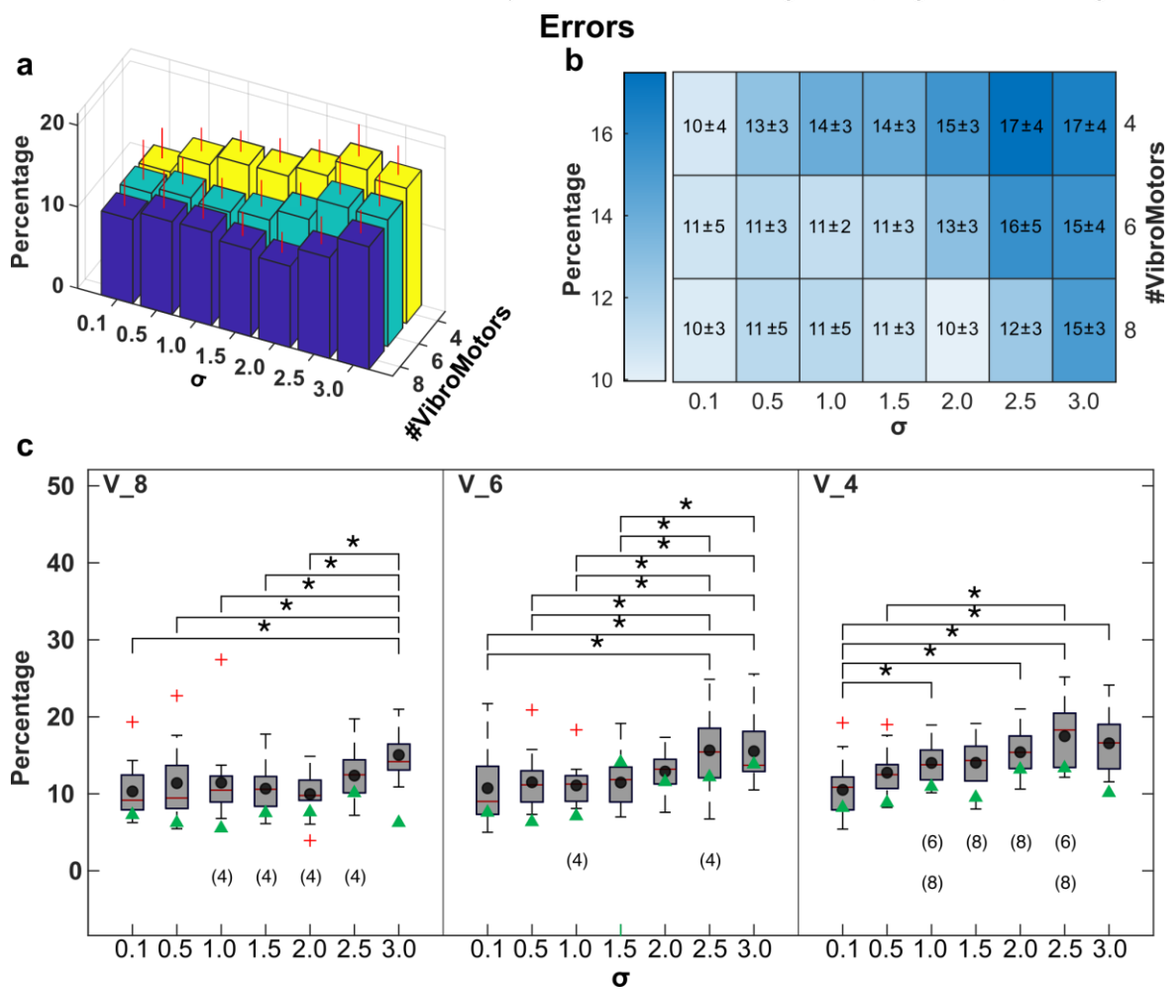

Figure 57 Summary results for the error in the form of: a) bar plot; b) heatmap; and c) boxplots.
In the heatmap, darker color indicates larger error (lower performace). In the boxplots, V indicates the number of vibromotors, the small circles and green triangles are the means for the able-bodied subjects and amputee participant, respectively, the red lines indicate the medians, boxes are interquartile ranges, whiskers represent min/max values and crosses are outliers. The horizontal lines denote statistically significant differences for the comparisons across the values of σ for the given number of motors (8, 6 and 4) (*, $p < 0.05$ with Bonferroni correction) while the numbers in parentheses denote statistically significant differences across the number of motors for the given σ.

Figure 57 shows that, in general, an increase in σ leads to a decrease in performance (i.e., an increase in error); however, the impact of σ is less pronounced when the feedback is provided using more motors in the array. This is clearly visible from the 3D bars (Figure 57 a) and heatmap (Figure 57 b). For instance, the heatmap has a characteristic diagonal structure, where the area above the diagonal has darker colors (higher errors). As shown in Figure 57 c, the performance with 8 and 6 vibromotors was rather resilient to the changes in σ. For 8 motors, the error increased significantly only for the highest value of σ. Specifically, the error for $\sigma = 3.0$ (~15.04 ± 2.9%) was significantly higher than that achieved with all other σ values (~10.7 ± 3.6%) except $\sigma = 2.5$ (~12.4 ± 3.4%). Similar results were obtained with 6 vibromotors where the σ of 2.5 (~15.6 ± 2.9%) was the first value to produce a significant change in performance (~11.5 ± 3.4% for σ of 0.1-2.0). On the contrary, the performance with 4 vibromotors was rather sensitive to the change in σ, and the significant increase in error was registered already for $\sigma = 1.0$ (~14.01 ± 2.6% vs ~11.6 ± 3.3% for σ of 0.1 and 0.5, respectively). When comparing the performance across the number of vibromotors for the given σ, there was no significant difference between 8 and 6 motors for any value of σ, while there was a significant drop in performance for 4 motors. More specifically, the difference arose in the medium range (σ between 1 and 2.5), while in the case of low (0.1 and 0.5) and high (3.0) σ, the error was not significantly different.

Differently from the error, the efficiency (Figure 58) was not significantly affected by σ regardless of the number of motors (~27.4 ± 6.1%, Figure 58 c). When comparing across the number of motors, the efficiency with 8 vibromotors was in a few cases significantly higher (~29.2 ± 5.7%) compared to that obtained with 4 vibromotors (~25.7 ± 6.9%), as indicated by the numbers between parentheses in Figure 58 c. Again, the trends are particularly visible in the heatmap (Figure 58 b). For the efficiency, the heatmap is diagonal but the colour is mirrored compared to that of the errors, indicating that efficiency decreased with fewer motors and higher σ (however, as explained, the effect was significant only across the number of motors).

Regarding the amputee subject, the results in both performance measures were within the ranges, and mostly below the mean performance, obtained in able-bodied subjects, as indicated by the green triangles in Figure 57 c and Figure 58 c. This is an encouraging preliminary result showing that the developed method can be successfully interpreted and exploited for control by a prospective prosthesis user.

Finally, the performance was analyzed for each target angle individually. Figure 59 shows the error (panels a and b) and efficiency (panels c and d) for different target angles grouped by the number of vibromotors (panels a and c) and Gaussian σ (panels b and d). The trends in the heatmaps further support the results presented in Figure 57 and Figure 58, showing that the error generally increased with fewer vibromotors and for higher σ values, while the efficiency was not impacted by those factors. However, Figure 59 reveals that performance depends on the angle. Specifically, for the angles in the middle of the range of motion, the error slightly increased (dark heatmap) while the efficiency decreased (lighted heatmap). We computed the overall error and efficiency averaged over the number of motors and σ and

we found that they were 11 ± 7% (error) and 32.3 ± 5% (efficiency) for the extreme positions whereas for the angle of 90° they were 14 ± 6% (error) and 21 ± 8% (efficiency), respectively, and the difference was statistically significant ($p < 0.001$) only for the efficiency.

Regarding subjective preference, most subjects (11) selected 8 vibromotors. Five of them chose σ = 1.0, three selected σ = 0.5, two preferred σ = 0.1 (discrete feedback), and one preferred σ = 1.5. The remaining subjects chose 4 (2 subjects, σ = 0.5) and 6 motors (2 subjects, σ of 1 and 1.5, respectively). The amputee participant preferred 8 vibromotors with a σ of 1.0.

4.1.4. Discussion

The present study proposed a novel approach to convey proprioceptive information that can be flexibly configured by adjusting the smoothness of the moving sensation (σ) and the number of

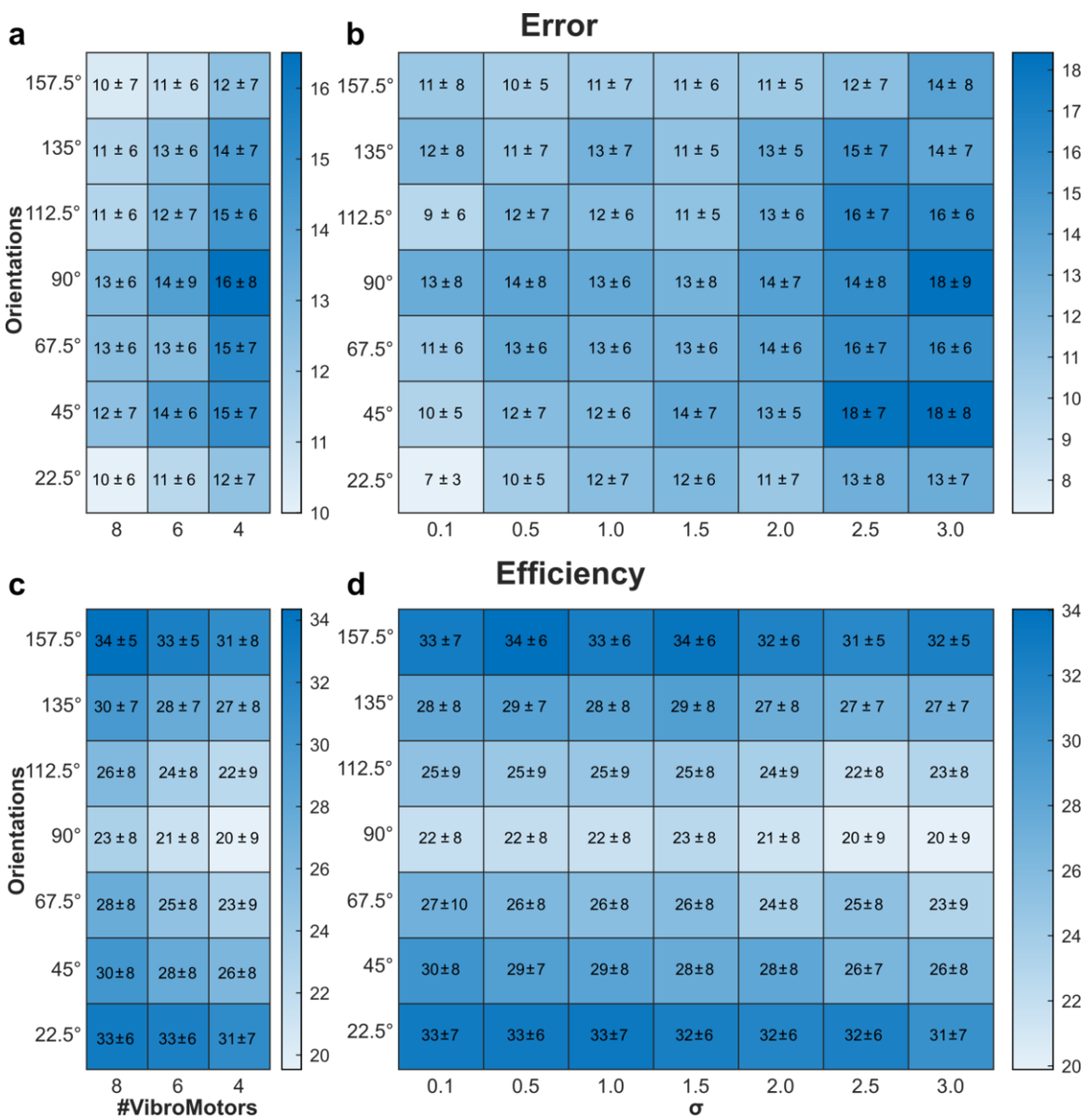

Figure 59 Average peformance across the target orientation angles.
a) Error and c) efficiency for different number of vibromotors; **b**) Error and d) efficiency for different values of σ.

vibromotors used. Most of the methods in the literature assume a single configuration based on heuristically selected parameters, while the present study systematically explored the parameter space of the proposed method and provides important insights for its successful application. The main conclusions of the experimental assessment are: 1) discrete feedback consistently showed high performance regardless of the number of motors; 2) nevertheless, with enough motors, the smoothness of feedback can be increased over a broad range without impacting the localization of sensation; 3) the subjects prefer smooth rather than discrete feedback; and 4) the number of motors can be safely decreased from 8 to 6 and, if smoothness is not the priority, even to 4. Importantly, the second point additionally reveals that σ might be used not only to adjust the smoothness but possibly as an extra "degree of freedom" to convey another feedback variable, as discussed later. Overall, the novel method allowed an effective closed-loop control (average error < 10% for some parameter combinations) in able-bodied as well as in an amputee subject. Although the method was used to convey wrist rotation, other variables could be transmitted using identical mapping via a circular or linear array (e.g., aperture and grasping force). Therefore, the key contribution of the present study is an effective feedback approach that can be flexibly customized in terms of sensation quality and potentially the nature and the number of feedback variables, according to the requirements of an application and/or user preference. The aforementioned outcomes are further discussed below in dedicated paragraphs.

The results demonstrated that the Gaussian interpolation of intensity is an effective method to generate smoothly moving sensations around the forearm. When enough motors were available in the array (8 and 6), the amount of smoothing set by the value of σ could be modulated substantially without significant impact on performance (Figure 57 b and d). Therefore, the spread of sensation did not negatively affect the subject's ability to locate the peak of intensity and thereby determine the associated wrist orientation.

The possibility of modulating σ without significant impact on the ability to locate the peak of sensation is an important result for the application of this feedback approach. First, this means that the value of σ can be selected based on the subject's preference. The subject can choose the feedback configuration with more or less spreading and/or continuity in transition. Indeed, when asked to indicate their preference, in most cases, the subjects indicated that they prefer smooth rather than discrete feedback, selecting different values of σ in the low to medium range, namely, from 0.5 to 1.5. Second, since σ does not affect the perception of rotation, this parameter could be used to encode an additional variable, for instance, hand aperture. Increasing σ spreads the sensation around the forearm, resembling thereby the movement of the hand enclosing an object. Such encoding would therefore allow for a compact solution, where the same interface could be used to provide the simultaneous feedback of wrist rotation and hand aperture. However, the results also show that this approach would work only with enough motors in the array. With 4 motors, for instance, the range in which σ can be modulated without affecting the performance is narrow. Hence, in the case of a small number of vibromotors, it could be challenging for the subject to clearly perceive the change in the feedback variable associated with σ.

Decreasing the number of motors required to provide feedback is an important advantage for the envisioned clinical application. Our experimental results showed that the number of motors can be decreased from 8 to 6 while still maintaining both the smoothness of the feedback (higher σ) and the performance. The number of vibromotors can be reduced even to 4 if the participant can "tolerate" discrete sensations (smaller σ). Fewer motors reduce the complexity of the interface, which can improve robustness and simplify the integration of the feedback into the socket. The present results demonstrate that there is a tradeoff between the value of σ and the number of motors, where the former parameter puts a limit on how many vibromotors can be decreased without incurring a significant loss of performance. For low values of σ (0.1 and 0.5), the number of vibromotors (i.e., feedback interface) can be halved, from 8 to 4, while $\sigma > 0.5$ allows only a smaller reduction (from 8 to 6).

Our initial assumption was that the small σ would be more sensitive to the decrease in the number of motors. Small σ (0.1) produced discrete feedback that jumps from motor to motor (no interpolation across motors), and hence, with fewer motors, the feedback resolution is presumably lower. Contrary to our assumption, the subjects achieved good results with small σ even when using only 4 motors. The expression (1) that was used to generate the intensity introduced a brief period of no stimulation when changing between the neighboring motors, and we believe that this cue allowed the subjects to effectively increase the feedback resolution. Nevertheless, such a stimulation pattern was not intuitively related to the prosthesis movements (discrete feedback vs. continuous rotation). This was confirmed by the qualitative, subjective outcomes, as most subjects selected at least some level of interpolation, even when using 8 motors. The interpolation produced continuous sensation around the forearm by generating virtual tactile points between the motors. However, it seemed that this approach needed a certain minimal number of motors to be effective (8 and 6 vs. 4). Finally, the amount of interpolation can be also excessive, as the highest values of σ (2.5 and 3) produced a blurred sensation that confused the perception of the continuous movement around the forearm. Indeed, the highest values of σ decreased the performance regardless of the number of motors.

The overall recommendation for the configuration of the proposed feedback interface, therefore, depends on the weighing of the subjective versus objective factors. If priority is given to the subjects' preference, 8 motors should be used with a medium level of interpolation (smooth sensation). However, if there is a need to decrease the number of motors in the array, 6 motors could be used with a similar amount of interpolation to maintain both the continuity of sensation and closed-loop performance.

The results obtained for each target angle (Figure 59) show that it was more difficult for the subjects to adjust the wrist orientation for the positions towards the middle of the range of motion (RoM). This is an intuitive result because the subjects could use the positions at the end of RoM as the well-defined anchors since the stimulation stopped changing when the subject reached the RoM end.

The next step in this research will be to expand the proposed approach to implement the proprioceptive feedback for all DoFs of a multifunctional prosthetic hand. As explained above, the second DoF can be added by exploiting the presumed "independence" of the two parameters (Gaussian profile peak and σ),

i.e., using σ to encode the hand aperture simultaneously with the rotation of the wrist. To accommodate more DoFs (e.g., wrist flexion/extension and force), however, additional motors need to be added.

The proprioceptive feedback was already employed for prosthesis control [136, 443, 463], but not in the form presented in this study, where Gaussian interpolation was combined with spatial encoding to produce the sensation of continuous movement around the forearm. A previous study used the principle of generating phantom sensations [450] and also reported good results with 6 motors. However, they employed a fixed number of motors, discrete activation (instead of Gaussian interpolation) thereby producing discrete sensations, and the application was wrist guidance and not prosthesis control.

The present experiment was performed by controlling a virtual prosthesis via keyboard using the contralateral hand, as the focus was on comparing the feedback parameters. However, in the envisioned practical application, both control and feedback will be performed ipsilaterally, and this could affect the effectiveness of feedback (e.g., forearm movements and muscle activation can impact the perception of sensations). The placement of a feedback interface was investigated in a recent study, albeit in a different context (control of balance), and the results demonstrated that the placement can be indeed an important factor [464]. Therefore, the next step in this research will be to test the interaction between feedback and pattern classification control in both able-bodied and amputee subjects. Importantly, the results of the present study will inform the design of the feedback (parameter selection) for this future assessment.

The aim of the present study was not a direct clinical translation but a systematic investigation of the novel feedback scheme and the effect of its parameters on the performance of closed-loop control, i.e., wrist rotation using an ideal command interface and the novel feedback method. Nevertheless, the results obtained in an amputee who could use the feedback as effectively as able-bodied subjects are encouraging from the viewpoint of future clinical translation.

4.1.5. Conclusion

The present study is the first effort to investigate the application of a novel feedback scheme that combines spatial encoding with Gaussian interpolation to provide continuous proprioceptive sensation for wrist rotation in prosthetic applications. The quality of the produced sensation, namely, the location of the peak intensity and the amount of spreading, depends on the number of vibromotors used in the array and the value of the parameter σ of the Gaussian interpolation profile. Overall, the present study has shown that the novel approach provided clear rotational feedback that was easy to interpret and use for closed-loop control. Nevertheless, there was a clear preference for a higher number of vibromotors (8 and 6). An increased number of vibromotors was also more robust with respect to the change in σ, i.e., the amount of spreading of sensation (continuity of the feedback) could be increased to higher values without the decrease in performance. This is an important outcome for the application of proprioceptive feedback, as it points out that the spatial modulation and σ could be used to simultaneously encode two feedback variables using a compact solution (i.e., an array of vibromotors).

4.2. Closed-loop Control of 2DoF Hannes Arm Prosthesis using Pattern Recognition and Spatial Encoding for Proprioceptive Feedback

4.2.1. Introduction

An amputation is a debilitating event with substantial physical, social and psychological consequences [6], but the lost motor functions can be partially restored using myoelectric prostheses [1, 2, 6, 8, 9]. Modern devices include advanced robotic hands with several degrees of freedom capable of performing multiple grasp types [2, 7, 8, 423, 465-467], but they do not provide somatosensory feedback and, hence, the reconstruction of the lost limb is not complete. Only two commercial hands provide simple feedback to the user (e.g., Ability hand [30] and Vincent hand [27]) but the feedback conveys only the grasping force, while the natural feedback from biological hands include both exteroception and proprioception. The artificial proprioceptive feedback is important as it allows amputees to perceive the configuration of the bionic limb without looking at it. The ability to "feel" the prosthesis movements can facilitate the embodiment, thus promoting the acceptance and the usability of the system [9, 468].

The methods and technologies for restoring the missing sensory information and consequently enrich the prosthesis-user interaction were the focus of recent research efforts [5, 6, 103, 126, 127, 469, 470]. Artificial feedback can be conveyed to the subject either invasively [88, 106, 155, 434, 435], by activating peripheral nerves using electrical stimulation, or non-invasively [5, 100, 220, 436, 437, 471], by delivering mechanical or electrical stimulation to the skin of the residual limb. Both methods can provide different kinds of information (e.g., pressure [120], textures [155], slippage [438], pain [106]), but grasping force is still the most common choice of the feedback variable [5, 100, 217, 220, 428, 437, 439-442]. The artificial proprioceptive feedback, conveying the position of the prosthesis joints (e.g., wrist rotation and hand aperture), was rarely considered [408, 436, 443-446] and it was typically limited to hand aperture [5, 88, 472] while fewer studies investigated wrist rotation feedback [443, 450, 455].

Non-invasive methods to provide feedback typically rely on sensory substitution. In this approach, the prosthesis variables are translated into stimulation profiles, according to a predefined encoding scheme, and the stimulation is delivered to the participant. Hand aperture and wrist rotation were conveyed more often using parameter modulation, which means that the value of the feedback variable was associated to the stimulation intensity or frequency [473, 474]. An alternative approach is to employ spatial encoding, where the movement of the prosthesis is intuitively represented as a tactile sensation moving across the residual limb [454, 475-478].

Nowadays, modern prostheses integrate several active DoFs [4, 6, 7], usually combining hand opening and closing with active wrist rotation. Therefore, to convey the full state of the prosthesis to the user, the artificial feedback needs to transmit two feedback variables, one encoding hand aperture and

one for wrist rotation. However, only few studies have so far proposed feedback methods that can convey both variables [80, 454]. In addition, although the two DoFs can be controlled using a simple 2-channel myoelectric interface, this approach is slow and cognitively taxing, as the user needs to manually switch between the active functions [6]. Therefore, pattern classification is the preferred method in this case, because it eliminates the tedious switching by directly translating the user motion intention into prosthesis movements [7, 9, 41, 73, 74, 87, 94, 177, 411, 479-481]. However, only a few studies have tested the integration of feedback on multiple DoFs [131] with pattern classification [136, 436, 454, 482, 483]. For example, Shehata, et al. [482] proposed an augmented audio feedback to provide 2-DoFs movements of a cursor using different sound frequencies. The audio feedback was then applied to control a real prosthesis by adjusting the hand aperture and the thumb abduction/adduction during a Virtual Egg Test [67]. Patel, et al. [436] assessed multichannel electrotactile feedback to provide fingers position when controlling a dexterous robotic hand. Similarly, Garenfeld, et al. [454] proposed discrete proprioceptive feedback to encode 2-DoF movements of a cursor simulating a prosthesis in a target-reaching task, using multi-pad electrodes.

In a recent study, it was proposed an approach to convey wrist rotation via an array of vibration motors placed around the forearm. The feedback variable was transmitted through spatial encoding and Gaussian interpolation of intensity to generate a sensation that smoothly moves around the forearm, congruently to the rotation of the prosthesis. Importantly, our tests showed that the smoothness of the tactile sensation, determined by the standard deviation (σ) of the Gaussian can be modulated without affecting the subjects' ability to localize the sensation, determined by the mean (μ) of the Gaussian (see section 4.1). Based on those results, our assumption was that the two parameters of Gaussian interpolation can be used to provide two proprioceptive feedback variables independently and simultaneously. In the present study, we therefore propose a novel 2-DoF encoding scheme in which the hand aperture and the wrist rotation are respectively mapped to the parameters σ and μ. This produces intuitive feedback because the parameter μ moves the peak of sensation around the forearm congruently with the wrist rotation, while σ maps the hand aperture to the spread of sensation (i.e., larger hand opening, more spread sensation). The advantage of the novel method is that it can lead to a Compact feedback interface that can convey the full kinematic state of the prosthetic hand through a single array of eight vibromotors (Compact feedback).

To assess the validity of this approach, we implemented the novel feedback method together with pattern classification into an embedded platform and used it for the closed-loop control of the Hannes prosthesis [11, 13]. The novel feedback was compared to the Conventional approach where the feedback was provided using two vibromotor arrays (with eight and four motors, respectively), each dedicated to conveying a single DoF (Conventional feedback). Reducing the number of vibromotors in the feedback array is an important step to facilitate the integration of the feedback interface into the prosthesis socket. The experimental assessment included ten able-bodied subjects and four transradial amputees, who performed a Target Achievement Control Test (TAC) [457] using pattern classification to control

rotation and hand aperture, while the state of the prosthesis was provided to the subject through the vibrotactile feedback using either the Compact or the Conventional interface.

4.2.2. Materials and Methods

4.2.2.1. Subjects

Ten heathy able-bodied subjects (aged 27.3 ± 3.1, 5 males), and four transradial amputees (aged 53.3 ± 14.7, all males), with no prior experience with proprioceptive tactile feedback, participated in this study. The amputees were expert users of hand prosthesis with single active DoF (see Table 19). Before starting the experiment, the subjects were informed about the protocol, and they signed the informed consent form. The healthy subjects performed the experiment at the Center for Sensory-Motor Interaction in Aalborg (Denmark) following the experimental protocol approved by the Research Ethics Committee of the Nordjylland Region (approval number N-20 190 036). The amputees performed the experiment at Istituto Italiano di Tecnologia (IIT) in Genova (Italy) following the experimental protocol approved by the Ethical Committee of Liguria Region (approval number 363/2022 - DB id 12494).

4.2.2.2. Experimental Setup

The experimental setup (Figure 60 A) comprised the following components: (1) a standard laptop (DELL XPS 15, Intel Core i9 @2.60GHz, 32GB RAM) running Windows 10, a keyboard, and a 24'' computer monitor, showing a user interface to collect EMG data and to train the pattern recognition algorithm to decode the user movements (E-DATS, EMG - Data Acquisition & Training Software [12, 13]); (2) a virtual reality (VR) environment simulating the Hannes prosthetic hand (Hannes) [11-13, 15] with three active DoFs (hand open/close, wrist pronation/supination, and wrist flexion/extension); (3) the interface to select the type of feedback (Compact vs. Conventional), configure the feedback parameters and select the number of vibromotors used; (4) Hannes prosthetic hand [11] with three active DoFs (hand open/close, wrist pronation/supination, and wrist flexion/extension); (5) twelve eccentric rotating mass (ERM) vibromotors (Vybronics, VC0625B001L) with a custom-made control unit to provide tactile feedback; (6) six EMG electrodes (Otto Bock, 13E200=50 AC) with a custom-made

Table 19 population of amputees

Amputees	Age	Time from amputation	Dominant Limb (before amputation)	Amputated Limb	Etiology	Level of Amputation	Type of Prosthesis
P1	32	7 years	Right	Right	Work accident	Unilateral Proximal	BeBionic Hand
P2	68	53 years	Right	Right	Work accident	Unilateral Distal	Michelangelo Hand
P3	54	22 years	Right	Right	Work accident	Unilateral Medial	Variplus Hand
P4	58	37 years	Right	Right	Work accident	Unilateral Distal	Michelangelo Hand

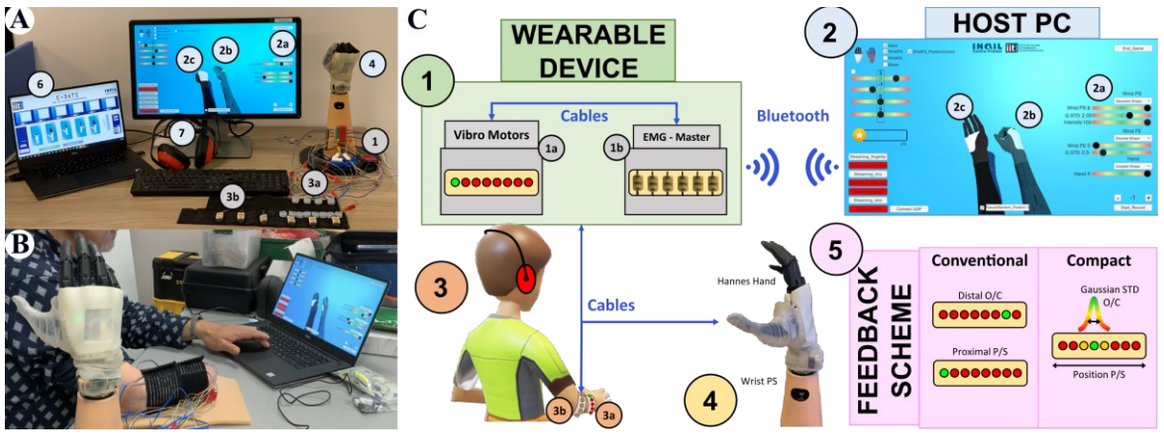

Figure 60 Experimental setup and the scheme of closed-loop control.
A: experimental equipment used. B: testing session with an amputee. C: The closed-loop control of Hannes Arm and its virtual representation . The subject (3) was seated in front of a monitor wearing the armband with EMG sensors (3b) placed equidistantly around the right forearm, and vibromotors (3a) distributed equidistantly around the interior aspect of the right forearm. The virtual reality interface (2) showed the orientation of the target (2b) and the controlled hand (2c) to implement target achievement test. Importantly, during the test, the subjects controlled a real prosthesis (4). The graphical controls (2a) allowed setting the paramenters of the feedback scheme (5). A PC application (6) governed the training of the pattern recognition model and later the controlled real prosthesis, while prosthesis state (wrist angle and hand aperture) was conveyed to the subject through vibrotactile feedback. The subject wore headphones (7) to block the incidental noise coming from the Hannes prosthesis (4). In the text more details of the setup and the experimental protocol were provided.

master board to record the data, establish the communication between a host PC, Hannes hand and the feedback control unit; (7) and headphones to cancel the noise of the Hannes's motors during movements. The master board (Figure 60 C-1b) communicates with Hannes hand (Figure 60 C-4) and with the feedback controller (Figure 60 C-1a) using a CAN Bus protocol, it collects data from EMG sensors (Figure 60 C-3b) using an onboard ADC unit, and connects to the laptop via Bluetooth (Figure 60 C-2). The master board implements a Non-Linear Regression (NLR) to decode the subject's motion intention and generate control commands for Hannes and VR hands, after an offline calibration [12, 13]. The algorithm was trained to recognize wrist pronation/supination and hand opening/closing and activate the prosthesis motion accordingly. The prosthesis velocity was proportional to the strength of muscle contraction estimated by averaging the mean absolute value of the EMG recorded over the six electrodes. The E-DATS software responsible of collecting EMG data and calibrating the NLR algorithm, was developed using Labview and MATLAB 2020b (The MathWorks, Inc., Natick, MA, USA) [12, 13]. The VR framework was developed using the Unity development suite and C# language.

Another master board collected the data from the Hannes hand (joint references, encoders, currents, EMGs) and sent that information to the VR framework. The framework computed the control commands for the vibromotors, depending on the selected encoding and transmitted the commands to the master board, which activated the feedback controller to generate the desired vibrotactile stimulation. Therefore, the real hand performed the movements decoded by the master board through the pattern recognition algorithm, while the virtual hand replicated the position of the real hand.

Six EMG sensors were placed circumferentially and equidistantly around the subject's forearm, approximately 5cm distal to the elbow (Figure 1C-3a,3b). Each electrode was enclosed in a plastic block

with the conductive pads in contact with the skin. The blocks were equidistantly fixed with Velcro to an elastic band and the band was strapped around the forearm by applying a level of pressure which was enough to hold the electrodes securely in place, while avoiding discomfort during a prolonged use. The EMG data was recorded at a sampling frequency of 1 kHz with 16 bits of resolution, and the signals were hardware rectified.

For feedback delivery, two configurations of vibromotors were used. In one condition (Conventional interface), twelve vibromotors were arranged in two arrays (first array of eight vibromotors and second array of four vibromotors), and in the other condition (Compact solution), only one array of eight vibromotors was used. The arrays were placed semi circumferentially and equidistantly around the internal aspect of the subject's forearm, approximately 15cm distal to the elbow (first array) and 20cm distal to the elbow (second array) (Figure 60 B). The diameter of each vibromotor was 6.3mm with a thickness of 2.5mm. Each vibromotor was covered with a soft silicon case (size 14.2x14.2x6.8mm) to localize and absorb the radiating stimulation and avoid heating the skin during prolonged continuous vibration. The silicone case was fixed to the elastic band using Velcro, to prevent slips. The case had a housing to place the vibromotor vertically, thereby bringing the side of a coin motor in contact with the skin, as a pilot test showed that this produced stronger and more focused sensations. The motors were placed at a minimum distance of 20mm between them to facilitate the localization of vibrations. The elastic band was strapped to the subject with Velcro by applying a level of pressure which was enough to hold the motors securely in place, but without masking the vibration sensation and/or constricting the blood flow. To check the tightness, the subject was asked to rotate the forearm, and if the elastic band moved accordingly without slipping, the band was deemed tight enough. The first vibromotor in each array was placed at the volar side while the last was positioned at the dorsal side, covering thereby only half of the forearm (its internal portion). This placement was selected because the spatial extent of the vibrotactile interface matched the range of motion of the prosthesis wrist. For each vibromotor, the vibration frequency was set to 200 Hz [459], which is within the range of maximum sensitivity of the Pacinian corpuscles [460]. The gain of each vibromotor was individually adjusted for every subject (see section I.4.2.2.4).

The subject sat comfortably in front of the monitor, with their right arm (residual limb) relaxed and placed on a desk, ensuring that the vibromotors did not contact the table. The computer monitor was placed approximately 50cm from the subject, and the Hannes hand was placed behind the screen so that the subject could not see it while he/she also wore noise-cancelling headphones to block the sound from the prosthesis motors. The VR environment displayed two virtual Hannes hands, where one showed the target position (Figure 60 C-2b, transparent Hannes) while the other was controlled by the subject (Figure 60 C-2c, solid Hannes). As explained above, the subject controlled the movements of the real prostheses through pattern recognition by moving their hand (able-bodied subjects) or phantom limb (amputee participants). The VR environment was therefore employed to present the task to the subjects

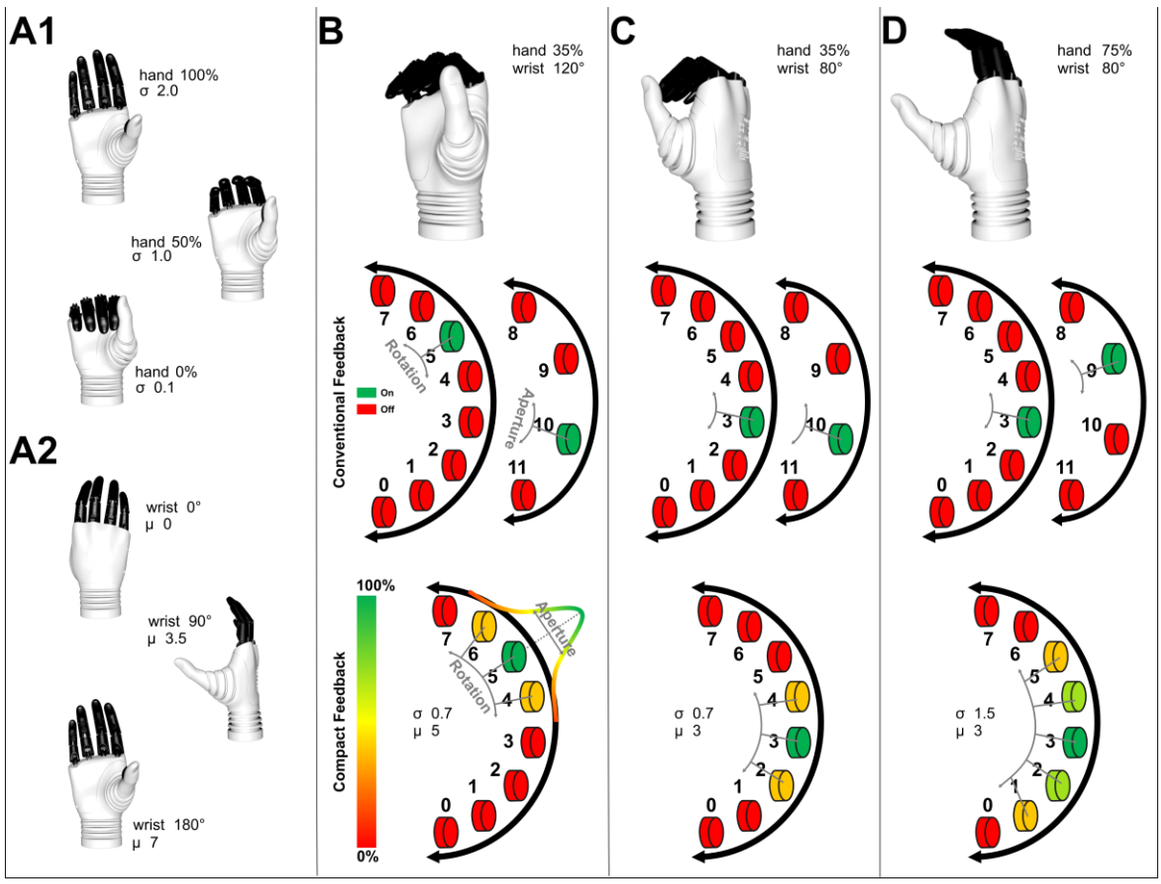

Figure 61 Illustration of the two feedback encoding approaches.
A1: Representation of Hand aperture range of motion. A2: Representation of the wrist rotation range of motion. B, C and D: Vibromotor activations determined by the two encoding approaches for three different hand configurations (top). The Conventional Feedback (middle) used two arrays of vibromotors to separately convey wrist rotation and hand aperture. The Compact Feedback (bottom) employs a single array of vibromotors and transmits the feedback information by modulating the Gaussian mean (μ) for wrist orientation and standard deviation (σ) for hand aperture.

(target configuration) while the real hand ensured that they actually controlled the real dynamics of a physical prosthesis.

4.2.2.3. Vibrotactile feedback encoding

A novel encoding scheme was implemented to provide the proprioceptive feedback (Figure 61, Compact feedback) and compared to the standard spatial encoding [450] (Figure 61, Conventional feedback). With the latter, the information about wrist rotation and the hand aperture was provided using two arrays of vibromotors. In particular, eight vibromotors were used to convey wrist rotation while a separate array of four vibromotors provided hand aperture, reflecting larger range of motion in the wrist compared to that of the hand. The range of motion of each DoF was divided into equisized intervals and the intervals were then sequentially associated to the vibromotors. Therefore, as the wrist rotation changed from 180° to 0°, the vibromotors were activated sequentially from the motor on the dorsal side to the motor on the volar side of the forearm, and similarly for the hand aperture. For instance, vibromotor 5 was activated when the wrist angle was 120° (Figure 61 B), and then as the wrist continued

rotating, motor 4 and motor 3 were activated in succession when the wrist angle reached 100° and 80° (**Figure 61** C), respectively, and analogously for the hand aperture (**Figure 61** A, **Figure 61** D).

The novel encoding scheme conveyed two feedback variables using a single array of 8 vibromotors, and hence, represented a more Compact solution (4 vibromotors less). This approach was based on a recent work (see section 4.1), where they investigated Gaussian interpolation of vibrotactile stimulation and showed that the location and spread of the Gaussian profile could be perceived independently by the subjects. Therefore, the rotation angle of the prosthesis wrist was conveyed to the subject by modulating vibration location (i.e., the location of the peak intensity, μ in equation (24)), while the hand aperture was transmitted by varying the spread of sensations (i.e., the number of active motors, σ in equation (24)), as shown in Figure 61 (Compact feedback, see also below). The feedback was therefore intuitively related to prosthesis motion, as the rotation of the wrist produced a sensation that rotated around the forearm, while with the hand opening, the elicited sensation spread spatially in both directions from the current location.

The following equation was used to define the Gaussian mapping between wrist position and hand aperture:

$$\begin{cases} y = e^{-\frac{(k-\mu)^2}{g*\sigma^2}} \\ \mu = p * N \\ \sigma = \left(\frac{h}{100} * (2.0 - 0.1)\right) + 0.1 \end{cases} \quad (24)$$

where y is the normalized vibration amplitude of the motor k, μ is the mean of the Gaussian computed as the normalized position (p) of the wrist multiplied by the number of motors (N = 8) in the array, g is a parameter set to 2.25, and σ is the standard deviation of Gaussian ranging from 0.1 for fully closed hand (0%) and 2.0 for fully open hand (100%), calculated as the normalized position of the hand (h) multiplied by the range of σ ([0.1 2.0]). The values and ranges of the parameters were selected based on the outcomes of a recent study (see section 4.1). The parameter μ, which was mapped to wrist position, determined the location of the peak of intensity within the array of vibration motors (increasing μ means that the prosthesis is supinating), while σ was mapped to hand aperture and adjusted the spread of intensity across the motors (increasing σ means that the prosthesis is opening).

An example of the Compact encoding is provided in Figure 61. The peak of intensity was centered at the vibromotor 5 when the wrist angle was 120° (Figure 61 B), then gradually moved across the vibromotors as the wrist continued rotating, to reach the third vibromotor when the wrist angle was 80° (Figure 61 C). Regarding the hand aperture, three vibromotors were simultaneously active (with different intensities) when the hand aperture was at 35% (Figure 61 B), and then further motors were added so that five vibromotors were active when the hand aperture was 75% (Figure 61 C). Figure 61 also provides the feedback pattern for the Conventional approach (middle row with two arrays), which is based on discrete activation of individual motors, so that the two methods can be directly compared.

4.2.2.4. Experimental protocol

Subjects were seated comfortably in front of a monitor placed at a distance of approx. 50cm. The band with EMG electrodes and vibromotors was mounted on the forearm of the dominant hand (able-bodied subjects) and/or residual limb (amputee participants). The minimum and maximum amplitude for each vibromotor was determined using the method of limits [461] as described in a recent work (see section 4.1). Briefly, vibration intensity was increased in small steps (i.e., 4-5% of maximum activation) until the subjects reported a sensation or discomfort. During the experiment, the vibration intensity was modulated between the sensation and discomfort thresholds, to generate clearly perceivable and localized, but still not intrusive sensations.

Subsequently, the gain of the EMG electrodes was adjusted by visualizing the signals to ensure that the maximum contraction did not saturate the recording. After this, EMG data to be used for classifier training was collected. To this aim, the subject was asked to perform four different movements (hand close and open, wrist pronation and supination) at three different contraction levels (weak, medium and strong). Each movement was maintained for 2s with 5s rest between the repetitions. After the data collection, the NLR classifier was trained, and its parameters were sent to the master control board for real-time decoding of subject movements and prosthesis control. The detected movement class activated the corresponding DoF of the prosthesis, while the average magnitude of the myoelectric signal determined movement speed. The latter was additionally finetuned for each subject until he/she was satisfied how the prosthesis reacted to his/her commands.

Subjects then practiced prosthesis control and when confident, they proceeded to the feedback familiarization phase. In this phase, they were trained to associate prosthesis movements to the activation of vibromotors. The order of the feedback schemes (e.g., Conventional vs Compact) was chosen pseudo-randomly so that half of the subjects started with the Conventional and half with the Compact configuration. The subjects were asked to move the prosthesis one joint at a time for five times across the full range of motion, while they watched the prosthesis moving with haptic feedback active. Then, they commanded sequential movements around 2-DoFs to experience the vibration patterns related to such combined activations.

After the control and feedback familiarization, the subjects performed the experiment. The experiment was based on a target achievement control test (TAC) in which they adjusted the configuration of the controlled hand to match that of the visual target shown on the computer screen. Importantly, the subjects controlled a real prosthesis, while the incidental feedback from the device (sound and vision) was blocked, as described before. A sequence of 21 pseudo random trials, hereafter named “block”, was generated by pairing 21 pseudo random wrist targets (3 repetitions x 7 orientations) with 21 pseudo random hand targets (5 repetition x 4 level of aperture +1). The seven target orientations of the wrist and four target positions of the hand aperture were equally distributed between 0°-180° and 0-100% excluding the extremities, respectively (see Figure 62). In addition, to prevent the subjects from using feedforward control and motivate them to rely on the feedback, the prosthesis velocity was

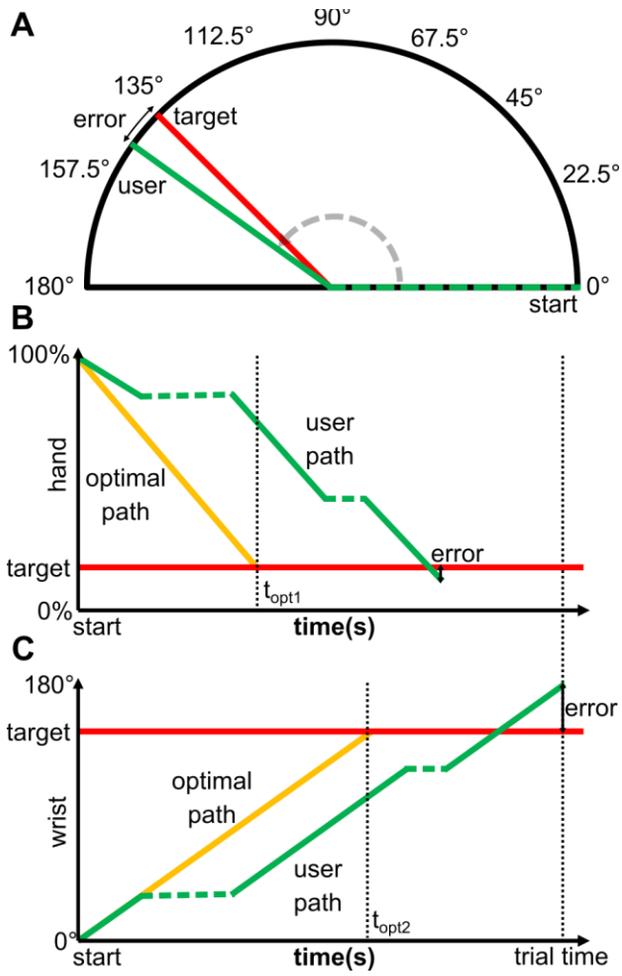

Figure 62 Target positions and outcome measures. A: error between target and reached position (control accuracy) when adjusting the wrist. B/C: path efficiency, optimal and genearted paths for hand/wrist. Trial time as well as optimal times (t_{opt1} and t_{opt2}) to adjust each DoF are annotated as well.

changed across trials by multiplying the maximum speed (1.26 rad/s) with a gain randomly selected from the interval 0.4 – 1. At the beginning of each trial, the subject could see the starting configuration of the controlled hand, visualized on the computer screen. Its position was selected to be at the end of the range of motion furthest from the target configuration (Figure 62 A green dashed line), i.e., if the target wrist orientation was over 90°, the wrist of the controlled hand would start at 0°, and similarly, if the target hand aperture was over 50%, the controlled hand would start fully closed (hand aperture of 0%).

After a sound notification indicated the trial start, the subjects were asked to adjust the controlled hand using pattern classification control while the state of the hand was provided only by the tactile feedback. The subjects could control different DoFs as they wished, and once they judged that the desired target configuration was reached, they pushed the space bar. The reached position was then revealed to them by showing the controlled hand on the screen, and after a short break (5s), the next trial started. After finishing the block of 21 trials, a 5min resting phase was provided, and then another block of trials was performed (three blocks in total). After ten minutes of rest, the second feedback scheme was tested following the same protocol. At the conclusion of the experiment, subjects were asked to choose the feedback scheme that they preferred.

4.2.2.5. Data Analysis

The primary outcome measure was the end-point error between the target configuration and the controlled hand. This measure was computed for each DoF as the difference between the target position and the position of the hand at the moment the subject pressed the space bar to indicate the end of the trial (Figure 62 B and C). The position errors were expressed as the percentage of the range of motion. In addition, for the given motion speed of the controlled hand in each trial, the path efficiency was calculated for each DoF as the ratio between the length of the optimal trajectory (Figure 62 B and C, yellow line) and the trajectory generated by the subject (Figure 62 B and C, green line). The optimal trajectory was the shortest path from the initial to the target configuration. The generated trajectory, instead, was calculated as the sum of the length of the slope segments (Figure 62 B and C, green full lines). The horizontal segments (Figure 62 B and C, green dashed line) were not counted into the length because they correspond to the phases in which the subject did not move the prosthesis.

Another parameter used to assess performance was the DoF time, i.e. the amount of time that the DoF was activated during the trial expressed as the percent of the total trial time. The time efficiency was also calculated as the ratio between the optimal time to perform the trial for the given motion speed, and the time that the subject took to perform the trial (Figure 62 B and C, trial time). The optimal time was computed as the sum of the time to adjust the two DoF (topt1 + topt2) following the respective optimal paths because the subject was able to adjust them sequentially and not simultaneously. Note that, contrary to path efficiency, which was computed for each DoF separately, the time efficiency was estimated per trial (because the rest time could not be separated to individual DoFs). Importantly, the path and time efficiency were calculated only in the trials where the positioning error was less then ± 15%, which was achieved in the 40% of all trials. This threshold was chosen to ensure that we consider only those trials in which the subjects reasonably completed the assignment (e.g., if the subjects finished the trial quickly, without even attempting to reach the target, the time and path efficiency would be high but essentially meaningless).

For able-bodied subjects, the average of the outcome measures (error, path efficiency, DoF time and trial time) was computed for each subject and feedback condition and statistically compared between the conditions for each DoF. Data was tested for normality using the Shapiro-Wilk test. A 1-way ANOVA or Friedman test was conducted depending on the outcome of the normality test, while post-hoc pairwise comparisons were performed using paired t-test or Wilcoxon signed rank test with Bonferroni correction. OriginPro 2020 Graphic & Analysis (OriginLab Corporation, Northampton, MA, USA) and MATLAB 2020b (The MathWorks, Inc., Natick, MA, USA) were used for the statistical analysis. The threshold for statistical significance was set at $p<0.05$, and the outliers were excluded from the statistical comparisons.

In four transradial amputees, the average of the outcome measures was computed for each DoF, each feedback scheme, and each subject, and reported overall and separately across three blocks to assess potential learning. Furthermore, for each DoF and condition, the mean of the three blocks was reported

to assess and compare the two feedback schemes. For consistency, the results in the text are reported as mean ± standard deviation in all cases.

4.2.3. Results

The overall results for able-bodied subjects for error, path and time efficiency are summarized in Figure 63. Importantly, no statistically significant differences were detected between the two feedback schemes in either of the performance measures. Nevertheless, it seems that the accuracy of positioning was somewhat more consistent (lower inter-subject variability) when using the Compact approach to adjust the hand aperture (Figure 63 A) and vice versa for the DoF time (Figure 63 C). Both feedback schemes were characterized with low time efficiency of approximately 40 ± 18.6% (Figure 63 D). Regarding the individual DoFs, the end-point error (Figure 63 A) and path efficiency (Figure 63 B) were

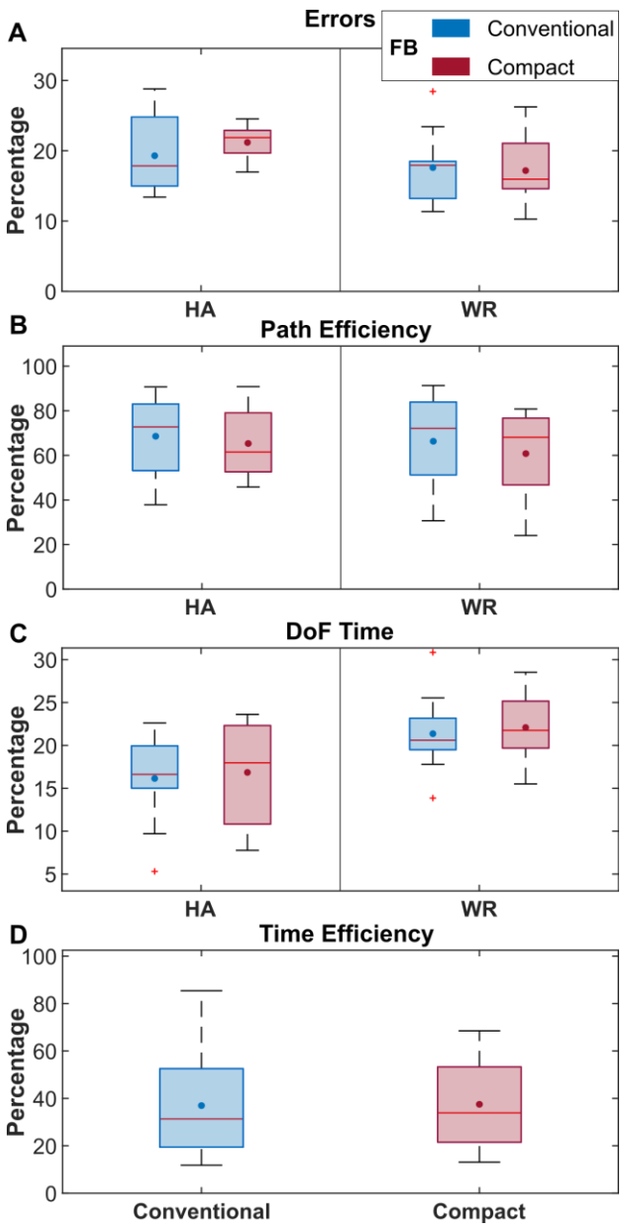

Figure 63
Summary results for the positioning error (A), path (B) and time efficiency (D), and time per DoF (C) in the form of boxplots for able-bodied subjects. HA indicates the aperture and WR indicates the prono/supination DoF. The small circles are the means, the red lines indicate the medians, boxes are interquartile ranges, whiskers represent min/max values and the crosses are outliers. There were no-statistically significant differences between the two feedback types.

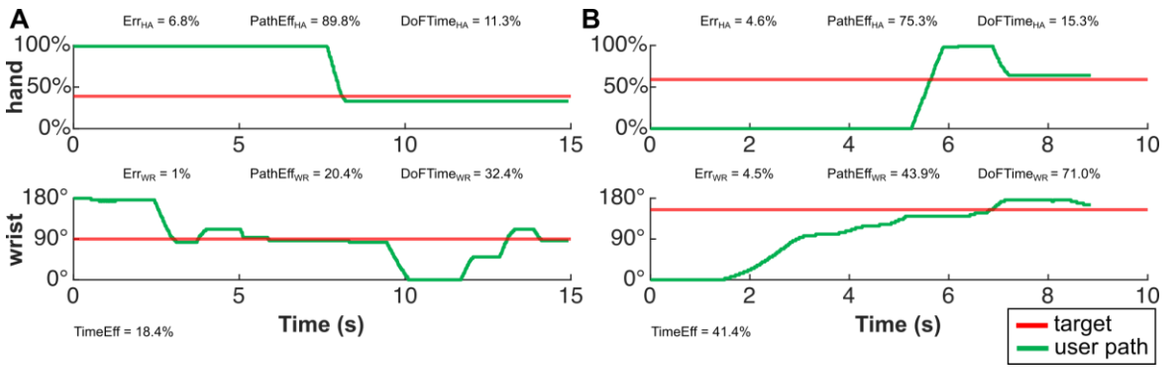

Figure 64
Two example trials performed by an amputee participant using the two feedback methods compared in the manuscript, namely, Conventional (A), and Compact Feedback (B). The plots show the trajectories generated by the participant when adjusting the wrist rotation and hand aperture. Err, PathEff, TimeEff and DoFTime denote positioning error, path and time efficiency, and time per DoF, while the subscripts HA and WR denote hand and wrist, respectively.

similar for the two DOFs with an overall average (mean and STD) around 20 ± 5.4% and 65 ± 17.4%, respectively. The only difference between the hand and wrist was in the DoF time (Figure 63 C), where the active time for the hand (overall average 16.5 ± 5.5) was lower compared to that of the wrist (21.7 ± 4.4) but also in this case the difference was not significant ($p = 0.24$). Finally, regarding the subjective preference, six out of 10 able-bodied subjects chose the Conventional encoding as the preferred approach.

Figure 64 shows representative trajectories (green line) generated by an amputee subject when adjusting the configuration of the prosthesis using the two vibrotactile feedback encoding schemes (Figure 64 A for the Conventional and Figure 64 B for the Compact feedback). The target positions for the wrist rotation and hand aperture are shown using red lines. In both cases, the subject first adjusted one DoF fully and then proceeded to the next one, namely, wrist rotation and then hand aperture. However, in the trial with the Conventional feedback (Figure 64 A), the subject came back to readjust the wrist as he did not consider it to be completely correct. The control of wrist rotation took longer time and included more feedback-driven corrections (flat segments) compared to the hand aperture, which was adjusted in one (Figure 64 A) and two (Figure 64 B) continuous motions. This observation was the same in both feedback conditions. In two cases (wrist in Figure 64 A and hand in Figure 64 B), the subject reached the end of the range of motion and used this as a well-defined and easy to recognize "anchor" point, from which to then readjust to the desired position. Finally, with both feedback schemes, the end positions achieved in both DoFs matched closely the target values. Figure 64 also reports the outcome measures for these specific trials to illustrate their range and meaning.

The results for the amputees are shown individually for each subject and block of trials in Figure 65. In general, the amputee performance (Figure 65) was comparable to that obtained in the able-bodied subjects, except for P1 that obtained better accuracy but worst results in all the efficiency parameters. When comparing the two conditions, Conventional and Compact, neither of them showed a clear advantage, reflecting thereby the overall results obtained in able-bodied participants. Overall, the

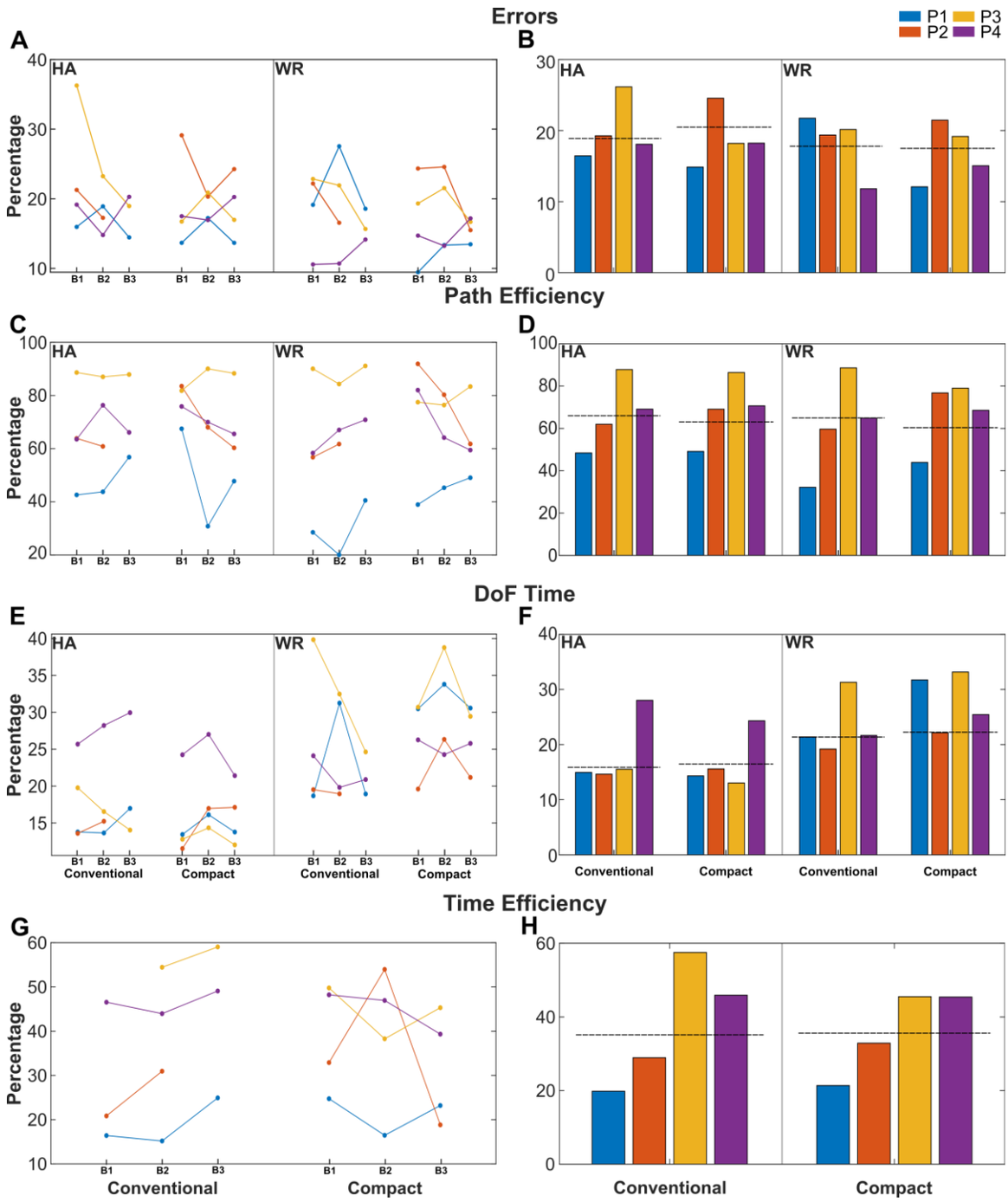

Figure 65 The results obtained by 4 amputee participants using Compact and Conventional feedback.
Left panels show the performance for each block of trials, to assess the potential learning effect, while the right panels representthe average across blocks. HA indicates aperture, and WR represents prono/supination DoF. Plot colours are associated to different amputated participants (P1-P4). The horizontal dashed lines in the right pannels indicate the mean performance of able-bodied subjects. B*n* in the left plots denotes different testing blocks.

difference in performance ([min, max]) between the encoding schemes was not large in any case, specifically, [0.2%, 9.7%] for error, [0.5%, 18.6%] for path efficiency, [0.6%, 17.0%] for DoF time, and [2%, 9.3%] for time efficiency. The condition with the lower error depended on the subject and even on the degree of freedom. There seem to be a slight trend for better efficiency of the Compact solution, as it is higher in most cases with that approach. For instance, P1 was the least efficient but he also made

smallest errors in most cases, whereas P3 was most efficient while maintaining good accuracy. Across blocks, there is no consistent learning across subjects and conditions, but only sporadic tendencies. For instance, P3 and P2 decreased while P4 somewhat increased the error from the first to the third block.

Finally, P1 and P3 preferred the Compact condition while P2 and P4 preferred the Conventional condition, and therefore, the subjects preferred the interface with which they achieved better accuracy.

4.2.4. Discussion

The present study proposed a novel approach to convey proprioceptive information simultaneously for two feedback variables, namely, hand aperture and wrist rotation, by using a single array of vibration motors. The approach employs spatial encoding with Gaussian interpolation, in which the location of the peak intensity was modulated to convey wrist orientation (μ in equation (24)), while the spread of sensation (σ in equation (24)) was associated to the hand aperture. Most methods in the literature use multiple arrays of stimulators to provide information from different DoFs [484, 485], while the encoding proposed in the present study enables conveying multiple information through a single array. The latter is an important strategy as it allows making the feedback interfaces more compact and therefore easier to be integrated in the prosthetic socket. The approaches to establish parallel feedback channels through the same interface were investigated in the literature using multimodal (hybrid vibro- and electrotactile stimulation) [475-478] and multiparameter (amplitude and frequency) [5, 126, 473, 474, 486] modulations. Our approach is based on spatial encoding, which enables superimposing two feedback variables using an intuitive mapping, i.e., rotating sensation to convey rotation and spreading sensation to indicate hand opening.

Importantly, the novel approach based on Compact encoding was compared to the Conventional mapping that used two independent arrays and the results demonstrated that the two approaches were similarly effective in conveying two-DoF proprioceptive information. There was no significant difference in either the accuracy or efficiency when using the two encoding schemes for the closed-loop prosthesis control. Our initial assumption was that the subjects would perform better with the Conventional scheme, as the interpretation was in this case simple (identifying a single active motor). In addition to similar accuracy, the subjective preference was also similarly distributed between the two encoding schemes (6 vs. 4 in able bodied and 2 vs. 2 in amputee participants). In able bodied subjects, the preference was slightly in favor of Conventional feedback scheme. Nevertheless, our results demonstrated that Compact solution can still be used in the case that there is not enough space to fit all vibromotors. In some subjects, this could decrease user experience (lower preference) but will not jeopardize the performance.

The present study has therefore proven the hypothesis inspired by a recent work that the two parameters defining the Gaussian interpolation strategy can be independently modulated and recognized by the participants (see section 4.1). In that study, the subjects controlled only the wrist rotation of a virtual prosthesis, whereas the parameter σ was imposed externally as “noise”. In the present

experiment, however, they actively adjusted the configuration (both wrist and hand) of a real prosthesis. Note that the feedback encoding in the Compact interface is intrinsically coupled. For instance, the same target hand aperture will lead to different sensations depending on the target wrist rotation. This effect does not exist in the Conventional approach, and the coupling therefore did not negatively affect the control.

This is an important result as it shows that the number of vibromotors can be safely decreased from twelve to eight without loss of performance. Therefore, the excess vibromotors can be removed to make the interface easier to be integrated or they can be used to encode additional information, such as wrist flexion/extension or grasping force. Such an interface could be used to provide the simultaneous feedback of three different DoFs: hand aperture, wrist rotation, and wrist flexion and extension, hence full kinematic state of a prosthetic hand (complete proprioceptive feedback).

In line with the previous goals, note that the setup for closed-loop control used in the present study was realized using an embedded platform, which is therefore ready to be integrated into a prosthesis for rapid clinical use. The embedded platform includes recording of EMG signals, pattern classification and control of vibromotor as well as bidirectional communication with the real prosthesis. In general, tactile feedback was rarely demonstrated in combination with pattern classification and multiple DoF control [454], especially when using an embedded setup [409].

Recently, multichannel electrotactile stimulation was used to convey two degrees of freedom [454]. The authors exploited the compactness of electrotactile stimulation to provide feedback through a flexible electrode integrating an array of 16 pads. Nevertheless, the encoding scheme utilized a Conventional approach where the array was segmented into non-overlapping sectors allocated to different DoFs, which is equivalent to the multi-array feedback of the present study. An additional advantage of vibrotactile interface is that it does not interfere with the recording of EMG and hence does not require a specialized hardware and software.

Importantly, the amputee participants have achieved the performance that was subject specific but coherent with the able-bodied population (Figure 65). This is an important outcome for the prospective clinical application of the proposed closed-loop control, especially considering that the amputee subjects employed pattern classification control and feedback interface, which were mounted on the same forearm. This is the same setup that will be used in the clinical system.

Overall, the novel method allowed an effective closed-loop control (average error < 20%) in able-bodied as well as in amputee subjects. However, the average error is higher than that obtained in a recent study where Gaussian interpolation was used to adjust wrist orientation (see section 4.1). Nevertheless, in that study, the subjects controlled a virtual prosthesis using keyboard, hence, both the system and the control interface were ideal. We also assume that in the clinical application a precise control of wrist orientation and hand aperture will not be critical. Both wrist rotation and hand opening can be adjusted with a margin of error without jeopardizing the successful grasp. In addition, with prolonged training the closed-loop control is expected to improve due to both better use of pattern classification and more

reliable interpretation of the feedback. Similarly, the prolonged use could also change the subjective preference, but these remain to be tested.

The subjects in general spent more time adjusting the wrist compared to the hand. This is not unexpected, as the wrist has larger range of motion, more target and feedback levels, and adjusting the wrist was, therefore, a more complicated task. However, it is still an encouraging result that, despite this difference, both DoFs could be controlled with similar relative accuracy. In general, the time efficiency was overall not high, and this is likely due to the cognitive demands related to interpreting the feedback but also generating commands using pattern classification. Nevertheless, it is overall promising that the subject could successfully exploit the closed-loop control of multiple DoFs, after only a brief training. A prolonged training is likely to have a stronger effect particularly on the time efficiency. Finally, despite in the present work the participants used to control DoFs sequentially via pattern classification, the same feedback scheme can be used in combination with regression to allow simultaneous control. In this case, the elicited tactile sensation would change both in the location and the extent of spreading concomitantly. It remains to be tested how well and how fast the participants can accommodate such dynamically changing feedback.

Following the encouraging results of the present study, especially regarding amputee subjects, the next step in our research will be to integrate the system into a prosthesis socket and test the closed-loop control during functional prosthesis use. The final aim is to accommodate all DoFs of the Hannes prosthesis both in control (pattern classification) and feedback (full proprioceptive and exteroceptive substitution).

4.2.5. Conclusion

The present study proposed a novel Compact approach to provide artificial vibrotactile feedback about two DoFs using a single array of vibromotors. In the proposed approach, the wrist rotation was conveyed by moving the peak of sensation around the forearm, while the hand aperture was transmitted by increasing the spread of sensations from the peak location as the hand was opening. Hence, the two variables were conveyed using an intuitive mapping. The tests demonstrated that the novel approach performs similarly to the Conventional feedback scheme, where separate arrays were used to covey individual DoFs. Our study therefore indicates that, by using the proposed method, the number of vibration motors required to provide feedback can be decreased without any significant loss of performance. This, in combination with the fact that the feedback was integrated with pattern recognition, represents an important step towards the development of clinical applications embedding both feedback and control into a single prosthesis socket.

frontiers | Frontiers in Neuroscience
ORIGINAL RESEARCH
published: 27 August 2021
doi: 10.3389/fnbot.2021.683653

4.3. Object Stiffness Recognition and Vibratory Feedback without Ad-hoc sensing on the Hannes Prosthesis: a Machine Learning Approach

4.3.1. Introduction

Upper limb loss is a serious impairment due to its explicit and direct interaction with the external world. To compensate this loss, prostheses have been introduced to restore the functionality of human limbs during Activities of Daily Living (ADLs). This necessity led to the development of high-tech devices with multiple degrees of freedom [487, 488], capable to perform a variety of gestures and grasps. However, the embodiment of these devices into human body scheme and their acceptance are also essential elements for the reconnection with the outside world [129, 243]. With the term "Embodiment" is meant the integration of an external object in the internal corporal scheme, as if it was part of the body itself. In this specific context, the external object is, precisely, the prosthesis [257]. Embodiment comprises three correlated factors: ownership, localization, and agency [489], and it has been suggested to promote intuitive control, learning and comfort when using new tools, thus providing the opportunity to improve the user interface for devices such as artificial limbs. The introduction of direct feedback modalities can prevent amputees to rely exclusively on sight [371, 490], reducing the mental effort and, therefore, facilitating the communication between user intention and prosthesis action [156, 428, 431]. In fact, it has been demonstrated that the introduction of haptic feedback improves the control of the prosthesis [5, 442, 470, 491] due to its fundamental role during human-objects interactions [88, 156, 432, 433, 449, 486], allowing subjects to embody the device [88, 127, 132], hence improving the compliancy among the user, the prosthesis and the grasped objects [492]. In literature, this interaction is mainly assessed providing grasp force or proprioceptive information [493]. Contrarily, it is our aim to deliver information about the grasped object's stiffness that in normal conditions, occurs thanks to the combination of visual sensory information, proprioceptive sensations related to shape and size, and tactile sensations related to stiffness [494]. Therefore, the current research activity wants to offer an intuitive, non-invasive and easy-to-use prosthetic system capable to identify simple grasped object proprieties when visual sensory information of the user is not available or limited [5]. For instance, when the user is taking an object from a bag without looking at it or when the light in the environment is off. This situation was also treated by Cybathlon 2020 competition, which introduced the Haptic Box task, considering it as a common Activity of Daily Living (ADL) [17].

Focusing on tactile sensations, several studies tried to reproduce the properties of human skin endow the device with tactile sensing technologies that typically requires cumbersome ad-on like sensing skin with different kind of sensors such as piezoresistive [120], capacitive [495], piezoelectric [496] and also optical [497]. The measurements acquired by these tactile sensors are often given as input to machine

learning algorithms, which extract useful information that may be conveyed to the prostheses users as described in Jamali and Sammut [498], Liarokapis, et al. [499], Konstantinova, et al. [500], Devaraja, et al. [501], Huang and Rosendo [502].

Once the tactile information has been extracted, it is necessary to effectively provide it to the subject. The sensory substitution process can be exploited non-invasively, involving the connection of a certain event with specific feedback that is not the natural one, such as tactile sensory feedback [5, 100, 220, 436, 437]. For example, the subject can be taught to associate a certain vibratory stimulus to the contact of the prosthesis with an object [100, 217, 220, 428, 437, 439-441]. On the other hand, superficial stimulation could target portions of missing limb's skin that are innervated by afferent neurons after the amputation, the so called referred touch, to stimulate the phantom limb and improve the embodiment [132, 503], such as kinesthetic sensory feedback.

The most common feedback restoration method is through vibration [503], given its compatibility with EMG control and better acceptance by the subjects with respect to electrostimulation, capable to stimulate phantom limb sensation with electric surface charge [504-506]. It is possible to provide different type of information acting on the amplitude and frequency of the vibration, as exploited in the study of Witteveen, et al. [507], in which the magnitude of the grasp force was transmitted using different levels of amplitude. An alternative to this feedback is the mechanotactile, which can be exerted, for example, with a tactor, as in Meek, et al. [508] hence producing a one-to-one correspondence of touch sensation to user stimulation, or with a cuff, as proposed by Casini, et al. [509].

However, despite the high potentiality offered by these solutions, they mainly result bulky, heavy, and difficult to integrate, along with high power consumption due to high computational burden. An example is proposed by Antfolk, et al. [407], which designed a touch sensory feedback via air mediated pressure from the hand to the forearm skin. This is a no-power solution which has no impact on power consumption nor on computational burdening. However, the final integration within the prosthesis does not guarantee the anthropomorphism of the hand device. It is also important to point out that the quick disconnection among the socket and the hand prosthesis is lost due to the mechanical connections running from the fingers' hand to the on-socket actuators. Standard devices use electronic slipring combined with a quick disconnect mechanism integrated in the prono-supinator wrist to guarantee the overall disconnection of the hand prosthesis from the socket in case of emergency. However, in the proposed design this feature is compromised. Other examples are Oddo, et al. [155], Shehata, et al. [483] which proposed an artificial fingertip to improve performance of prosthetic hands by using intraneural stimulation. That solution can be nicely integrated into a fingertip by maintaining the anthropomorphic. However, the on-board electronics which record, process the tactile information and encode the stimulation is cumbersome. Moreover, the high-power consumption of the FPGA-based solution does not permit the entire system to last for an entire day and to fit into a standard socket. Similarly, Clemente, et al. [428] purpose a solution whose electronic skin offers high sensitivity ranging from light touch and heavy touch. However, similar integration problem of the dedicated board occurs. On the other hand,

Vargas, et al. [445], finally, proposed force and position sensors on the fingers to provide object stiffness recognition on amputees through vibrotactile feedback. That solution can be easily integrated; however, the performances of such solution are limited in comparison to our results. Due to these issues, the lack of a suitable feedback restitution method in the prosthetic field is still far from being solved. Two other solutions for object stiffness recognition, without dedicated sensors, were implemented by [510] as well as by [511]. Their works demonstrated the feasibility of these approaches in a robotic scenario using an actuated mechanical gripper.

Considering the advantages of providing feedback to amputees to improve the comfort between the user and the device, in this study we first investigated the possibility of detecting void grasp and object grasp. Then, we identify softness and hardness of the objects therefore permitting the user to discriminate among "void grasp", "rigid object" and "soft object" without visual sensory information. In a first preliminary study [512], a virtual multi-body model of Hannes was developed to offline demonstrate, with a virtual simulation, how the motor-side current absorption and the position measurement could be correlated with the hand grasp force and the grasped object's stiffness. Subsequently, in a following study [513] an Ensemble Bagged Trees classifier was implemented and offline tested with simulated data to validate an approach to distinguish two different objects' stiffnesses.

Consequently, in the presented paper we exploited the previously preliminary validated approach to develop an online (real-time) solution to perform object stiffness recognition and sensory feedback. The performance of this solution was assessed on end-users, both able-bodied and amputees. A Non-Linear Logistic regression classifier was used to recognize rigid or soft objects and void grasps. We excluded embedded force sensors, whose introduction would require facing many challenges, starting from the choice of the right sensor with basic requirements like high resolution, high sensitivity and robustness, to the difficulties of managing the wiring [514]. Instead, we propose a methodology that uses *intrinsic sensors* (sensors and parameters already available on the prosthesis) for the normal functionality of the prosthesis which does not increase cost and complexity of the device. In particular, we exploited the following intrinsic sensors: the motor-side current, whose relationship with the contact stiffness has been analytically demonstrated by Deng, et al. [515], the reference position, given as input to control the device closure, and the position effectively measured by the encoder (encoder position). We implemented a close-loop vibratory feedback, using a single vibromotor embedded in the Hannes system, closely related to the predictions made by the classifier. In details we applied the strategy of strong vibration for rigid objects and small vibration for soft objects, identified in this work as 'Two Feedback (2FB) condition' [516, 517]. In a first phase, the classifier performance and the 2FB effectiveness were evaluated with 18 able-bodied subjects by measuring the classification accuracy through F1Score. In a second phase, a comparison between our proposed feedback method (2FB) and three other control feedback conditions was carried out on 5 amputees. This comparison was performed both objectively by measuring F1Score, users' response time and proprioceptive drift, and subjectively

through questionnaire to investigate the users' appreciation of the feedback strategies and to identify the most intuitive and effective one.

4.3.2. Material & Methods

4.3.2.1. Subjects

Eighteen able-bodied subjects aged between 24 and 50 years (28.8 ± 6.2) and 5 mono-lateral amputees (right trans-radial amputees, users of active prostheses) were recruited for this study, Table 20. Written informed consent was obtained from all subjects. Experimental protocol was approved by the AVEC (Area Vasta Emilia Centro) Ethics Committee (Protocol Code: CP-PPRAS1/1-03) and performed in accordance with the guideline of the Declaration of Helsinki.

4.3.2.2. Experimental setup

The experimental setup used for performing the entire experiment, Figure **66**, was composed by: (A) the myoelectric prosthesis Hannes, fixed on a rigid cone; (B) a custom master-board to control the hand, decode the stiffness of the grasped object, and communicate with the PC via Bluetooth; (C) two EMG sensors (standard Ottobock, 13E200=50 AC) to close or open the hand; (D) an eccentric rotating mass (ERM) vibromotor to convey the feedback; (E) a power supply for the prosthetic system; (F) two wristbands to attach the EMG sensors and the vibromotor to the subject's forearm; (G) three rigid objects and three soft objects with spherical, cubic and cylindrical shape used during the Cybathlon 2020 edition (Caserta et al., 2022, ETH-Zurich, 2020); (H) a laptop to choose the feedback condition and to collect the data; (I) a keyboard, placed in front of the subject, to press the left (rigid object) and right (soft object) arrows to indicate the guessed stiffness of the grasped object; (J) headphones reproducing white noise to prevent the users from hearing the prosthesis motor.

Table 20 Population of amputees.

Amputees	*Age*	*Time from amputation*	*Dominant Limb (before amputation)*	*Amputated Limb*	*Etiology*	*Level of Amputation*	*Type of Prosthesis*
A1	53	32 years	Right	Right	Work accident	Unilateral medial	Michelangelo Hand
A2	42	18 years	Right	Right	Car accident	Unilateral proximal	Variplus Hand
A3	58	37 years	Right	Right	Work accident	Unilateral distal	Michelangelo Hand
A4	35	12 years	Right	Right	Work accident	Unilateral distal	Variplus Hand
A5	68	53 years	Right	Right	Work accident	Unilateral distal	Michelangelo Hand

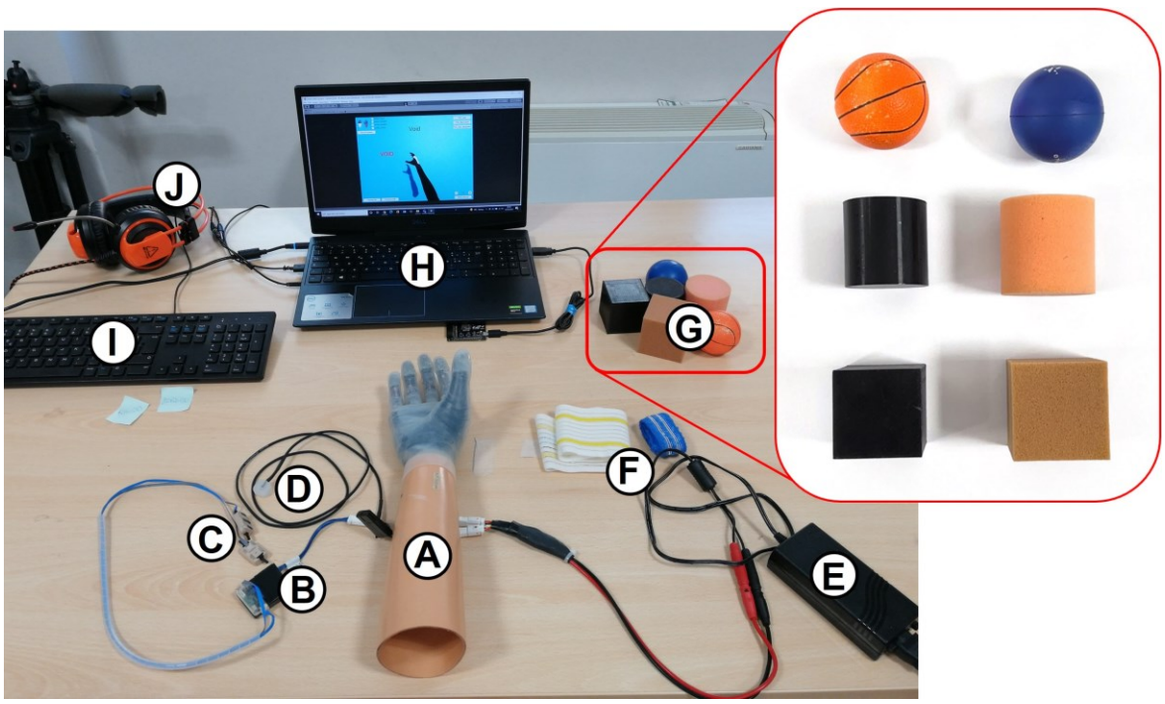

Figure 66 Experimental setup used to perform the task on healthy subjects and amputees.
It consists of: A) socket with the Hannes prosthesis; B) the EMGM to control the Hannes hand, recognize the grasped object and provide feedback; C) EMG sensors; D) vibromotors; E) power supply; F) elastic band to attach the EMGs and vibromotors to the forearm; G) the objects used to perform the task; H) laptop with the virtual reality; I) keyboard to choose between rigid, soft or void; J) headphones to isolate the participants during the experiment.

The vibromotor was inserted in a custom silicone holder to localize and absorb the radiating stimulation and to avoid the possible heating of the skin due to prolonged vibration. The vibromotor was placed vertically with respect to the skin to produce a stronger and focused sensation. The vibration frequency was set to 200 Hz, using a supply voltage of 2.5 V [459], and the amplitude was varied through the Pulse Width Modulation (PWM).

4.3.2.2.1. The Hannes hand

Hannes is an under-actuated poly-articulated prosthetic hand characterized by a leader-follower wire configuration used to control the movements of fingers [11]. The hand powertrain consists of a single DC motor coupled with a custom planetary gearhead, which drives the grasping movement (see Supplementary Materials). The actuation system is controlled by a position reference (ϑ_{ref}) synthetized from the user's electromyography (EMG) signals. A magnetic encoder measures the slow shaft position (ϑ_{out}) of the hand drive train, therefore controlling the desired grasp configuration. The low-level control system is based on a series of Proportional-Integrative-Derivative (PID) controllers. The outer loop is position based (where only Proportional and Derivative – PD terms are deployed) whilst the inner loop is current based and concerns Proportional and Integrative – PI terms only. In particular, the error (ε_{pos}) between the ϑ_{ref} (hand control command) and the ϑ_{out} (outer feedback) is fed to the outer PD loop. The related output is then multiplied by a proportional gain resulting in a current reference (i_{ref}) which is subtracted with the measured one (i_{out}, inner secondary feedback which is the current absorbed by the DC motor during hand movement and grasp). As consequence, the related error (ε_i) is then fed to the

inner PI controller hence generating the control command (V) to be delivered to the motor driver. As many under-actuated prostheses, Hannes is under-sensorized. Indeed, the only available measurements are motor-side current and position.

4.3.2.2.2. Feedback conditions

Four different feedback conditions were assessed in this study: (i) no FB condition (NoFB); (ii) audio FB condition (AFB); (iii) one FB condition (1FB); (iv) two FB condition (2FB). The NoFB condition was characterized by the absence of any possible feedback. Subjects were visibly (with closed eyes) and auditory (headphones with white noise) blind and without any vibratory feedback. In the AFB condition no vibratory feedback was supplied to the user, but the absence of the headphones permitted accidental auditory feedback of the moving prosthesis. In the 1FB condition the vibratory feedback was provided, but the same vibration intensity (30% of PWM) was associated to both rigid and soft objects, while no vibration was given during void closures, see Figure 67 table. The 2FB condition provided a strong vibration for rigid objects (100% of PWM) and a light vibration for soft objects (30% of PWM, value found during some previous pilot tests to be perceived sufficiently different from the 100% used for rigid objects), see Figure 67 table. As in the 1FB condition, void closures did not provide any kind of vibration. The no FB condition was implemented as a baseline for validation and comparison of subjects' performance. In fact, in total absence of feedback, subjects' performance should be close to a random guess. The audio FB condition was introduced, since it represents a reasonable scenario of use of the prosthetic hand by amputees, namely with no direct vision of the prosthesis but accidental auditory information from the prosthesis motion. Therefore, this second condition works as a real-case scenario ground-truth for the user. The other two conditions - 1FB and 2FB - were implemented to observe, respectively, if an additional vibratory feedback could improve the stiffness estimation performance, and if a different degree of vibration could further help amputees in discerning between harder and softer objects.

4.3.2.3. Non-Linear Logistic Regression

4.3.2.3.1. Algorithm Model

The algorithm chosen for the object stiffness discrimination task is the Non-Linear Logistic Regression (NLR) classifier. This machine learning algorithm was selected given the good performance shown for multiclass classification problems, and for simplicity reasons, since the NLR is already employed for Hannes pattern recognition control strategy [12, 13]. It is based on the calculation of the class membership probability through the following formulation:

$$P(1|x,\vartheta) = \begin{cases} g(\vartheta^T \cdot x) = \dfrac{1}{1+e^{-(\vartheta^T \cdot x + \vartheta_0)}} \\ 1 - P(y=0|x,\vartheta) \end{cases} \tag{25}$$

Where ϑ and ϑ_0 are the internal parameters vector of the classifier and the bias term respectively, x is the input feature vector while g(·) is the sigmoid logistic function. The class prediction is obtained from the comparison between the distribution P(y|x) with a decision threshold (TH) as:

$$h_\vartheta(x) = \begin{cases} P(1|x,\vartheta) \geq \text{TH} \rightarrow 1 \\ P(1|x,\vartheta) \leq \text{TH} \rightarrow 0 \end{cases} \quad (26)$$

The TH value was obtained after an optimization phase on the validation set. Since the NLR is a binary classifier, a One-vs-All approach was implemented to address the multiclass classification problem for the discrimination between rigid, soft and void closures. This involves the use of as many binary classifiers as the classes to predict, and each of them is trained to recognize the specific class. The model parameters (ϑ) are the result of an optimization process which involves the minimization of a cost function called cross-entropy error J:

$$J(\vartheta,\vartheta_0) = -\frac{1}{m}\cdot\left[\sum_{i=1}^{m} y(i)\cdot\ln\left(g(\vartheta^T\cdot x+\vartheta_0)\right)\right]-\frac{1}{m}\cdot\left[\sum_{i=1}^{m}(1-y^{(i)})\cdot\ln\left(1-g(\vartheta^T\cdot x+\vartheta_0)\right)\right] \quad (27)$$

Where m is the number of samples used to train the algorithm and y(i) is the known class membership of the i_{th} sample [13, 77].

4.3.2.3.2. Algorithm Training

To adapt the model to distinguish multiple rigidities, the classifier required a training phase involving the repetitive closure of the prosthesis on objects of different stiffness. To simplify this work and to create a reproducible acquisition set up, a custom-made object was 3D printed. This device, shown in Figure **68**, was designed to reproduce the same shape and dimension of the Go Direct ® Hand Dynamometer [518], used in the previous study [512], which offers the possibility to insert springs of different stiffness, simulating the grasping of soft and rigid objects as shown in Figure 68 table.

Table 21 Dataset realization for training the NLR for object stiffness recognition algorithm.

# closures	***Grasped object***	***Stiffness***	***Control signal***
10	Void	Void	Sinusoidal
10	Hand Dynam	Rigid	Sinusoidal
10	Hand Dynam	Rigid	EMG
5	4xS1	Soft	Sinusoidal
5	4xS1	Soft	EMG
5	2xS1	Soft	Sinusoidal
5	2xS1	Soft	EMG
5	4xS2	Rigid	Sinusoidal
5	4xS2	Rigid	EMG
5	4xS3	Rigid	Sinusoidal
5	4xS3	Rigid	EMG
5	2xS1-2xS4	Soft	Sinusoidal
5	2xS1-2xS4	Soft	EMG

The device was mounted in an ad-hoc designed test bench. It is composed by movable parallel arms and a two-cuffs system acting as holder. The prosthesis was fixed at the base of this test bench, as shown in Figure **68**, in such a way that only the distal phalanges of the four fingers had impact on the upper plate of the device when performing a closure.

Hannes was controlled through a USB GUI, which allowed the data acquisition (motor-side current and encoder position) as well.

The NLR model generation was performed offline through Matlab and it required a training and a test dataset, both characterized by the following four-columns structure: (i) the motor-side current, (ii) the reference position sent as input, (iii) the encoder position measured, and (iv) the labels of the objects (rigid, soft, void), as it is a supervised learning algorithm. All these measurements are fed to the classifier as analog signals, thus they are directly used as input dataset. Moreover, the label zero was associated to void closures (for motor-side currents below 300 mA), one to the rigid objects and two to the soft objects. The dataset was created using the test bench described in Figure 68.

The choice of relying on only the motor current and the reference and measured motor encoder position was based on the immediate and relevant available sensor information on the prosthesis. Specifically, the motor current is proportional to the motor torque, and, thus, to the grasp force, while the encoder position is related to grasping motion of the fingers. Additionally, the difference between reference and measured encoder position provides good information regarding the distinction between a void closure and the actual grasping of an object (this is due to the variation between the reference encoder position that continues to grow due to EMG residuals, while the actual measured encoder

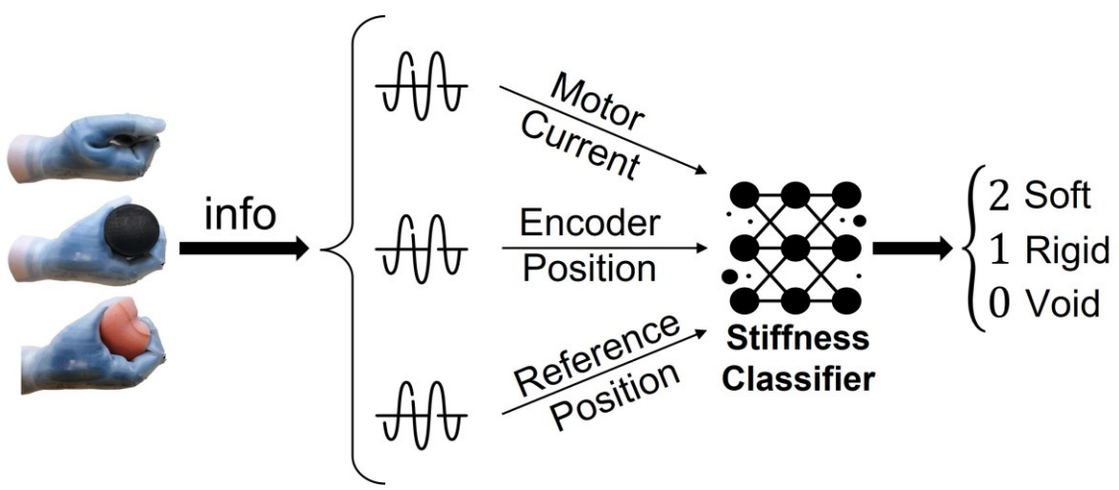

	NoFB	AudioFB	1FB	2FB
Soft	-	-	30% PWM	30% PWM
Rigid	-	-	30% PWM	100% PWM
Void	-	-	0% PWM	0% PWM

Figure 67 Scheme representing the object stiffness classification process.
The motor-side current, the reference and the encoder positions are acquired from Hannes and sent as input to the classifier, which gives as output the resulting stiffness.

position stops when encountering an object during grasp). These three quantities (current, reference and measured position) represent – to the authors – the minimum set of variables to properly classify the different types of grasping (see Results Section for details on the performances). Nonetheless, it is worth mentioning that additional sensors or derived quantities could be beneficial for more complex classifier structure. For example, motor speed – if not particularly noisy or delayed – could help in more advanced classification algorithms.

To generate variability of the data, multiple grasps with various stiffness were performed by the prosthesis, which was controlled by both EMG and sinusoidal references. The hand dynamometer was used to simulate rigid objects, whilst four type of springs with distinct stiffness were used to reproduce

	Spring 1	***Spring 2***	***Spring 3***	***Spring 4***
K [N/mm]	1.55	4.09	4.09	2.9
L_0 [mm]	40	40	40	35
Deflection max [mm]	26	25	24	12.5

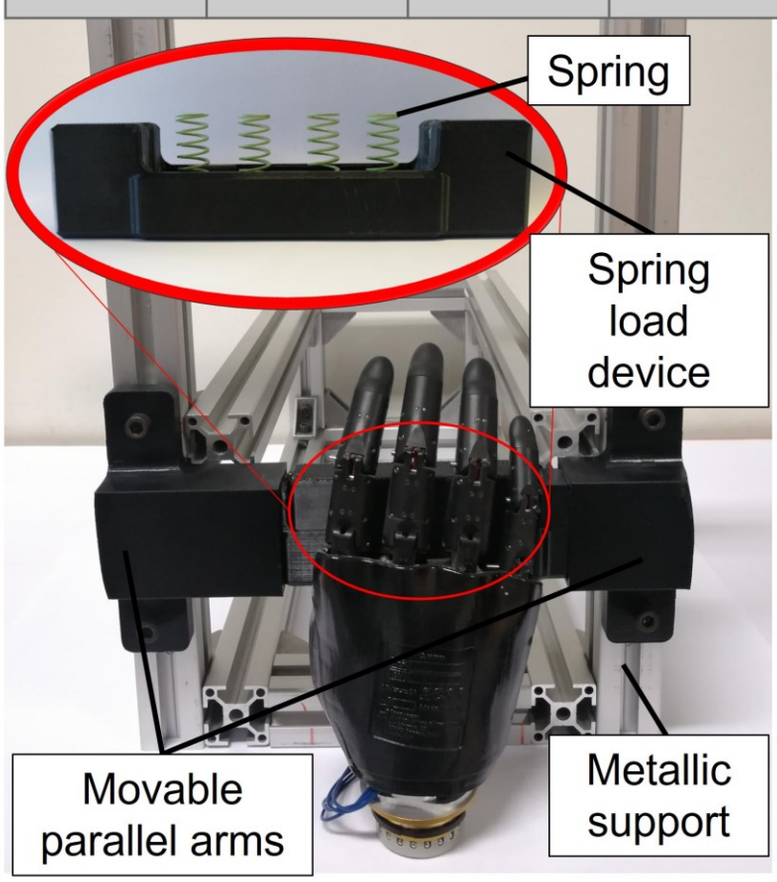

Figure 68 Custom-made hand dynamometer mounted on test bench used for the classifier training.
The device is composed of a base where at maximum four strings can be inserted, and a cover which can slide along the base when compressed by the prosthesis fingers. The test bench consists of a custom -made system composed by movable parallel arms and a two-cuffs system acting as holder. The table represents the different spring force and levels to characterize the stiffness of the dynamometer.

a range of softness/soft objects, as shown in the table of Figure 68. The springs are placed under a bar to distribute the stiffness of their combination to the entire grasp. The chosen combination of springs is different for each case because the total stiffness of parallel springs varies according with their sum, thus affecting the total grasp behavior. In particular, several closures were performed for each case, as described in Table 21, to collect data for the training and validation of the NLR model. The training dataset was split in training set (80%), used for the model generation (selection of the best model parameters (ϑ) by minimizing the cost function J) and validation set (20%) to find the best threshold (TH). Lastly, the classifier was evaluated on the test dataset.

4.3.2.4. Experimental protocol

Subjects were seated comfortably in front of a table (see Figure 69) with EMG sensors positioned on the forearm or stump using an elastic band. The electrodes measured the activity of the forearm muscles involved in the opening and closing of the hand (Flexor Carpi Ulnaris and Extensor Carpi Ulnaris respectively), which were selected by manual inspection. The Hannes system was detached from the users' body (except for the two EMGs) and fixed on the table, lying between the subjects' arms with the palm up, to let the experimenter place the objects to be grasped within the prosthetic hand. Hence, subjects were only asked to close and open the hand, not to approach or grasp the objects. The prosthesis was commanded in proportional-speed-control mode through the EMG signals. To convey the vibratory feedback, the vibromotor was positioned on the pisiform bone for able-bodied subjects and on the lateral epicondyle for the amputees by means of a second elastic band.

First, the minimum and maximum amplitude for the vibromotor was determined using the method of limits [461], to determine the minimum level of perception and avoid discomfort. To this aim, the vibration intensity was increased in small steps (4-5% in the normalized scale of PWM). When the subject warned, as soon as it was perceptible, the sensing of a small and then of a strong sensation, the respective PWM was saved. Subsequently, the 30% of the PWM range was adopted for Soft objects and the 100% was adopted for Rigid objects. The vibration intensity was then modulated between these two values to generate clearly perceivable and localized vibrations that were not intrusive to the subject but intuitive for the encoding of the object stiffness.

Six objects (Figure 66) were randomly presented three times to the user by the experimenter and three void closures were also inserted along the test, to have a total number of 21 trials. Before the test phase, a training phase was performed to let the user become familiar with the feedback. A total of 6 closures were performed, alternating between rigid and soft objects without headphones and with open eyes, so that the user could learn to associate the proper feedback to the right stiffness. Furthermore, the involved upper limb side was covered with a black blanket to strengthen a possible embodiment effect.

In a first phase to evaluate the classifier performance and the feedback effectiveness, the able-bodied subjects underwent a single test with a single condition. They performed the test with the 2FB condition. The participant was asked to wear the headphones with white noise and to close the eyes (avoiding the

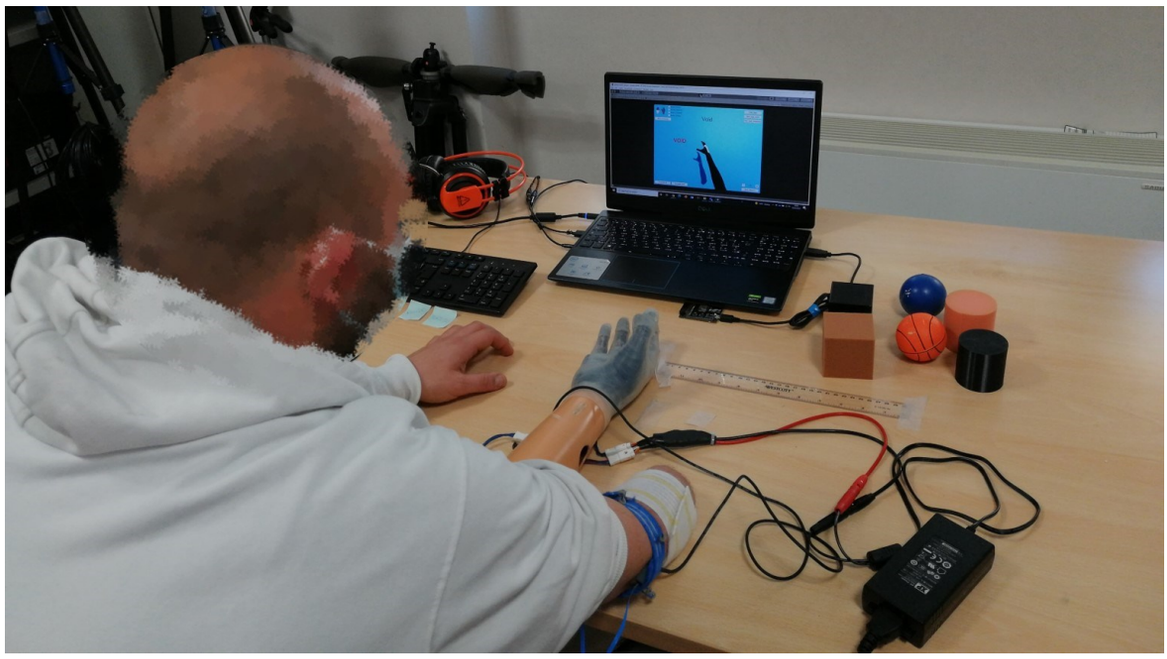

Figure 69 Example of trial involving an amputee.
Two EMGs are attached to the stump for the dual side control of the prosthesis with an elastic band. The vibromotor is fixed to the upper side of the stump with a second elastic band for the feedback restitution. The objects are placed within Hannes hand by the experimenter while the participant has closed eyes. The keyboard, placed in front of the participant, is used to indicate the grasped object stiffness by the user using the left hand.

sight of the prosthesis and the grasped object). The subject was not required to reach out to the object. Instead, the experimenter proceeded to insert it directly into the prosthesis, asking the subject to perform a full closure, and then to identify the stiffness of the squeezed object. The answer was provided by subject's left hand pressing the keyboard arrows, left for rigid objects and right for soft objects. No button needed to be pressed when the prosthesis performed a void closure. Finally, the subject could reopen the eyes to check if the answer was correct.

In a second phase, a comparison between the 4 different feedback conditions, discussed in section 4.3.2.2.2, was carried out by 5 transradial amputees. The order of these 4 sessions was randomly presented to the amputees. Each condition had the same test protocol already described in the first phase with able-bodied subjects, in which the experimenter places the object inside the prosthetic hand, the amputee performs a grasp with closed eyes and gives the answer using the keyboard. At the end of each session the proprioceptive drift was detected with respect to the initial arm position (see section 4.3.2.5.2) and an ad-hoc questionnaire was administered (see supplementary materials).

4.3.2.5. Data Analysis

All the outcomes and the evaluation methods used in this study were tested for normality using the Shapiro-Wilk test. A repeated measure 1-way ANOVA or Friedman test was conducted depending on the outcome of the normality test (for the analysis of dataset with missing data the Skilling's Mack was applied in substitution of Friedman test), while the multiple comparison test with Bonferroni correction was used for post-hoc analysis. Mathworks Matlab 2020b were used for the statistical analysis. The average of the measures used (error and efficiency) was computed for each subject and condition and

compared across conditions. The threshold for statistical significance was set at $p<0.05$. The results in the text are reported as mean and standard deviation.

4.3.2.5.1. Able-bodied subjects

The primary outcome measure was the F1score of classifier on detecting the grasped object's stiffness expressed as percentage, which takes into account the rate of false and true positives and of false negatives [404]. This result allowed to demonstrate that our approach of intrinsic sensor stiffness detection works properly. In addition, the F1score was calculated on users' performance on recognizing objects' stiffness using the 2FB approach described in section 4.3.2.2.2. This latter was used to verify the usability and clarity of our feedback method.

4.3.2.5.2. Amputees

The second phase involving 5 amputees was carried out to compare the four feedback conditions. To validate and demonstrate that the 2FB condition was effective and the best feedback restoration for the recognition of objects' stiffness, our hypothesis, four evaluation methods were used: (i) F1score of performance; (ii) reaction time to recognize the stiffness of the objects; (iii) proprioceptive drift; (iv) ad-hoc questionnaire.

The F1score of amputees' performance was calculated in all feedback conditions. Furthermore, the response time of each trial was also recorded for the four conditions. Low response times were considered positive results. For each amputee, the mean response time of each feedback condition was calculated to allow comparison.

As a quantitative measure of the embodiment, the proprioceptive drift toward the artificial limb was detected [240]. Before covering the involved upper limb side with a black blanket, the initial position of the hand was marked with white tape. Immediately after the experiment, the blanket was removed and the amputees were asked to close their eyes, raise their stump and to replace it in the perceived initial position. The lateral distance between the initial position and the one estimated after the trials was measured by the experimenter with a ruler in centimeter, together with the direction of the deviation [18]. Deviations towards the prosthesis were considered an effect of the embodiment process.

At the end of each session, amputees also had to complete a Likert-type 5-point questionnaire, providing a subjective evaluation. The questionnaire (see supplementary materials) aimed to assess subjectively the intuitiveness and comfortability of the feedback (7 questions), its utility for ADLs (3 questions) and the embodiment (4 questions). The possible answers ranged between 1 (strongly disagree) and 5 (strongly agree). Since all amputees performed the test in all condition, the experimental design is within-subject.

4.3.3. Results

4.3.3.1. Able-bodied subjects

The classifier average accuracy in identifying the objects stiffness was tested on a total of 378 grasps

(21 grasps X 18 subjects). Its average F1Score resulted to be 94.93% ± 3.94. The able-bodied subjects instead, thanks to the 2FB condition, reached an average F1Score of 94.08% ± 4.0 for the object's stiffness discrimination task.

Figure 70 A shows the F1Score obtained by able-bodied subjects during the 2FB condition compared to the F1Score of the classifier performance. Since these data did not present a normal distribution, the Friedman test was applied to demonstrate that no statistical difference was detected between the two populations ($p = 0.1$).

4.3.3.2. Amputees

Figure 70 B shows the boxplot of F1Score obtained by amputees for each of the four feedback conditions. It is possible to observe an ascending trend in the scores from the NoFB condition to the 2FB condition. In the NoFB condition, Amputee A3 data is missing because he found impossible to accomplish the task without any feedback, stating that it was not possible to understand neither if the prosthesis was opened or closed. In the 1FB condition, Amputee A5 data is missing due to a recording problem.

The F1Score among amputees for the NoFB condition is 31.41% ± 8.57, indicated in Figure 70 B with points, which is below the random chance probability of 33%. The statistically significant difference is indicated by "*" ($p < 0.05$). Only Amputee A1 achieved a higher F1Score with respect to random chance (F1Score = 44.03%). The distributions resulted to be normal, so the statistical analysis applied was the ANOVA. As shown in Figure 70 B, the 2FB condition presents a statistically significant difference with respect to the NoFB condition ($p < 0.001$) and AFB ($p < 0.001$) conditions. Furthermore, 1FB condition is statistically different from the NoFB condition ($p = 0.0031$). The average F1Score calculated from the 5 amputees' responses during the 2FB experimental session is 86.41% ± 11.6.

Figure 70 C shows the average response time for amputees in each feedback condition, in which the statistically significant difference is indicated by "*" ($p < 0.05$). All amputees, except A1, achieved the lowest response time during the 2FB condition (2.82 s ± 1.2), which also produced the best results in terms of F1Scores. A statistical analysis was performed between the different conditions. The distribution resulted to be not normal and, given the presence of some missing data, the Skillings Mack test was applied. As shown in Figure 70 C, there is statistically significant difference between AFB and 1FB condition ($p = 0.02$) and between 1FB condition and 2FB condition ($p = 0.04$).

The mean proprioceptive drift for each feedback condition was calculated and it is reported in Figure 70 D as barplots with standard deviations. On average, the 5 amputees estimated the position of their right arm after the experiment 1.8 cm ± 1.17 right (in the opposite side of the prosthesis) during the NoFB condition, whilst 0.4 cm ± 0.58, 0.3 cm ± 0.4 and 0.7 cm ± 1.17 towards left and hence Hannes during the AFB, 1FB and 2FB conditions respectively. The only significant difference was found between the NoFB and 2FB condition ($p = 0.017$) with the Nemenyi test for a post-hoc comparison.

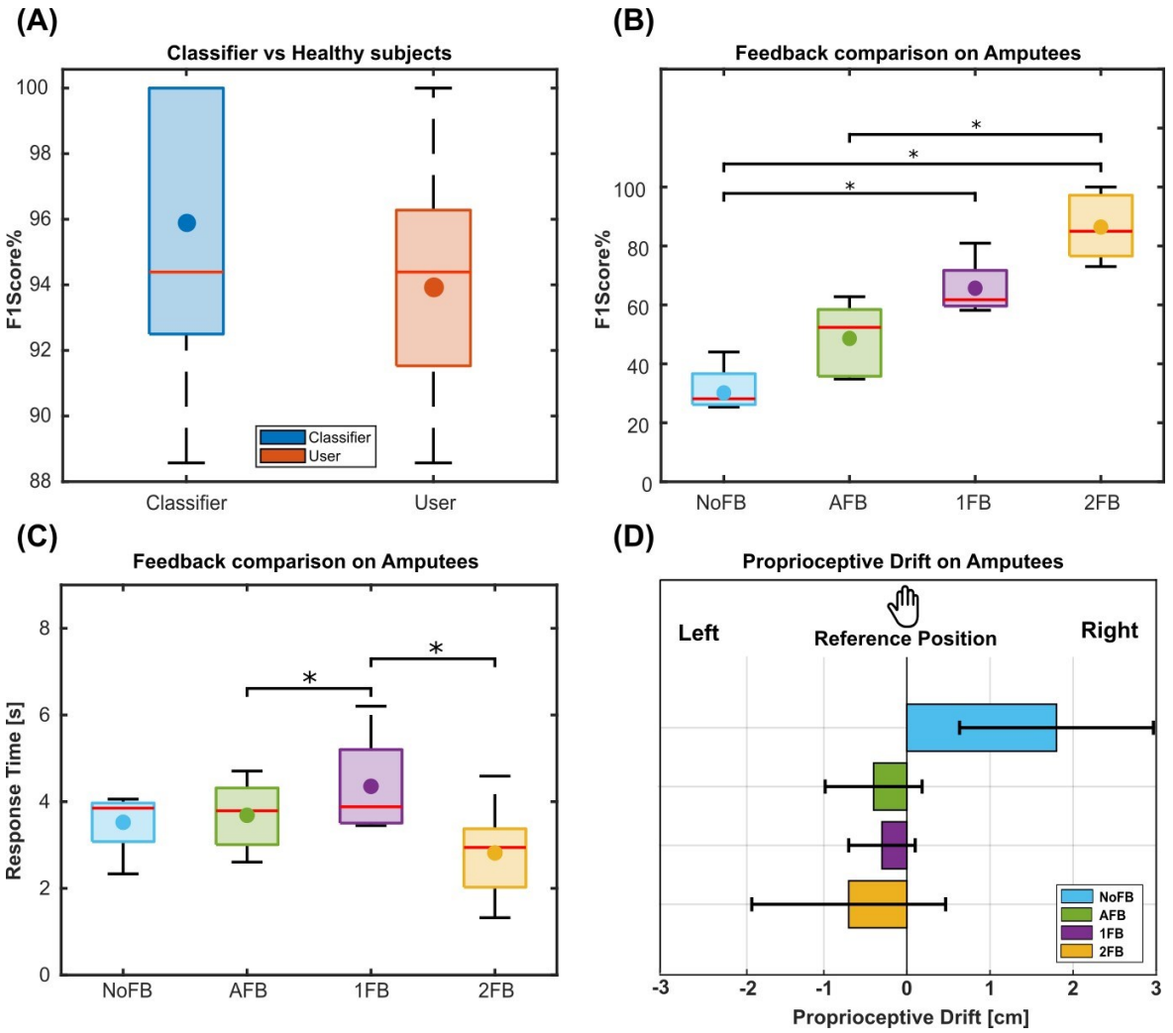

Figure 70 Stiffness Recognition results.
A: F1Scores results of classifier with respect to able-bodied subjects. First the F1Score of the classifier is calculated (blue box). Then the F1Score of 18 able-bodied subjects is evaluated, based on the answer of classifier, in recognizing the objects' stiffness while receiving the 2FB condition (red box). A comparison between classifier's and subjects' F1Score was assessed and no significant difference was found between the two populations. **B:** F1Scores results for amputees. F1Score obtained by amputees for each feedback condition. The Box chart shows the comparison between the distributions of the F1Scores obtained in each condition. The statistically significant difference is indicated by "*" ($p < 0.05$). **C:** Response Time results for amputees. Response Time obtained by amputees for each experimental condition. The Box chart shows the comparison between the distributions of the Response Time obtained in each condition. The statistically significant difference is indicated by "*" ($p < 0.05$). **D:** Proprioceptive drift of amputees for the different feedback conditions as a quantitative embodiment measure. The barplot shows the mean and standard deviation of the drift over amputees for each condition, the left direction is toward Hannes hand, whilst the right direction indicates a movement on the opposite side of Hannes hand. Deviations towards the prosthesis were considered an effect of the embodiment process.

According to comparisons performed through the Friedman test (because the scales are discrete and the actual data does not match the assumptions for other inferential techniques), 3 scales of the questionnaire showed significant effects of the feedback conditions. The subjective evaluations collected about the sessions show that in the 2FB condition:

- Scale 1) made significantly easier to perceive the difference between soft and hard objects ($p = 0.027$);
- Scale 2) was significantly more intuitive for soft objects ($p = 0.015$);
- Scale 3) was significantly intuitive for rigid objects ($p = 0.005$).

According to Scale 3 scores, post-hoc comparisons performed through the Nemenyi Test show how the proposed feedback condition was significantly more intuitive for rigid objects than the NoFB condition ($p = 0.025$) and 1FB condition ($p = 0.017$). Furthermore, the Friedman test showed a significant effect of the 2FB condition ($p = 0.019$), especially considering the results of the Nemenyi test for the post-hoc comparison between 2FB and NoFB conditions ($p = 0.017$).

4.3.4. Discussion

The present study explored the possibility to recognize objects' stiffness with an under-sensorized prosthesis. The reference position, the encoder position, and the motor-side current available on Hannes were used to feed a pattern recognition algorithm, capable to generate different vibratory feedbacks to allow the subject to decode the relative objects' stiffness.

The F1Score of the classifier during the 2FB condition tested with able-bodied subjects (Figure 70 A) was very high (94.93% ± 3.94), demonstrating that the only sensors available on Hannes (motor-side current and encoder position) provide sufficient information for an object stiffness discrimination task using a Non-Linear Logistic Regression algorithm. However, it is necessary to consider that the classifier, during this experiment, was only tested on 6 objects of different shapes, but with almost the same dimensions (chosen to replicate the objects used during the Cybathlon race [17]). Further, also the F1Score obtained by able-bodied subjects (Figure 70 A) on discriminating the object stiffness was very good, proving the usability and efficacy of this feedback approach on a user case.

The positive results of the first phase allowed to evaluate the object stiffness recognition approach on 5 transradial amputees. In this second phase, we tested four approaches of feedback scheme (Figure 70 B). In the NoFB condition we expected a correct identification of the right stiffness around the random chance probability (33%). Actually, the F1Score for NoFB condition was even lower than this percentage (F1Score = 31.41% ± 8.57), as amputees stated they were forced to guess since being deprived of any possible clue. The AFB condition presents a higher average F1Score (48.62% ± 12.56) with respect to the NoFB one, indicating that the motor noise provides a little help in this kind of task. This is true for expert users like Amputee A1, who reached the highest score (62.78%), while it is less evident from others like Amputee A3 (34.85%) and A5 (36.11%), who scored almost as random chance. Differently, in the 1FB condition almost everyone improved their performance (F1Score = 65.67% ± 10.34) respect to NoFB and AFB. In this condition the users were clearly helped in recognizing the void closures, since those were the only ones without vibratory feedback. Moreover, most of the amputees declared that even if the intensity of the vibration was the same for rigid and soft objects, they were able to perceive a difference based on the vibration onset. Since soft objects are more compliant, the motor-side current takes more time to rise with respect to a rigid object. Hence, the vibration is slightly late. For this reason, the 1FB condition resulted statistically better than the NoFB one, unlike the AFB condition which has no significant difference with respect to the NoFB. Overall, the 2FB condition provided the best results (F1score 86.41% ± 11.6), demonstrating to be significantly more helpful with

respect to the other conditions and indicating that the difference in vibration, correspondent to the rigid and soft objects, was sufficiently distinguishable by the users, as we expected. This proves the advantages that this type of feedback can provide to prosthesis users as additional information to the incidental feedback (i.e., auditory feedback).

The reduction in the response time (Figure 70 C) in the 2FB condition (2.82 s ± 1.2) is another proof of the efficiency of the implemented distinct vibratory feedback, meaning the amputees needed a short time to understand object's stiffness and enhancing the intuitiveness of the method. This parameter is significantly lower in 2FB (2.82 s ± 1.2) condition with respect to the NoFB (3.52 s ± 0.8), AFB (3.7 s ± 0.83) and 1FB (4.35 s ± 1.28) ones, suggesting that in these latter the amputees needed to put quite effort in discriminating between the objects instead.

The proprioceptive drift (Figure 70 D) shows an effect of the feedback on the embodiment, especially according to the comparison between 2FB (0.7 cm ± 1.17 towards Hannes hand) and NoFB (1.8 cm ± 1.17 opposite to Hannes hand) condition. Interestingly, the results could indicate that the presence of a source of feedback is important for summoning the embodiment process. Precisely, the highest impact on the proprioceptive drift was found with the 2FB condition, suggesting that this specific vibratory feedback was the most effective one during the embodiment process. However, a larger sample size is necessary to check potentially higher effects caused by the 2FB condition.

Three scales in the subjective questionnaire significantly highlight the benefits offered by the stimulations provided in the 2FB condition as intuitive feedback, especially for rigid objects. This indicates a possible effect of the feedback on the embodiment (see Figure 70 D). However, a larger sample is necessary to deepen our understanding of potential effects of 2FB condition on embodiment measures in dedicated experiments. Overall, and regardless of the statistical significance, the results seem pointing at the superiority of the 2FB condition over all aspects of user experience considered in this study. The qualitative observations provided by the amputees need a larger sample to extract potential user requirements.

4.3.5. Conclusion

This study presents the implementation of an online i.e., real-time, dedicated stiffness detection strategy to provide grasp oriented vibratory feedback using the Hannes prosthetic hand in a close-loop scenario. As a further progression of our previous studies, in which we exploited a virtual simulation to find the intrinsic variables correlated to the grasped object's stiffness, this work builds upon those preliminary findings and presents a refined and improved methodology, its implementation and its clinical validation. The main aim was to implement an online strategy exploiting such measurements (motor-side current, encoder position, and reference position) to detect the stiffness of real objects (without increasing the system complexity with ad-hoc force sensing) and to validate such strategy with a first preliminary study with end-users.

The classifier was tested by 18 able-bodied subjects on 6 objects and resulted to be sufficiently accurate in discriminating between void, soft and rigid grasps. The stiffness information was conveyed to the users through a single vibromotor, whose intensity changed based on the grasp type, high intensity for rigid objects and low intensity for soft objects in our proposed feedback condition (2FB condition). This feedback modality was compared to other three control conditions (NoFB, AFB, 1FB) in a user study involving 5 mono-lateral amputees. Results showed a statistically significant improvement in users' performances both in terms of F1Score and response time for the 2FB condition. Moreover, this condition was appreciated by the users, as demonstrated from the subjective questionnaires, which highlighted its intuitiveness, comfortability, and usefulness. This result was also confirmed by the analysis of the proprioceptive drift, which showed an improvement in the prosthesis embodiment. Hence, we can state our proposed feedback modality was the best among those tested.

In the future, the classifier should be tested on a higher variety of objects with different dimensions and stiffness, especially to investigate the influence of the dimension on the algorithm's performance. Reach and grasp tasks, with active usage of prosthesis, will be implemented to provide a more realistic validation of the usability and effectiveness of our solution within ADL and real scenarios. A higher number of prosthesis users will be involved to better assess the effect of the feedback on the embodiment and its appreciation.

The presented work can have a relevant impact for the application of intrinsic sensor detection of object stiffness, as it points out that this object recognition strategy and vibrotactile feedback restitution on upper limb prosthesis could be effectively used as an intuitive and effective close-loop daily living solution. Such solution could facilitate the identification of a precise and delicate grasp rather than a strength and power one during different object manipulation.

4.4. Chapter Discussion and Remarks

The three studies presented innovative approaches for improving the effectiveness and efficiency of vibrotactile feedback in conveying proprioceptive information and recognizing object stiffness on the Hannes prosthesis. Despite these methods are far from being biomimetic, the studies showed promising results in developing flexible customization options and improving the interface's robustness, making it easier to integrate into a prosthetic socket. The novel feedback approaches proved to be effective and usable in user cases with significant improvements in performance and user experience. These outcomes contribute to the development of advanced prosthetic technologies that aim to enhance the quality of life for amputees.

In summary, the following outcomes were achieved in the three studies:

1. A new method for conveying proprioceptive information using vibrotactile feedback was developed and found to be effective in conveying information with flexible customization options. The use of Gaussian interpolation for intensity and modulation of sigma were effective in generating smoothly moving sensations with fewer motors, improving the interface's robustness. The results we obtained showed minimal differences across settings with difference in the error of 5-10% demonstrating that the number of vibromotors can be safely decreased without loss of performance. In this way subjects can decide to have smoot sensations based on their preferences and the excess vibromotors can be removed to make the interface easier to integrate or encode additional information.
2. A novel approach for providing proprioceptive feedback for two variables using a single array of vibration motors was proposed and found to be similarly effective to the conventional mapping method using two independent arrays. The study also demonstrated that a single array of vibration motors could convey multiple information, making the feedback interfaces more compact and easier to integrate into a prosthetic socket. The study used an embedded platform ready for integration into a prosthesis and demonstrated an effective closed-loop control in both able-bodied and amputee participants.
3. A study explored the possibility of recognizing object stiffness without ad-hoc sensing on the Hannes prosthesis using a machine learning approach. The study found that, although the approach for object stiffness recognition is far from being biomimetic, it was effective and usable on a user case. The algorithm based on intrinsic prosthetic sensors, in combination with the 2FB condition had a very high F1Score with able-bodied subjects, and this was also confirmed in amputees. Such result was also confirmed by the embodiment process and user experience promoted by 2FB condition.

Chapter 4

General Conclusions

The primary objective of this thesis was to develop a Bidirectional Body - Machine Interface, which is crucial for restoring lost functionality after amputation. This two-way communication between the user and prosthesis plays a significant role in determining the level of acceptance, as the lack of it often leads to abandonment of the prosthetic hand, eliminating any chance of improvement in the control skills of the user [243]. The integration of a control component with a suitable feedback mechanism aims to create artificial limbs that can be used by amputees as naturally as their own, promoting the process of *embodiment*. This technology enhances intuitive control, resulting in an improved user experience and acceptance [269, 278, 519]. While an invasive approach may offer a more natural and biomimetic feedback experience, as highlighted in paragraph 1.2.3.2, it also brings with it certain limitations that hinder its suitability for long-term and widespread commercial use. Consequently, the exploration of artificial feedback through non-invasive approaches emerges as the most promising solution for the immediate translation of this technology into a commercial setting.

Through a meticulous three-year journey, the ultimate goal was achieved by systematically progressing through three primary Aims (**A**). The first aim (**A1**) involved the construction of a modular multi-DoF prosthesis, named Hannes, which could be configured to meet the unique needs and capabilities of the user (section 2.3). This accomplishment marked a significant advancement compared to commercially available alternatives, which only incorporate one additional active DoF, such as wrist rotation [359, 360].

The second aim (**A2**) focused on developing pattern recognition algorithms capable of efficiently and robustly controlling up to three DoFs (i.e., hand aperture, wrist rotation, and wrist flexion) in a simultaneous manner. The limitation of linear commercial systems, which experience performance and accuracy degradation when managing more than two DoFs [76, 78], was overcome by introducing non-linearity into the classification algorithm. The optimization of the entire system in terms of robustness, efficiency, computational load, and encumbrance ensured its whole integration into a practical device for direct clinical translation. These outcomes provided valuable insights for future research to explore the application of non-linear classification, optimization methods, and encumbrance level integration into a real prosthesis.

By combining the first two aims (**A1** and **A2**), a realistic BMI was achieved, by narrowing the gap between technology and controllability. However, the inclusion of multimodal sensory feedback was deemed essential for next-generation prostheses. The bidirectional communication provided by such a feedback approximates the user experience of a natural limb and it affects the spontaneous and effective user capabilities. To this end, the role of haptic feedback was analyzed in Aim three (**A3**), demonstrating successful methods for restoring proprioceptive information (section 4.1), its interaction with the control component (sections 4.2), and touch information (section 4.3), thereby restoring interaction of soft or

rigid objects [16]. The results provided guidelines for realizing vibrotactile feedback solutions, which could potentially reduce device bulk for direct integration into a prosthetic socket. This overcomes the limitations of commercial devices that lack of feedback solutions, thereby precluding bidirectional communication.

In summary, this research made a significant impact on the field of Bidirectional BMI by demonstrating the effectiveness of pattern recognition strategies and vibrotactile feedback in upper limb prostheses, as an intuitive and efficient close-loop daily living solution (section 4.2 and 4.3). Bidirectional BMI has several advantages, including improved usability of prostheses through improved user-system interaction (section 4.1), promoting embodiment of the device (section 2.2), and potentially reducing abandonment rates. This enhances engagement and prosthesis ownership, thereby bridging the gap between technology (section 2.3) and controllability (section 3.3 and 3.4). Overall, this solution has facilitated the use of prostheses, enabling the users to have greater control and improved interaction with the external world.

References

[1] F. Cordella *et al.*, "Literature review on needs of upper limb prosthesis users," *Frontiers in neuroscience,* vol. 10, p. 209, 2016.

[2] N. Das, N. Nagpal, and S. S. Bankura, "A review on the advancements in the field of upper limb prosthesis," *Journal of medical engineering & technology,* vol. 42, no. 7, pp. 532-545, 2018.

[3] I. Kyranou, S. Vijayakumar, and M. S. Erden, "Causes of performance degradation in non-invasive electromyographic pattern recognition in upper limb prostheses," *Frontiers in neurorobotics,* 2018.

[4] L. Trent *et al.*, "A narrative review: current upper limb prosthetic options and design," *Disability and Rehabilitation: Assistive Technology,* 2019.

[5] J. W. Sensinger and S. Dosen, "A review of sensory feedback in upper-limb prostheses from the perspective of human motor control," *Frontiers in Neuroscience,* vol. 14, 2020.

[6] A. Marinelli *et al.*, "Active upper limb prostheses: A review on current state and upcoming breakthroughs," *Progress in Biomedical Engineering,* 2022.

[7] T. J. Bates, J. R. Fergason, and S. N. Pierrie, "Technological Advances in Prosthesis Design and Rehabilitation Following Upper Extremity Limb Loss," *Current Reviews in Musculoskeletal Medicine,* vol. 13, pp. 485-493, 2020.

[8] R. Brack and E. H. Amalu, "A review of technology, materials and R&D challenges of upper limb prosthesis for improved user suitability," *Journal of Orthopaedics,* 2020.

[9] H. Shahsavari *et al.*, "Upper limb amputation; Care needs for reintegration to life: An integrative review," *International journal of orthopaedic and trauma nursing,* vol. 38, p. 100773, 2020.

[10] J. Qu, K. Ma, and B. Hommel, "Cognitive load dissociates explicit and implicit measures of body ownership and agency," *Psychonomic Bulletin & Review,* pp. 1-12, 2021.

[11] M. Laffranchi *et al.*, "The Hannes hand prosthesis replicates the key biological properties of the human hand," *Science Robotics,* 2020.

[12] D. Di Domenico *et al.*, "Hannes Prosthesis Control Based on Regression Machine Learning Algorithms," presented at the 2021 IEEE/RSJ International Conference on Intelligent Robots and Systems (IROS 2021), 2021.

[13] A. Marinelli *et al.*, "Performance Evaluation of Pattern Recognition Algorithms for Upper Limb Prosthetic Applications," in *8th IEEE RAS/EMBS International Conference for Biomedical Robotics and Biomechatronics (BioRob)*, 2020: IEEE.

[14] A. Marinelli *et al.*, "Improved Pattern Recognition Control of Hannes," presented at the IRIM, 2021.

[15] A. Marinelli *et al.*, "Miniature EMG Sensors for Prosthetic Applications," 2021.

[16] G. Bruni *et al.*, "Object stiffness recognition and vibratory feedback without ad-hoc sensing on the Hannes prosthesis: A machine learning approach," (in English), *Frontiers in Neuroscience,* Original Research vol. 17, 2023-February-16 2023, doi: 10.3389/fnins.2023.1078846.

[17] G. Caserta *et al.*, "Benefits of the Cybathlon 2020 experience for a prosthetic hand user: a case study on the Hannes system," *Journal of NeuroEngineering and Rehabilitation,* vol. 19, no. 1, pp. 1-15, 2022.

[18] G. Barresi *et al.*, "Exploring the Embodiment of a Virtual Hand in a Spatially Augmented Respiratory Biofeedback Setting," (in English), *Frontiers in Neurorobotics,* Original Research vol. 15, no. 114, 2021-August-27 2021, doi: 10.3389/fnbot.2021.683653.

[19] S. Salminger *et al.*, "Current rates of prosthetic usage in upper-limb amputees–have innovations had an impact on device acceptance?," *Disability and Rehabilitation,* pp. 1-12, 2020.

[20] A. O. P. A. AOPA. (2016) Where Science Meets Art. *American Orthotic & Prosthetic Association (AOPA)*. Available: https://issuu.com/americanoandp/docs/april_2016_almanac

[21] J. Ribeiro *et al.*, "Analysis of man-machine interfaces in upper-limb prosthesis: A review," *Robotics,* vol. 8, no. 1, p. 16, 2019.

[22] Ottobock. "MyoHand VariPlus Speed." https://shop.ottobock.us/Prosthetics/Upper-Limb-Prosthetics/Myo-Hands-and-Components/Myo-Terminal-Devices/MyoHand-VariPlus-Speed/p/8E38~59 (accessed.

[23] Fillauer. "Motion Control Hand." https://fillauer.com/products/motion-control-hand/ (accessed.
[24] Ottobock. "Michelangelo hand." https://www.ottobock.it/soluzioni-protesiche/arto-superiore/panoramica-delle-soluzioni/sistema-axon-bus-con-mano-michelangelo/ (accessed.
[25] Ottobock. "Bebionic hand." https://www.ottobock.it/protesizzazioni/prodotti-dalla-a-alla-z/mano-bebionic/ (accessed.
[26] Ossur. "i-Limb® Ultra titanium." https://www.ossur.com/it-it/protesi/arto-superiore/i-limb-ultra-titanium (accessed.
[27] V. Systems. "Vincent hand." https://www.vincentsystems.de/ (accessed.
[28] Taska. "Taska Hand Gen 2." https://www.taskaprosthetics.com/it/prodotti/taska-hand/ (accessed.
[29] **BrainRobotics**. "BrainRobotics Hand." https://brainrobotics.com/brainrobotics-hand/ (accessed.
[30] Psyonic. "Ability Hand." https://www.psyonic.io/ability-hand (accessed.
[31] COVVI. "COVVI hand." https://www.covvi.com/ (accessed.
[32] D. A. Bennett, S. A. Dalley, D. Truex, and M. Goldfarb, "A multigrasp hand prosthesis for providing precision and conformal grasps," *IEEE/ASME Transactions on Mechatronics,* vol. 20, no. 4, pp. 1697-1704, 2014.
[33] M. Controzzi, F. Clemente, D. Barone, A. Ghionzoli, and C. Cipriani, "The SSSA-MyHand: a dexterous lightweight myoelectric hand prosthesis," *IEEE Transactions on Neural Systems and Rehabilitation Engineering,* vol. 25, no. 5, pp. 459-468, 2016.
[34] S. B. Godfrey *et al.*, "The SoftHand Pro: Functional evaluation of a novel, flexible, and robust myoelectric prosthesis," *PloS one,* vol. 13, no. 10, p. e0205653, 2018.
[35] P. Weiner, J. Starke, F. Hundhausen, J. Beil, and T. Asfour, "The KIT prosthetic hand: design and control," in *2018 IEEE/RSJ International Conference on Intelligent Robots and Systems (IROS)*, 2018: IEEE, pp. 3328-3334.
[36] R. Meattini, L. Biagiotti, G. Palli, D. De Gregorio, and C. Melchiorri, "A Control Architecture for Grasp Strength Regulation in Myocontrolled Robotic Hands Using Vibrotactile Feedback: Preliminary Results," in *2019 IEEE 16th International Conference on Rehabilitation Robotics (ICORR)*, 2019: IEEE, pp. 1272-1277.
[37] S. R. Company. "Shadow Robot." https://www.shadowrobot.com/ (accessed.
[38] R. Harte *et al.*, "A human-centered design methodology to enhance the usability, human factors, and user experience of connected health systems: a three-phase methodology," *JMIR human factors,* vol. 4, no. 1, p. e5443, 2017.
[39] M. A. Wilke, C. Niethammer, B. Meyer, D. Farina, and S. Dosen, "Psychometric characterization of incidental feedback sources during grasping with a hand prosthesis," *Journal of neuroengineering and rehabilitation,* vol. 16, no. 1, pp. 1-13, 2019.
[40] M. A. Gonzalez, C. Lee, J. Kang, R. B. Gillespie, and D. H. Gates, "Getting a Grip on the Impact of Incidental Feedback From Body-Powered and Myoelectric Prostheses," *IEEE Transactions on Neural Systems and Rehabilitation Engineering,* vol. 29, pp. 1905-1912, 2021.
[41] R. Merletti, M. Aventaggiato, A. Botter, A. Holobar, H. Marateb, and T. M. Vieira, "Advances in surface EMG: recent progress in detection and processing techniques," *Critical Reviews™ in Biomedical Engineering,* vol. 38, no. 4, 2010.
[42] C. Cipriani, J. L. Segil, J. A. Birdwell, and R. F. ff Weir, "Dexterous control of a prosthetic hand using fine-wire intramuscular electrodes in targeted extrinsic muscles," *IEEE Transactions on Neural Systems and Rehabilitation Engineering,* vol. 22, no. 4, pp. 828-836, 2014.
[43] M. Ortiz-Catalan, E. Mastinu, P. Sassu, O. Aszmann, and R. Brånemark, "Self-contained neuromusculoskeletal arm prostheses," *New England Journal of Medicine,* vol. 382, no. 18, pp. 1732-1738, 2020.
[44] Z. G. Xiao and C. Menon, "A review of force myography research and development," *Sensors,* vol. 19, no. 20, p. 4557, 2019.
[45] S. Wilson and R. Vaidyanathan, "Upper-limb prosthetic control using wearable multichannel mechanomyography," in *2017 International Conference on Rehabilitation Robotics (ICORR)*, 2017: IEEE, pp. 1293-1298.

[46] W. Guo, X. Sheng, H. Liu, and X. Zhu, "Mechanomyography assisted myoeletric sensing for upper-extremity prostheses: A hybrid approach," *IEEE Sensors Journal,* vol. 17, no. 10, pp. 3100-3108, 2017.
[47] C. S. M. Castillo, S. Wilson, R. Vaidyanathan, and S. F. Atashzar, "Wearable MMG-Plus-One Armband: Evaluation of Normal Force on Mechanomyography (MMG) to Enhance Human-Machine Interfacing," *IEEE Transactions on Neural Systems and Rehabilitation Engineering,* vol. 29, pp. 196-205, 2020.
[48] A. S. Dhawan *et al.*, "Proprioceptive Sonomyographic Control: A novel method for intuitive and proportional control of multiple degrees-of-freedom for individuals with upper extremity limb loss," *Scientific reports,* vol. 9, no. 1, pp. 1-15, 2019.
[49] M. Paleari, R. Luciani, and P. Ariano, "Towards NIRS-based hand movement recognition," in *2017 International Conference on Rehabilitation Robotics (ICORR)*, 2017: IEEE, pp. 1506-1511.
[50] Y. Zhang, R. Xiao, and C. Harrison, "Advancing hand gesture recognition with high resolution electrical impedance tomography," in *Proceedings of the 29th Annual Symposium on User Interface Software and Technology*, 2016, pp. 843-850.
[51] Y. Wu, D. Jiang, X. Liu, R. Bayford, and A. Demosthenous, "A human–machine interface using electrical impedance tomography for hand prosthesis control," *IEEE transactions on biomedical circuits and systems,* vol. 12, no. 6, pp. 1322-1333, 2018.
[52] J. Cheng, O. Amft, G. Bahle, and P. Lukowicz, "Designing sensitive wearable capacitive sensors for activity recognition," *IEEE Sensors Journal,* vol. 13, no. 10, pp. 3935-3947, 2013.
[53] H. Truong *et al.*, "Capband: Battery-free successive capacitance sensing wristband for hand gesture recognition," in *Proceedings of the 16th ACM Conference on Embedded Networked Sensor Systems*, 2018, pp. 54-67.
[54] S. Zuo, H. Heidari, D. Farina, and K. Nazarpour, "Miniaturized magnetic sensors for implantable magnetomyography," *Advanced Materials Technologies,* vol. 5, no. 6, p. 2000185, 2020.
[55] A. T. Nguyen *et al.*, "A bioelectric neural interface towards intuitive prosthetic control for amputees," *Journal of neural engineering,* vol. 17, no. 6, p. 066001, 2020.
[56] L. R. Hochberg *et al.*, "Neuronal ensemble control of prosthetic devices by a human with tetraplegia," *Nature,* vol. 442, no. 7099, pp. 164-171, 2006.
[57] L. R. Hochberg *et al.*, "Reach and grasp by people with tetraplegia using a neurally controlled robotic arm," *Nature,* vol. 485, no. 7398, pp. 372-375, 2012.
[58] J. L. Collinger *et al.*, "High-performance neuroprosthetic control by an individual with tetraplegia," *The Lancet,* vol. 381, no. 9866, pp. 557-564, 2013.
[59] B. Wodlinger, J. Downey, E. Tyler-Kabara, A. Schwartz, M. Boninger, and J. Collinger, "Ten-dimensional anthropomorphic arm control in a human brain− machine interface: difficulties, solutions, and limitations," *Journal of neural engineering,* vol. 12, no. 1, p. 016011, 2014.
[60] W. Wang *et al.*, "An electrocorticographic brain interface in an individual with tetraplegia," *PloS one,* vol. 8, no. 2, p. e55344, 2013.
[61] M. S. Fifer *et al.*, "Simultaneous neural control of simple reaching and grasping with the modular prosthetic limb using intracranial EEG," *IEEE transactions on neural systems and rehabilitation engineering,* vol. 22, no. 3, pp. 695-705, 2013.
[62] M. G. Bleichner, Z. V. Freudenburg, J. M. Jansma, E. J. Aarnoutse, M. J. Vansteensel, and N. F. Ramsey, "Give me a sign: decoding four complex hand gestures based on high-density ECoG," *Brain Structure and Function,* vol. 221, no. 1, pp. 203-216, 2016.
[63] G. Hotson *et al.*, "Individual finger control of a modular prosthetic limb using high-density electrocorticography in a human subject," *Journal of neural engineering,* vol. 13, no. 2, p. 026017, 2016.
[64] D. J. McFarland, W. A. Sarnacki, and J. R. Wolpaw, "Electroencephalographic (EEG) control of three-dimensional movement," *Journal of neural engineering,* vol. 7, no. 3, p. 036007, 2010.
[65] J. Yang *et al.*, "Channel selection and classification of electroencephalogram signals: an artificial neural network and genetic algorithm-based approach," *Artificial intelligence in medicine,* vol. 55, no. 2, pp. 117-126, 2012.

[66] B. J. Edelman *et al.*, "Noninvasive neuroimaging enhances continuous neural tracking for robotic device control," *Science robotics,* vol. 4, no. 31, 2019.
[67] J. Fuentes-Gonzalez, A. Infante-Alarcón, V. Asanza, and F. R. Loayza, "A 3d-printed eeg based prosthetic arm," in *2020 IEEE International Conference on E-health Networking, Application & Services (HEALTHCOM)*, 2021: IEEE, pp. 1-5.
[68] U. Syed, Z. Kausar, and N. Yousaf, "Control of a Prosthetic Arm using fNIRS, A Neural-Machine Interface," 2020.
[69] H. Schmidl, "The inail myoelectric b/e prosthesis," *Orthotics and Prosthetics,* vol. 19, no. 4, pp. 298-303, 1965.
[70] R. Merletti and D. Farina, "Surface electromyography for man-machine interfacing in rehabilitation technologies," 2016.
[71] B. Hudgins, P. Parker, and R. N. Scott, "A new strategy for multifunction myoelectric control," *IEEE transactions on biomedical engineering,* vol. 40, no. 1, pp. 82-94, 1993.
[72] M. Z. Jamal, "Signal acquisition using surface EMG and circuit design considerations for robotic prosthesis," *Computational Intelligence in Electromyography Analysis-A Perspective on Current Applications and Future Challenges,* vol. 18, pp. 427-448, 2012.
[73] G. Drost, D. F. Stegeman, B. G. van Engelen, and M. J. Zwarts, "Clinical applications of high-density surface EMG: a systematic review," *Journal of Electromyography and Kinesiology,* vol. 16, no. 6, pp. 586-602, 2006.
[74] M. Zheng, M. S. Crouch, and M. S. Eggleston, "Surface Electromyography as a Natural Human-Machine Interface: A Review," *arXiv preprint arXiv:2101.04658,* 2021.
[75] R. Merletti and S. Muceli, "Tutorial. Surface EMG detection in space and time: Best practices," *Journal of Electromyography and Kinesiology,* vol. 49, p. 102363, 2019.
[76] COAPT, "COAPT - Complete control handbook," 2017.
[77] A. Dellacasa Bellingegni *et al.*, "NLR, MLP, SVM, and LDA: a comparative analysis on EMG data from people with trans-radial amputation," *J Neuroeng Rehabil,* Aug 14 2017. [Online]. Available: https://www.ncbi.nlm.nih.gov/pubmed/28807038.
[78] Ottobock. "Myo Plus pattern recognition." https://www.ottobock.it/protesizzazioni/arto-superiore/panoramica-delle-soluzioni/myo-plus-pattern-recognition/ (accessed.
[79] J. M. Winters, "Hill-based muscle models: a systems engineering perspective," in *Multiple muscle systems*: Springer, 1990, pp. 69-93.
[80] M. Sartori, G. Durandau, S. Došen, and D. Farina, "Robust simultaneous myoelectric control of multiple degrees of freedom in wrist-hand prostheses by real-time neuromusculoskeletal modeling," *Journal of neural engineering,* vol. 15, no. 6, p. 066026, 2018.
[81] J. Chen, S. Bi, G. Zhang, and G. Cao, "High-density surface EMG-based gesture recognition using a 3D convolutional neural network," *Sensors,* vol. 20, no. 4, p. 1201, 2020.
[82] C. J. De Luca, "The use of surface electromyography in biomechanics," *Journal of applied biomechanics,* vol. 13, no. 2, pp. 135-163, 1997.
[83] E. D. Adrian and D. W. Bronk, "The discharge of impulses in motor nerve fibres: Part II. The frequency of discharge in reflex and voluntary contractions," *The Journal of physiology,* vol. 67, no. 2, pp. 9-151, 1929.
[84] R. Merletti and D. Farina, "Analysis of intramuscular electromyogram signals," *Philosophical Transactions of the Royal Society A: Mathematical, Physical and Engineering Sciences,* vol. 367, no. 1887, pp. 357-368, 2009.
[85] D. I. Rubin, "Needle electromyography: Basic concepts," *Handbook of clinical neurology,* vol. 160, pp. 243-256, 2019.
[86] L. J. Hargrove, K. Englehart, and B. Hudgins, "A comparison of surface and intramuscular myoelectric signal classification," *IEEE transactions on biomedical engineering,* vol. 54, no. 5, pp. 847-853, 2007.
[87] A. Cloutier and J. Yang, "Control of hand prostheses: A literature review," in *International Design Engineering Technical Conferences and Computers and Information in Engineering Conference*, 2013, vol. 55935: American Society of Mechanical Engineers, p. V06AT07A016.
[88] S. Raspopovic, G. Valle, and F. M. Petrini, "Sensory feedback for limb prostheses in amputees," *Nature Materials,* vol. 20, no. 7, pp. 925-939, 2021.

[89] R. F. Weir, P. R. Troyk, G. A. DeMichele, D. A. Kerns, J. F. Schorsch, and H. Maas, "Implantable myoelectric sensors (IMESs) for intramuscular electromyogram recording," *IEEE Transactions on Biomedical Engineering,* vol. 56, no. 1, pp. 159-171, 2008.
[90] L. H. Smith, T. A. Kuiken, and L. J. Hargrove, "Real-time simultaneous and proportional myoelectric control using intramuscular EMG," *Journal of neural engineering,* vol. 11, no. 6, p. 066013, 2014.
[91] T. A. Kuiken *et al.*, "Targeted muscle reinnervation for real-time myoelectric control of multifunction artificial arms," *Jama,* vol. 301, no. 6, pp. 619-628, 2009.
[92] T. A. Kuiken, A. K. Barlow, L. Hargrove, and G. A. Dumanian, "Targeted muscle reinnervation for the upper and lower extremity," *Techniques in orthopaedics (Rockville, Md.),* vol. 32, no. 2, p. 109, 2017.
[93] J. E. Cheesborough, L. H. Smith, T. A. Kuiken, and G. A. Dumanian, "Targeted muscle reinnervation and advanced prosthetic arms," in *Seminars in plastic surgery*, 2015, vol. 29, no. 01: Thieme Medical Publishers, pp. 062-072.
[94] F. Mereu, F. Leone, C. Gentile, F. Cordella, E. Gruppioni, and L. Zollo, "Control Strategies and Performance Assessment of Upper-Limb TMR Prostheses: A Review," *Sensors,* vol. 21, no. 6, p. 1953, 2021.
[95] P. P. Vu, C. A. Chestek, S. R. Nason, T. A. Kung, S. W. Kemp, and P. S. Cederna, "The future of upper extremity rehabilitation robotics: research and practice," *Muscle & nerve,* vol. 61, no. 6, pp. 708-718, 2020.
[96] M. G. Urbanchek, Z. Baghmanli, J. D. Moon, K. B. Sugg, N. B. Langhals, and P. S. Cederna, "Quantification of regenerative peripheral nerve interface signal transmission," *Plastic and reconstructive surgery,* vol. 130, no. 5S-1, pp. 55-56, 2012.
[97] P. P. Vu *et al.*, "A regenerative peripheral nerve interface allows real-time control of an artificial hand in upper limb amputees," *Science translational medicine,* vol. 12, no. 533, 2020.
[98] P. Tropea, A. Mazzoni, S. Micera, and M. Corbo, "Giuliano Vanghetti and the innovation of “cineplastic operations”," *Neurology,* vol. 89, no. 15, pp. 1627-1632, 2017.
[99] C. W. Heckathorne and D. S. Childress, "Cineplasty as a control input for externally powered prosthetic components," *Journal of Rehabilitation Research & Development,* vol. 38, no. 4, 2001.
[100] F. Clemente, M. D'Alonzo, M. Controzzi, B. B. Edin, and C. Cipriani, "Non-invasive, temporally discrete feedback of object contact and release improves grasp control of closed-loop myoelectric transradial prostheses," *IEEE Transactions on Neural Systems and Rehabilitation Engineering,* vol. 24, no. 12, pp. 1314-1322, 2015.
[101] A. Schmitz, M. Maggiali, M. Randazzo, L. Natale, and G. Metta, "A prototype fingertip with high spatial resolution pressure sensing for the robot iCub," in *Humanoids 2008-8th IEEE-RAS International Conference on Humanoid Robots*, 2008: IEEE, pp. 423-428.
[102] B. C. Tee, C. Wang, R. Allen, and Z. Bao, "An electrically and mechanically self-healing composite with pressure-and flexion-sensitive properties for electronic skin applications," *Nature nanotechnology,* vol. 7, no. 12, pp. 825-832, 2012.
[103] C. Lucarotti, C. M. Oddo, N. Vitiello, and M. C. Carrozza, "Synthetic and bio-artificial tactile sensing: A review," *Sensors,* vol. 13, no. 2, pp. 1435-1466, 2013.
[104] M. L. Hammock, A. Chortos, B. C. K. Tee, J. B. H. Tok, and Z. Bao, "25th anniversary article: the evolution of electronic skin (e-skin): a brief history, design considerations, and recent progress," *Advanced materials,* vol. 25, no. 42, pp. 5997-6038, 2013.
[105] T. Taunyazov *et al.*, "Extended Tactile Perception: Vibration Sensing through Tools and Grasped Objects," in *2021 IEEE/RSJ International Conference on Intelligent Robots and Systems (IROS)*, 2021: IEEE, pp. 1755-1762.
[106] M. M. Iskarous and N. V. Thakor, "E-skins: Biomimetic sensing and encoding for upper limb prostheses," *Proceedings of the IEEE,* vol. 107, no. 10, pp. 2052-2064, 2019.
[107] D. Dimante, I. Logina, M. Sinisi, and A. Krūmiņa, "Sensory Feedback in Upper Limb Prostheses," in *Proceedings of the Latvian Academy of Sciences. Section B. Natural, Exact, and Applied Sciences.*, 2020, vol. 74, no. 5, pp. 308-317.
[108] A. L. Ciancio *et al.*, "Control of prosthetic hands via the peripheral nervous system," *Frontiers in neuroscience,* vol. 10, p. 116, 2016.

[109] P. Maiolino, M. Maggiali, G. Cannata, G. Metta, and L. Natale, "A flexible and robust large scale capacitive tactile system for robots," *IEEE Sensors Journal,* vol. 13, no. 10, pp. 3910-3917, 2013.
[110] N. Jamali, M. Maggiali, F. Giovannini, G. Metta, and L. Natale, "A new design of a fingertip for the iCub hand," in *2015 IEEE/RSJ International Conference on Intelligent Robots and Systems (IROS)*, 2015: IEEE, pp. 2705-2710.
[111] L. Beccai *et al.*, "Design and fabrication of a hybrid silicon three-axial force sensor for biomechanical applications," *Sensors and Actuators A: Physical,* vol. 120, no. 2, pp. 370-382, 2005.
[112] N. A. Zainuddin, N. F. Anuar, A. L. Mansur, N. I. M. Fauzi, W. F. Hanim, and S. H. Herman, "Resistive-based sensor system for prosthetic fingers application," *Procedia Computer Science,* vol. 76, pp. 323-329, 2015.
[113] M. Alameh *et al.*, "Live demonstration: System based on electronic skin and cutaneous electrostimulation for sensory feedback in prosthetics," in *2018 IEEE Biomedical Circuits and Systems Conference (BioCAS)*, 2018: IEEE, pp. 1-1.
[114] R. Ahmadi, M. Packirisamy, J. Dargahi, and R. Cecere, "Discretely loaded beam-type optical fiber tactile sensor for tissue manipulation and palpation in minimally invasive robotic surgery," *IEEE Sensors Journal,* vol. 12, no. 1, pp. 22-32, 2011.
[115] C. H. Lin, T. W. Erickson, J. A. Fishel, N. Wettels, and G. E. Loeb, "Signal processing and fabrication of a biomimetic tactile sensor array with thermal, force and microvibration modalities," in *2009 IEEE International Conference on Robotics and Biomimetics (ROBIO)*, 2009: IEEE, pp. 129-134.
[116] L. Massari, C. M. Oddo, E. Sinibaldi, R. Detry, J. Bowkett, and K. C. Carpenter, "Tactile sensing and control of robotic manipulator integrating fiber Bragg grating strain-sensor," *Frontiers in neurorobotics,* vol. 13, p. 8, 2019.
[117] A. Mazzoni *et al.*, "Morphological neural computation restores discrimination of naturalistic textures in trans-radial amputees," *Scientific reports,* vol. 10, no. 1, pp. 1-14, 2020.
[118] H. Gunasekaran, G. Spigler, A. Mazzoni, E. Cataldo, and C. M. Oddo, "Convergence of regular spiking and intrinsically bursting Izhikevich neuron models as a function of discretization time with Euler method," *Neurocomputing,* vol. 350, pp. 237-247, 2019.
[119] A. Alfadhel and J. Kosel, "Magnetic nanocomposite cilia tactile sensor," *Advanced Materials,* vol. 27, no. 47, pp. 7888-7892, 2015.
[120] L. E. Osborn *et al.*, "Prosthesis with neuromorphic multilayered e-dermis perceives touch and pain," *Science robotics,* vol. 3, no. 19, 2018.
[121] S. Robot. "Shadow Dexterous Hand Series." https://www.shadowrobot.com/dexterous-hand-series/ (accessed.
[122] J. A. Fishel and G. E. Loeb, "Sensing tactile microvibrations with the BioTac—Comparison with human sensitivity," in *2012 4th IEEE RAS & EMBS international conference on biomedical robotics and biomechatronics (BioRob)*, 2012: IEEE, pp. 1122-1127.
[123] Ottobock. "SensorHand Speed." https://shop.ottobock.us/Prosthetics/Upper-Limb-Prosthetics/Myo-Hands-and-Components/Myo-Terminal-Devices/SensorHand-Speed/p/8E39~58 (accessed.
[124] S. Raspopovic *et al.*, "Restoring natural sensory feedback in real-time bidirectional hand prostheses," *Science translational medicine,* vol. 6, no. 222, pp. 222ra19-222ra19, 2014.
[125] M. Alameh, Y. Abbass, A. Ibrahim, and M. Valle, "Smart tactile sensing systems based on embedded CNN implementations," *Micromachines,* vol. 11, no. 1, p. 103, 2020.
[126] C. Antfolk, M. D'alonzo, B. Rosén, G. Lundborg, F. Sebelius, and C. Cipriani, "Sensory feedback in upper limb prosthetics," *Expert review of medical devices,* vol. 10, no. 1, pp. 45-54, 2013.
[127] P. Svensson, U. Wijk, A. Björkman, and C. Antfolk, "A review of invasive and non-invasive sensory feedback in upper limb prostheses," *Expert review of medical devices,* vol. 14, no. 6, pp. 439-447, 2017.
[128] W. T. Navaraj, H. Nassar, and R. Dahiya, "Prosthetic hand with biomimetic tactile sensing and force feedback," in *2019 IEEE International Symposium on Circuits and Systems (ISCAS)*, 2019: IEEE, pp. 1-4.

[129] I. Cuberovic, A. Gill, L. J. Resnik, D. J. Tyler, and E. L. Graczyk, "Learning of artificial sensation through long-term home use of a sensory-enabled prosthesis," *Frontiers in neuroscience,* vol. 13, p. 853, 2019.
[130] K. Bark *et al.*, "Effects of vibrotactile feedback on human learning of arm motions," *IEEE Transactions on Neural Systems and Rehabilitation Engineering,* vol. 23, no. 1, pp. 51-63, 2014.
[131] M. Markovic, M. Varel, M. A. Schweisfurth, A. F. Schilling, and S. Dosen, "Closed-loop multi-amplitude control for robust and dexterous performance of myoelectric prosthesis," *IEEE Transactions on Neural Systems and Rehabilitation Engineering,* vol. 28, no. 2, pp. 498-507, 2019.
[132] C. Antfolk *et al.*, "Transfer of tactile input from an artificial hand to the forearm: experiments in amputees and able-bodied volunteers," *Disability and Rehabilitation: Assistive Technology,* vol. 8, no. 3, pp. 249-254, 2013.
[133] J. Tchimino, M. Markovic, J. L. Dideriksen, and S. Dosen, "The effect of calibration parameters on the control of a myoelectric hand prosthesis using EMG feedback," *Journal of Neural Engineering,* vol. 18, no. 4, p. 046091, 2021.
[134] N. Jorgovanovic, S. Dosen, D. J. Djozic, G. Krajoski, and D. Farina, "Virtual grasping: closed-loop force control using electrotactile feedback," *Computational and mathematical methods in medicine,* vol. 2014, 2014.
[135] H. Xu, D. Zhang, J. C. Huegel, W. Xu, and X. Zhu, "Effects of different tactile feedback on myoelectric closed-loop control for grasping based on electrotactile stimulation," *IEEE Transactions on Neural Systems and Rehabilitation Engineering,* vol. 24, no. 8, pp. 827-836, 2015.
[136] M. A. Garenfeld, C. K. Mortensen, M. Strbac, J. L. Dideriksen, and S. Dosen, "Amplitude versus spatially modulated electrotactile feedback for myoelectric control of two degrees of freedom," *Journal of Neural Engineering,* vol. 17, no. 4, p. 046034, 2020.
[137] A. Gigli, D. Brusamento, R. Meattini, C. Melchiorri, and C. Castellini, "Feedback-aided data acquisition improves myoelectric control of a prosthetic hand," *Journal of Neural Engineering,* vol. 17, no. 5, p. 056047, 2020.
[138] F. Clemente, S. Dosen, L. Lonini, M. Markovic, D. Farina, and C. Cipriani, "Humans can integrate augmented reality feedback in their sensorimotor control of a robotic hand," *IEEE Transactions on Human-Machine Systems,* vol. 47, no. 4, pp. 583-589, 2016.
[139] M. Markovic, H. Karnal, B. Graimann, D. Farina, and S. Dosen, "GLIMPSE: Google Glass interface for sensory feedback in myoelectric hand prostheses," *Journal of neural engineering,* vol. 14, no. 3, p. 036007, 2017.
[140] A. Sharma *et al.*, "A mixed-reality training environment for upper limb prosthesis control," in *2018 IEEE Biomedical Circuits and Systems Conference (BioCAS)*, 2018: IEEE, pp. 1-4.
[141] S. Hazubski, H. Hoppe, and A. Otte, "Hand prosthetic controlled via augmented reality," 2020.
[142] T. Sun, Q. Hu, P. Gulati, and S. F. Atashzar, "Temporal dilation of deep LSTM for agile decoding of sEMG: Application in prediction of Upper-Limb motor intention in NeuroRobotics," *IEEE Robotics and Automation Letters,* vol. 6, no. 4, pp. 6212-6219, 2021.
[143] G. Lundborg, B. Rosén, and S. Lindberg, "Hearing as substitution for sensation: a new principle for artificial sensibility," *The Journal of hand surgery,* vol. 24, no. 2, pp. 219-224, 1999.
[144] J. Gonzalez, H. Soma, M. Sekine, and W. Yu, "Psycho-physiological assessment of a prosthetic hand sensory feedback system based on an auditory display: a preliminary study," *Journal of neuroengineering and rehabilitation,* vol. 9, no. 1, pp. 1-14, 2012.
[145] M. Markovic, M. A. Schweisfurth, L. F. Engels, D. Farina, and S. Dosen, "Myocontrol is closed-loop control: incidental feedback is sufficient for scaling the prosthesis force in routine grasping," *Journal of neuroengineering and rehabilitation,* vol. 15, no. 1, pp. 1-11, 2018.
[146] P. Milgram and F. Kishino, "A taxonomy of mixed reality visual displays," *IEICE TRANSACTIONS on Information and Systems,* vol. 77, no. 12, pp. 1321-1329, 1994.
[147] M. Speicher, B. D. Hall, and M. Nebeling, "What is mixed reality?," in *Proceedings of the 2019 CHI Conference on Human Factors in Computing Systems*, 2019, pp. 1-15.
[148] F. Anderson and W. F. Bischof, "Augmented reality improves myoelectric prosthesis training," *International Journal on Disability and Human Development,* vol. 13, no. 3, pp. 349-354, 2014.

[149] E. Lamounier, K. Lopes, A. Cardoso, A. Andrade, and A. Soares, "On the use of virtual and augmented reality for upper limb prostheses training and simulation," in *2010 Annual International Conference of the IEEE Engineering in Medicine and Biology*, 2010: IEEE, pp. 2451-2454.
[150] Y. Sun *et al.*, "A Comparison between Virtual Reality and Augmented Reality on Upper-limb Prosthesis Control," in *2021 International Symposium on Electrical, Electronics and Information Engineering*, 2021, pp. 521-528.
[151] C. Nissler *et al.*, "VITA—An everyday virtual reality setup for prosthetics and upper-limb rehabilitation," *Journal of neural engineering,* vol. 16, no. 2, p. 026039, 2019.
[152] A. Cutrone and S. Micera, "Implantable neural interfaces and wearable tactile systems for bidirectional neuroprosthetics systems," *Advanced healthcare materials,* vol. 8, no. 24, p. 1801345, 2019.
[153] G. Shannon, "A myoelectrically-controlled prosthesis with sensory feedback," *Medical and Biological Engineering and Computing,* vol. 17, no. 1, pp. 73-80, 1979.
[154] A. Benvenuto *et al.*, "Intrafascicular thin-film multichannel electrodes for sensory feedback: Evidences on a human amputee," in *2010 Annual International Conference of the IEEE Engineering in Medicine and Biology*, 2010: IEEE, pp. 1800-1803.
[155] C. M. Oddo *et al.*, "Intraneural stimulation elicits discrimination of textural features by artificial fingertip in intact and amputee humans," *elife,* vol. 5, p. e09148, 2016.
[156] G. Valle *et al.*, "Biomimetic intraneural sensory feedback enhances sensation naturalness, tactile sensitivity, and manual dexterity in a bidirectional prosthesis," *Neuron,* vol. 100, no. 1, pp. 37-45. e7, 2018.
[157] D. W. Tan, M. A. Schiefer, M. W. Keith, J. R. Anderson, J. Tyler, and D. J. Tyler, "A neural interface provides long-term stable natural touch perception," *Science translational medicine,* vol. 6, no. 257, pp. 257ra138-257ra138, 2014.
[158] J. A. George *et al.*, "Biomimetic sensory feedback through peripheral nerve stimulation improves dexterous use of a bionic hand," *Science Robotics,* vol. 4, no. 32, 2019.
[159] M. Liu, A. Batista, S. Bensmaia, and D. J. Weber, "Information about contact force and surface texture is mixed in the firing rates of cutaneous afferent neurons," *Journal of Neurophysiology,* vol. 125, no. 2, pp. 496-508, 2021.
[160] P. D. Marasco, K. Kim, J. E. Colgate, M. A. Peshkin, and T. A. Kuiken, "Robotic touch shifts perception of embodiment to a prosthesis in targeted reinnervation amputees," *Brain,* vol. 134, no. 3, pp. 747-758, 2011.
[161] P. D. Marasco *et al.*, "Neurorobotic fusion of prosthetic touch, kinesthesia, and movement in bionic upper limbs promotes intrinsic brain behaviors," *Science Robotics,* vol. 6, no. 58, p. eabf3368, 2021.
[162] S. L. Carey, D. J. Lura, and M. J. Highsmith, "Differences in myoelectric and body-powered upper-limb prostheses: Systematic literature review," *Journal of Rehabilitation Research & Development,* vol. 52, no. 3, 2015.
[163] S. Millstein, H. Heger, and G. Hunter, "Prosthetic use in adult upper limb amputees: a comparison of the body powered and electrically powered prostheses," *Prosthetics and orthotics international,* vol. 10, no. 1, pp. 27-34, 1986.
[164] R. Scott and P. Parker, "Myoelectric prostheses: state of the art," *Journal of medical engineering & technology,* vol. 12, no. 4, pp. 143-151, 1988.
[165] J. M. Hahne, M. A. Schweisfurth, M. Koppe, and D. Farina, "Simultaneous control of multiple functions of bionic hand prostheses: Performance and robustness in end users," *Science Robotics,* vol. 3, no. 19, 2018.
[166] B. Siciliano, L. Sciavicco, L. Villani, and G. Oriolo, *Robotics: modelling, planning and control*. Springer Science & Business Media, 2010.
[167] B. Siciliano, O. Khatib, and T. Kröger, *Springer handbook of robotics*. Springer, 2008.
[168] P. I. Corke and O. Khatib, *Robotics, vision and control: fundamental algorithms in MATLAB*. Springer, 2011.
[169] L. Resnik, H. H. Huang, A. Winslow, D. L. Crouch, F. Zhang, and N. Wolk, "Evaluation of EMG pattern recognition for upper limb prosthesis control: a case study in comparison with

direct myoelectric control," *Journal of neuroengineering and rehabilitation,* vol. 15, no. 1, pp. 1-13, 2018.
[170] I. Moon, M. Lee, J. Chu, and M. Mun, "Wearable EMG-based HCI for electric-powered wheelchair users with motor disabilities," in *Proceedings of the 2005 IEEE International Conference on Robotics and Automation*, 2005: IEEE, pp. 2649-2654.
[171] A. d'Avella and E. Bizzi, "Shared and specific muscle synergies in natural motor behaviors," *Proceedings of the national academy of sciences,* vol. 102, no. 8, pp. 3076-3081, 2005.
[172] N. Jiang, H. Rehbaum, I. Vujaklija, B. Graimann, and D. Farina, "Intuitive, online, simultaneous, and proportional myoelectric control over two degrees-of-freedom in upper limb amputees," *IEEE transactions on neural systems and rehabilitation engineering,* vol. 22, no. 3, pp. 501-510, 2013.
[173] G. Liu, L. Wang, and J. Wang, "A novel energy-motion model for continuous sEMG decoding: from muscle energy to motor pattern," *Journal of Neural Engineering,* vol. 18, no. 1, p. 016019, 2021.
[174] A. Furui *et al.*, "A myoelectric prosthetic hand with muscle synergy–based motion determination and impedance model–based biomimetic control," *Science Robotics,* vol. 4, no. 31, p. eaaw6339, 2019.
[175] S. Guo, M. Pang, B. Gao, H. Hirata, and H. Ishihara, "Comparison of sEMG-based feature extraction and motion classification methods for upper-limb movement," *sensors,* vol. 15, no. 4, pp. 9022-9038, 2015.
[176] E. Scheme and K. Englehart, "Electromyogram pattern recognition for control of powered upper-limb prostheses: state of the art and challenges for clinical use," *Journal of Rehabilitation Research & Development,* vol. 48, no. 6, 2011.
[177] N. Parajuli *et al.*, "Real-time EMG based pattern recognition control for hand prostheses: a review on existing methods, challenges and future implementation," *Sensors,* vol. 19, no. 20, p. 4596, 2019.
[178] A. Hartwell, V. Kadirkamanathan, and S. R. Anderson, "Compact deep neural networks for computationally efficient gesture classification from electromyography signals," in *2018 7th IEEE International Conference on Biomedical Robotics and Biomechatronics (Biorob)*, 2018: IEEE, pp. 891-896.
[179] R. Boostani and M. H. Moradi, "Evaluation of the forearm EMG signal features for the control of a prosthetic hand," *Physiological measurement,* 2003.
[180] K. Englehart, B. Hudgins, and A. D. Chan, "Continuous multifunction myoelectric control using pattern recognition," *Technology and Disability,* vol. 15, no. 2, pp. 95-103, 2003.
[181] i-biomed. "Sense Pattern Recognition system." https://www.i-biomed.com/sense.html (accessed.
[182] J. M. Hahne *et al.*, "Linear and nonlinear regression techniques for simultaneous and proportional myoelectric control," *IEEE Transactions on Neural Systems and Rehabilitation Engineering,* vol. 22, no. 2, pp. 269-279, 2014.
[183] M. T. Hagan, H. B. Demuth, and M. Beale, *Neural network design*. PWS Publishing Co., 1997.
[184] A. Cloutier and J. Yang, "Design, control, and sensory feedback of externally powered hand prostheses: a literature review," *Critical Reviews™ in Biomedical Engineering,* vol. 41, no. 2, 2013.
[185] M. Z.-E.-A. Amrani, A. Daoudi, N. Achour, and M. Tair, "Artificial neural networks based myoelectric control system for automatic assistance in hand rehabilitation," in *2017 26th IEEE International Symposium on Robot and Human Interactive Communication (RO-MAN)*, 2017: IEEE, pp. 968-973.
[186] M. Shahzaib and S. Shakil, "Hand electromyography circuit and signals classification using artificial neural network," in *2018 14th International Conference on Emerging Technologies (ICET)*, 2018: IEEE, pp. 1-6.
[187] C. Piazza, M. Rossi, M. G. Catalano, A. Bicchi, and L. J. Hargrove, "Evaluation of a Simultaneous Myoelectric Control Strategy for a Multi-DoF Transradial Prosthesis," *IEEE Transactions on Neural Systems and Rehabilitation Engineering,* 2020.

[188] L. Pan, D. Zhang, N. Jiang, X. Sheng, and X. Zhu, "Improving robustness against electrode shift of high density EMG for myoelectric control through common spatial patterns," *Journal of neuroengineering and rehabilitation,* vol. 12, no. 1, pp. 1-16, 2015.
[189] W. Geng, Y. Du, W. Jin, W. Wei, Y. Hu, and J. Li, "Gesture recognition by instantaneous surface EMG images," *Scientific reports,* vol. 6, no. 1, pp. 1-8, 2016.
[190] R. Merletti, A. Holobar, and D. Farina, "Analysis of motor units with high-density surface electromyography," *Journal of electromyography and kinesiology,* vol. 18, no. 6, pp. 879-890, 2008.
[191] A. Holobar and D. Zazula, "Multichannel blind source separation using convolution kernel compensation," *IEEE Transactions on Signal Processing,* vol. 55, no. 9, pp. 4487-4496, 2007.
[192] D. Y. Barsakcioglu and D. Farina, "A real-time surface emg decomposition system for non-invasive human-machine interfaces," in *2018 IEEE Biomedical Circuits and Systems Conference (BioCAS)*, 2018: IEEE, pp. 1-4.
[193] A. E. Olsson, P. Sager, E. Andersson, A. Björkman, N. Malešević, and C. Antfolk, "Extraction of multi-labelled movement information from the raw HD-sEMG image with time-domain depth," *Scientific reports,* vol. 9, no. 1, pp. 1-10, 2019.
[194] X. Zhai, B. Jelfs, R. H. Chan, and C. Tin, "Self-recalibrating surface EMG pattern recognition for neuroprosthesis control based on convolutional neural network," *Frontiers in neuroscience,* vol. 11, p. 379, 2017.
[195] G. Vasan and P. M. Pilarski, "Learning from demonstration: Teaching a myoelectric prosthesis with an intact limb via reinforcement learning," in *2017 International Conference on Rehabilitation Robotics (ICORR)*, 2017: IEEE, pp. 1457-1464.
[196] R. Wu, M. Li, Z. Yao, W. Liu, J. Si, and H. Huang, "Reinforcement learning impedance control of a robotic prosthesis to coordinate with human intact knee motion," *IEEE Robotics and Automation Letters,* vol. 7, no. 3, pp. 7014-7020, 2022.
[197] H. H. Huang, J. Si, A. Brandt, and M. Li, "Taking both sides: seeking symbiosis between intelligent prostheses and human motor control during locomotion," *Current Opinion in Biomedical Engineering,* vol. 20, p. 100314, 2021.
[198] R. Amado Laezza, "Deep neural networks for myoelectric pattern recognition-An implementation for multifunctional control," 2018.
[199] W. Li, P. Shi, and H. Yu, "Gesture Recognition Using Surface Electromyography and Deep Learning for Prostheses Hand: State-of-the-Art, Challenges, and Future," *Frontiers in Neuroscience,* vol. 15, 2021.
[200] M. Montazerin, S. Zabihi, E. Rahimian, A. Mohammadi, and F. Naderkhani, "ViT-HGR: Vision Transformer-based Hand Gesture Recognition from High Density Surface EMG Signals," *arXiv preprint arXiv:2201.10060,* 2022.
[201] A. Burrello *et al.*, "Bioformers: embedding transformers for ultra-low power sEMG-based gesture recognition," in *2022 Design, Automation & Test in Europe Conference & Exhibition (DATE)*, 2022: IEEE, pp. 1443-1448.
[202] L. Resnik, "Development and testing of new upper-limb prosthetic devices: research designs for usability testing," *Journal of Rehabilitation Research & Development,* vol. 48, no. 6, 2011.
[203] L. Pan, D. L. Crouch, and H. Huang, "Myoelectric control based on a generic musculoskeletal model: Toward a multi-user neural-machine interface," *IEEE Transactions on Neural Systems and Rehabilitation Engineering,* vol. 26, no. 7, pp. 1435-1442, 2018.
[204] J. Zhao, Y. Yu, X. Wang, S. Ma, X. Sheng, and X. Zhu, "A musculoskeletal model driven by muscle synergy-derived excitations for hand and wrist movements," *Journal of Neural Engineering,* 2022.
[205] E. Cho, R. Chen, L.-K. Merhi, Z. Xiao, B. Pousett, and C. Menon, "Force myography to control robotic upper extremity prostheses: a feasibility study," *Frontiers in bioengineering and biotechnology,* vol. 4, p. 18, 2016.
[206] E. Mainardi and A. Davalli, "Controlling a prosthetic arm with a throat microphone," in *2007 29th Annual International Conference of the IEEE Engineering in Medicine and Biology Society*, 2007: IEEE, pp. 3035-3039.

[207] O. S. Alkhafaf, M. K. Wali, and A. H. Al-Timemy, "Improved prosthetic hand control with synchronous use of voice recognition and inertial measurements," in *IOP Conference Series: Materials Science and Engineering*, 2020, vol. 745, no. 1: IOP Publishing, p. 012088.
[208] D. Johansen, C. Cipriani, D. B. Popović, and L. N. Struijk, "Control of a robotic hand using a tongue control system—A prosthesis application," *IEEE Transactions on Biomedical Engineering,* vol. 63, no. 7, pp. 1368-1376, 2016.
[209] J. Mouchoux, S. Carisi, S. Dosen, D. Farina, A. F. Schilling, and M. Markovic, "Artificial Perception and Semiautonomous Control in Myoelectric Hand Prostheses Increases Performance and Decreases Effort," *IEEE Transactions on Robotics,* 2021.
[210] A. Krasoulis, I. Kyranou, M. S. Erden, K. Nazarpour, and S. Vijayakumar, "Improved prosthetic hand control with concurrent use of myoelectric and inertial measurements," *Journal of neuroengineering and rehabilitation,* vol. 14, no. 1, pp. 1-14, 2017.
[211] A. Krasoulis, S. Vijayakumar, and K. Nazarpour, "Multi-grip classification-based prosthesis control with two EMG-IMU sensors," *IEEE Transactions on Neural Systems and Rehabilitation Engineering,* vol. 28, no. 2, pp. 508-518, 2019.
[212] M. Nowak, T. Eiband, E. R. Ramírez, and C. Castellini, "Action interference in simultaneous and proportional myocontrol: Comparing force-and electromyography," *Journal of neural engineering,* vol. 17, no. 2, p. 026011, 2020.
[213] S. Jiang, Q. Gao, H. Liu, and P. B. Shull, "A novel, co-located EMG-FMG-sensing wearable armband for hand gesture recognition," *Sensors and Actuators A: Physical,* vol. 301, p. 111738, 2020.
[214] D. Ferigo, L.-K. Merhi, B. Pousett, Z. G. Xiao, and C. Menon, "A case study of a force-myography controlled bionic hand mitigating limb position effect," *Journal of Bionic Engineering,* vol. 14, no. 4, pp. 692-705, 2017.
[215] W. Guo, X. Sheng, H. Liu, and X. Zhu, "Toward an enhanced human–machine interface for upper-limb prosthesis control with combined EMG and NIRS signals," *IEEE Transactions on Human-Machine Systems,* vol. 47, no. 4, pp. 564-575, 2017.
[216] T. Zhao, J. Liu, Y. Wang, H. Liu, and Y. Chen, "Towards Low-cost Sign Language Gesture Recognition Leveraging Wearables," *IEEE Transactions on Mobile Computing,* vol. 20, no. 4, pp. 1685-1701, 2019.
[217] P. Mamidanna, J. L. Dideriksen, and S. Dosen, "The impact of objective functions on control policies in closed-loop control of grasping force with a myoelectric prosthesis," *Journal of Neural Engineering,* vol. 18, no. 5, p. 056036, 2021.
[218] S. Jiang, L. Li, H. Xu, J. Xu, G. Gu, and P. B. Shull, "Stretchable e-skin patch for gesture recognition on the back of the hand," *IEEE Transactions on Industrial Electronics,* vol. 67, no. 1, pp. 647-657, 2019.
[219] M. A. Schweisfurth, M. Markovic, S. Dosen, F. Teich, B. Graimann, and D. Farina, "Electrotactile EMG feedback improves the control of prosthesis grasping force," *Journal of neural engineering,* vol. 13, no. 5, p. 056010, 2016.
[220] M. Štrbac *et al.*, "Integrated and flexible multichannel interface for electrotactile stimulation," *Journal of neural engineering,* vol. 13, no. 4, p. 046014, 2016.
[221] Y. Li, J. Chen, and Y. Yang, "A method for suppressing electrical stimulation artifacts from electromyography," *International journal of neural systems,* vol. 29, no. 06, p. 1850054, 2019.
[222] M. Luchetti, A. G. Cutti, G. Verni, R. Sacchetti, and N. Rossi, "Impact of Michelangelo prosthetic hand: Findings from a crossover longitudinal study," *Journal of rehabilitation research and development,* vol. 52, 5, p. 13, 2015, doi: http://dx.doi.org/10.1682/JRRD.2014.11.0283.
[223] H. Jones *et al.*, "Co-creation and user perspectives for upper limb prosthetics," *Frontiers in Neurorobotics,* 2021.
[224] R. Riener, "The Cybathlon promotes the development of assistive technology for people with physical disabilities," *Journal of neuroengineering and rehabilitation,* vol. 13, no. 1, pp. 1-4, 2016.
[225] M. Zahabi *et al.*, "Application of cognitive task performance modeling for assessing usability of transradial prostheses," *IEEE Transactions on Human-Machine Systems,* vol. 49, no. 4, pp. 381-387, 2019.

[226] E. A. Biddiss and T. T. Chau, "Upper limb prosthesis use and abandonment: a survey of the last 25 years," *Prosthetics and orthotics international,* vol. 31, no. 3, pp. 236-257, 2007.
[227] E. Biddiss, D. Beaton, and T. Chau, "Consumer design priorities for upper limb prosthetics," *Disability and rehabilitation: Assistive technology,* vol. 2, no. 6, pp. 346-357, 2007.
[228] C. Davis and M. S. Onge, "Myoelectric and body-powered upper-limb prostheses: the users' perspective," in *JPO: Journal of Prosthetics and Orthotics*, 2017, vol. 29, no. 4S: LWW, pp. P30-P34.
[229] J. Uellendahl, "Myoelectric versus body-powered upper-limb prostheses: a clinical perspective," in *JPO: Journal of Prosthetics and Orthotics*, 2017, vol. 29, no. 4S: LWW, pp. P25-P29.
[230] L. C. Smail, C. Neal, C. Wilkins, and T. L. Packham, "Comfort and function remain key factors in upper limb prosthetic abandonment: findings of a scoping review," *Disability and rehabilitation: Assistive technology,* pp. 1-10, 2020.
[231] N. Kerver, S. van Twillert, B. Maas, and C. K. van der Sluis, "User-relevant factors determining prosthesis choice in persons with major unilateral upper limb defects: A meta-synthesis of qualitative literature and focus group results," *PloS one,* vol. 15, no. 6, p. e0234342, 2020.
[232] C. A. Garske, M. Dyson, S. Dupan, and K. Nazarpour, "Perception of Game-Based Rehabilitation in Upper Limb Prosthetic Training: Survey of Users and Researchers," *JMIR serious games,* vol. 9, no. 1, p. e23710, 2021.
[233] A. Tabor, W. Hill, S. Bateman, and E. Scheme, "Quantifying muscle control in myoelectric training games," in *Proc Myoelectr Control Symp (MEC)*, 2017, vol. 4.
[234] C. A. Garske, M. Dyson, S. Dupan, G. Morgan, and K. Nazarpour, "Serious Games Are Not Serious Enough for Myoelectric Prosthetics," *JMIR serious games,* vol. 9, no. 4, p. e28079, 2021.
[235] P. Beckerle *et al.*, "Feel-good robotics: requirements on touch for embodiment in assistive robotics," *Frontiers in neurorobotics,* vol. 12, p. 84, 2018.
[236] D. M. Page *et al.*, "Motor control and sensory feedback enhance prosthesis embodiment and reduce phantom pain after long-term hand amputation," *Frontiers in human neuroscience,* vol. 12, p. 352, 2018.
[237] P. M. McDonnell, R. N. Scott, J. Dickison, R. A. Theriault, and B. Wood, "Do artificial limbs become part of the user? New evidence," *Journal of rehabilitation research and development,* vol. 26, no. 2, pp. 17-24, 1989.
[238] P. Beckerle, C. Castellini, and B. Lenggenhager, "Robotic interfaces for cognitive psychology and embodiment research: a research roadmap," *Wiley Interdisciplinary Reviews: Cognitive Science,* vol. 10, no. 2, p. e1486, 2019.
[239] M. Botvinick and J. Cohen, "Rubber hands 'feel'touch that eyes see," *Nature,* vol. 391, no. 6669, pp. 756-756, 1998.
[240] M. Tsakiris and P. Haggard, "The rubber hand illusion revisited: visuotactile integration and self-attribution," *Journal of Experimental Psychology: Human Perception and Performance,* vol. 31, no. 1, p. 80, 2005.
[241] H. H. Ehrsson, B. Rosén, A. Stockselius, C. Ragnö, P. Köhler, and G. Lundborg, "Upper limb amputees can be induced to experience a rubber hand as their own," *Brain,* vol. 131, no. 12, pp. 3443-3452, 2008.
[242] D. Romano, A. Maravita, and M. Perugini, "Psychometric properties of the embodiment scale for the rubber hand illusion and its relation with individual differences," *Scientific reports,* vol. 11, no. 1, pp. 1-16, 2021.
[243] C. Castellini, "Upper Limb Active Prosthetic systems—Overview," in *Wearable Robotics*: Elsevier, 2020, pp. 365-376.
[244] A. Saradjian, A. R. Thompson, and D. Datta, "The experience of men using an upper limb prosthesis following amputation: positive coping and minimizing feeling different," *Disability and Rehabilitation,* vol. 30, no. 11, pp. 871-883, 2008.
[245] D. K. Kumar, B. Jelfs, X. Sui, and S. P. Arjunan, "Prosthetic hand control: A multidisciplinary review to identify strengths, shortcomings, and the future," *Biomedical Signal Processing and Control,* vol. 53, p. 101588, 2019.

[246] M. C. Bettoni and C. Castellini, "Interaction in assistive robotics: a radical constructivist design framework," *Frontiers in Neurorobotics,* vol. 15, p. 675657, 2021.
[247] M. Laffranchi *et al.*, "The Hannes hand prosthesis replicates the key biological properties of the human hand," *Science Robotics,* vol. 5, no. 46, 2020.
[248] K. Baur, F. L. Haufe, R. Sigrist, K. Dorfschmid, and R. Riener, "The CYBATHLON-Bionic Olympics to Benchmark Assistive Technologies," in *International Conference on Inclusive Robotics for a better Society*, 2018: Springer, pp. 175-179.
[249] C. ETH Zurich, "Race task decription Cybathlon 2020 Global Edition, V_2020-11-03," 2020.
[250] A. Ochando and L. Zago, "What are the contributions of handedness, sighting dominance, hand used to bisect, and visuospatial line processing to the behavioral line bisection bias?," *Frontiers in psychology,* vol. 9, p. 1688, 2018.
[251] T. R. Makin, M. Wilf, I. Schwartz, and E. Zohary, "Amputees "neglect" the space near their missing hand," *Psychological science,* vol. 21, no. 1, pp. 55-57, 2010.
[252] L. Haverkate, G. Smit, and D. H. Plettenburg, "Assessment of body-powered upper limb prostheses by able-bodied subjects, using the Box and Blocks Test and the Nine-Hole Peg Test," *Prosthetics and orthotics international,* vol. 40, no. 1, pp. 109-116, 2016.
[253] V. Mathiowetz, G. Volland, N. Kashman, and K. Weber, "Adult norms for the Box and Block Test of manual dexterity," *American Journal of Occupational Therapy,* vol. 39, no. 6, pp. 386-391, 1985.
[254] D. E. Beaton, J. G. Wright, J. N. Katz, and U. E. C. Group, "Development of the QuickDASH: comparison of three item-reduction approaches," *JBJS,* vol. 87, no. 5, pp. 1038-1046, 2005.
[255] A. W. Heinemann, R. Bode, and C. O'reilly, "Development and measurement properties of the Orthotics and Prosthetics Users' Survey (OPUS): a comprehensive set of clinical outcome instruments," *Prosthetics and orthotics international,* vol. 27, no. 3, pp. 191-206, 2003.
[256] L. Resnik and M. Borgia, "Reliability and validity of outcome measures for upper limb amputation," *JPO: Journal of Prosthetics and Orthotics,* vol. 24, no. 4, pp. 192-201, 2012.
[257] M. R. Longo, F. Schüür, M. P. Kammers, M. Tsakiris, and P. Haggard, "What is embodiment? A psychometric approach," *Cognition,* vol. 107, no. 3, pp. 978-998, 2008.
[258] M. Freddolini, A. Corvi, L. Barni, and F. Esposito, "Data processing techniques may influence numerical results and interpretation of single leg stance test," *IRBM,* vol. 42, no. 2, pp. 106-111, 2021.
[259] M. Pau *et al.*, "Relationship between static and dynamic balance abilities in Italian professional and youth league soccer players," *Physical Therapy in Sport,* vol. 16, no. 3, pp. 236-241, 2015.
[260] W. Plom, S. Strike, and M. Taylor, "The effect of different unstable footwear constructions on centre of pressure motion during standing," *Gait & posture,* vol. 40, no. 2, pp. 305-309, 2014.
[261] J. Zbinden, E. Lendaro, and M. Ortiz-Catalan, "Prosthetic embodiment: systematic review on definitions, measures, and experimental paradigms," *Journal of NeuroEngineering and Rehabilitation,* vol. 19, no. 1, pp. 1-16, 2022.
[262] A. G. Mirnig, A. Meschtscherjakov, D. Wurhofer, T. Meneweger, and M. Tscheligi, "A formal analysis of the ISO 9241-210 definition of user experience," in *Proceedings of the 33rd annual ACM conference extended abstracts on human factors in computing systems*, 2015, pp. 437-450.
[263] O. Christ *et al.*, "User-centered prosthetic development: comprehension of amputees' needs," *Biomedical Engineering/Biomedizinische Technik,* vol. 57, no. SI-1-Track-R, pp. 1098-1101, 2012.
[264] S. G. Hart, "NASA-task load index (NASA-TLX); 20 years later," in *Proceedings of the human factors and ergonomics society annual meeting*, 2006, vol. 50, no. 9: Sage Publications Sage CA: Los Angeles, CA, pp. 904-908.
[265] E. A. Bustamante and R. D. Spain, "Measurement invariance of the Nasa TLX," in *Proceedings of the Human Factors and Ergonomics Society Annual Meeting*, 2008, vol. 52, no. 19: SAGE Publications Sage CA: Los Angeles, CA, pp. 1522-1526.
[266] J. Brooke, "SUS-A quick and dirty usability scale," *Usability evaluation in industry,* vol. 189, no. 194, pp. 4-7, 1996.
[267] P. Gallagher and M. Maclachlan, "The Trinity Amputation and Prosthesis Experience Scales and quality of life in people with lower-limb amputation," (in eng), *Archives of Physical*

Medicine and Rehabilitation, vol. 85, no. 5, pp. 730-736, 2004/05// 2004, doi: 10.1016/j.apmr.2003.07.009.
[268] F. Franchignoni, S. Vercelli, A. Giordano, F. Sartorio, E. Bravini, and G. Ferriero, "Minimal clinically important difference of the disabilities of the arm, shoulder and hand outcome measure (DASH) and its shortened version (QuickDASH)," *Journal of orthopaedic & sports physical therapy,* vol. 44, no. 1, pp. 30-39, 2014.
[269] E. C. Nelson, A. M. Sools, M. M. Vollenbroek-Hutten, T. Verhagen, and M. L. Noordzij, "Embodiment of Wearable Technology: Qualitative Longitudinal Study," *JMIR mHealth and uHealth,* vol. 8, no. 11, p. e16973, 2020.
[270] T. R. Makin, F. de Vignemont, and S. Micera, "Soft Embodiment for Engineering Artificial Limbs," *Trends in Cognitive Sciences,* 2020.
[271] G. Fusco, E. Tidoni, N. Barone, C. Pilati, and S. M. Aglioti, "Illusion of arm movement evoked by tendon vibration in patients with spinal cord injury," *Restorative neurology and neuroscience,* vol. 34, no. 5, pp. 815-826, 2016.
[272] I. Iturrate, R. Chavarriaga, L. Montesano, J. Minguez, and J. d. R. Millán, "Teaching brain-machine interfaces as an alternative paradigm to neuroprosthetics control," *Scientific reports,* vol. 5, no. 1, pp. 1-10, 2015.
[273] E. Tidoni *et al.*, "Local and remote cooperation with virtual and robotic agents: a P300 BCI study in healthy and people living with spinal cord injury," *IEEE Transactions on Neural Systems and Rehabilitation Engineering,* vol. 25, no. 9, pp. 1622-1632, 2016.
[274] U. B. Rongala, A. Mazzoni, D. Camboni, M. C. Carrozza, and C. M. Oddo, "Neuromorphic artificial sense of touch: bridging robotics and neuroscience," in *Robotics Research*: Springer, 2018, pp. 617-630.
[275] C. D. Murray, "An interpretative phenomenological analysis of the embodiment of artificial limbs," *Disability and rehabilitation,* vol. 26, no. 16, pp. 963-973, 2004.
[276] R. O. Maimon Mor and T. R. Makin, "Is an artificial limb embodied as a hand? Brain decoding in prosthetic limb users," *Plos Biology,* vol. 18, no. 6, p. e3000729, 2020.
[277] M. Pazzaglia and M. Molinari, "The embodiment of assistive devices—from wheelchair to exoskeleton," *Physics of life reviews,* vol. 16, pp. 163-175, 2016.
[278] A. Toet, I. A. Kuling, B. N. Krom, and J. B. Van Erp, "Toward enhanced teleoperation through embodiment," *Frontiers in Robotics and AI,* vol. 7, p. 14, 2020.
[279] N. Ratcliffe and R. Newport, "The effect of visual, spatial and temporal manipulations on embodiment and action," *Frontiers in human neuroscience,* vol. 11, p. 227, 2017.
[280] V. Brugada-Ramentol, I. Clemens, and G. G. de Polavieja, "Active control as evidence in favor of sense of ownership in the moving Virtual Hand Illusion," *Consciousness and cognition,* vol. 71, pp. 123-135, 2019.
[281] M. Allen and M. Tsakiris, "The body as first prior: Interoceptive predictive processing and the primacy," *The interoceptive mind: From homeostasis to awareness,* vol. 27, 2018.
[282] M. Czub and M. Kowal, "Respiration entrainment in virtual reality by using a breathing avatar," *Cyberpsychology, Behavior, and Social Networking,* vol. 22, no. 7, pp. 494-499, 2019.
[283] B. Bornemann, "Body awareness, voluntary physiological regulation, and their modulation by contemplative training," Humboldt University Berlin, 2017.
[284] M. Niedernhuber, D. G. Barone, and B. Lenggenhager, "Prostheses as extensions of the body: Progress and challenges," *Neuroscience & Biobehavioral Reviews,* vol. 92, pp. 1-6, 2018.
[285] H. Shaw, D. A. Ellis, and F. V. Ziegler, "The Technology Integration Model (TIM). Predicting the continued use of technology," *Computers in Human Behavior,* vol. 83, pp. 204-214, 2018.
[286] R. Bekrater-Bodmann, I. Reinhard, M. Diers, X. Fuchs, and H. Flor, "Relationship of prosthesis ownership and phantom limb pain: results of a survey in 2383 limb amputees," *Pain,* vol. 162, no. 2, pp. 630-640, 2021.
[287] K. Kilteni, R. Groten, and M. Slater, "The sense of embodiment in virtual reality," *Presence: Teleoperators and Virtual Environments,* vol. 21, no. 4, pp. 373-387, 2012.
[288] H. Ramakonar, E. A. Franz, and C. R. Lind, "The rubber hand illusion and its application to clinical neuroscience," *Journal of Clinical Neuroscience,* vol. 18, no. 12, pp. 1596-1601, 2011.
[289] M. P. Kammers, F. de Vignemont, L. Verhagen, and H. C. Dijkerman, "The rubber hand illusion in action," *Neuropsychologia,* vol. 47, no. 1, pp. 204-211, 2009.

[290] H. H. Ehrsson, N. P. Holmes, and R. E. Passingham, "Touching a rubber hand: feeling of body ownership is associated with activity in multisensory brain areas," *Journal of neuroscience,* vol. 25, no. 45, pp. 10564-10573, 2005.
[291] M. Tsakiris, G. Prabhu, and P. Haggard, "Having a body versus moving your body: How agency structures body-ownership," *Consciousness and cognition,* vol. 15, no. 2, pp. 423-432, 2006.
[292] D. Romano, E. Caffa, A. Hernandez-Arieta, P. Brugger, and A. Maravita, "The robot hand illusion: Inducing proprioceptive drift through visuo-motor congruency," *Neuropsychologia,* vol. 70, pp. 414-420, 2015.
[293] E. Lewis and D. M. Lloyd, "Embodied experience: A first-person investigation of the rubber hand illusion," *Phenomenology and the Cognitive Sciences,* vol. 9, no. 3, pp. 317-339, 2010.
[294] D. Crivelli and M. Balconi, "Extending the Body Ownership to Affective Experience of an Embodied Artificial Hand: a Power Spectra Investigation," *Multisensory Research,* vol. 1, no. aop, pp. 1-13, 2020.
[295] M. Prikken *et al.*, "Multisensory integration underlying body-ownership experiences in schizophrenia and offspring of patients: a study using the rubber hand illusion paradigm," *Journal of psychiatry & neuroscience: JPN,* vol. 44, no. 3, p. 177, 2019.
[296] M. Chancel, H. H. Ehrsson, and W. J. Ma, "Uncertainty-based inference of a common cause for body ownership," 2021.
[297] K. Grechuta, J. Guga, G. Maffei, B. R. Ballester, and P. F. Verschure, "Visuotactile integration modulates motor performance in a perceptual decision-making task," *Scientific reports,* vol. 7, no. 1, pp. 1-13, 2017.
[298] K. Ma, J. Qu, L. Yang, W. Zhao, and B. Hommel, "Explicit and implicit measures of body ownership and agency: affected by the same manipulations and yet independent," *Experimental Brain Research,* pp. 1-12, 2021.
[299] M. Tsakiris, "My body in the brain: a neurocognitive model of body-ownership," *Neuropsychologia,* vol. 48, no. 3, pp. 703-712, 2010.
[300] B. M. Herbert and O. Pollatos, "The body in the mind: on the relationship between interoception and embodiment," *Topics in cognitive science,* vol. 4, no. 4, pp. 692-704, 2012.
[301] M. Tsakiris, A. T.-. Jiménez, and M. Costantini, "Just a heartbeat away from one's body: interoceptive sensitivity predicts malleability of body-representations," *Proceedings of the Royal Society B: Biological Sciences,* vol. 278, no. 1717, pp. 2470-2476, 2011.
[302] K. Suzuki, S. N. Garfinkel, H. D. Critchley, and A. K. Seth, "Multisensory integration across exteroceptive and interoceptive domains modulates self-experience in the rubber-hand illusion," *Neuropsychologia,* vol. 51, no. 13, pp. 2909-2917, 2013.
[303] H.-D. Park *et al.*, "Neural sources and underlying mechanisms of neural responses to heartbeats, and their role in bodily self-consciousness: an intracranial EEG study," *Cerebral Cortex,* vol. 28, no. 7, pp. 2351-2364, 2018.
[304] A. Xu, B. Cullen, C. Penner, C. Zimmerman, C. Kerr, and L. Schmalzl, "Comparing embodiment experiences in expert meditators and non-meditators using the rubber hand illusion," *Consciousness and cognition,* vol. 65, pp. 325-333, 2018.
[305] A. Cebolla *et al.*, "Embodiment and body awareness in meditators," *Mindfulness,* vol. 7, no. 6, pp. 1297-1305, 2016.
[306] J. Brenner *et al.*, "Mindfulness with paced breathing reduces blood pressure," *Medical hypotheses,* vol. 142, p. 109780, 2020.
[307] M. A. Russo, D. M. Santarelli, and D. O'Rourke, "The physiological effects of slow breathing in the healthy human," *Breathe,* vol. 13, no. 4, pp. 298-309, 2017.
[308] M. Leganes-Fonteneau *et al.*, "The cardiovascular mechanisms of interoceptive awareness: effects of resonance breathing," *Int J Psychophysiol Stage,* vol. 1, 2021.
[309] H. Y. Weng, J. L. Feldman, L. Leggio, V. Napadow, J. Park, and C. J. Price, "Interventions and manipulations of interoception," *Trends in neurosciences,* vol. 44, no. 1, pp. 52-62, 2021.
[310] J. Blum, C. Rockstroh, and A. S. Göritz, "Development and pilot test of a virtual reality respiratory biofeedback approach," *Applied psychophysiology and biofeedback,* vol. 45, no. 3, pp. 153-163, 2020.
[311] M. de Zambotti, M. Sizintsev, S. Claudatos, G. Barresi, I. M. Colrain, and F. C. Baker, "Reducing bedtime physiological arousal levels using immersive audio-visual respiratory bio-

feedback: a pilot study in women with insomnia symptoms," *Journal of behavioral medicine,* vol. 42, no. 5, pp. 973-983, 2019.
[312] L. Raz, P. L. Weiss, and M. Reiner, "The virtual hand illusion and body ownership," in *International Conference on Human Haptic Sensing and Touch Enabled Computer Applications*, 2008: Springer, pp. 367-372.
[313] T. D. Parsons, A. Gaggioli, and G. Riva, "Extended Reality for the Clinical, Affective, and Social Neurosciences," *Brain Sciences,* vol. 10, no. 12, p. 922, 2020.
[314] G. Tieri, A. Gioia, M. Scandola, E. F. Pavone, and S. M. Aglioti, "Visual appearance of a virtual upper limb modulates the temperature of the real hand: a thermal imaging study in Immersive Virtual Reality," *European Journal of Neuroscience,* vol. 45, no. 9, pp. 1141-1151, 2017.
[315] F. Škola, S. Tinková, and F. Liarokapis, "Progressive training for motor imagery brain-computer interfaces using gamification and virtual reality embodiment," *Frontiers in human neuroscience,* vol. 13, p. 329, 2019.
[316] W. A. IJsselsteijn, Y. A. W. de Kort, and A. Haans, "Is this my hand I see before me? The rubber hand illusion in reality, virtual reality, and mixed reality," *Presence: Teleoperators and Virtual Environments,* vol. 15, no. 4, pp. 455-464, 2006.
[317] M. Slater, D. Pérez Marcos, H. Ehrsson, and M. V. Sanchez-Vives, "Towards a digital body: the virtual arm illusion," *Frontiers in human neuroscience,* vol. 2, p. 6, 2008.
[318] F. Škola and F. Liarokapis, "Examining the effect of body ownership in immersive virtual and augmented reality environments," *The Visual Computer,* vol. 32, no. 6, pp. 761-770, 2016.
[319] M. Matamala-Gomez, A. Maselli, C. Malighetti, O. Realdon, F. Mantovani, and G. Riva, "Virtual Body Ownership Illusions for Mental Health: A Narrative Review," *Journal of Clinical Medicine,* vol. 10, no. 1, p. 139, 2021.
[320] O. A. Kannape, E. J. Smith, P. Moseley, M. P. Roy, and B. Lenggenhager, "Experimentally induced limb-disownership in mixed reality," *Neuropsychologia,* vol. 124, pp. 161-170, 2019.
[321] A. Boschmann, D. Neuhaus, S. Vogt, C. Kaltschmidt, M. Platzner, and S. Dosen, "Immersive augmented reality system for the training of pattern classification control with a myoelectric prosthesis," *Journal of neuroengineering and rehabilitation,* vol. 18, no. 1, pp. 1-15, 2021.
[322] A. Monti, G. Porciello, G. Tieri, and S. M. Aglioti, "The “embreathment” illusion highlights the role of breathing in corporeal awareness," *Journal of Neurophysiology,* vol. 123, no. 1, pp. 420-427, 2020.
[323] F. Faul, E. Erdfelder, A.-G. Lang, and A. Buchner, "G* Power 3: A flexible statistical power analysis program for the social, behavioral, and biomedical sciences," *Behavior research methods,* vol. 39, no. 2, pp. 175-191, 2007.
[324] P. Beckerle, "Virtual Hand Experience," in *Human-Robot Body Experience*: Springer, 2021, pp. 41-53.
[325] R. Raskar, G. Welch, and H. Fuchs, "Spatially augmented reality," *Augmented Reality: Placing Artificial Objects in Real Scenes,* pp. 64-71, 1999.
[326] O. Bimber and R. Raskar, *Spatial augmented reality: merging real and virtual worlds*. AK Peters/CRC Press, 2019.
[327] Z. Visnovcova *et al.*, "Spectral and Nonlinear Analysis of Electrodermal Activity in Adolescent Anorexia Nervosa," *Applied Sciences,* vol. 10, no. 13, p. 4514, 2020.
[328] E. Gümüslü, D. Erol Barkana, and H. Köse, "Emotion Recognition using EEG and Physiological Data for Robot-Assisted Rehabilitation Systems," in *Companion Publication of the 2020 International Conference on Multimodal Interaction*, 2020, pp. 379-387.
[329] A. Pacholik-Żuromska, "Self-Regulation in the Time of Lockdown," *Frontiers in Neuroinformatics,* vol. 15, p. 7, 2021.
[330] D. S. Avalur, "Human breath detection using a microphone," Master Thesis, Faculty of Science and Engineering, University of Groningen, Netherlands 2013. [Online]. Available: https://fse.studenttheses.ub.rug.nl/11311/
[331] A. R. Schwerdtfeger, G. Schwarz, K. Pfurtscheller, J. F. Thayer, M. N. Jarczok, and G. Pfurtscheller, "Heart rate variability (HRV): From brain death to resonance breathing at 6 breaths per minute," *Clinical Neurophysiology,* vol. 131, no. 3, pp. 676-693, 2020.

[332] I. T. Fonkoue *et al.*, "Acute effects of device-guided slow breathing on sympathetic nerve activity and baroreflex sensitivity in posttraumatic stress disorder," *American Journal of Physiology-Heart and Circulatory Physiology,* vol. 315, no. 1, pp. H141-H149, 2018.
[333] I. Senna, A. Maravita, N. Bolognini, and C. V. Parise, "The marble-hand illusion," *PloS one,* vol. 9, no. 3, p. e91688, 2014.
[334] K. C. Armel and V. S. Ramachandran, "Projecting sensations to external objects: evidence from skin conductance response," *Proceedings of the Royal Society of London. Series B: Biological Sciences,* vol. 270, no. 1523, pp. 1499-1506, 2003.
[335] M. Pyasik, G. Tieri, and L. Pia, "Visual appearance of the virtual hand affects embodiment in the virtual hand illusion," *Scientific reports,* vol. 10, no. 1, pp. 1-11, 2020.
[336] J. Love *et al.*, "JASP: Graphical statistical software for common statistical designs," *Journal of Statistical Software,* vol. 88, no. 1, pp. 1-17, 2019.
[337] D. S. Kerby, "The simple difference formula: An approach to teaching nonparametric correlation," *Comprehensive Psychology,* vol. 3, p. 11. IT. 3.1, 2014.
[338] G. Riva, F. Davide, and W. A. IJsselsteijn, "Being there: The experience of presence in mediated environments," *Being there: Concepts, effects and measurement of user presence in synthetic environments,* vol. 5, 2003.
[339] N. Rosa, P. Werkhoven, W. Hürst, and R. C. Veltkamp, "A Model for Virtual Hand Ownership in Augmented Reality," in *2020 IEEE Conference on Virtual Reality and 3D User Interfaces Abstracts and Workshops (VRW)*, 2020: IEEE, pp. 224-229.
[340] A. Kalckert and H. Ehrsson, "The onset time of the ownership sensation in the moving rubber hand illusion," *Frontiers in psychology,* vol. 8, p. 344, 2017.
[341] M. Riemer, J. Trojan, M. Beauchamp, and X. Fuchs, "The rubber hand universe: On the impact of methodological differences in the rubber hand illusion," *Neuroscience & Biobehavioral Reviews,* vol. 104, pp. 268-280, 2019.
[342] S. L. Winkler, M. Schlesinger, A. Krueger, and A. Ludwig, "Amputee Perspectives of Virtual Patient Education," *The Qualitative Report,* vol. 24, no. 6, pp. 1309-1318, 2019.
[343] D. Grynberg and O. Pollatos, "Alexithymia modulates the experience of the rubber hand illusion," *Frontiers in human neuroscience,* vol. 9, p. 357, 2015.
[344] N. Kanayama, M. Hara, and K. Kimura, "Virtual reality alters cortical oscillations related to visuo-tactile integration during rubber hand illusion," *Scientific reports,* vol. 11, no. 1, p. 1436, 2021.
[345] T. Hinterberger, N. Walter, C. Doliwa, and T. Loew, "The brain's resonance with breathing—decelerated breathing synchronizes heart rate and slow cortical potentials," *Journal of breath research,* vol. 13, no. 4, p. 046003, 2019.
[346] G. Northoff, "Slow cortical potentials and "inner time consciousness"—A neuro-phenomenal hypothesis about the "width of present"," *International Journal of Psychophysiology,* vol. 103, pp. 174-184, 2016.
[347] J. Ratcliffe, F. Soave, N. Bryan-Kinns, L. Tokarchuk, and I. Farkhatdinov, "Extended Reality (XR) remote research: a survey of drawbacks and opportunities," in *Proceedings of the 2021 CHI Conference on Human Factors in Computing Systems*, 2021, pp. 1-13.
[348] W. E. Mehling, C. Price, J. J. Daubenmier, M. Acree, E. Bartmess, and A. Stewart, "The multidimensional assessment of interoceptive awareness (MAIA)," *PloS one,* vol. 7, no. 11, p. e48230, 2012.
[349] D. Burin *et al.*, "Relationships between personality features and the rubber hand illusion: an exploratory study," *Frontiers in psychology,* vol. 10, p. 2762, 2019.
[350] F. Dehais, W. Karwowski, and H. Ayaz, "Brain at Work and in Everyday Life as the Next Frontier: Grand Field Challenges for Neuroergonomics," *Front Neuroergonomics,* 2020.
[351] A. J. a. G. Spiers, Yuri and Dollar, Aaron M., "Examining the Impact of Wrist Mobility on Reaching Motion Compensation Across a Discretely Sampled Workspace," presented at the IEEE International Conference on Biomedical obotics and Biomechatronics (Biorob), Enshede, The Netherlands, August 26-29, 2018.
[352] G. Gillen, R. Goldberg, S. Muller, and J. Straus, "The Effect of Wrist Position on Upper Extremity Function While Wearing a Wrist Immobilizing Splint," *JPO: Journal of Prosthetics and Orthotics,* vol. 20, no. 1, pp. 19-23, 2008, doi: 10.1097/JPO.0b013e31815f013f.

[353] N. R. Olsen *et al.*, "An adaptable prosthetic wrist reduces subjective workload," *bioRxiv,* p. 808634, 2019.
[354] A. G. Mell, B. L. Childress, and R. E. Hughes, "The effect of wearing a wrist splint on shoulder kinematics during object manipulation," *Arch Phys Med Rehabil,* vol. 86, no. 8, pp. 1661-4, Aug 2005, doi: 10.1016/j.apmr.2005.02.008.
[355] T. a. F. Bertels, Kerstin and Schmalz, Thomas, "Biomechanical Analysis in Arm Prosthetics - Objectifying of Functional Advantages offered by Wrist Flexion," presented at the Myoelectric Controls/Powered Prosthetics Symposium, Fredericton, New Brunswick, Canada, August 13-15, 2008.
[356] B. Peerdeman *et al.*, "Myoelectric forearm prostheses: state of the art from a user-centered perspective," *J Rehabil Res Dev,* vol. 48, no. 6, pp. 719-37, 2011, doi: 10.1682/jrrd.2010.08.0161.
[357] N. M. a. S. Bajaj, Adam J. and Dollar, Aaron M., "State of the Art in Prosthetic Wrists: Commercial and Research Devices," *IEEE International Conference on Rehabilitation Robotics (ICORR),* p. 8, 2015.
[358] F. Montagnani, M. Controzzi, and C. Cipriani, "Is it Finger or Wrist Dexterity That is Missing in Current Hand Prostheses?," *IEEE Trans Neural Syst Rehabil Eng,* vol. 23, no. 4, pp. 600-9, Jul 2015, doi: 10.1109/TNSRE.2015.2398112.
[359] Ottobock. "Eletric wrist rotator." https://shop.ottobock.us/Prosthetics/Upper-Limb-Prosthetics/Myo-Hands-and-Components/Myo-Wrist-Units-and-Rotation/Electric-Wrist-Rotator/p/10S17 (accessed.
[360] Fillauer. "MC standard wrist rotator." https://fillauer.com/products/mc-standard-wrist-rotator/ (accessed.
[361] F. f. M. Control, "Powered flexion wrist." [Online]. Available: https://fillauer.com/wp-content/uploads/2020/07/MC-Powered-Flexion-Wrist-Sell-Sheet-07-28-2020.pdf.
[362] Keshen. "KS-Bionic Hand." http://en.keshen.com/product-2.html (accessed.
[363] P. J. Kyberd, A. S. Poulton, L. Sandsjö, S. Jönsson, B. Jones, and D. Gow, "The ToMPAW Modular Prosthesis: A Platform for Research in Upper-Limb Prosthetics," *JPO: Journal of Prosthetics and Orthotics,* vol. 19, no. 1, pp. 15-21, 2007, doi: 10.1097/JPO.0b013e31802d46f8.
[364] J. H. U.-A. P. L. (APL). "Modular Prosthetic Limb (MPL) v1." https://www.jhuapl.edu/prosthetics/program (accessed.
[365] M. Bionics. "Luke Arm." https://www.mobiusbionics.com/luke-arm/ (accessed.
[366] "Atom Touch artificial arm." https://atomlimbs.com (accessed.
[367] K. Nazarpour, "A more human prosthetic hand," *Science Robotics,* vol. 5, no. 46, p. eabd9341, 2020, doi: 10.1126/scirobotics.abd9341.
[368] I. A. Kapandji, Monduzzi, Ed. *Fisiologia articolare, vol. 1, Arto Superiore*, 6 ed. 2011.
[369] D. A. Neumann, *Kinesiology of the Muscoloskeletal System* (Foundations for Physical Rehabilitation). Mosby.
[370] R. Tubiana, J.-M. Thomine, and E. Mackin, *Examination of the Hand and Wrist*. Taylor & Francis Group, 1998.
[371] E. Biddiss and T. Chau, "Upper-limb prosthetics: critical factors in device abandonment," *Am J Phys Med Rehabil,* vol. 86, no. 12, pp. 977-87, Dec 2007, doi: 10.1097/PHM.0b013e3181587f6c.
[372] C. Cipriani, R. Sassu, M. Controzzi, and M. C. Carrozza, "Influence of the weight actions of the hand prosthesis on the performance of pattern recognition based myoelectric control: Preliminary study," 2011.
[373] ISHN. "https://www.ishn.com/articles/97844-statistics-on-hand-and-arm-loss." (accessed.
[374] NASA. "https://msis.jsc.nasa.gov/sections/section03.htm." (accessed.
[375] J. C. Perry, J. Rosen, and S. Burns, "Upper-limb powered exoskeleton design," *IEEE/ASME transactions on mechatronics,* vol. 12, no. 4, pp. 408-417, 2007.
[376] C. M. Light, P. H. Chappell, and P. J. Kyberd, "Establishing a standardized clinical assessment tool of pathologic and prosthetic hand function: normative data, reliability, and validity," *Archives of physical medicine and rehabilitation,* vol. 83, no. 6, pp. 776-783, 2002.

[377] S. A. Taylor, A. E. Kedgley, A. Humphries, and A. F. Shaheen, "Simulated activities of daily living do not replicate functional upper limb movement or reduce movement variability," *Journal of Biomechanics,* vol. 76, pp. 119-128, 2018.
[378] H. Burger, F. Franchignoni, A. W. Heinemann, S. Kotnik, and A. Giordano, "Validation of the orthotics and prosthetics user survey upper extremity functional status module in people with unilateral upper limb amputation," *Journal of rehabilitation medicine,* vol. 40, no. 5, pp. 393-399, 2008.
[379] P. J. Kyberd *et al.*, "Two-degree-of-freedom powered prosthetic wrist," *J Rehabil Res Dev,* vol. 48, no. 6, pp. 609-17, 2011, doi: 10.1682/jrrd.2010.07.0137.
[380] D. A. Bennett, J. E. Mitchell, D. Truex, and M. Goldfarb, "Design of a Myoelectric Transhumeral Prosthesis," *IEEE/ASME Transactions on Mechatronics,* vol. 21, no. 4, pp. 1868-1879, 2016, doi: 10.1109/TMECH.2016.2552999.
[381] N. M. Bajaj, A. J. Spiers, and A. M. Dollar, "State of the art in artificial wrists: A review of prosthetic and robotic wrist design," *IEEE Transactions on Robotics,* vol. 35, no. 1, pp. 261-277, 2019.
[382] Southampton. "Southampton Hand Assessment Procedure (SHAP) " http://www.shap.ecs.soton.ac.uk/index.php (accessed.
[383] R. Safaee-Rad, E. Shwedyk, A. O. Quanbury, and J. E. Cooper, "Normal functional range of motion of upper limb joints during performance of three feeding activities," (in eng), *Arch Phys Med Rehabil,* vol. 71, no. 7, pp. 505-9, Jun 1990.
[384] D. H. Gates, L. S. Walters, J. C. Cowley, J. M. Wilken, and L. J. Resnik, "Range of Motion Requirements for Upper-Limb Activities of Daily Living," *The American journal of occupational therapy : official publication of the American Occupational Therapy Association,* vol. 70 1, pp. 7001350010p1-7001350010p10, 2016.
[385] A. Naceri *et al.*, "From human to robot grasping: force and kinematic synergies: Close comparison between human and robotic hands in both force and kinematic domain," in *Tactile Sensing, Skill Learning, and Robotic Dexterous Manipulation*: Elsevier, 2022, pp. 133-148.
[386] M. Semprini *et al.*, "Clinical evaluation of Hannes: measuring the usability of a novel polyarticulated prosthetic hand," in *Tactile Sensing, Skill Learning, and Robotic Dexterous Manipulation*: Elsevier, 2022, pp. 205-225.
[387] J. R. Binda, "Multiple degrees of freedom wrist prostheses," Master of Science, Biorobotics, Delft University of Technology, 2018.
[388] Ottobock. "Ottobock Hand Chassis." https://shop.ottobock.us/c/Hand-Chassis-with-Quick-Disconnect-Wrist/p/9S266 (accessed.
[389] Ottobock. "Coaxial Plug." https://shop.ottobock.us/Prosthetics/Upper-Limb-Prosthetics/bebionic/Myoelectric-Accessories/Coaxial-Plug/p/9E169 (accessed.
[390] Ottobock. "Co-Axial Bushing." https://shop.ottobock.us/c/Co-Axial-Bushing/p/9E397 (accessed.
[391] D. Shah, Y. Wu, A. Scalzo, G. Metta, and A. Parmiggiani, "A Comparison of Robot Wrist Implementations for the iCub Humanoid †," *Robotics,* vol. 8, no. 1, p. 11, 2019. [Online]. Available: https://www.mdpi.com/2218-6581/8/1/11.
[392] R. Damerla *et al.*, "Design and Testing of a Novel, High-Performance Two DoF Prosthetic Wrist," *IEEE Transactions on Medical Robotics and Bionics,* 2022.
[393] Ottobock. "Hand Chassis with Quick Disconnect Wrist." https://shop.ottobock.us/c/Hand-Chassis-with-Quick-Disconnect-Wrist/p/9S266 (accessed.
[394] TQ. "TQ ILM25x04 Datasheet." https://www.tq-group.com/filedownloads/files/products/robodrive/data-sheets/en/DRVA_DB_Servo-Kits_ILM_EN_Rev408_Web.pdf (accessed.
[395] Ottobock. "Lamination Ring." https://shop.ottobock.us/Prosthetics/Upper-Limb-Prosthetics/Myo-Hands-and-Components/Myo-Wrist-Units-and-Rotation/Lamination-Ring/p/10S1 (accessed.
[396] Ottobock. "Electric Wrist Rotator." https://shop.ottobock.us/Prosthetics/Upper-Limb-Prosthetics/Myo-Hands-and-Components/Myo-Wrist-Units-and-Rotation/Electric-Wrist-Rotator/p/10S17 (accessed.

[397] T. Instruments. "Microcontroller." https://www.ti.com/lit/ds/symlink/tm4c123gh6pm.pdf (accessed.
[398] B. Sensortech. "BNO055 Datasheet." https://www.bosch-sensortec.com/media/boschsensortec/downloads/datasheets/bst-bno055-ds000.pdf (accessed.
[399] AMS. "Magnetic Encoder." https://ams.com/documents/20143/36005/AS5045B_DS000397_2-00.pdf (accessed.
[400] R. Khusainov, D. Azzi, I. E. Achumba, and S. D. Bersch, "Real-time human ambulation, activity, and physiological monitoring: Taxonomy of issues, techniques, applications, challenges and limitations," *Sensors,* vol. 13, no. 10, pp. 12852-12902, 2013.
[401] A. D. Roche, B. Lakey, I. Mendez, I. Vujaklija, D. Farina, and O. C. Aszmann, "Clinical Perspectives in Upper Limb Prostheses: An Update," *Current Surgery Reports,* 2019.
[402] A. Chadwell, L. Kenney, S. Thies, A. Galpin, and J. Head, "The reality of myoelectric prostheses: understanding what makes these devices difficult for some users to control," *Frontiers in neurorobotics,* 2016.
[403] T. Kapelner, F. Negro, O. C. Aszmann, and D. Farina, "Decoding motor unit activity from forearm muscles: perspectives for myoelectric control," *IEEE Transactions on Neural Systems and Rehabilitation Engineering,* vol. 26, no. 1, pp. 244-251, 2017.
[404] D. M. Powers, "Evaluation: from precision, recall and F-measure to ROC, informedness, markedness and correlation," 2011.
[405] S. Amsüss, P. M. Goebel, N. Jiang, B. Graimann, L. Paredes, and D. Farina, "Self-correcting pattern recognition system of surface EMG signals for upper limb prosthesis control," *IEEE Transactions on Biomedical Engineering,* 2013.
[406] J. Demšar, "Statistical comparisons of classifiers over multiple data sets," *Journal of Machine learning research,* 2006.
[407] C. Antfolk, A. Björkman, S.-O. Frank, F. Sebelius, G. Lundborg, and B. Rosen, "Sensory feedback from a prosthetic hand based on air-mediated pressure from the hand to the forearm skin," *Journal of rehabilitation medicine,* vol. 44, no. 8, pp. 702-707, 2012.
[408] H. Cha, S. An, S. Choi, S. Yang, S. Park, and S. Park, "Study on Intention Recognition and Sensory Feedback: Control of Robotic Prosthetic Hand through EMG Classification and Proprioceptive Feedback using Rule-based Haptic Device," *IEEE Transactions on Haptics,* 2022.
[409] A. T. Nguyen *et al.*, "A Portable, Self-Contained Neuroprosthetic Hand with Deep Learning-Based Finger Control," *arXiv preprint arXiv:2103.13452,* 2021.
[410] H. Sun and Q. Wu, "Regularized least square regression with dependent samples," *Advances in Computational Mathematics,* vol. 32, no. 2, pp. 175-189, 2010.
[411] S. Dreiseitl and L. Ohno-Machado, "Logistic regression and artificial neural network classification models: a methodology review," *Journal of biomedical informatics,* vol. 35, no. 5-6, pp. 352-359, 2002.
[412] C.-C. Chang and C.-J. Lin, "LIBSVM: A library for support vector machines," *ACM transactions on intelligent systems and technology (TIST),* vol. 2, no. 3, pp. 1-27, 2011.
[413] N. Chaiyaratana, A. M. Zalzala, and D. Datta, "Myoelectric signals pattern recognition for intelligent functional operation of upper-limb prosthesis," 1996.
[414] A. Ameri, E. N. Kamavuako, E. J. Scheme, K. B. Englehart, and P. A. Parker, "Support vector regression for improved real-time, simultaneous myoelectric control," *IEEE Transactions on Neural Systems and Rehabilitation Engineering,* vol. 22, no. 6, pp. 1198-1209, 2014.
[415] N. Baykal and A. M. Erkmen, "Resilient backpropagation for RBF networks," in *KES'2000. Fourth International Conference on Knowledge-Based Intelligent Engineering Systems and Allied Technologies. Proceedings (Cat. No. 00TH8516)*, 2000, vol. 2: IEEE, pp. 624-627.
[416] C.-W. Hsu and C.-J. Lin, "A comparison of methods for multiclass support vector machines," *IEEE transactions on Neural Networks,* vol. 13, no. 2, pp. 415-425, 2002.
[417] Y. Ding, E. Lushi, and Q. Li, "Investigation of quasi-Newton methods for unconstrained optimization," *Simon Fraser University, Canada,* 2004.
[418] A. J. Young, L. H. Smith, E. J. Rouse, and L. J. Hargrove, "A comparison of the real-time controllability of pattern recognition to conventional myoelectric control for discrete and

simultaneous movements," *Journal of neuroengineering and rehabilitation,* vol. 11, no. 1, pp. 1-10, 2014.
[419] D. D. Lee and H. S. Seung, "Learning the parts of objects by non-negative matrix factorization," *Nature,* vol. 401, no. 6755, pp. 788-791, 1999.
[420] D. Proaño-Guevara, J. Procel-Feijóo, J. Zhingre-Balcazar, and L. Serpa-Andrade, "Biomimetical arm prosthesis: A new proposal," in *International Conference on Applied Human Factors and Ergonomics*, 2017.
[421] J. W. Robertson, K. B. Englehart, and E. J. Scheme, "Effects of confidence-based rejection on usability and error in pattern recognition-based myoelectric control," *IEEE journal of biomedical and health informatics,* 2018.
[422] P. K. Artemiadis and K. J. Kyriakopoulos, "An EMG-based robot control scheme robust to time-varying EMG signal features," *IEEE Transactions on Information Technology in Biomedicine,* vol. 14, no. 3, pp. 582-588, 2010.
[423] I. Vujaklija, D. Farina, and O. C. Aszmann, "New developments in prosthetic arm systems," *Orthopedic research and reviews,* vol. 8, p. 31, 2016.
[424] A. J. Young, L. J. Hargrove, and T. A. Kuiken, "The effects of electrode size and orientation on the sensitivity of myoelectric pattern recognition systems to electrode shift," *IEEE Transactions on Biomedical Engineering,* vol. 58, no. 9, pp. 2537-2544, 2011.
[425] B. Wan *et al.*, "Study on fatigue feature from forearm SEMG signal based on wavelet analysis," in *2010 IEEE International Conference on Robotics and Biomimetics*, 2010: IEEE, pp. 1229-1232.
[426] C. Castellini, A. E. Fiorilla, and G. Sandini, "Multi-subject/daily-life activity EMG-based control of mechanical hands," *Journal of neuroengineering and rehabilitation,* vol. 6, no. 1, pp. 1-11, 2009.
[427] S. Amsuess *et al.*, "Context-dependent upper limb prosthesis control for natural and robust use," *IEEE Transactions on Neural Systems and Rehabilitation Engineering,* vol. 24, no. 7, pp. 744-753, 2015.
[428] F. Clemente *et al.*, "Intraneural sensory feedback restores grip force control and motor coordination while using a prosthetic hand," *Journal of neural engineering,* vol. 16, no. 2, p. 026034, 2019.
[429] F. Popa and P. Kyberd, "Identification of patterns in upper limb prosthetic usage by analysis of visual attention to areas of interest," in *Proceedings of the 2011 MyoElectric Controls/Powered Prosthetics Symposium Fredericton, New Brunswick, Canada: August*, 2011, pp. 14-19.
[430] S. Lewis, M. F. Russold, H. Dietl, and E. Kaniusas, "User demands for sensory feedback in upper extremity prostheses," in *2012 IEEE international symposium on medical measurements and applications proceedings*, 2012: Ieee, pp. 1-4.
[431] M. Markovic *et al.*, "The clinical relevance of advanced artificial feedback in the control of a multi-functional myoelectric prosthesis," *Journal of neuroengineering and rehabilitation,* vol. 15, no. 1, pp. 1-15, 2018.
[432] G. Di Pino *et al.*, "Sensory-and action-oriented embodiment of neurally-interfaced robotic hand prostheses," *Frontiers in Neuroscience,* vol. 14, p. 389, 2020.
[433] A. W. Shehata, M. Rehani, Z. E. Jassat, and J. S. Hebert, "Mechanotactile sensory feedback improves embodiment of a prosthetic hand during active use," *Frontiers in neuroscience,* vol. 14, p. 263, 2020.
[434] E. D'Anna *et al.*, "A closed-loop hand prosthesis with simultaneous intraneural tactile and position feedback," *Science Robotics,* vol. 4, no. 27, p. eaau8892, 2019.
[435] S. Micera *et al.*, "Decoding information from neural signals recorded using intraneural electrodes: toward the development of a neurocontrolled hand prosthesis," *Proceedings of the IEEE,* vol. 98, no. 3, pp. 407-417, 2010.
[436] G. K. Patel, S. Dosen, C. Castellini, and D. Farina, "Multichannel electrotactile feedback for simultaneous and proportional myoelectric control," *Journal of neural engineering,* vol. 13, no. 5, p. 056015, 2016.
[437] S. Dosen *et al.*, "Multichannel electrotactile feedback with spatial and mixed coding for closed-loop control of grasping force in hand prostheses," *IEEE Transactions on Neural Systems and Rehabilitation Engineering,* vol. 25, no. 3, pp. 183-195, 2016.

[438] K. Horch, S. Meek, T. G. Taylor, and D. T. Hutchinson, "Object discrimination with an artificial hand using electrical stimulation of peripheral tactile and proprioceptive pathways with intrafascicular electrodes," *IEEE Transactions on Neural Systems and Rehabilitation Engineering,* vol. 19, no. 5, pp. 483-489, 2011.
[439] M. N. Nemah, O. H. Aldulaymi, C. Y. Low, N. A. C. Zakaria, and S. Mohamaddan, "A hybrid haptic feedback stimulation device to recover the missing sensation of the upper limb amputees," in *IOP Conference Series: Materials Science and Engineering*, 2020, vol. 834, no. 1: IOP Publishing, p. 012013.
[440] C. Antfolk *et al.*, "Artificial redirection of sensation from prosthetic fingers to the phantom hand map on transradial amputees: vibrotactile versus mechanotactile sensory feedback," *IEEE transactions on neural systems and rehabilitation engineering,* vol. 21, no. 1, pp. 112-120, 2012.
[441] A. M. De Nunzio *et al.*, "Tactile feedback is an effective instrument for the training of grasping with a prosthesis at low-and medium-force levels," *Experimental brain research,* vol. 235, no. 8, pp. 2547-2559, 2017.
[442] R. M. Mayer *et al.*, "Tactile feedback in closed-loop control of myoelectric hand grasping: conveying information of multiple sensors simultaneously via a single feedback channel," *Frontiers in Neuroscience,* vol. 14, p. 348, 2020.
[443] O. Kayhan, A. K. Nennioglu, and E. Samur, "A skin stretch tactor for sensory substitution of wrist proprioception," in *2018 IEEE Haptics Symposium (HAPTICS)*, 2018: IEEE, pp. 26-31.
[444] E. Battaglia, J. P. Clark, M. Bianchi, M. G. Catalano, A. Bicchi, and M. K. O'Malley, "Skin stretch haptic feedback to convey closure information in anthropomorphic, under-actuated upper limb soft prostheses," *IEEE Transactions on Haptics,* vol. 12, no. 4, pp. 508-520, 2019.
[445] L. Vargas, H. Huang, Y. Zhu, and X. Hu, "Object Recognition via Evoked Sensory Feedback during Control of a Prosthetic Hand," *IEEE Robotics and Automation Letters,* vol. 7, no. 1, pp. 207-214, 2021.
[446] A. Blank, A. M. Okamura, and K. J. Kuchenbecker, "Identifying the role of proprioception in upper-limb prosthesis control: Studies on targeted motion," *ACM Transactions on Applied Perception (TAP),* vol. 7, no. 3, pp. 1-23, 2008.
[447] M. Rossi, M. Bianchi, E. Battaglia, M. G. Catalano, and A. Bicchi, "HapPro: a wearable haptic device for proprioceptive feedback," *IEEE Transactions on Biomedical Engineering,* vol. 66, no. 1, pp. 138-149, 2018.
[448] R. W. Mann and S. D. Reimers, "Kinesthetic Sensing for the EMG Controlled" Boston Arm"," *IEEE Transactions on Man-Machine Systems,* vol. 11, no. 1, pp. 110-115, 1970.
[449] A. E. Pena, L. Rincon-Gonzalez, J. J. Abbas, and R. Jung, "Effects of vibrotactile feedback and grasp interface compliance on perception and control of a sensorized myoelectric hand," *PloS one,* vol. 14, no. 1, p. e0210956, 2019.
[450] J. V. S. Luces, K. Okabe, Y. Murao, and Y. Hirata, "A phantom-sensation based paradigm for continuous vibrotactile wrist guidance in two-dimensional space," *IEEE Robotics and Automation Letters,* vol. 3, no. 1, pp. 163-170, 2017.
[451] L. Vargas, H. H. Huang, Y. Zhu, and X. Hu, "Closed-loop control of a prosthetic finger via evoked proprioceptive information," *Journal of Neural Engineering,* vol. 18, no. 6, p. 066029, 2021.
[452] R. Yunus *et al.*, "Development and testing of a wearable vibrotactile haptic feedback system for proprioceptive rehabilitation," *IEEE Access,* vol. 8, pp. 35172-35184, 2020.
[453] H. J. Witteveen, H. S. Rietman, and P. H. Veltink, "Vibrotactile grasping force and hand aperture feedback for myoelectric forearm prosthesis users," *Prosthetics and orthotics international,* vol. 39, no. 3, pp. 204-212, 2015.
[454] M. A. Garenfeld *et al.*, "A compact system for simultaneous stimulation and recording for closed-loop myoelectric control," *Journal of NeuroEngineering and Rehabilitation,* vol. 18, no. 1, pp. 1-17, 2021.
[455] A. Erwin and F. C. Sup IV, "A haptic feedback scheme to accurately position a virtual wrist prosthesis using a three-node tactor array," *PloS one,* vol. 10, no. 8, p. e0134095, 2015.
[456] S.-W. Shim and H. Z. Tan, "palmScape: Calm and pleasant vibrotactile signals," in *International Conference on Human-Computer Interaction*, 2020: Springer, pp. 532-548.

[457] M. Ortiz-Catalan, B. Håkansson, and R. Brånemark, "Real-time and simultaneous control of artificial limbs based on pattern recognition algorithms," *IEEE Transactions on Neural Systems and Rehabilitation Engineering,* vol. 22, no. 4, pp. 756-764, 2014.
[458] M. Solomonow, J. Lyman, and A. Freedy, "Electrotactile two-point discrimination as a function of frequency, body site, laterality, and stimulation codes," *Annals of biomedical engineering,* vol. 5, no. 1, pp. 47-60, 1977.
[459] I. Vybronics. "VC0625B001L." https://www.vybronics.com/wp-content/uploads/datasheet-files/Vybronics-VC0625B001L-datasheet.pdf (accessed.
[460] S. Gilman, "Joint position sense and vibration sense: Anatomical organisation and assessment," *Journal of neurology, neurosurgery, and psychiatry,* vol. 73, pp. 473-7, 12/01 2002, doi: 10.1136/jnnp.73.5.473.
[461] N. Prins, *Psychophysics: a practical introduction*. Academic Press, 2016.
[462] D. G. Buma, J. R. Buitenweg, and P. H. Veltink, "Intermittent stimulation delays adaptation to electrocutaneous sensory feedback," *IEEE Transactions on Neural Systems and Rehabilitation Engineering,* vol. 15, no. 3, pp. 435-441, 2007.
[463] F. S. di Luzio, C. Lauretti, F. Cordella, F. Draicchio, and L. Zollo, "Visual vs vibrotactile feedback for posture assessment during upper-limb robot-aided rehabilitation," *Applied ergonomics,* vol. 82, p. 102950, 2020.
[464] J. Azbell, J. Park, S.-H. Chang, M. P. Engelen, and H. Park, "Plantar or palmar tactile augmentation improves lateral postural balance with significant influence from cognitive load," *IEEE Transactions on Neural Systems and Rehabilitation Engineering,* vol. 29, pp. 113-122, 2020.
[465] L. Biagiotti, F. Lotti, C. Melchiorri, and G. Vassura, "How far is the human hand," *A review on anthropomorphic robotic end-effectors,* 2004.
[466] J. T. Belter, J. L. Segil, A. M. Dollar, and R. F. Weir, "Mechanical design and performance specifications of anthropomorphic prosthetic hands: A review," *Journal of Rehabilitation Research & Development,* vol. 50, no. 5, 2013.
[467] M. Controzzi, C. Cipriani, and M. C. Carrozza, "Design of artificial hands: A review," in *The Human Hand as an Inspiration for Robot Hand Development*: Springer, 2014, pp. 219-246.
[468] E. Scaliti, E. Gruppioni, and C. Becchio, "And Yet It Moves: What We Currently Know about Phantom Arm Movements," *The Neuroscientist,* vol. 26, no. 4, pp. 328-342, 2020.
[469] M. Ortiz-Catalan, R. Brånemark, B. Håkansson, and J. Delbeke, "On the viability of implantable electrodes for the natural control of artificial limbs: review and discussion," *Biomedical engineering online,* vol. 11, no. 1, pp. 1-24, 2012.
[470] K. A. Yildiz, A. Y. Shin, and K. R. Kaufman, "Interfaces with the peripheral nervous system for the control of a neuroprosthetic limb: a review," *Journal of neuroengineering and rehabilitation,* vol. 17, no. 1, pp. 1-19, 2020.
[471] J. S. Schofield, M. R. Dawson, J. P. Carey, and J. S. Hebert, "Characterizing the effects of amplitude, frequency and limb position on vibration induced movement illusions: Implications in sensory-motor rehabilitation," *Technology and Health Care,* vol. 23, no. 2, pp. 129-141, 2015.
[472] P. D. Marasco *et al.*, "Illusory movement perception improves motor control for prosthetic hands," *Science translational medicine,* vol. 10, no. 432, p. eaao6990, 2018.
[473] P. Chaubey, T. Rosenbaum-Chou, W. Daly, and D. Boone, "Closed-loop vibratory haptic feedback in upper-limb prosthetic users," *JPO: Journal of Prosthetics and Orthotics,* vol. 26, no. 3, pp. 120-127, 2014.
[474] P. Shi and X. Shen, "Sensation feedback and muscle response of electrical stimulation on the upper limb skin: A case study," in *2015 Seventh International Conference on Measuring Technology and Mechatronics Automation*, 2015: IEEE, pp. 969-972.
[475] M. D'Alonzo, S. Dosen, C. Cipriani, and D. Farina, "HyVE—hybrid vibro-electrotactile stimulation—is an efficient approach to multi-channel sensory feedback," *IEEE transactions on haptics,* vol. 7, no. 2, pp. 181-190, 2013.
[476] J. Lee, M. H. Choi, J. H. Jung, and F. L. Hammond, "Multimodal sensory feedback for virtual proprioception in powered upper-limb prostheses," in *2017 26th IEEE International Symposium on Robot and Human Interactive Communication (RO-MAN)*, 2017: IEEE, pp. 277-283.

[477] H. Huang *et al.*, "Multi-modal sensory feedback system for upper limb amputees," in *2017 New Generation of CAS (NGCAS)*, 2017: IEEE, pp. 193-196.
[478] F. Clemente and C. Cipriani, "A novel device for multi-modal sensory feedback in hand prosthetics: Design and preliminary prototype," in *2014 IEEE Haptics Symposium (HAPTICS)*, 2014: IEEE, pp. 569-573.
[479] T. Basu. "Facebook is making a bracelet that lets you control computers with your brain." https://www.technologyreview.com/2021/03/18/1021021/facebook-augmented-reality-wristband/?truid=6d1563793eef118b900759ed00bfef6f&utm_source=the_download&utm_medium=email&utm_campaign=the_download.unpaid.engagement&utm_term=&utm_content=03-19-2021&mc_cid=f1e3644b4e&mc_eid=de470f7d14 (accessed March 18, 2021.
[480] M. Zecca, S. Micera, M. C. Carrozza, and P. Dario, "Control of multifunctional prosthetic hands by processing the electromyographic signal," *Critical Reviews™ in Biomedical Engineering,* vol. 30, no. 4-6, 2002.
[481] R. M. Palnitkar and J. Cannady, "A review of adaptive neural networks," in *IEEE SoutheastCon, 2004. Proceedings.*, 2004: IEEE, pp. 38-47.
[482] A. W. Shehata, E. J. Scheme, and J. W. Sensinger, "Audible feedback improves internal model strength and performance of myoelectric prosthesis control," *Scientific reports,* vol. 8, no. 1, pp. 1-10, 2018.
[483] A. W. Shehata, L. F. Engels, M. Controzzi, C. Cipriani, E. J. Scheme, and J. W. Sensinger, "Improving internal model strength and performance of prosthetic hands using augmented feedback," *Journal of neuroengineering and rehabilitation,* vol. 15, no. 1, pp. 1-12, 2018.
[484] A. Smith, B. Ward-Cherrier, A. Etoundi, and M. J. Pearson, "Evaluating Multi-Channel Vibrational Feedback Arrays in a Digit Discrimination Task," in *2022 International Symposium on Electrical, Electronics and Information Engineering (ISEEIE)*, 2022: IEEE, pp. 202-207.
[485] T. Boljanić *et al.*, "Design of multi-pad electrotactile system envisioned as a feedback channel for supernumerary robotic limbs," *Artificial Organs,* 2022.
[486] S. S. Hsiao, M. Fettiplace, and B. Darbandi, "Sensory feedback for upper limb prostheses," *Progress in brain research,* vol. 192, pp. 69-81, 2011.
[487] C. Medynski and B. Rattray, "Bebionic prosthetic design," 2011: Myoelectric Symposium.
[488] O. Van Der Niet and C. K. van der Sluis, "Functionality of i-LIMB and i-LIMB Pulse hands: Case report," *Journal of rehabilitation research and development,* vol. 50, no. 8, p. 1123, 2013.
[489] C. Stiegelmar, D. Blustein, J. Sensinger, J. Hebert, and A. Shehata, "TOWARDS QUANTIFYING THE SENSE OF AGENCY AND ITS CONTRIBUTION TO EMBODIMENT OF MYOELECTRIC PROSTHESES," in *MEC20 Symposium*, 2020.
[490] C. Pylatiuk, S. Schulz, and L. Döderlein, "Results of an Internet survey of myoelectric prosthetic hand users," *Prosthetics and orthotics international,* vol. 31, no. 4, pp. 362-370, 2007.
[491] G. Chai, H. Wang, G. Li, X. Sheng, and X. Zhu, "Electrotactile feedback improves grip force control and enables object stiffness recognition while using a myoelectric hand," *IEEE Transactions on Neural Systems and Rehabilitation Engineering,* 2022.
[492] L. Osborn, R. R. Kaliki, A. B. Soares, and N. V. Thakor, "Neuromimetic event-based detection for closed-loop tactile feedback control of upper limb prostheses," *IEEE transactions on haptics,* vol. 9, no. 2, pp. 196-206, 2016.
[493] B. Stephens-Fripp, G. Alici, and R. Mutlu, "A review of non-invasive sensory feedback methods for transradial prosthetic hands," *IEEE Access,* vol. 6, pp. 6878-6899, 2018.
[494] S. J. Garland and T. S. Miles, "Control of motor units in human flexor digitorum profundus under different proprioceptive conditions," *The Journal of physiology,* vol. 502, no. 3, pp. 693-701, 1997.
[495] G. Cannata, M. Maggiali, G. Metta, and G. Sandini, "An embedded artificial skin for humanoid robots," in *2008 IEEE International conference on multisensor fusion and integration for intelligent systems*, 2008: IEEE, pp. 434-438.
[496] Z. Yi and Y. Zhang, "Bio-inspired tactile FA-I spiking generation under sinusoidal stimuli," *Journal of Bionic Engineering,* vol. 13, no. 4, pp. 612-621, 2016.
[497] H. Zhao, K. O'Brien, S. Li, and R. F. Shepherd, "Optoelectronically innervated soft prosthetic hand via stretchable optical waveguides," *Science robotics,* vol. 1, no. 1, p. eaai7529, 2016.

[498] N. Jamali and C. Sammut, "Majority voting: Material classification by tactile sensing using surface texture," *IEEE Transactions on Robotics,* vol. 27, no. 3, pp. 508-521, 2011.
[499] M. V. Liarokapis, B. Calli, A. J. Spiers, and A. M. Dollar, "Unplanned, model-free, single grasp object classification with underactuated hands and force sensors," in *2015 IEEE/RSJ International Conference on Intelligent Robots and Systems (IROS)*, 2015: IEEE, pp. 5073-5080.
[500] J. Konstantinova, G. Cotugno, A. Stilli, Y. Noh, and K. Althoefer, "Object classification using hybrid fiber optical force/proximity sensor," in *2017 IEEE SENSORS*, 2017: IEEE, pp. 1-3.
[501] R. R. Devaraja, R. Maskeliūnas, and R. Damaševičius, "Design and evaluation of anthropomorphic robotic hand for object grasping and shape recognition," *Computers,* vol. 10, no. 1, p. 1, 2020.
[502] J. Huang and A. Rosendo, "Variable Stiffness Object Recognition with a CNN-Bayes Classifier on a Soft Gripper," *Soft Robotics,* 2022.
[503] A. Masteller, S. Sankar, H. B. Kim, K. Ding, X. Liu, and A. H. All, "Recent developments in prosthesis sensors, texture recognition, and sensory stimulation for upper limb prostheses," *Annals of biomedical engineering,* vol. 49, no. 1, pp. 57-74, 2021.
[504] G. Shannon, "A comparison of alternative means of providing sensory feedback on upper limb prostheses," *Medical and biological engineering,* vol. 14, no. 3, pp. 289-294, 1976.
[505] K. A. Kaczmarek, J. G. Webster, P. Bach-y-Rita, and W. J. Tompkins, "Electrotactile and vibrotactile displays for sensory substitution systems," *IEEE transactions on biomedical engineering,* vol. 38, no. 1, pp. 1-16, 1991.
[506] L. Vargas, H. Shin, H. H. Huang, Y. Zhu, and X. Hu, "Object stiffness recognition using haptic feedback delivered through transcutaneous proximal nerve stimulation," *Journal of neural engineering,* vol. 17, no. 1, p. 016002, 2019.
[507] H. J. Witteveen, F. Luft, J. S. Rietman, and P. H. Veltink, "Stiffness feedback for myoelectric forearm prostheses using vibrotactile stimulation," *IEEE transactions on neural systems and rehabilitation engineering,* vol. 22, no. 1, pp. 53-61, 2013.
[508] S. G. Meek, S. C. Jacobsen, and P. P. Goulding, "Extended physiologic taction: design and evaluation of a proportional force feedback system," *J Rehabil Res Dev,* vol. 26, no. 3, pp. 53-62, 1989.
[509] S. Casini, M. Morvidoni, M. Bianchi, M. Catalano, G. Grioli, and A. Bicchi, "Design and realization of the cuff-clenching upper-limb force feedback wearable device for distributed mechano-tactile stimulation of normal and tangential skin forces," in *2015 IEEE/RSJ International Conference on Intelligent Robots and Systems (IROS)*, 2015: IEEE, pp. 1186-1193.
[510] A. B. Balasubramanian, D. P. Magee, and D. G. Taylor, "Stiffness Estimation in Single Degree of Freedom Mechanisms using Regression," in *IECON 2021–47th Annual Conference of the IEEE Industrial Electronics Society*, 2021: IEEE, pp. 1-6.
[511] L. Wang, Q. Li, J. Lam, and Z. Wang, "Tactual recognition of soft objects from deformation cues," *IEEE Robotics and Automation Letters,* vol. 7, no. 1, pp. 96-103, 2021.
[512] G. Bruni and A. Bucchieri, "Analysis and optimization of Hannes prosthetic hand: a multi-body approach," 2021.
[513] G. Bruni *et al.*, "A Multi-Body Model of an upper-limb prosthesis for grip force estimation and related object interaction application," in *2022 9th IEEE RAS/EMBS International Conference for Biomedical Robotics and Biomechatronics (BioRob)*, 2022: IEEE, pp. 01-07.
[514] Z. Kappassov, J.-A. Corrales, and V. Perdereau, "Tactile sensing in dexterous robot hands," *Robotics and Autonomous Systems,* vol. 74, pp. 195-220, 2015.
[515] H. Deng, X. Xu, W. Zhuo, and Y. Zhang, "Current-sensor-based contact stiffness detection for prosthetic hands," *IEEE Access,* vol. 8, pp. 29456-29466, 2020.
[516] C. Cipriani, M. D'Alonzo, and M. C. Carrozza, "A miniature vibrotactile sensory substitution device for multifingered hand prosthetics," *IEEE transactions on biomedical engineering,* vol. 59, no. 2, pp. 400-408, 2011.
[517] C. Tejeiro, C. E. Stepp, M. Malhotra, E. Rombokas, and Y. Matsuoka, "Comparison of remote pressure and vibrotactile feedback for prosthetic hand control," in *2012 4th IEEE RAS & EMBS*

International Conference on Biomedical Robotics and Biomechatronics (BioRob), 2012: IEEE, pp. 521-525.
[518] Vernier. "Go Direct® Hand Dynamometer." https://www.vernier.com/product/go-direct-hand-dynamometer/ (accessed.
[519] T. R. Makin, F. de Vignemont, and A. A. Faisal, "Neurocognitive barriers to the embodiment of technology," *Nature Biomedical Engineering,* vol. 1, no. 1, pp. 1-3, 2017.